

Mass measurements near the $Z=N$ line with JYFLTRAP

Anu Kankainen and the JYFLTRAP Collaboration

Department of Physics, University of Jyväskylä, FI-40014 University of Jyväskylä, Finland

Abstract. Masses of nuclides involved in astrophysical rp and νp processes have to be known precisely in order to model these processes reliably. Mass excesses for 90 ground state and 8 isomeric states of neutron-deficient nuclides have been determined with a precision of better than 10 keV with the JYFLTRAP double Penning trap mass spectrometer at the Ion-Guide Isotope Separator On-Line facility in Jyväskylä. Highlights of the measurements related to nuclear astrophysics are given. Some of the measured isomers, such as $^{53}\text{Co}^m$, $^{90}\text{Tc}^m$, and $^{95}\text{Pd}^m$, and implications for the excitation energy of the 21^+ isomer in ^{94}Ag are briefly discussed.

Keywords: Penning trap, atomic masses, isomers, rp process, νp process

PACS: 21.10.Dr, 27.40.+z, 27.50.+e, 27.60.+j

INTRODUCTION

Penning traps have opened a new, direct way to determine atomic masses with high precision ($\delta m/m \approx 10^{-8}$). In addition to ground-state mass measurements, traps can be used to identify isomeric states and to measure related excitation energies. The JYFLTRAP double Penning trap mass spectrometer at the Ion-Guide Isotope Separator On-Line (IGISOL) facility [1] has been used to measure 90 ground state and 8 isomeric state masses of neutron-deficient nuclides during the years 2005-2010. These measurements have made an impact on nuclear astrophysics calculations in two ways. Firstly, determined proton-separation energies have a direct effect on calculated proton-capture rates which depend exponentially on the proton-capture Q values. The abundances in each isotonic chain also depend exponentially on the Q values according to the Saha equation [2]. Thus, the masses have a clear effect e.g. on the path and final abundances as well as on x-ray burst light curves. Secondly, the Penning trap mass measurements have revealed that many of the masses based previously on beta-decay endpoint energies have been underestimated. The new measurements have paved the way for a new Atomic Mass Evaluation where the nuclides far from the stability are less bound in the $A \approx 80 - 100$ region.

Figure 1 shows the nuclei studied at JYFLTRAP and related astrophysical processes. The measurements near the $Z = N$ line have been important for the studies of nucleosynthesis in novae as well as for rp [3, 4] or νp processes [5, 6]. Here, we will focus on νp and rp processes by giving three highlights of the JYFLTRAP mass measurements. In addition, isomeric states $^{53}\text{Co}^m$, $^{90}\text{Tc}^m$, and $^{95}\text{Pd}^m$, and implications for the 21^+ isomer in ^{94}Ag will be discussed.

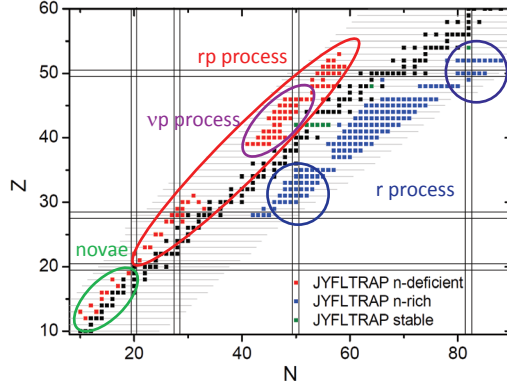


FIGURE 1. (Color online) Measured nuclides at JYFLTRAP and astrophysical motivation for different regions.

JYFLTRAP AND MASS MEASUREMENTS

The ions of interest are produced with the IGISOL technique [1]. The ions produced via light ion (p or ${}^3\text{He}$) or heavy ion induced fusion-evaporation reactions are stopped in the ion-guide gas cell, extracted and guided with a sextupole ion guide (SPIG) [7] towards the high vacuum region of the mass separator. The beam is accelerated to 30 keV and mass-separated with a dipole magnet. The continuous beam has to be cooled and bunched with a radio-frequency quadrupole (RFQ) [8] before injecting into the JYFLTRAP double Penning trap mass spectrometer [9] inside a 7-T superconducting solenoid. The ions are purified isobarically in the first trap: elements within the same mass number A and in some cases even isomers can be resolved via the buffer gas cooling technique [10] coupled with ion extraction. High-precision mass measurements take place in the second trap via the time-of-flight (TOF) ion cyclotron resonance method [11, 12]. When extracted from the trap, the ions in resonance gain more energy in the magnetic field gradient and have a shorter time-of-flight to the multi-channel plate detector at the end of the trap line. The cyclotron frequency of the ion, $\nu_c = qB/(2\pi m)$, depends inversely on its mass. Since the majority of the ions produced at IGISOL have charge state $q = 1^+$, and as the magnetic field B can be calibrated with a reference ion with a well-known mass m_{ref} , the atomic mass of the nuclide of interest m is obtained as $m = (\nu_c^{ref}/\nu_c) \cdot (m_{ref} - m_e) + m_e$. Therefore, the basic quantity to be measured is the frequency ratio between the reference and the ion of interest. For the details of the used analysis methods and mass-dependent and residual uncertainties studied via carbon cluster measurements, see Refs. [13, 14].

NUCLEAR ASTROPHYSICS: HIGHLIGHTS

rp-process waiting point ${}^{56}\text{Ni}$

${}^{56}\text{Ni}$ has a half-life of 6.075(10) days [15]. This is long enough to inhibit further nucleosynthesis towards heavier elements unless the proton captures on ${}^{56}\text{Ni}$ are fast

enough. The proton capture rate depends exponentially on the Q value of $^{56}\text{Ni}(p, \gamma)^{57}\text{Cu}$ [16]. This has been recently determined via a direct frequency ratio measurement between ^{57}Cu and ^{56}Ni at JYFLTRAP. The resulting Q value is close to the Atomic Mass Evaluation 2003 (AME03) [17] value but is 40 times more precise. This will enable a more reliable rp process modeling in the future.

S_p values and the νp process

In the $A \approx 80 - 100$ region, plenty of measurements have been carried out at JYFLTRAP [13, 18, 19, 20] and also at SHIPTRAP [13, 21]. The new mass values have been used to calculate proton capture Q values (or proton separation energies S_p) needed to model the νp process [5]. Large deviations have been found in the S_p values of the measured Tc, Mo and Nb isotopes. These results have an effect on the calculated final abundances after decaying to stability in the νp process [13]. For example, the proton separation energy of ^{90}Tc has been found to be 490(240) keV [13] lower than in the AME03 [17]. This increases the photodisintegration of ^{90}Tc and thus there will be less $A = 90$ in the final abundance pattern. Another example is the S_p value of ^{88}Tc , which was found to be 1030(480) keV [13] lower than in the AME03. A lower Q value favors the reaction $^{87}\text{Mo}(n, p)^{87}\text{Nb}$ instead of $^{87}\text{Mo}(p, \gamma)^{88}\text{Tc}$. As a result, there will be more mass $A = 87$ in the abundance pattern. However, a recent measurement at SHIPTRAP [22] shows that the mass excess of ^{87}Mo was off by 810(220) keV. After this update, the S_p value of ^{88}Tc is 220(320) keV lower than in the AME03. The νp process has not yet been modeled with this new value. Nevertheless, the observed large deviations in this mass region further confirm that Penning trap measurements are essential for obtaining more accurate mass values.

The endpoint of the rp process

The rp process has been predicted to end in a so called SnSbTe cycle where subsequent proton captures on Sn and Sb isotopes lead to alpha-unbound Te isotopes which then decay back to Sn isotopes. In this way, material is cycled and He produced towards the end of the rp process. Mass measurements performed at JYFLTRAP [19] have shown that the proton separation energies of ^{106}Sb and ^{107}Sb are relatively low. The only measurement on the S_p value of ^{106}Sb gives a value of 930(210) keV [23] and a branching of about 50(30) % to the SnSbTe cycle. This value has been considered as uncertain, and it was already rejected from the AME03 compilation. The new JYFLTRAP value, 424(8) keV, yields a branching of 3 %. This suppresses the cycle considerably. The S_p value of ^{107}Sb is also quite low yielding only about 13 % branching to the SnSbTe cycle. Since the half-life of ^{106}Sn is long compared to x-ray burst time scales, the cycle through ^{108}Sb is also weak. In summary, new mass measurements have shown that the SnSbTe cycle is not so strong as expected. This yields a slightly longer and less luminous burst tail and a broader distribution of final abundances (not so concentrated on ^{104}Pd).

TABLE 1. Excitation energies of some isomers determined at JYFLTRAP compared to the NUBASE 2003 [30].

Isomer	$E_{x,JYFL}$ (keV)	E_x [30] (keV)
$^{53}\text{Co}^m$	3174.3(10) [25]	3197(29)
$^{94}\text{Ag}^m$ (1p)	6960(400)# [27]	6500(2000)#
$^{94}\text{Ag}^m$ (2p)	8360(370)# [27]	6500(2000)#
$^{95}\text{Pd}^m$	1875.4(67) [13]	1860(500)#

ISOMERIC STATES

The region around $A = 80 - 100$ is rich in isomers and special attention should be paid to the measured state in Penning trap measurements. With JYFLTRAP mass spectrometer, isomers having half-lives above ≈ 100 ms and excitation energies above ≈ 100 keV can be resolved from the ground state. Information on the possible mixture of states can be obtained both from the TOF spectra and from post-trap spectroscopy. Even a simple half-life measurement of beta particles at the selected mass number is in some cases enough to identify the state. This has been demonstrated for example for ^{90}Tc [24]. The time-of-flight spectrum of ^{90}Tc shows clearly two components of which the lower-mass state is much more dominant. The time behaviour of the beta particles at $A = 90$ after the IGISOL dipole magnet confirms that the ground state is the 8^+ state with a half-life of around 50 s. The excitation energy of the isomer was determined by measuring the isomeric and ground states separately against the reference ^{86}Kr .

JYFLTRAP has also been capable of measuring the masses and excitation energies of high-spin, spin-gap isomers $^{53}\text{Co}^m$ ($19/2^-$) [25] and $^{95}\text{Pd}^m$ ($21/2^+$) [13]. The measured excitation energies are collected in Table 1. $^{95}\text{Pd}^m$ was the first of this type of isomeric state measured at JYFLTRAP, and it confirms the results from in-beam γ spectroscopy [26]. The excitation energy of $^{53}\text{Co}^m$ [25] yields a more precise value for the mirror energy difference in the $T = 1/2$ pair at $A = 53$.

We have also estimated the excitation energy for the spin-gap isomer (21^+) in ^{94}Ag based on JYFLTRAP measurements [27]. Firstly, the Coulomb displacement energy of ^{94}Ag was extrapolated from the values of well-known odd-odd $Z = N$ nuclei. The resulting Q_{EC} value was combined with the measured mass of ^{94}Pd to obtain the ground-state mass of ^{94}Ag . The two-proton separation energy, S_{2p} , is then determined with the measured ^{92}Rh mass. Combining this with the data from the two-proton decay of the 21^+ isomer [28] yields an excitation energy of 8360(370)# keV. On the other hand, the mass of ^{93}Pd can be interpolated from the smooth trend of S_{2p} values of the $N = 47$ isotones, and from the measured ^{91}Ru mass. Together with the measured ^{92}Rh mass, a proton separation energy of 3730(160)# keV is obtained for ^{93}Pd . When this S_p value is summed up with the one-proton decay data [29], the resulting excitation energy, 6960(400)# keV, disagrees with the value based on two-proton decay data. A direct Penning trap mass measurement of this isomer would solve this discrepancy in the future.

SUMMARY AND OUTLOOK

JYFLTRAP has been very successful in measuring atomic masses of neutron-deficient nuclei owing to the chemically insensitive IGISOL method and a large variety of beams and targets available. At the moment, IGISOL is being moved to a new laboratory area. There, it will be possible to use beams from two cyclotrons: K-30 and K-130. Two 70 % HPGe detectors have been ordered for more efficient measurements at a permanent yield station after the IGISOL dipole magnet, and for post-trap spectroscopy measurements after the trap. These improvements will help to identify the measured states. Tests for laser ionization of silver in the hot-cavity laser ion source have been performed [31] and the aim is to produce $^{94}\text{Ag}^m (21^+)$ at the new facility.

ACKNOWLEDGMENTS

This work has been supported by the EU 6th Framework programme “Integrating Infrastructure Initiative - Transnational Access”, Contract Number: 506065 (EURONS) and by the Academy of Finland under the Finnish Centre of Excellence Programme 2006-2011 (Nuclear and Accelerator Based Physics Programme at JYFL). A.K. acknowledges the support from the Academy of Finland under the project 127301.

REFERENCES

1. J. Äystö, *Nucl. Phys. A* **693**, 477 – 494 (2001).
2. H. Schatz, *Int. J. Mass Spectrom.* **251**, 293 – 299 (2006).
3. R. K. Wallace, and S. E. Woosley, *Astrophys. J. Suppl. Ser.* **45**, 389–420 (1981).
4. H. Schatz, A. Aprahamian, J. Görres, M. Wiescher, T. Rauscher, J. F. Rembges, F. K. Thielemann, B. Pfeiffer, P. Möller, K. L. Kratz, H. Herndl, B. A. Brown, and H. Rebel, *Phys. Rep.* **294**, 167 – 263 (1998).
5. C. Fröhlich, G. Martínez-Pinedo, M. Liebendörfer, F.-K. Thielemann, E. Bravo, W. R. Hix, K. Langanke, and N. T. Zinner, *Phys. Rev. Lett.* **96**, 142502 (2006).
6. J. Pruet, R. D. Hoffman, S. E. Woosley, H.-T. Janka, and R. Buras, *Astrophys. J.* **644**, 1028 (2006).
7. P. Karvonen, I. Moore, T. Sonoda, T. Kessler, H. Penttilä, K. Peräjärvi, P. Ronkanen, and J. Äystö, *Nucl. Instrum. and Methods in Phys. Res. B* **266**, 4794 – 4807 (2008).
8. A. Nieminen, J. Huikari, A. Jokinen, J. Äystö, P. Campbell, and E. C. A. Cochrane, *Nucl. Instrum. Methods Phys. Res. A* **469**, 244 – 253 (2001).
9. V. S. Kolhinen, S. Kopecky, T. Eronen, U. Hager, J. Hakala, J. Huikari, A. Jokinen, A. Nieminen, S. Rinta-Antila, J. Szerypo, and J. Äystö, *Nucl. Instrum. Methods Phys. Res. A* **528**, 776 – 787 (2004).
10. G. Savard, S. Becker, G. Bollen, H. J. Kluge, R. B. Moore, T. Otto, L. Schweikhard, H. Stolzenberg, and U. Wiess, *Phys. Lett. A* **158**, 247 – 252 (1991).
11. G. Gräff, H. Kalinowsky, and J. Traut, *Z. Phys. A* **297**, 35–39 (1980).
12. M. König, G. Bollen, H. J. Kluge, T. Otto, and J. Szerypo, *Int. J. Mass Spectrom. Ion Processes* **142**, 95 – 116 (1995).
13. C. Weber, V.-V. Elomaa, R. Ferrer, C. Fröhlich, D. Ackermann, J. Äystö, G. Audi, L. Batist, K. Blaum, M. Block, A. Chaudhuri, M. Dworschak, S. Eliseev, T. Eronen, U. Hager, J. Hakala, F. Herfurth, F. P. Heßberger, S. Hofmann, A. Jokinen, A. Kankainen, H.-J. Kluge, K. Langanke, A. Martín, G. Martínez-Pinedo, M. Mazzocco, I. D. Moore, J. B. Neumayr, Y. N. Novikov, H. Penttilä, W. R. Plaß, A. V. Popov, S. Rahaman, T. Rauscher, C. Rauth, J. Rissanen, D. Rodríguez, A. Saastamoinen, C. Scheidenberger, L. Schweikhard, D. M. Seliverstov, T. Sonoda, F.-K. Thielemann, P. G. Thirolf, and G. K. Vorobjev, *Phys. Rev. C* **78**, 054310 (2008).

14. V.-V. Elomaa, T. Eronen, J. Hakala, A. Jokinen, A. Kankainen, I. Moore, S. Rahaman, J. Rissanen, C. Weber, and J. Äystö, *Nucl. Instrum. Methods Phys. Res. A* **612**, 97 – 102 (2009).
15. M. T. F. da Cruz, Y. Chan, R.-M. Larimer, K. T. Lesko, E. B. Norman, R. G. Stokstad, F. E. Wietfeldt, and I. Žilimen, *Phys. Rev. C* **46**, 1132–1135 (1992).
16. O. Forstner, H. Herndl, H. Oberhammer, H. Schatz, and B. A. Brown, *Phys. Rev. C* **64**, 045801 (2001).
17. G. Audi, A. H. Wapstra, and C. Thibault, *Nucl. Phys. A* **729**, 337 – 676 (2003).
18. A. Kankainen, L. Batist, S. Eliseev, V. Elomaa, T. Eronen, U. Hager, J. Hakala, A. Jokinen, I. Moore, Y. Novikov, H. Penttilä, K. Peräjärvi, A. Popov, S. Rahaman, S. Rinta-Antila, P. Ronkanen, A. Saastamoinen, D. Seliverstov, T. Sonoda, G. Vorobjev, and J. Äystö, *Eur. Phys. J. A* **29**, 271–280 (2006).
19. V.-V. Elomaa, G. K. Vorobjev, A. Kankainen, L. Batist, S. Eliseev, T. Eronen, J. Hakala, A. Jokinen, I. D. Moore, Y. N. Novikov, H. Penttilä, A. Popov, S. Rahaman, J. Rissanen, A. Saastamoinen, H. Schatz, D. M. Seliverstov, C. Weber, and J. Äystö, *Phys. Rev. Lett.* **102**, 252501 (2009).
20. V. Elomaa, T. Eronen, U. Hager, J. Hakala, A. Jokinen, A. Kankainen, I. Moore, S. Rahaman, J. Rissanen, V. Rubchenya, C. Weber, and J. Äystö, *Eur. Phys. J. A* **40**, 1–9 (2009).
21. A. Martín, D. Ackermann, G. Audi, K. Blaum, M. Block, A. Chaudhuri, Z. Di, S. Eliseev, R. Ferrer, D. Habs, F. Herfurth, F. Heßberger, S. Hofmann, H. Kluge, M. Mazzocco, M. Mukherjee, J. Neumayr, Y. Novikov, W. Plaß, S. Rahaman, C. Rauth, D. Rodríguez, C. Scheidenberger, L. Schweikhard, P. Thierolf, G. Vorobjev, and C. Weber, *Eur. Phys. J. A* **34**, 341–348 (2007).
22. E. Haettner, D. Ackermann, G. Audi, K. Blaum, M. Block, S. Eliseev, T. Fleckenstein, F. Herfurth, F. P. Heßberger, S. Hofmann, J. Ketelaer, J. Ketter, H.-J. Kluge, G. Marx, M. Mazzocco, Y. N. Novikov, W. R. Plaß, S. Rahaman, T. Rauscher, D. Rodríguez, H. Schatz, C. Scheidenberger, L. Schweikhard, B. Sun, P. G. Thirolf, G. Vorobjev, M. Wang, and C. Weber, *Phys. Rev. Lett.* **106**, 122501 (2011).
23. A. Plochocki, J. Zylicz, R. Kirchner, O. Klepper, E. Roeckl, P. Tidemand-Petersson, I. S. Grant, P. Misaelides, and W. D. Schmidt-Ott, *Phys. Lett. B* **106**, 285 – 288 (1981).
24. A. Kankainen, *Hyperfine Interact.* (2011), to be published.
25. A. Kankainen, V.-V. Elomaa, T. Eronen, D. Gorelov, J. Hakala, A. Jokinen, T. Kessler, V. S. Kolhinen, I. D. Moore, S. Rahaman, M. Reponen, J. Rissanen, A. Saastamoinen, C. Weber, and J. Äystö, *Phys. Rev. C* **82**, 034311 (2010).
26. N. Mărginean, D. Bucurescu, C. Rossi Alvarez, C. A. Ur, L. D. Skouras, L. P. Johnstone, D. Bazzacco, S. Lunardi, G. de Angelis, M. Axiotis, E. Farnea, A. Gadea, M. Ionescu-Bujor, A. Iordăchescu, W. Krolas, T. Kröll, S. M. Lenzi, T. Martinez, R. Mărginean, R. Menegazzo, D. R. Napoli, P. Pavan, M. De Poli, B. Quintana, C. Rusu, P. Spolaore, and J. Wrzesinski, *Phys. Rev. C* **67**, 061301 (2003).
27. A. Kankainen, V.-V. Elomaa, L. Batist, S. Eliseev, T. Eronen, U. Hager, J. Hakala, A. Jokinen, I. D. Moore, Y. N. Novikov, H. Penttilä, A. Popov, S. Rahaman, S. Rinta-Antila, J. Rissanen, A. Saastamoinen, D. M. Seliverstov, T. Sonoda, G. Vorobjev, C. Weber, and J. Äystö, *Phys. Rev. Lett.* **101**, 142503 (2008).
28. I. Mukha, E. Roeckl, L. Batist, A. Blazhev, J. Döring, H. Grawe, L. Grigorenko, M. Huyse, Z. Janas, R. Kirchner, M. La Commara, C. Mazzocchi, S. L. Tabor, and P. Van Duppen, *Nature* **439**, 298–302 (2006).
29. I. Mukha, E. Roeckl, J. Döring, L. Batist, A. Blazhev, H. Grawe, C. R. Hoffman, M. Huyse, Z. Janas, R. Kirchner, M. La Commara, C. Mazzocchi, C. Plettner, S. L. Tabor, P. V. Duppen, and M. Wiedeking, *Phys. Rev. Lett.* **95**, 022501 (2005).
30. G. Audi, O. Bersillon, J. Blachot, and A. H. Wapstra, *Nucl. Phys. A* **729**, 3 – 128 (2003).
31. M. Reponen, T. Kessler, I. Moore, S. Rothe, and J. Äystö, *Eur. Phys. J. A* **42**, 509–515 (2009).

Mass Measurements of Proton-rich Nuclides at the Cooler Storage Ring at IMP

Y. H. Zhang^{*}, X. L. Tu^{*,†}, H. S. Xu^{*}, M. Wang^{*}, Yu. A. Litvinov^{**,‡},
Y. Sun^{§,*}, H. Schatz[¶], X. H. Zhou^{*}, Y. J. Yuan^{*}, J. W. Xia^{*}, G. Audi^{||},
K. Blaum^{††}, C. M. Du^{*,†}, P. Geng^{*,†}, Z. G. Hu^{*}, W. X. Huang^{*}, S. L. Jin^{*,†},
L. X. Liu^{*,†}, Y. Liu^{*}, X. Ma^{*}, R. S. Mao^{*}, B. Mei^{*}, P. Shuai^{‡‡}, Z. Y. Sun^{*},
H. Suzuki^{§§}, S. W. Tang^{*,†}, J. S. Wang^{*}, S. T. Wang^{*,†}, G. Q. Xiao^{*},
X. Xu^{*,†}, T. Yamaguchi^{¶¶}, Y. Yamaguchi^{***}, X. L. Yan^{*}, J. C. Yang^{*},
R. P. Ye^{*,†}, Y. D. Zang^{*,†}, H. W. Zhao^{*}, T. C. Zhao^{*}, X. Y. Zhang^{*} and
W. L. Zhan^{*}

^{*}*Institute of Modern Physics, Chinese Academy of Sciences, Lanzhou 730000, China*

[†]*Graduate University of Chinese Academy of Sciences, Beijing, 100049, China*

^{**}*Max-Planck-Institut für Kernphysik, Saupfercheckweg, D-69117 Heidelberg, Germany*

[‡]*GSI Helmholtzzentrum für Schwerionenforschung, Planckstraße 1, 64291 Darmstadt, Germany*

[§]*Department of Physics, Shanghai Jiao Tong University, Shanghai 200240, China*

[¶]*Department of Physics and Astronomy, National Superconducting Cyclotron Laboratory and the Joint Institute for Nuclear Astrophysics, Michigan State University, East Lansing, Michigan 48824, USA*

^{||}*CSNSM-IN2P3-CNRS, Université de Paris Sud, F-91405 Orsay, France*

^{††}*Max-Planck-Institut für Kernphysik, Saupfercheckweg 1, D-69117 Heidelberg, Germany*

^{‡‡}*Department of Modern Physics, University of Science and Technology of China, Hefei 230026, China*

^{§§}*Institute of Physics, University of Tsukuba, Ibaraki 305-8571, Japan*

^{¶¶}*Department of Physics, Saitama University, Saitama 338-8570, Japan*

^{***}*RIKEN Nishina Center, RIKEN, Saitama 351-0198, Japan*

Abstract.

Recent results and progress of mass measurements of proton-rich nuclei using isochronous mass spectrometry (IMS) are reported. The nuclei under investigation were produced via fragmentation of relativistic energy heavy ions of ^{78}Kr and ^{58}Ni . After in-flight separation by the fragment separator RIBLL-2, the nuclei were injected and stored in the experimental storage ring CSRe, and their masses were determined from measurements of the revolution times. The impact of these measurements on the stellar nucleosynthesis in the rp-process is discussed.

Keywords: Mass spectrometry, storage rings, proton-rich nuclides

PACS: 21.10.Dr, 26.30.Ca, 29.20.db

INTRUDUCTION

Nuclear mass is a fundamental property of the nucleus. The complex interplay of strong, weak and electromagnetic interactions in a nucleus contributes to the difference between its mass and the sum of the masses of its constituent nucleons. Precise and systematic measurements of nuclear masses not only provide information on nuclear structure, but also find their important applications in nuclear astrophysics [1, 2]. In recent years, the

majority of new atomic masses have been obtained from Penning trap and storage ring mass spectrometry [3]. Recent commissioning of the Cooler Storage Ring at the Heavy Ion Research Facility in Lanzhou (HIRFL-CSR) [4] has allowed us for direct mass measurements at the Institute of Modern Physics in Lanzhou (IMP), Chinese Academy of Sciences. Great efforts have been made for a realization of the isochronous mass spectrometry in IMP. Proton-rich nuclei from Ti through Kr have been produced via fragmentation of the energetic beams of ^{78}Kr and ^{58}Ni . 22 masses of $T_z = -1/2, -1, -3/2$ nuclides have been measured among which half of the mass values are determined for the first time, providing fundamental data for investigating the nucleosynthesis in the astrophysical rp-process.

EXPERIMENT AND DATA ANALYSIS

The experiments were performed at the HIRFL-CSR accelerator complex with the combination of an in-flight fragment separator RIBLL-2 and the experimental storage ring CSRe in IMP; the layout of experimental facilities was shown in Fig. 1 of Ref. [4]. In order to fulfill an isochronous condition for the nuclides of interest (^{65}As and ^{47}Mn with ^{78}Kr and ^{58}Ni beams, respectively), the $^{78}\text{Kr}^{28+}$ ($^{58}\text{Ni}^{19+}$) beams of 483.4 MeV/u (463.36 MeV/u) were accelerated by the main ring CSRm and impinged on a ~ 15 mm beryllium target placed at the entrance of RIBLL-2. The exotic nuclei were produced by projectile fragmentation of the energetic beams and emerged from the target predominantly as bare ions. After in-flight separation of the fragments in RIBLL-2, the cocktail beam of exotic nuclei within an $B\rho$ -acceptance of $\sim \pm 0.2\%$ was injected into the experimental storage ring.

Setting the CSRe in an isochronous mode [5], the revolution times, T , of various stored ions in CSRe were measured using a timing detector [6] equipped with a $19 \mu\text{g}/\text{cm}^2$ carbon foil of 40 mm in diameter. The time resolution of the detector was about 50 ps, and the detection efficiency varied from 20% to 70% depending on the ion type and the number of the ions stored. The signals from the detector were sampled with a digital oscilloscope Tektronix DPO 71254 at a sampling rate of 50 GHz. The recording time was 200 μs for each injection corresponding to ~ 320 revolutions. Figures 1 presents the revolution time spectra for a part of the $T_z = -1/2, -1, -3/2$ nuclei; the insert in Fig. 1(a) shows the revolution time spectrum zoomed in on the well-resolved peaks of the ground and $E_x = 3173.3(1.0)$ keV isomeric states of ^{53}Co . The nuclides with known masses [7] were used to fit m/q versus T employing a second order polynomial. The unknown masses were obtained by either extrapolation (in the case of ^{78}Kr beam, see Fig. 1(a)) or interpolation (in the case of ^{58}Ni , see Fig. 1(b)).

RESULTS AND DISCUSSION

A summary of the mass measurements in CSRe is shown in Fig. 2. From the experiment using ^{78}Kr beam we have obtained the mass excesses of $ME(^{63}\text{Ge}) = -46921(37)$ keV, $ME(^{65}\text{As}) = -46937(85)$ keV, $ME(^{67}\text{Se}) = -46580(67)$ keV, and $ME(^{71}\text{Kr}) = -46320(141)$ keV, respectively. These new mass excess values are compared in Fig. 2(a)

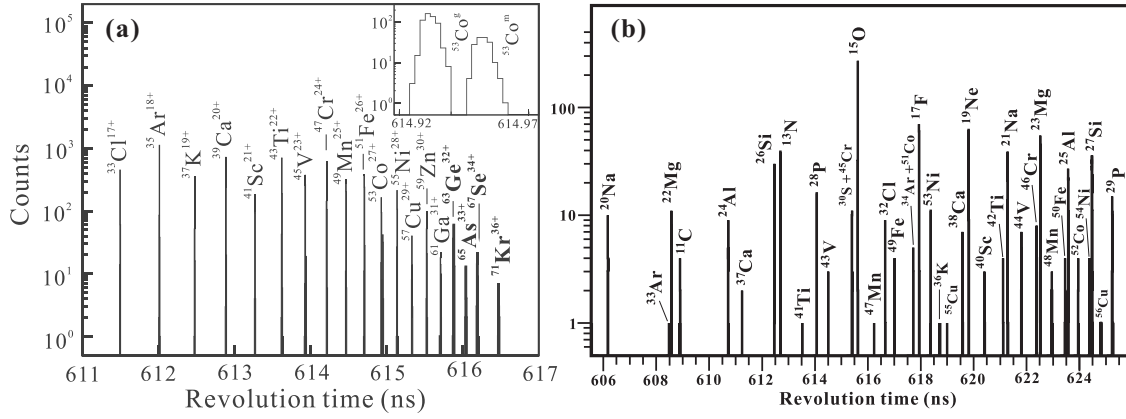


FIGURE 1. (a) The revolution time spectrum zoomed in on a subset of the $T_z = -1/2$ nuclides obtained using ^{78}Kr beam. (b) The revolution time spectrum for the $T_z = -1/2, -1, -3/2$ nuclides obtained using ^{58}Ni beam

with those calculated by the CDE method [8] and those from the AME03 [7]. Good agreement between CSRe and CDE is found for ^{63}Ge , ^{65}As , and ^{67}Se , which confirms the predictive power of the CDE method in this mass region and shows that at least for these three nuclei the method is reliable. In the case of ^{71}Kr , the CDE value differs by more than one standard deviation from our result. The disagreement of the CDE value with ours for ^{71}Kr may hint at a structure change along the $N = Z$ line at $N = Z = 35$, and the deformation effect and shape-coexistence are the factors that future CDE calculations may need to consider.

By using the precise mass excess of $ME(^{64}\text{Ge}) = 54315.7(3.8)$ keV [9], a negative proton separation energy of $S_p(^{65}\text{As}) = -90(85)$ keV is deduced, confirming that ^{65}As is slightly unbound against proton emission. Particularly, the precise $S_p(^{65}\text{As})$ value allowed us to determine the degree to which ^{64}Ge is an rp -process waiting point.

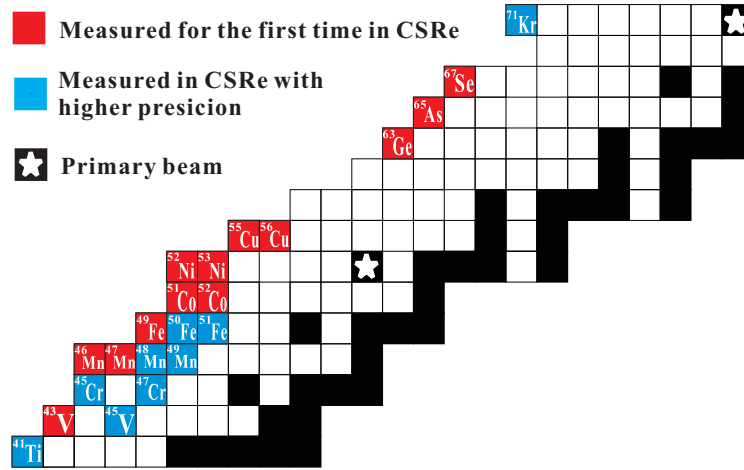


FIGURE 2. A summary of atomic masses measured in CSRe.

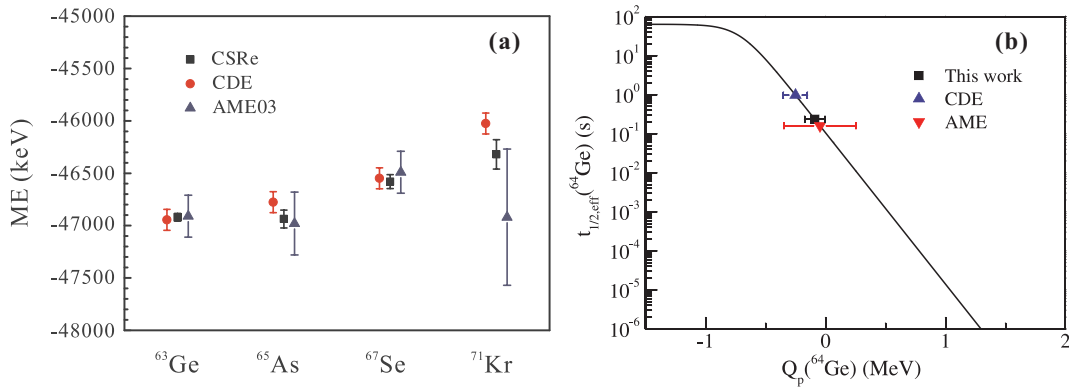


FIGURE 3. (a) Comparison of measured mass excesses with those of CDE calculations [8] and AME03 [7]. (b) The effective stellar half-life of ^{64}Se as a function of $Q_p(^{64}\text{Ge})$ using the ^{65}As masses of this work, AME03, and CDE calculation.

Fig. 2(b) shows the effective stellar half-life [10] of ^{64}Ge as a function of $Q_p(^{64}\text{Ge})$, where typical conditions for x-ray burst models were used (temperature $T=1.3$ GK, density $\rho = 10^6 \text{g/cm}^3$, solar hydrogen abundance, $\langle p\gamma \rangle$ rates taken from Ref. [10]), and the photodisintegration of ^{66}Se is assumed to be negligible [10]. With the present uncertainty in $Q_p(^{64}\text{Ge})$, the effective stellar half-life of ^{64}Ge is between 0.1 and 0.5 s, indicating that the rp process is not slowed down at ^{64}Ge . Furthermore, the realistic x-ray burst model calculations show that [11] varying the $S_p(^{65}\text{As})$ value within 2σ provides essentially identical light curves, and 89-90% of the reaction flow passes through ^{64}Ge via proton capture indicating that ^{64}Ge is not a significant rp-process waiting point.

In the experiment using ^{58}Ni beam, the masses of $T_z = -3/2$ nuclei from ^{41}Ti through ^{55}Cu have been measured. Although the data of this experiment is under analysis, we may expect that the experimental mass values for these nuclei allow to test the isobaric analog multiplet equation in the $1f_{7/2}$ shell. Furthermore the precise masses of ^{43}V and ^{47}Mn are particularly important for the reliable theoretical calculations of nucleosynthesis of in the Type I x-ray burst models [12].

REFERENCES

1. K. Blaum, Phys. Rep. **425** (2006) 1.
2. D. Lunney, *et al.* Rev. Mod. Phys. **75** (2003) 1021.
3. Yu. A. Litvinov, *et al.*, Proc. of Science (NIC XI) (2011) 073.
4. W. L. Zhan, *et al.*, Nucl. Phys. **A 834**, 694c (2006).
5. M. Hausmann *et al.*, Nucl. Instr. Meth. **A 446**, 569 (2000).
6. B. Mei *et al.*, Nucl. Instr. Meth. **A 624**, 109 (2010).
7. G. Audi *et al.*, Nucl. Phys. **A729**, 337 (2003).
8. B. A. Brown, *et al.*, Phys. Rev. C **65**, 045802 (2002).
9. J. A. Clark *et al.*, Phys. Rev. C **75**, 032801(R) (2007).
10. H. Schatz *et al.*, Phys. Rep. **294**, 167 (1998).
11. X. L. Tu, *et al.*, Phys. Rev. Lett. **106** (2011) 112501.
12. A. Parikh, *et al.*, Phys. Rev. C **79**, 045802 (2009).

Proton-Rich Sulphur and Nucleosynthesis in Classical Novae

A. A. Chen^a, K. Setoodehnia^a, J. Chen^a, J. A. Clark^b, C. M. Deibel^{b,c}, S. D. Geraedts^a, D. Kahl^d, P. D. Parker^e, D. Seiler^f, and C. Wrede^g

^a*Department of Physics and Astronomy, McMaster University, Hamilton, ON L8S 4M1, Canada*

^b*Physics Division, Argonne National Laboratory, Argonne, IL 60439, USA*

^c*Joint Institute for Nuclear Astrophysics, Michigan State University, East Lansing, MI 48824, USA*

^d*Center for Nuclear Study, University of Tokyo, RIKEN branch, Wako, Saitama 351-0198, Japan*

^e*Wright Nuclear Structure Laboratory, Yale University, New Haven, CT 06520, USA*

^f*Physik Department E12, Technische Universität München, D-85748 Garching, Germany*

^g*Department of Physics, University of Washington, Seattle, WA 98195, USA*

Abstract. The structure of proton-unbound states in ^{30}S and ^{31}S is important for determining the $^{29}\text{P}(p,\gamma)^{30}\text{S}$ and $^{30}\text{P}(p,\gamma)^{31}\text{S}$ reaction rates, which influence explosive hydrogen burning in classical novae. The former reaction rate in this temperature regime had been previously predicted to be dominated by two low-lying, unobserved, $J^\pi = 3^+$ and 2^+ resonances in ^{30}S . To search for evidence for these levels, the structure of ^{30}S was studied using the $^{32}\text{S}(p,t)^{30}\text{S}$ reaction with a magnetic spectrograph. We provide an update on the status of the ongoing analysis and some preliminary results.

Keywords: nucleosynthesis, reaction rates, proton-rich sulphur isotopes, classical novae

PACS: 26.30.Ca, 26.50.+x, 27.30.+t, 29.30.Ep, 25.60.Je

INTRODUCTION

The $^{29}\text{P}(p,\gamma)^{30}\text{S}$ reaction rate plays a role in classical novae, which are energetic stellar explosions powered by thermonuclear runaway in close interacting binary systems. The temperature characteristic of explosive hydrogen burning in novae covers about 0.1–0.4 GK. An interesting area of inquiry in this context is the identification of presolar grains of potential nova origin [1,2]. In particular, silicon isotopic ratios (i.e., $^{29}\text{Si}/^{28}\text{Si}$ and $^{30}\text{Si}/^{28}\text{Si}$) may help determine the main nucleosynthesis flow followed by the thermonuclear runaway during the burst [3]. To improve the prediction of silicon isotopic abundances in nova ejecta, it is important to know the rates of the reactions that influence silicon production and destruction. One such reaction is $^{29}\text{P}(p,\gamma)^{30}\text{S}$, which was shown to affect strongly the abundance of silicon isotopes in nova nucleosynthesis [4].

The rate depends sensitively on the level parameters of proton-unbound states of ^{30}S , and in particular on two predicted resonances in the 4.7 – 4.8 MeV region of excitation energy [5] (see Fig. 1). While one of these two states was found by the study of Ref. [6], no evidence for the second, higher-energy resonance was detected in past measurements. We have searched for evidence of these states by populating them

with the $^{32}\text{S}(p,t)^{30}\text{S}$ reaction, and in this contribution we report on the status of the ongoing analysis and preliminary results.

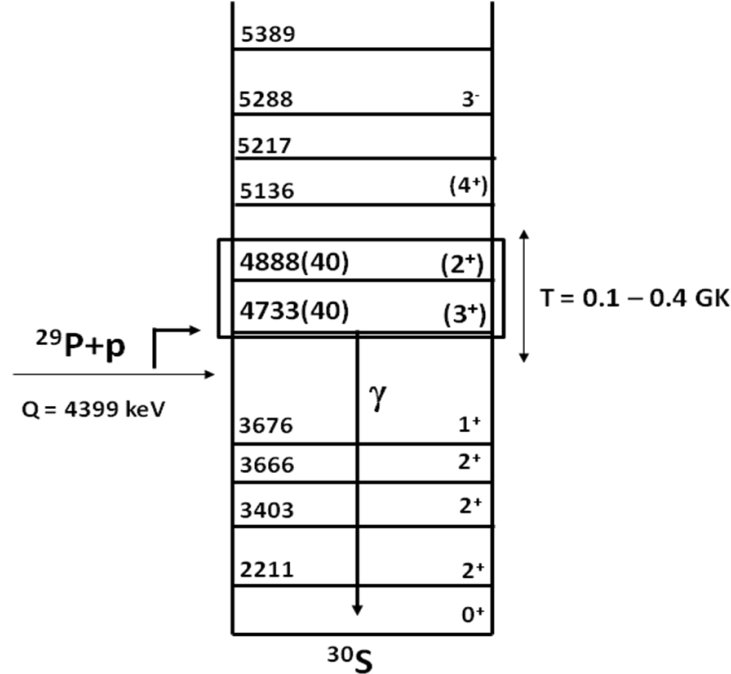


FIGURE 1. Level scheme of ^{30}S . The two important proton-unbound levels are shown in the box. The energies of these two states are the predicted values from Ref. [5]. The double-arrow covers the range of excitation energies relevant for classical nova explosions.

EXPERIMENT AND RESULTS

The experiment was carried out at the Wright Nuclear Structure Laboratory at Yale University. The proton beam had an energy of 34.5 MeV and intensities of about 90 enA. For the first phase of the experiment, reported in Ref. [7], the target was 249 $\mu\text{g}/\text{cm}^2$ of CdS evaporated onto a 20 $\mu\text{g}/\text{cm}^2$ natural carbon foil. The reaction ejectiles were momentum analyzed with an Enge split-pole magnetic spectrograph. The tritons were focused at the spectrograph's focal plane, and their momenta and energy losses (ΔE) measured with a position-sensitive ionization chamber. Those that passed through this detector deposited their residual energy (E) in a plastic scintillator. This first phase was carried out with a magnetic field strength of 10 kG for $\theta_{\text{lab}} = 10, 20, 22,$ and 62 degrees.

The tritons were selected with software gates in histograms of ΔE and E vs. momentum, and energy spectra of were generated for each angle. The background from (p,t) reactions on the Cd and carbon in the CdS target was determined with a 200- $\mu\text{g}/\text{cm}^2$ Cd foil on a 20 $\mu\text{g}/\text{cm}^2$ backing of natural carbon, along with a 75 $\mu\text{g}/\text{cm}^2$ 95.6% isotopically enriched ^{13}C target. The main contaminant peak is from the

$^{12}\text{C}(p,t)^{10}\text{C}(\text{g.s.})$ reaction, with its peak location away from the region of interest. Triton peaks corresponding to ^{30}S states were identified unambiguously through kinematic analysis.

The results from the first phase of the experiment, including the detection of a new state in the energy region of interest and its implications for the $^{29}\text{P}(p,\gamma)^{30}\text{S}$ reaction rate, were presented in Ref. [7] and will not be repeated here. This phase focused mainly on determining the excitation energies of the two important states to relatively high precision. In the second phase of the experiment, additional data were taken with a target of ^{32}S ($\sim 10 \mu\text{g}/\text{cm}^2$) implanted into an isotopically pure ^{12}C foil, which effectively removes background from the Cadmium, ^{13}C , and other stable sulphur isotopes in the original target. The improvement in the background level can be seen in the sample spectra shown in Figure 2.

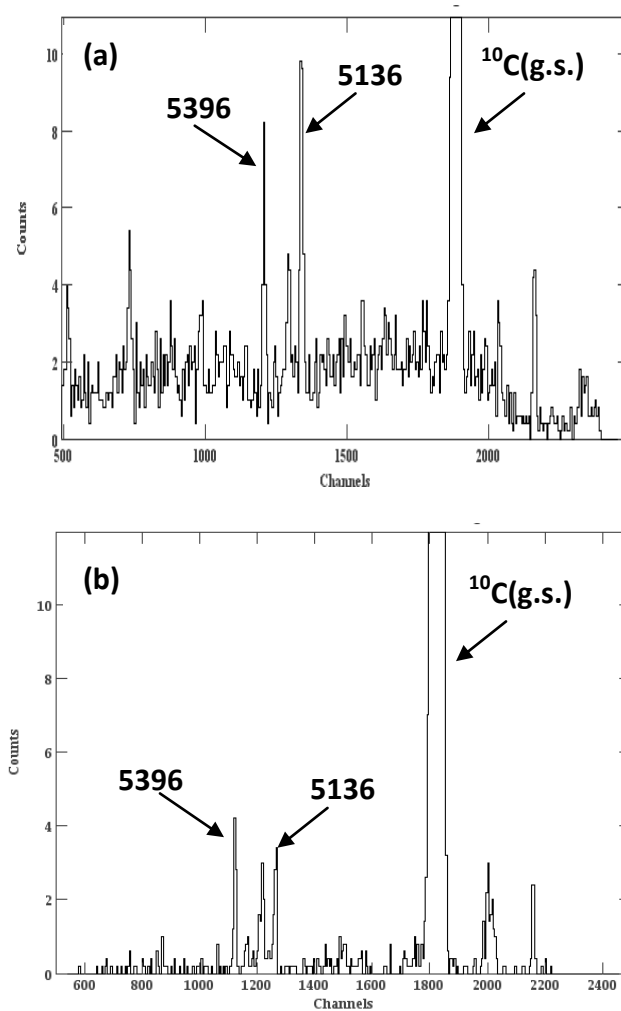


FIGURE 2. (a) Triton spectrum from $^{32}\text{S}(p,t)^{30}\text{S}$ taken with the CdS target and a carbon backing; (b) same as (a), but using a target of ^{32}S implanted into an isotopically pure ^{12}C foil. Some prominent peaks are labeled with energies in keV.

Furthermore, data were taken at additional angles during the second phase, in order to extract or constrain spin and parity assignments for the observed levels through a Distorted Wave Born Analysis (DWBA) of the triton angular distributions. This analysis so far supports the tentative assignments of 3^+ and 2^+ to the two most important resonances for the $^{29}\text{P}(p,\gamma)^{30}\text{S}$ reaction rate.

These results will be combined with further analysis of the experiment described in Ref. [8] on a measurement of the $^{28}\text{Si}(^3\text{He},n\gamma)^{30}\text{S}$ reaction, in which de-excitation γ -rays from the states of interest were measured. This will result in a more comprehensive level scheme of ^{30}S above the proton threshold, and a new thermonuclear $^{29}\text{P}(p,\gamma)^{30}\text{S}$ reaction rate from the Monte Carlo approach presented in Ref. [9]. A manuscript on this remaining work is currently in preparation [10].

ACKNOWLEDGMENTS

We thank the WNSL accelerator staff and acknowledge funding support from the Natural Sciences and Engineering Research Council of Canada; the US Department of Energy under Grants DE-FG02-91ER40609, DE-AC02-06CH11357, and DE-FG02-97ER41020; and the DFG cluster of excellence “Origin and Structure of the Universe.”

REFERENCES

1. S. Amari, X. Gao, L. R. Nittler, E. Zinner, J. José, M. Hernanz, and R. S. Lewis, *Astrophys. J.* **551**, 1065 (2001).
2. L. R. Nittler and P. Hoppe, *Astrophys. J.* **631**, L89 (2005).
3. J. José, M. Hernanz, S. Amari, K. Lodders, and E. Zinner, *Astrophys. J.* **612**, 414 (2004).
4. C. Iliadis, A. E. Champagne, J. José, S. Starrfield, and P. Tupper, *Astrophys. J. Suppl. Ser.* **142**, 105 (2002).
5. C. Iliadis, J. M. D’Auria, S. Starrfield, W. J. Thompson, and M. Wiescher, *Astrophys. J. Suppl. Ser.* **134**, 151 (2001).
6. D. W. Bardayan *et al.*, *Phys. Rev. C* **76**, 045803 (2007).
7. K. Setoodehnia *et al.*, *Phys. Rev. C* **82**, 022801(R) (2010).
8. K. Setoodehnia *et al.*, *Phys. Rev. C* **83**, 018883 (2011).
9. R. Longland *et al.*, *Nucl. Phys. A* **841**, 1 (2010).
10. K. Setoodehnia *et al.*, in preparation.

Exotic nuclear studies around and below $A=100$

B.S. Nara Singh^{*}, R. Wadsworth^{*}, P. Boutachkov[†], A. Blazhev^{**}, Z. Liu[‡],
H. Grawe[†], T.S. Brock^{*}, N. Braun^{**}, M. Górska[†], S. Pietri[†], D. Rudolph[§],
C. Domingo-Pardo[†], S.J. Steer[¶], A. Ataç^{||}, L. Bettermann^{**}, L. Cáceres[†],
K. Eppinger^{††}, T. Engert[†], T. Faestermann^{††}, F. Farinon[†], F. Finke^{**},
K. Geibel^{**}, J. Gerl[†], R. Gernhäuser^{††}, N. Goel[†], A. Gottardo[‡],
J. Grębosz^{‡‡}, C. Hinke^{††}, R. Hoischen^{§,†}, G. Ilie^{**}, H. Iwasaki^{**}, J. Jolie^{**},
A. Kaşkaş^{||}, I. Kojouharov[†], R. Krücken^{††}, N. Kurz[†], E. Merchán[†],
C. Nociforo[†], J. Nyberg^{§§}, M. Pfützner^{¶¶}, A. Prochazka[†], Zs. Podolyák^{¶¶},
P.H. Regan[¶], P. Reiter^{**}, S. Rinta-Antila^{***}, C. Scholl^{**}, H. Schaffner[†],
P.-A. Söderström^{§§}, N. Warr^{**}, H. Weick[†], H.-J. Wollersheim[†],
P.J. Woods[‡], F. Nowacki^{†††} and K. Sieja^{†††}

^{*}Department of Physics, University of York, Heslington, York, YO10 5DD, UK

[†]GSI Helmholtzzentrum für Schwerionenforschung, D-64291 Darmstadt, Germany

^{**}IKP, Universität Köln, D-50937 Köln, Germany

[‡]School of Physics and Astronomy, University of Edinburgh, Edinburgh, UK

[§]Department of Physics, Lund University, S-22100 Lund, Sweden

[¶]Department of Physics, University of Surrey, Guildford, GU2 7XH, UK

^{||}Department of Physics, Ankara University, 06100 Tandoğan, Ankara, Turkey

^{††}Physik Department E12, Technische Universität München, D-85748 Garching, Germany

^{‡‡}The Institute of Nuclear Physics PAN, Kraków, Poland

^{§§}Department of Physics and Astronomy, Uppsala University, SE-75120 Uppsala, Sweden

^{¶¶}Faculty of Physics, University of Warsaw, PL-00-681 Warsaw, Poland

^{***}Department of Physics, Oliver Lodge Laboratory, University of Liverpool, Liverpool, UK

^{†††}IPHC, IN2P3-CNRS et Université de Strasbourg, F-67037 Strasbourg, France

Abstract. A RISING experiment with an aim to study exotic Cd nuclei was carried out at GSI-FRS facility. Some preliminary results from this experiment are presented here. In particular, the β decay of ^{96}Cd to ^{96}Ag revealed the existence of a high spin isomer predicted a few decades ago. In this context, the structures of both these nuclei are discussed. Shell model calculations using the Gross-Frenkel interaction are used to interpret the results.

Keywords: Palladium, Silver, Cadmium nuclei with mass number 94, 96, gamma-ray spectroscopy, iso-scalar neutron-proton interaction, high spin isomer, isomer decay, beta decay

PACS: PACS 21.60.Cs, 23.20.Lv, 27.60.+j, 23.35.+g

INTRODUCTION

Self conjugate nuclear studies provide data needed for different fields of research including nuclear structure, nuclear astrophysics and the standard model of particle physics [1, 2]. As mass increases these nuclei reside in the land-scape around the proton drip-line and exhibit exotic decays that directly probe the force seen by the nucleons in the nucleus. In particular, the Sn region is experimentally known to be abundant with ‘spin-gap’ isomers. The ‘spin-gap’ isomerism is one of the expected manifestations of

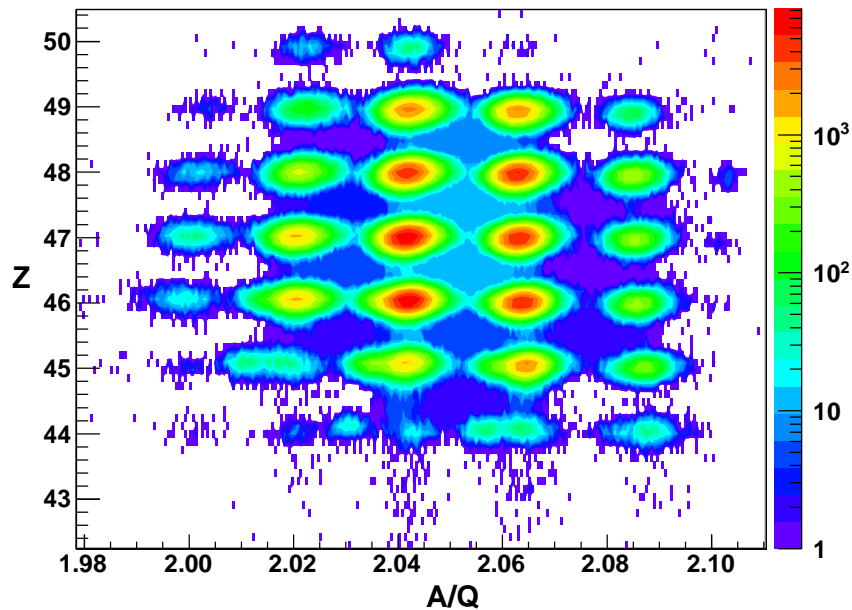


FIGURE 1. (Color online) Z versus A/Q identification plot. A clean separation enabled the study of nuclei produced with very low cross sections.

the effective proton-neutron interaction [3]. Long half-lives allow a competition between the decays via the proton, β -delayed proton, β , and isomeric γ rays, which serves as a highly sensitive probe to critically test the theoretical models. $N \approx Z \approx 50$ nuclei have been of special interest due to the purity of the wave-functions and a possibility to describe their properties using only a few orbitals of which the $g_{9/2}$ shell plays a dominant role [1, 4, 5, 6, 7]. Such data often guide theories in adapting the model spaces. Indeed such a situation was found while interpreting the data of ^{94}Pd and ^{96}Ag from our experiment, where the typically used model-spaces needed extension to reproduce the observed structural features [6, 8]. In spite of such great interest, the progress in this field has been hindered due to the difficulty in producing the nuclei and populating them in the isomeric states.

The present work utilizes data from an experiment using the set-up at the GSI that has played a major role in recent years in the field of isomer spectroscopy. This is due to the production and unique identification capabilities of the device for the isomers. Results on ^{94}Pd , ^{96}Ag and ^{98}Cd from our data have already been reported together with the shell model calculations [6, 7, 8]. Here, we present initial results on the β decay of a high spin isomer in ^{96}Cd to the (15^+) isomer in ^{96}Ag and discuss them in relation to the work presented in Refs. [6, 7, 8].

EXPERIMENT

The nuclei were produced via the fragmentation of an 850 MeV/u ^{124}Xe primary beam from SIS-18 synchrotron on a ^9Be target of 4 g/cm^2 at the entrance of the FRS sepa-

rator [9] at GSI. The fragments were transported to the focal plane of the device and implanted into an 'active stopper' (AS) that provided the information on the implantation position [10]. The AS also detected the particle decays from the fragments and was surrounded by the RISING array of 15 Ge EUROBALL cluster detectors, each cluster with 7 individual crystals, for the detection of γ rays [11, 12]. Unique identification for the fragments was possible due to their separation using the $B\rho$ - ΔE - $B\rho$ technique followed by time of flight and energy loss measurements. The latter provide A/Q , and Z of the fragments, respectively that are plotted in the identification plot shown in Fig. 1. Here, A , Q and Z are the mass, charge state and the atomic number of the fragments. It should be pointed out that the produced fragments were fully stripped of their electrons due to their relativistic energies, i.e. $Q = Z$. The active stopper consisted of nine double sided silicon strip detectors (DSSSD) that were arranged in 3 rows perpendicular to the beam direction and each row with 3 columns. Similar to Ref. [13], each DSSSD of 1 mm thickness and $5 \times 5 \text{ cm}^2$ area had 16 X- and 16 Y-strips. The primary beam and FRS settings were optimized so as to stop the Cd nuclei in the center of the AS. The geometry of the AS allowed an optimal solid angular coverage for the decays from the nuclei implanted in its center. A timing signal from the focal plane scintillator corresponded to the instance of fragment implantation, i.e. the 'implantation trigger' [11, 14] and was used for the time correlations with the decays. The AS timing signal, which we refer to as 'decay trigger', served as the start of a decay event. A software code, r2d2 [15], was developed and used by us to sort the data for decay spectroscopy involving spatial and temporal correlations between the implanted nuclei and the β and β delayed proton particles and γ rays following their decay. Subsequently, an analysis of the final spectra was done in the ROOT software package [16]. Our analysis was restricted to the data with clean events in the FRS diagnostic detectors [9].

RESULTS AND DISCUSSION

From our recent data analysis, a few isomers were found including those of 'spin-gap' in nature. We present here results on ^{96}Ag and ^{96}Cd from isomeric γ and β delayed γ decays, respectively.

^{96}Ag

Fig. 2 shows γ -ray spectrum observed between 75 ns to 90 μs following the implantation of ^{96}Ag nuclei into the AS. Due to the unique identification of the nucleus, the delayed γ spectrum is very clean and contains the transitions belonging only to the isomeric decays in ^{96}Ag . The intense 470 and 668 keV transitions were already observed in Ref. [17]. All the other transitions are new. For a largely extended level scheme with three new isomers from the present work using γ - γ coincidence and half-life analysis, we refer to Ref. [8]. In the inset of Fig. 2, we only show a partial level scheme together with that from shell model calculations using the Gross-Frenkel (GF) empirical interaction and $g_{9/2}$, $p_{1/2}$ model space [18]. The scheme is relevant for the interpretation of the β decay of ^{96}Cd which populates the (15^+) isomer in ^{96}Ag with a half-life of 1.56(3) μs

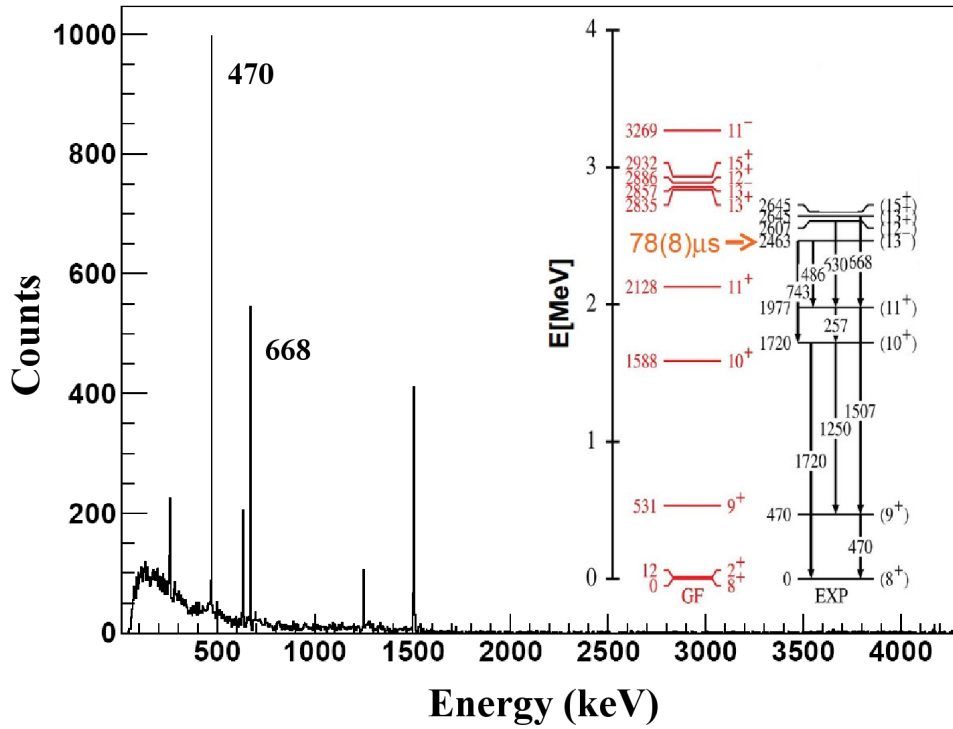


FIGURE 2. γ -ray spectra associated with isomeric decays in ^{96}Ag . The two marked transitions at energies of 470 and 668 keV were also observed in Ref. [17]. All the other transitions are new. The γ times are restricted to be between 75 ns to 90 μs following the implantation of ^{96}Ag . Calculated and partial experimental level schemes are shown in the inset. As discussed in the text, our data shows the existence of the 16^+ isomer in ^{96}Cd which feeds the 15^+ isomer with half-life of 1.56(3) μs in ^{96}Ag .

(see below). The spin and parity assignments for this state are discussed in Ref. [8]. Although the calculations reproduce the observed level ordering, the half-life and γ decay energy for one of the new isomers (13^-) indicated the presence of $E3$ and $M2$ isomeric transitions. In order to calculate the $B(E3)$ and $B(M2)$ transition probabilities and interpret this result, an extension of the model space e.g., inclusion of $p_{3/2}, f_{5/2}$ orbitals was needed [8].

^{96}Cd

Figs. 3a,b (Left) show the γ -ray spectra corresponding to the decay of ^{96}Cd and all the other nuclei those implanted into the central DSSSD [19]. The Si energies associated with the decay events are selected to be in the range of between 60 keV and 600 keV, just above the noise threshold and below the maximum expected energy loss for most of the β particles. In order to select only the isomeric decays, γ times were selected to fall between 200 ns to 4 μs following the decay trigger. Furthermore, a time difference of 1 s between the implantation and decay triggers, which we refer to as the decay correlation time, is considered. The 470, 668, 1506 keV γ rays can be seen in this delayed

spectrum. These lines disappear when the γ times are restricted to fall between 0 to 200 ns. Therefore, we conclude that the entire intensities come from the delayed γ rays. This strongly suggests that the γ decays are those which follow from the decay of the (15^+) isomer in ^{96}Ag [8], with a half-life of $1.56(3) \mu\text{s}$, populated via the β decay of ^{96}Cd . From the β -decay selection rules, the 0^+ ground state in ^{96}Cd can be excluded, but the long predicted 16^+ $E6$ 'spin-gap' isomer [20] is the only possible isomer to decay to the 15^+ high spin isomer in ^{96}Ag . The combined β decay time distribution when the three γ decays are simultaneously selected indicates a half-life of 0.3 s for the isomer in ^{96}Cd , which is similar to the predicted value for the 16^+ isomer [20]. Within the uncertainties, this half-life is similar to that observed in Ref. [21] for the β decay of ^{96}Cd . Furthermore, Fig. 3 (Left)b, which is same as fig. 3 (Left)a except that it corresponds to all the nuclei other than ^{96}Cd , does not have any peak corresponding to the decays of levels below the (15^+) isomer in ^{96}Ag . Clearly, this shows that there is no contribution from any other nuclear background produced in this experiment. Therefore, we conclude that the decay γ intensities essentially originate from the β decay of the 16^+ isomer in ^{96}Cd .

Figure 3 (Right) shows our shell model calculations on the level structure of ^{96}Cd using Gross-Frankel interaction and $g_{9/2}, p_{1/2}$ model space, with (column 1) and without (column 2) isoscalar neutron-proton, $T = 0$, np , interaction. As can be clearly seen, the $E6$ 'spin-gap' only appears when the $T = 0$ component is present, emphasizing its important role on the nuclear phenomenon. The very existence of the 16^+ isomer, found in this work, provides experimental confirmation of the important role of this component in the ^{100}Sn region. We note that this is only the second such experimental example apart from the recent case of ^{92}Pd [22]. On the other hand, we believe our result is more convincing and the first example which highlights the importance of the iso-scalar np interaction at high spins.

The analysis is still under progress. At this point it is clear that the statistics are too low for example to obtain the Gamow-Teller strength, $B(GT)$ distributions for the decay of 16^+ isomer in ^{96}Cd and to look for possible beta delayed proton decays. In future we aim to obtain further data for this purpose.

ACKNOWLEDGMENTS

This work has been supported by the UK STFC, the German BMBF under Contracts No. 06KY205I, No. 06KY9136I, and No. 06MT9156, the Swedish Research Council, and the DFG cluster of excellence Origin and Structure of the Universe.

REFERENCES

1. H. Grawe *et al.*, Eur. Phys. J A 27, S01, 2006, pp. 257–267.
2. H. Schatz *et al.*, Phys. Rep. 294, 1998, 167–263.
3. S. Zerguine and P. Van Isacker, Phys. Rev. C, 83, 2011, 064314-1–12 and the references therein.
4. A. Blazhev *et al.*, Phys. Rev. C, 69, 2004, 064304-1–8.
5. M. Gorska *et al.*, Phys. Rev. Lett., 79, 1997, 2415–2418.
6. T. S. Brock *et al.*, Phys. Rev. C, 82, (R), 2010, 061309-1–5.
7. A. Blazhev *et al.*, GSI Scientific Report, 2009, 206, J. Phys.: Conf. Ser. 205, 2010, 012035.
8. P. Butachkov *et al.*, submitted to Phys. Rev. C, Rapid Communications.

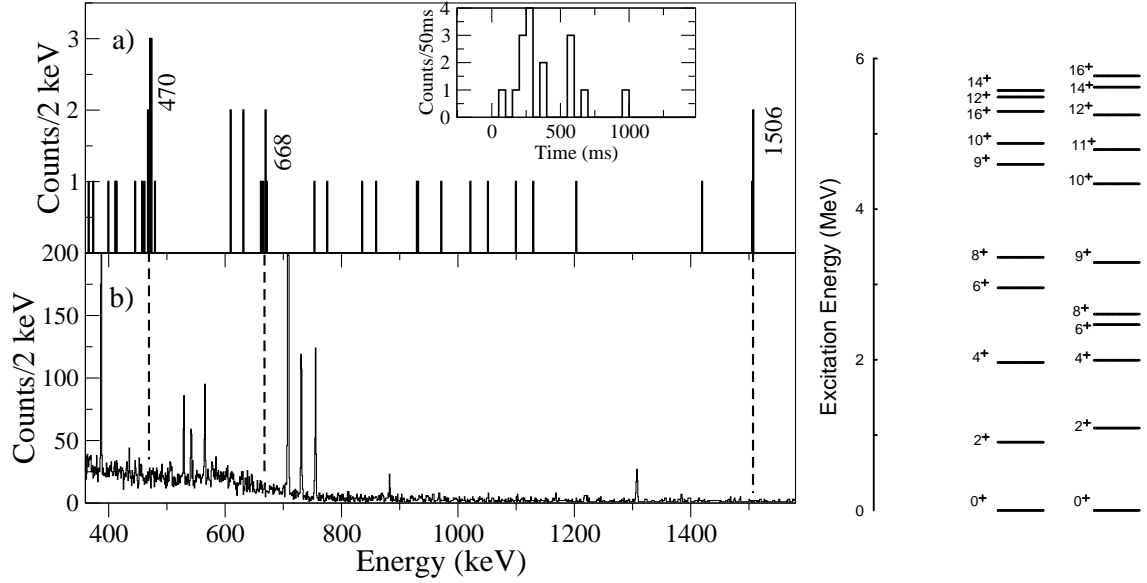


FIGURE 3. (Left) γ -ray spectra associated with the decays following implantation into the geometrically central DSSSD of the 'active stopper' for, Top: ^{96}Cd , Bottom: the nuclei other than ^{96}Cd . The γ times are restricted to be between 200 ns to 4 μs following the decay trigger. Furthermore, the events shown here correspond to the Si energy below 600 keV, since the energy losses of most of the β particles are estimated to fall into this range. The inset shows the combined correlation time distribution for 470, 668, 1506 keV γ rays with respect to ^{96}Cd implantation. (Right) Calculations on the level structure of ^{96}Cd using Gross-Frenkel interaction and $g_{9/2}$, $p_{1/2}$ model space: Column 1: With, Column 2: Without $T = 0$ np interaction. As can be seen, in the absence of the $T = 0$ component the 16^+ state loses the $E6$ 'spin-gap'. Consequently, the isomeric nature is no longer present.

9. H. Geissel, Nucl. Instrum. Methods Phys. Res. B, 70, 1992, 286–297.
10. Zs. Podolyak, *et al.*, Phys. Lett. B, 672, 2009, 116–119.
11. D. Rudolph *et al.*, Eur. Phys. J Special Topics, 150, 173, 2007, 173–176.
12. S. Pietri *et al.*, Nucl. Instrum. Methods Phys. Res. A, 261, 1079, 2007, 1079–1083.
13. R. Kumar *et al.*, Nucl. Instrum. Methods Phys. Res., 598, 2009, 754–758.
14. S. Pietri *et al.*, Eur. Phys. J Special Topics, 150, 2007, 319–320.
15. r2d2, software developed by the present collaboration.
16. root.cern.ch.
17. R. Grzywacz *et al.*, Phys. Rev. C, 55, 1997, 1126–1129.
18. R. Gross and A. Frenkel, Nucl. Phys. A, 267, 1976, 85–108.
19. B.S. Nara Singh *et al.*, submitted to Phys. Rev. Lett.
20. K. Ogawa, Phys. Rev. C, 28, 1983, pp. 958–960.
21. D. Bazin *et al.*, Phys. Rev. Lett., 101, 2008, 252501–1–4.
22. B. Cederwall *et al.*, Nature, 469, 2011, pp. 68–70.

Delayed and In-beam Spectroscopy on Francium and Astatine Nuclei at the Proton Drip Line

J. Uusitalo, U. Jakobsson,
RITU-Gamma collaboration

Department of Physics, University of Jyväskylä, Finland

Abstract: Delayed and in-beam spectroscopy on francium and astatine nuclei at and beyond the proton drip line has been performed. In neutron deficient astatine nuclei a shift to deformed shapes as a function of decreasing neutron has been obtained. In neutron deficient francium isotope the same shift is evident.

Keywords: Delayed spectroscopy, in-beam, proton drip line, odd-mass.

PACS: 23.20.LV, 23.35.+g, 23.60.+e

The proton-drip line above lead is a challenging research domain to perform spectroscopic studies. In the odd- Z nuclei the proton states $(\pi h_{9/2}^n i_{13/2}^1) 13/2^+$, $(\pi h_{9/2}^{n+2} s_{1/2}^{-1}) 1/2^+$ and $(\pi h_{9/2}^n f_{7/2}^1) 7/2^-$ are down sloping as a function of decreasing neutron number and the states become almost degenerate. These states coupled to an increasing number of valence neutron holes also leads to a shape change from spherical structures to deformed ones. The bismuth isotopes have been studied down to ^{185}Bi thoroughly. The in-beam studies performed for $^{191,193}\text{Bi}$ showed a transition to oblate deformed shapes at $N = 110$, associated with the down-sloping $13/2^+$ state [1]. Later on the studies utilized for $^{189,187}\text{Bi}$ gave the first evidence for a transition from oblate shapes to prolate shapes at $N = 106$ [2]. Finally in ^{185}Bi the (proton decaying) $1/2^+$ intruder state becomes the ground state whilst in the heavier bismuth isotopes the ground state has spin and parity of $9/2^-$ [3].

We have extended our studies on neutron deficient astatine and francium nuclei. Both delayed and in-beam spectroscopic studies have been utilized. In those cases where the production cross-sections are too low for in-beam studies, alpha decay studies were performed. Alpha decay studies after fast separation and performed far away from the production target allow higher beam intensities to be used. This together with high alpha-particle collection efficiency provides a viable means to obtain spectroscopic information even when the production cross sections are very low.

The neutron deficient astatine and francium isotopes were produced using heavy-ion induced fusion evaporation reactions. The targets and beam particles were selected in a way to minimize losses due to the strong fission channel open in this region. Bombarding energies close to the Coulomb barrier were used. The experiments were performed at the Accelerator Laboratory of the University of Jyväskylä, Finland. Prompt γ rays were recorded at the target position by the JUROGAM γ -ray spectrometer consisting of 43 Compton-suppressed high-purity germanium (HPGe) detectors of Eurogam Phase 1 [4] and GASP [5] type. The recoiling fusion-evaporation residues were separated from the primary beam and other unwanted reaction products by the gas-filled recoil separator RITU [6] and transported to the

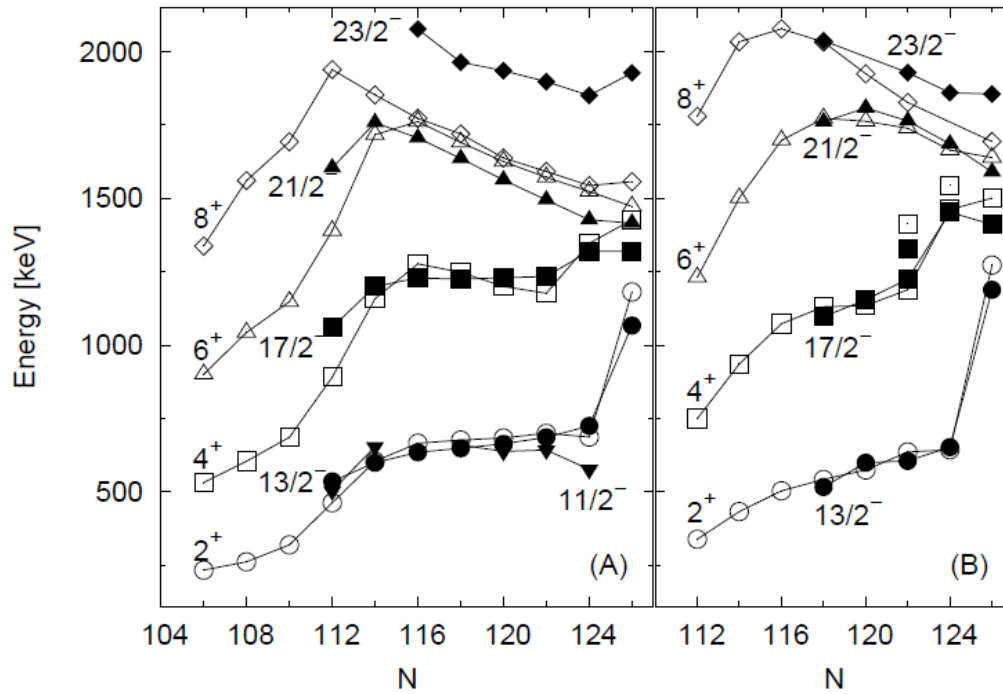


FIGURE 2. The energies of the negative parity states as function of neutron number in the odd-mass astatine and francium isotopes (closed symbols) are compared with the corresponding even-mass (core) polonium and radon, respectively, isotopes (open symbols). Data points are taken from ref. [9, 10, and 13] and from references therein.

For francium isotopes delayed and in-beam spectroscopy has been performed in ^{203}Fr and ^{205}Fr [13]; whilst only delayed study has been utilized for ^{201}Fr [14] and ^{199}Fr [15]. In francium isotopes the onset of ground state deformation occurs at $N = 112$ (^{199}Fr), ^{201}Fr being the first proton unbound francium isotope. From alpha-decay studies it was obtained that the $1/2^+$ intruder state becomes the ground state in ^{199}Fr . For the ^{203}Fr and ^{205}Fr both in-beam and delayed spectroscopy studies were performed. Isomeric $1/2^+$ and $13/2^+$ states were identified from these nuclei. The single-particle energies of odd-mass isotopes of interest are shown in Figure 3.

ACKNOWLEDGMENTS

This work has been supported through EURONS (European Commission contact no. RII3-CT-2004-506065) and by the Academy of Finland under the Finnish Centre of Excellence Programme 2006-2011 (Nuclear and Accelerator Based Physics contract no. 213503). The authors would like also to thank the UK/France (STFG/IN2P3) detector Loan Pool and GAMMAPOOL European Spectroscopy Resource for the loan of the detectors for JUROGAM. Support has also been provided by the UK Engineering and Physical Sciences Research Council. U. J. acknowledges the support from the Finnish Academy of Science and Letters; Vilho, Yrjö and Kalle Väisälä Foundation.

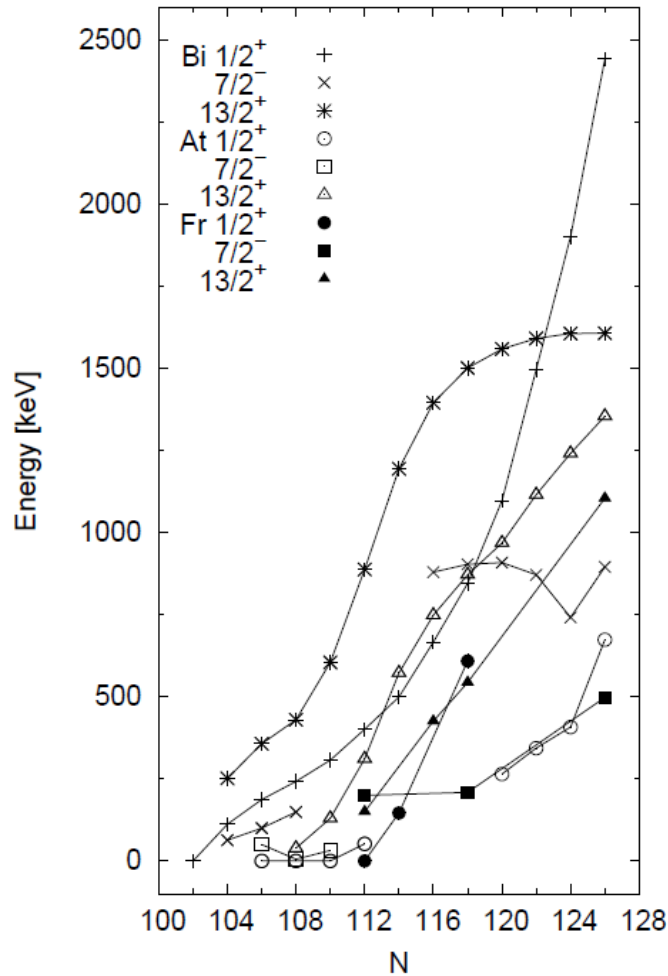


FIGURE 3. Experimental excitation energies for the low-lying states in odd-mass bismuth, astatine, and francium isotopes in the region of interest are shown. The $9/2^-$ states, in most of the cases the ground states, are not shown. Data points are taken from ref. [9-15] and from references therein.

REFERENCES

1. P. Nieminen *et al.*, Phys. Rev. C **69**, 064326 (2004)
2. A. Hürstel *et al.*, Eur. Phys. J A **21**, 365 (2004)
3. C. Davids *et al.*, Phys. Rev. Lett. **76**, 596 (1996)
4. C. W. Beusang *et al.*, Nucl. Instrum. Methods Phys. Res. A **313**, 37 (1992)
5. C. Rossi Alvarez, Nuclear Physics News **3**, 3 (1993)
6. M. Leino *et al.*, Nucl. Instrum. Methods Phys. Res. B **99**, 653 (1995)
7. R. Page *et al.*, Nucl. Instrum. Methods Phys. Res. B **204**, 634 (2003)
8. I. H. Lazarus *et al.*, IEEE Trans. Nucl. Sci. **48**, 567 (2001)
9. U. Jakobsson *et al.*, Phys. Rev. C **82**, 044302 (2010)
10. K. Andgren *et al.*, Phys. Rev. C **78**, 044328 (2008)
11. M. Nyman *et al.*, to be published
12. H. Kettunen *et al.*, Eur. Phys. J. A **16**, 457 (2003)
13. U. Jakobsson *et al.*, to be published
14. J. Uusitalo *et al.*, Phys. Rev. C **71**, 024306 (2005)
15. J. Uusitalo *et al.*, to be published

Probing the Collective Degrees of Freedom at the Proton Drip Line in the Extremely Neutron Deficient ^{172}Hg

M. Sandzelius^{*,†}, B. Cederwall[†], E. Ganioglu^{†,**}, B. Hadinia[†],
K. Andgren[†], T. Bäck[†], T. Grahn^{*}, P.T. Greenlees^{*}, U. Jakobsson^{*},
A. Johnson[†], P.M. Jones^{*}, R. Julin^{*}, S. Juutinen^{*}, S. Ketelhut^{*},
A. Khaplanov[†], M. Leino^{*}, M. Nyman^{*}, P. Peura^{*}, P. Rahkila^{*}, J. Sarén^{*},
C. Scholey^{*}, J. Sorri^{*}, J. Uusitalo^{*} and R. Wyss[†]

^{*}*Department of Physics, University of Jyväskylä, FIN-40014 Jyväskylä, Finland*

[†]*Department of Physics, Royal Institute of Technology, S-10691 Stockholm, Sweden*

^{**}*Science Faculty, Department of Physics, Istanbul University, 34459 Istanbul, Turkey*

Abstract. Excited states in the extremely neutron-deficient isotope ^{172}Hg have been established for the first time. The $^{96}\text{Ru}(^{78}\text{Kr},2n)$ reaction was employed to populate excited states in ^{172}Hg with a cross section $\sigma \approx 15$ nb. The highly selective Recoil-Decay Tagging (RDT) technique was used to obtain clean in-beam γ -ray spectra for ^{172}Hg . The yrast ground-state band has tentatively been established up to $I = 6\hbar$. The data have been interpreted within the framework of total Routhian surface and quasiparticle random phase approximation calculations. In addition to the well-known features of shape coexistence previously observed in light Hg isotopes, the systematic trends in the energy of the yrast 2^+ and 4^+ states in the chain of Hg isotopes indicate a pronounced vibrational collectivity which is reduced in strength, but at the same time shows a higher degree of harmonicity, as the neutron number decreases below the neutron midshell.

Keywords: JUROGAM and GREAT spectrometers, RITU gas-filled separator, ^{172}Hg , TRS calculations. QRPA calculations.

PACS: 21.10.Re,23.20.Lv,27.60.+j

The nucleus ^{172}Hg is situated at the proton drip-line, at the edge of the classical region of shape coexistence below the $Z=82$ shell gap. It may be noted that the shape coexistence phenomenon was first discovered in the neutron-deficient Hg isotopes [1]. The phenomenon of shape coexistence is particularly prolific in the Hg isotopes around the neutron midshell. For $N \leq 110$ that the weakly deformed oblate ground-state band is crossed by a prolate-deformed intruder band at low spins [2, 3, 4]. The prolate-deformed intruder band has been explained as due to proton $4p$ - $6h$ excitations across the $Z=82$ shell gap, into the $h_{9/2}$ orbital. For the Hg isotopes around the midshell this competition between low-lying oblate and prolate shapes is reproduced in Nilsson-Strutinsky type of calculations [6] as energy minima in the deformation surfaces of nearly the same depths for the two competing structures. The delicate balance between such coexisting structures is easily shifted when the neutron number is altered along an isotopic chain. It has been found that the prolate intruder structure reaches its minimum energy in ^{182}Hg , lying only slightly above the ground state [5]. For $N < 100$ the prolate minimum is predicted by total routhian surface calculations to be pushed up in energy compared to

the ground state until it disappears and gives way to a new prolate minimum at a larger superdeformed shape ($\beta_2 \approx 0.55$ at $E_x \approx 4.5$ MeV) [4]. The oblate ground state evolves steadily towards a more spherical shape with decreasing N as the $N=82$ closed shell is approached. The essential aim for probing ^{172}Hg is to investigate the transition between the collective and single particle regimes in the light Hg isotopes and to elucidate the character of the collective active collective degrees of freedom.

The experiment was performed at the Accelerator Laboratory of the University of Jyväskylä, Finland. Excited states in ^{172}Hg were populated with the minuscule cross section of $\sigma \approx 15$ nb using the $^{96}\text{Ru}(^{78}\text{Kr}, 2n)$ fusion-evaporation reaction at bombarding energies of 337-355 MeV. Prompt γ rays were detected at the target position by the JUROGAM array consisting of 43 EUROGAM phase I [7] and GASP [8] type Compton-suppressed germanium detectors. The fusion-evaporation residues were separated in-flight from fission products and scattered beam particles using the RITU gas-filled recoil separator [9, 10] and subsequently implanted into the Double-sided Silicon Strip Detectors (DSSDs) of the GREAT [11] spectrometer situated at the focal plane. The recoiling residues were discriminated from scattered beam components by means of the energy loss in the GREAT multiwire proportional counter (MWPC) and the time of flight between the MWPC and the DSSD. All detector signals were recorded independently by the Total Data Readout (RDT) system [12] and were given a time stamp of 10 ns precision. This allowed accurate temporal correlations to be performed between prompt γ rays detected at the target position, recoil implants at the RITU focal plane and their subsequent radioactive decays. Clean γ -ray spectra were obtained using the highly selective Recoil-Decay Tagging (RDT) technique [13, 14]. The characteristic energy and half-life of an α decay detected at the same position (pixel) as a previously implanted recoiling residue provided identification for the residue. Prompt γ rays emitted at the target position could then be associated with the implantation event.

A prompt energy spectrum of all the γ rays recorded at the target position in delayed coincidence with a detected recoil in the DSSD is shown in Fig. 1(a). It is dominated by much stronger fusion evaporation channels than the $2n$ -channel. The selective power of the RDT-technique is exhibited in Fig. 1(b), where a prompt recoil- α - γ spectrum is shown, obtained by selecting the ^{172}Hg α decays and using a 1 ms correlation time (corresponding to three half lives). Depicted in Fig 1(c) is a recoil- α - α - γ spectrum generated by additional tagging with the ^{168}Pt α -decay (daughter of ^{172}Hg). It confirms the assignment of the three strongest gamma lines to ^{172}Hg from the the recoil- α correlated spectrum. Also shown in Fig. 1 is the tentative level scheme deduced for ^{172}Hg . Based on the relative intensities and the energy systematics for the even-even Hg nuclei the γ rays assigned to ^{172}Hg are arranged as a cascade of stretched E2 transitions. The most intense 673 keV peak is hence assigned to the $2^+ \rightarrow 0^+$ transition in ^{172}Hg . On the basis of intensity arguments the 846 keV and 760 keV peaks are then associated with the $4^+ \rightarrow 2^+$ and $6^+ \rightarrow 4^+$ transitions in ^{172}Hg , respectively. However, due to almost similar measured intensity of the 760 and 846 keV transitions, together with the the large uncertainties, the possibility exist of a reversed ordering of the two transitions.

The data obtained in this work are compared with the energy systematics of excited low-lying levels for the entire Hg isotopic chain ranging from the $N=126$ (^{206}Hg) closed shell nucleus, see Fig. 2. The level energies of the first three excited states (2^+ , 4^+ and 6^+ states) of the Hg isotopes are also compared with the equivalent levels

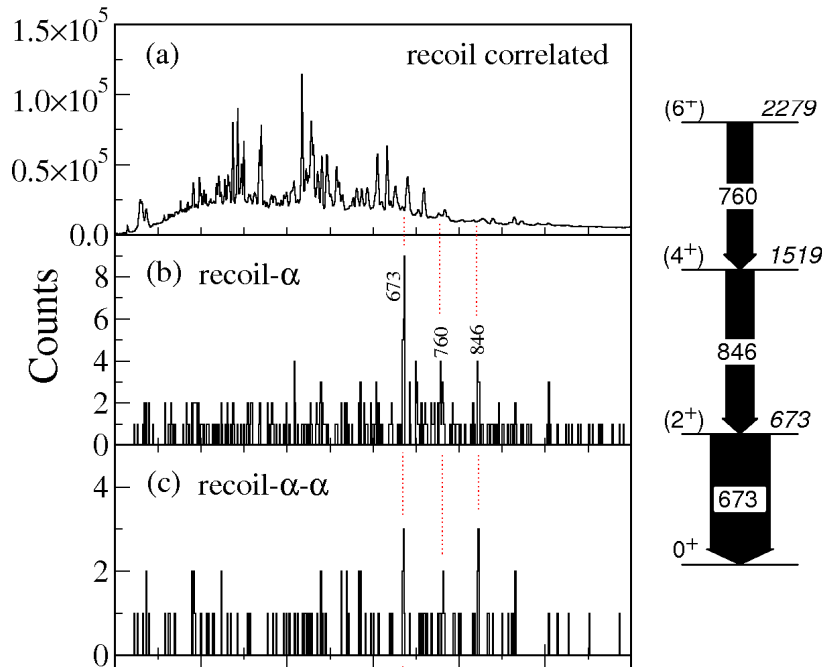


FIGURE 1. (a) Gamma-ray energy spectrum in coincidence with any fusion-evaporation residue detected in the DSSD. (b) Gamma-ray energy spectrum obtained by tagging with the ^{172}Hg α decays. (c) Gamma-ray energy spectrum obtained by additional tagging with the ^{168}Pt daughter α -decay. The width of the arrows in the proposed level scheme for ^{172}Hg are proportional to the measured relative efficiency-corrected intensities. Transition energies are given in keV.

in even- A Pt isotopes (where known). From Fig. 2 it is apparent that the excitation energies of the 2^+ , 4^+ and 6^+ levels in ^{172}Hg are higher than in any other Hg isotopes except for the closed-shell nucleus ^{206}Hg . The trend of increasing level energies as a function of decreasing neutron number from the neutron midshell at $N=104$ in the Hg isotopes is carried through down to ^{172}Hg . This is in line with the transition from a predominantly prolate structure, coexisting with a weakly-deformed oblate ground state, near the midshell to a near-spherical ground state for the lighter Hg isotopes below the midshell. Woods-Saxon-Strutinsky calculations predict a pronounced change in the potential energy surfaces from ^{180}Hg to ^{170}Hg [4]. In ^{170}Hg a single spherical minimum has replaced the coexisting oblate ground state and low-lying prolate intruder structures found in the even- A $^{180}\text{--}^{184}\text{Hg}$ nuclei. The deformed prolate intruder band, whose presence is reflected as a marked dip of the 2^+ - 6^+ energies around the neutron mid-shell, can be seen to disappear with decreasing N in Fig. 2 from the midshell towards the lightest Hg isotopes. This interpretation is confirmed by Total Routhian Surface (TRS) calculations (see Ref. [6] for details). TRS calculations for the even- A $^{172}\text{--}^{176}\text{Hg}$ isotopes are shown in Fig. 3. These nuclei are predicted to be weakly deformed ($\beta_2 \approx 0.10 - 0.15$) and soft with respect to both deformation parameters (β_2 and γ). The TRS calculations predict a gradual transition from the shape coexistence regime around midshell towards a dominance of lower deformation with decreasing neutron number.

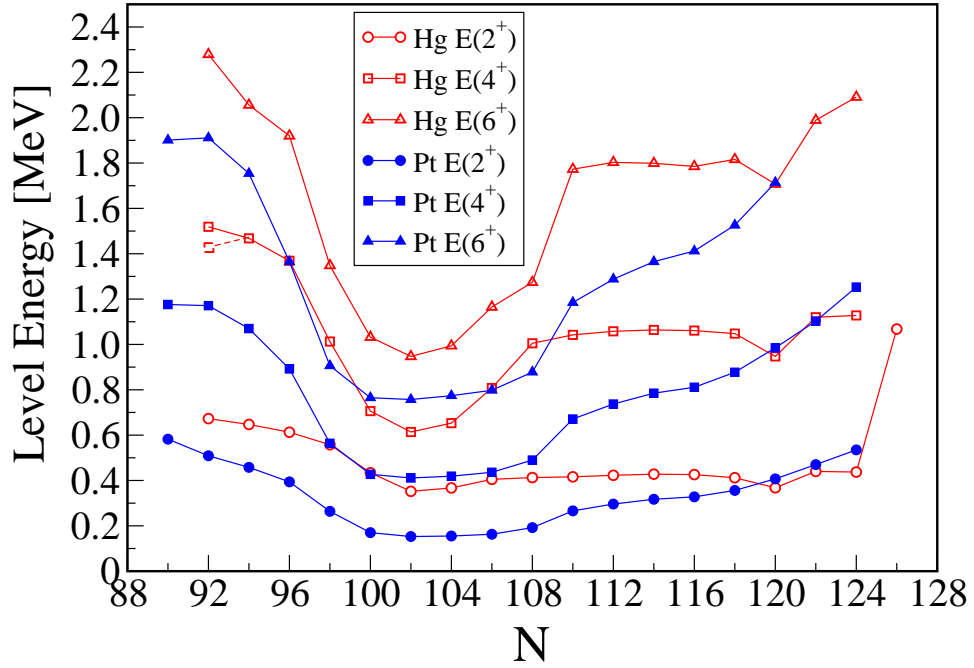


FIGURE 2. Energy level systematics for the yrast states in even-N Hg and Pt isotopes for the isotopic chain ranging from $N=126$ to $N=90$. The excitation energies of the 2^+ , 4^+ , and 6^+ levels for Hg (open symbols) are plotted together with those energy levels (closed symbols) for the even-N Pt isotopes. The level energy of the 4^+ state in ^{172}Hg is also indicated with an alternative level due the ambiguity of the placement of the 760 and 846 keV γ rays as described in the text. The data are taken from [15, 16, 17] and from the present work.

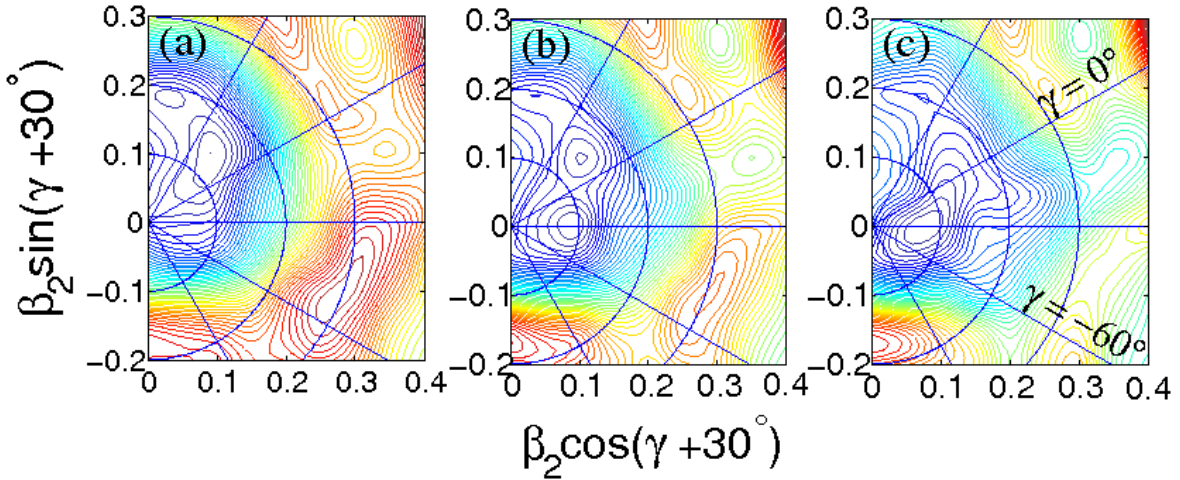


FIGURE 3. Total Routhian Surfaces calculated at a rotational frequency of $\hbar\omega = 0.240$ MeV for the yrast ground state band in ^{172}Hg (left), ^{174}Hg (middle) and ^{176}Hg (right). Weakly deformed collective and non-collective minima are visible at a deformation $\beta_2 \approx 0.10 - 0.15$. For increasing neutron number a well deformed ($\beta_2 \approx 0.35$, $\gamma \approx -15^\circ$) minimum starts to develop. The energy difference between contour lines is 100 keV.

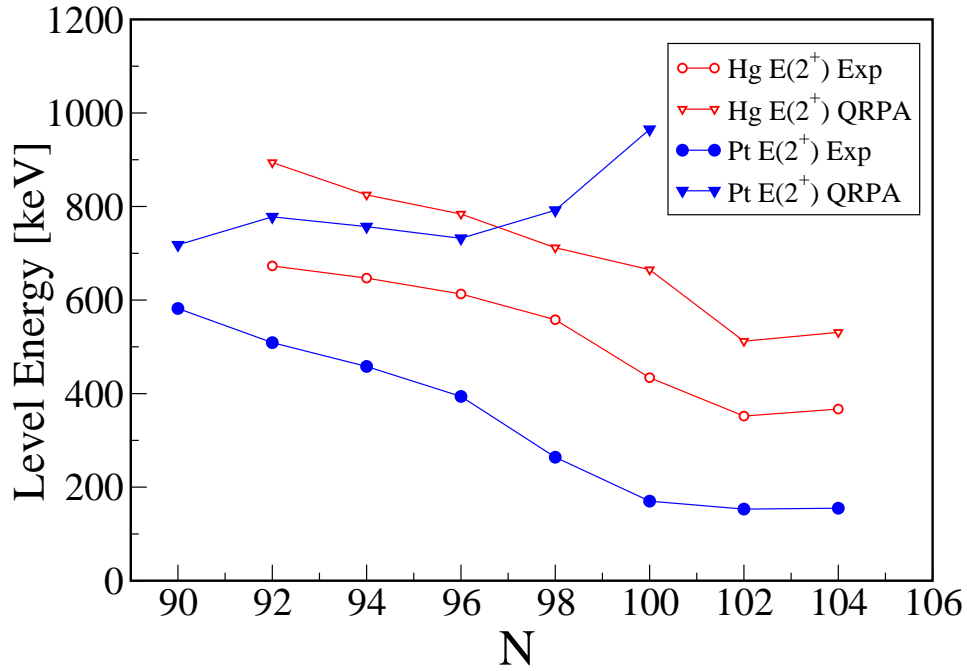


FIGURE 4. Experimental and calculated QRPA energy systematics of the 2^+ excited state for the lightest even-even Hg (open symbols) and Pt (filled symbols) isotopes. For the Hg isotopes the QRPA $E(2^+)$ values are calculated from the neutron midshell ($N=104$) and for Pt only the $E(2^+)$ values for $N \leq 100$ are considered.

The difference in the 2^+ level energies between the Pt and Hg isotopes, especially around the midshell, is also evidence of the predominantly oblate nature of the ground and low-lying excited states in Hg as compared with those in Pt, where the same states are predicted to be of a prolate character. A striking similarity between ^{172}Hg and the lightest even-even is the near constant level spacing between the lowest excited states, resembling those of a harmonic vibrator. The $E(4^+)/E(2^+)$ ratio is 2.26 (or 2.13 if the 760 and 846 keV transitions would be interchanged) which is closer to the harmonic vibrational limit of 2.0 than the values ~ 2.5 obtained for Hg isotopes with $N \geq 108$ (which are more similar to those of a gamma-soft rotor). These trends could also be regarded as an evolution of vibrational collectivity with a varying degree of harmonicity.

The collective nature of ^{172}Hg can be interpreted in the light of QRPA calculations [18]. The QRPA calculations are specifically aimed at characterising low-lying collective vibrational states. Such calculations have been performed for the even-even $N=92-104$ Hg and $N=90-100$ Pt isotopes. In Fig. 4 the experimental and calculated 2^+ level energies for the lightest even-even Hg and Pt isotopes are plotted below the neutron midshell. From the Pt energy systematics in Fig. 4 an overall drop in the QRPA 2^+ excitation energy can be inferred as the neutron number decreases below $N=100$. The lowering of the vibrational 2^+ state and the increasing closeness to the experimental 2^+ energies as the neutron number decreases suggests a significant vibrational admixture for the lightest platinum isotopes. From Fig. 4 it is also evident that the QRPA calculations deviate markedly from the experimental values, and that they cannot reproduce the

2^+ level energy for the Pt midshell nuclei, which is consistent with the interpretation that the low-lying energy levels in these Pt nuclei are predominantly of a rotational collective nature. A quite different trend can be observed in the comparison with the QRPA results for the Hg isotopes. Starting from the neutron midshell at $N=104$ an almost monotonic increase of the experimental 2^+ level energy can be observed with decreasing neutron number. This trend is reproduced by the QRPA 2^+ energies for every even-even nucleus below midshell, suggesting that the Hg isotopes have a vibrational character already at midshell, contrary to the Pt case. This marked difference can be explained by the softening of the nuclear potential in the Hg midshell isotopes, thereby causing a *lowering* of the vibrational 2^+ level energy as compared with the lightest Pt isotopes. Furthermore, the increasing QRPA 2^+ energies, similarly to the experimental 2^+ level energies, as a function of decreasing neutron number are indicative of a *decreased* degree of collectivity for the lightest Hg isotopes as compared to the midshell nuclei. However, the calculated near-spherical shape with its pronounced deformation softness and the 4^+ and 2^+ energy ratio close to 2.0 point to that the low-lying excitations in ^{172}Hg still could be close to those of harmonic vibrator.

In summary, excited states in the extremely neutron deficient ^{172}Hg have been populated in heavy-ion fusion-evaporation reactions and studied using the spectrometers JU-ROGAM and GREAT, coupled to the gas-filled RITU recoil separator. The yrast band have tentatively been delineated up to the $I^\pi = 6^+$ state. TRS calculations suggest that the prolate intruder band observed at the midshell is pushed up to higher energies in the lighter Hg isotopes below the neutron midshell and have disappeared in ^{172}Hg , well above the experimentally attained level energies. The QRPA calculations suggest that ^{172}Hg has a lower degree of vibrational collectivity than the midshell nuclei while the nearly constant level spacing in ^{172}Hg between the lowest excited 2^+ , 4^+ and 6^+ states may indicate a transition to a near-spherical harmonic collective vibrational structure as compared with heavier even-even Hg isotopes around the neutron midshell and above.

REFERENCES

1. J. Bonn *et al.*, Phys. Lett. **B38**, 308 (1972).
2. S. Frauendorf *and* V.V. Pashkevich, Phys. Lett. **B55**, 365 (1975).
3. J.L. Wood *et al.*, Phys. Rep. **215**, 101 (1992).
4. W. Nazarewicz, Phys. Lett. **B305**, 195 (1993).
5. G.D. Dracoulis *et al.*, Phys. Lett. **B208**, 365 (1988).
6. W. Nazarewicz *et al.*, Nucl. Phys. **A435**, 397 (1985).
7. C.W. Beausang *et al.*, Nucl. Instr. Meth. **A313**, 37 (1992).
8. C.R. Alvarez *et al.*, Nucl. Phys. News **3**(3), 10 (1993).
9. M. Leino *et al.*, Nucl. Instr. Meth. **B99**, 653 (1995).
10. M. Leino, Nucl. Instr. Meth. **B126**, 320 (1997).
11. R.D. Page *et al.*, Nucl. Instr. and Meth. in Phys. Res. **B204**, 634 (2003).
12. I.H. Lazarus *et al.*, IEEE Trans. Nucl. Sci **48**, 567 (2001).
13. E.S. Paul *et al.*, Phys. Rev. **C51**, 78 (1995).
14. R.S. Simon *et al.*, Z. Phys. **A325**, 197 (1986).
15. S.L. King *et al.*, Nucl. Phys. **A443**, 82 (1998).
16. R. Julin *et al.*, J. Phys. G: Nucl. Part. Phys. **27**, R109 (2001).
17. Nat. Nucl. Data Center, <http://www.nndc.bnl.com>.
18. H. Sakamoto and T. Kishimoto, Nucl. Phys. A **501** (1989) 205.

2p radioactivity studies with a TPC

P.Ascher*, L. Audirac*, N. Adimi*,[†], B. Blank*, C. Borcea**, B. A. Brown[‡],
I. Companis**, F. Delalee*, C.E. Demonchy*, F. de Oliveira Santos[§], J.
Giovinazzo*, S. Grévy[§], L. V. Grigorenko[¶], T. Kurtukian-Nieto*, S.
Leblanc*, J.-L. Pedroza*, L. Perrot[§], J. Pibernat*, L. Serani*, P. Srivastava^{||}
and J.-C. Thomas[§]

*Centre d'Études Nucléaires de Bordeaux Gradignan - Université Bordeaux 1 - UMR 5797
CNRS/IN2P3, Chemin du Solarium, BP 120, 33175 Gradignan, France

[†]Faculté de Physique, USTHB, B.P.32, El Alia, 16111 Bab Ezzouar, Alger, Algeria

**National Institute for Physics and Nuclear Engineering, P.O. Box MG6, Bucharest-Margurele,
Romania

[‡]Department of Physics and Astronomy, and National Superconducting Cyclotron Laboratory,
Michigan State University, East Lansing, Michigan 48824-1321, USA

[§]Grand Accélérateur National d'Ions Lourds, CEA/DSM - CNRS/IN2P3, 14076 Caen Cedex 05,
France

[¶]Flerov Laboratory of Nuclear Reactions, JINR, Dubna 141980, Russian Federation

^{||}Nuclear Physics Group, Department of Physics, University of Allahabad, India

Abstract. After the discovery of two-proton radioactivity in 2002, an important effort has been made in order to observe each emitted particle individually. Energy and angular correlations between the protons should reveal details about the mechanism of this exotic decay mode. In this frame, an experiment has been performed at LISE/GANIL, where the two protons emitted in the decay of ^{54}Zn have been individually observed for the first time. Angular and energy correlations were determined and allowed a first comparison with theoretical predictions.

Keywords: Two-proton radioactivity, Time Projection Chamber

PACS: 23.50.+z, 27.40.+z, 29.40.Cs, 29.40.Gx

INTRODUCTION

In 1960, Goldansky [1] predicted the 2p radioactivity for nuclei beyond the proton drip line, for which one-proton emission is energetically prohibited and only simultaneous two-proton emission is allowed. The pairing correlation of the last protons makes such a decay process possible, and the emitted particles may keep a trace of this correlation.

Experimentally, this new nuclear decay mode was observed first in the decay of ^{45}Fe in two independent experiments [2][3] and later also in ^{54}Zn [4] and possibly in ^{48}Ni [5]. In these experiments, the ions of interest were deeply implanted in silicon detectors in which the decay was observed. Therefore, only the total decay energy, the half-life, and the absence of β particles from the competing decay by β -delayed-particle emission could be clearly established. In addition, the observation of the daughter decay helped to unambiguously assign the observed decay to 2p radioactivity. These experimental results were found in reasonable agreement with predictions from different theoretical models [6], like the R-Matrix theory [7], the Shell Model embedded in the Continuum (SMC) [8] or the three-body model [9][10].

However, in none of these experiments, the two protons were identified separately, while the main physics question in the context of 2p radioactivity is how the two protons emitted are correlated in energy and in angle. An answer to that would enable us to investigate the decay dynamics of 2p radioactivity and thus reveal details of nuclear structure at the limits of stability.

In an experiment performed in 2005 at GANIL, emission of two protons in the decay of ^{45}Fe was observed directly for the first time with a Time Projection Chamber (TPC) [11]. The purpose of this detection set-up is to reconstruct the proton tracks in three dimensions. In another experiment performed at MSU [12] [13], the 2p emission in the decay of ^{45}Fe was observed with an Optical Time Projection Chamber in which images of ionizing particle trajectories are recorded optically. In this latter work, high statistics data allowed the authors to obtain a first meaningful comparison with a model including the three-body dynamics of the process [9][10].

This paper describes an experiment performed in 2008 where emission of two protons in the decay of ^{54}Zn was observed with the TPC. Angular and energy correlations have been determined. These results allowed a first comparison with theoretical predictions of the three-body model.

EXPERIMENT

The ^{54}Zn nuclei were produced by quasi-fragmentation of the projectile at GANIL. A primary $^{58}\text{Ni}^{26+}$ beam with an energy of 74.5 MeV/nucleon and an average intensity of $3.5\ \mu\text{A}$ was fragmented in a ^{nat}Ni target ($200\ \mu\text{m}$). The ^{54}Zn fragments were selected by a magnetic-rigidity, energy-loss, and velocity analysis by means of the LISE3 separator including an achromatic energy degrader ($500\ \mu\text{m}$ of beryllium).

Two silicon detectors located at the end of the spectrometer allowed to identify individually the fragments by means of an energy-loss and time-of-flight analysis. The identification parameters were first determined for frequently produced nuclei. Then, the parameters were extrapolated to unambiguously identify the nuclei produced with low probability. Details of this procedure can be found in [14].

The main setting of the spectrometer was optimized for the production and transmission of ^{54}Zn . During a two weeks experiment, 18 ^{54}Zn nuclei have been produced. These ions were finally implanted in the TPC [15] (see Fig.1).

This detector is based on the principle of a time-projection-chamber. Ions of interest are implanted in a gas volume (argon 90% - methane 10%) at 750 mbar, where the radioactive decay takes place. The electrons, produced by the slowing down of either the incoming ions or the decay products, drift in the electric field of the TPC towards a set of four gas electron multipliers (GEM) where they are multiplied and finally detected in a two dimensional strip detector. The analysis of energy signals allows to reconstruct the tracks of the particles in two dimensions; the drift-time analysis gives the third one. Details can be found in [15].

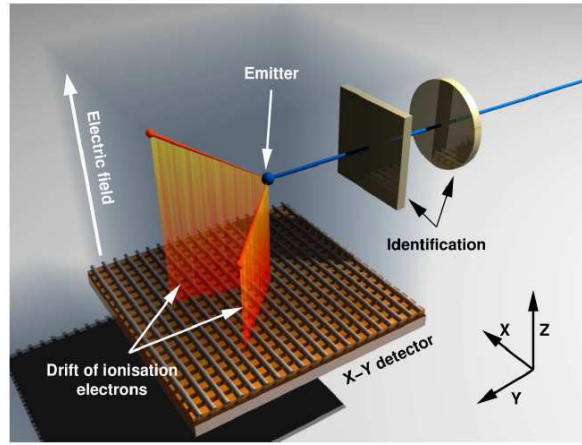


FIGURE 1. Schematic view of the TPC : the ions selected by the LISE separator go through a set of two silicon detectors used for identification of the ions, and are implanted in the gas volume of the TPC. The two protons from the decay are emitted and stopped in the gas. The ionization electrons (from ions or from protons) drift to the 2D strip detector, due to an electric field in the chamber. The amplitude of the signal on the strips reflects the 2D projection of the tracks. The third component Z is measured by means of the time information on each strip. The signal amplification by a set of 4 GEM located just above the X-Y detector is not shown in the Figure.

RESULTS

Among the eighteen ^{54}Zn implantation events, only thirteen could be correlated in time and space with decays. Five decay events were lost due to the data acquisition dead time and the short half-life of ^{54}Zn . For two decay events, no information about the energy was obtained because the protons emitted did not stop in the active volume of the chamber.

The half-life of ^{54}Zn determined as $1.59^{+0.60}_{-0.35}$ ms and the measured total decay energy $Q_{2p} = 1.28 \pm 0.21$ MeV are in agreement with those determined in [4].

Observables related to the measurements of individual protons were also determined. As an example, an implantation event spectrum is presented in Figure 2. The ion enters with an angle of 45° in the chamber and stops at a given (X_0, Y_0) position. The implantation signals are fitted with a Gaussian folded with a straight line. This function is a good approximation of the Bragg peak corresponding to the energy loss of the charged particles inside the gas chamber. It allowed to determine the implantation position of the ion (top part), which coincides with the emission position of the two protons (middle part). Their tracks in X and Y are fitted with the same function as for the implantation signals: the sum of two foldings of a straight line and a Gaussian. Figure 3a shows an example of a two-proton emission in two dimensions.

The energy fraction distribution of the individual protons as determined from the energy signals is plotted in Figure 4 and is found in good agreement with the predictions of the three body model. As expected in a simultaneous emission, the two protons share the decay energy equally in order to favor the barrier penetration. This theoretical approach [9, 10] is the only model of 2p radioactivity which takes into account correlations between the two protons.

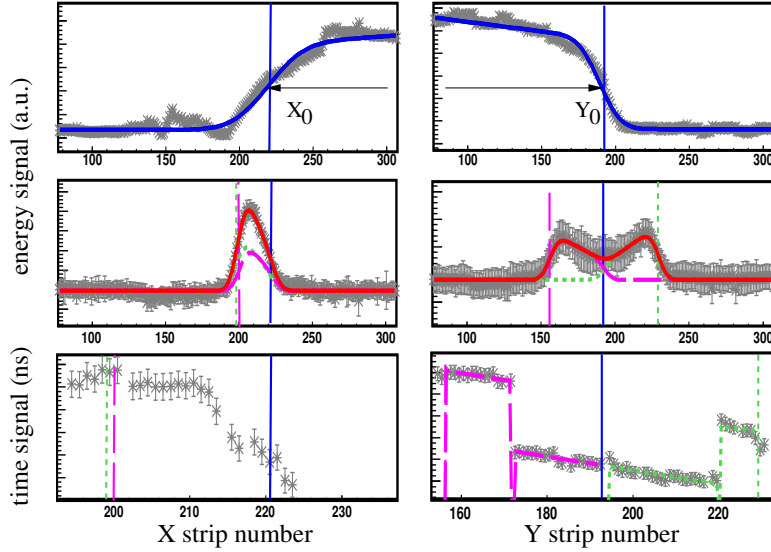


FIGURE 2. Example of energy loss spectra obtained with the XY strip detector and associated with the implantation of a 2p-emitter in the TPC. Top: Signals obtained for the implantation of ^{54}Zn : the ion enters in the chamber and stops at a given (X_0, Y_0) depth. The arrows indicate the direction of the incoming beam. The solid line is the fit of the implantation profile whereas the vertical line indicates the determined implantation position. Middle: The decay of ^{54}Zn takes place at the stopping point of the implantation event described above. The two protons are clearly identified. Their tracks are determined by fitting the decay signal with a sum of two foldings of a straight line and a Gaussian. The vertical full line corresponds to the starting point of the trajectories determined from the implantation profile of ^{54}Zn whereas the dashed lines are the two stopping points of the protons trajectories. Bottom: Corresponding time signals. The spectrum on the Y dimension is fitted by a straight line for each proton, giving the directions of each individual proton.

In a final step, the third component Z of the tracks was obtained. The bottom of Figure 2 shows the time spectra corresponding to the same event. Only the spectrum on the Y dimension is analyzed because the protons were emitted along the X strips. The spectrum is fitted by a straight line for each proton, giving the third component of each proton track. Briefly, due to the short range of the protons, the determination of Δz with the time signals is not very accurate. Therefore, the time signals were only used to determine whether the proton goes upwards or downwards. Then, we use the theoretical range r of the protons [16] to determine Δz with $\Delta z^2 = r^2 - \Delta x^2 - \Delta y^2$, with Δx and Δy given by the energy signal analysis. The theoretical range was calculated by taking the energy sharing of the protons, as determined from the energy spectra analysis, and the sum energy, as determined from the previous measurements [4].

Among the ten events, seven have been fully reconstructed in the three dimensional space. For the three remaining, the time signals did not allow to determine if the protons went up or down. Therefore, we have for these events two possible angles between the two protons. Figure 3b shows an example of a two-proton emission reconstructed in three dimensions.

The complete analysis of these decay events allowed to provide angular correlations between the protons. The upper part of Figure 5 shows each experimental angle, rep-

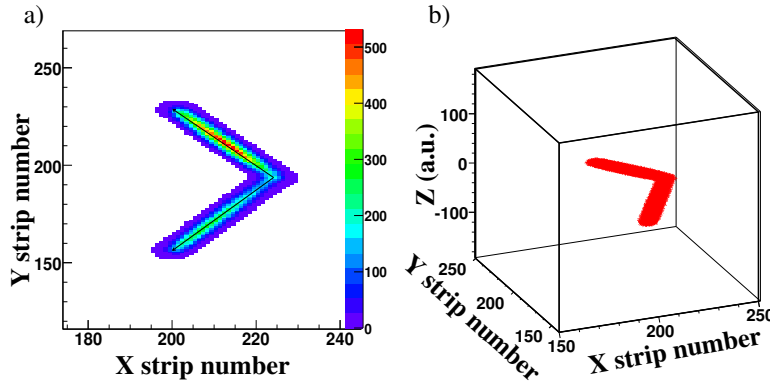


FIGURE 3. a) Two-dimensional view of a ^{54}Zn decay event as reconstructed from the XY strip detector. The color corresponds to the energy loss detected by the strips. b) Same decay event reconstructed in the three-dimensional space.

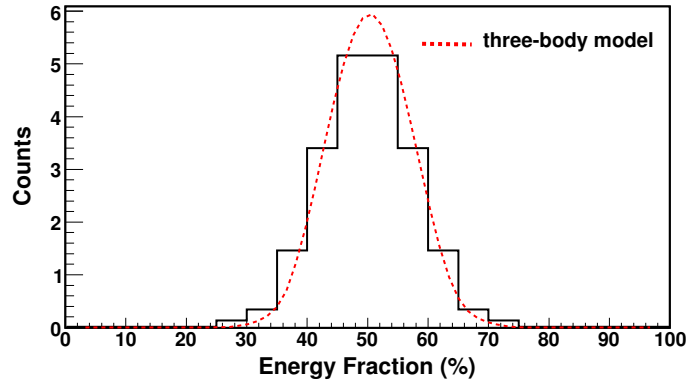


FIGURE 4. Energy sharing between the two protons emitted in the decay of ^{54}Zn . The dashed line is the energy distribution of the three-body model [10] folded with the response of the detector, which fits well the experimental distribution.

resented by a Gaussian reflecting the angular resolution. The middle part shows the angular distribution obtained. Seven events are represented in the histogram; the three other events, not fully reconstructed, are represented by full lines for the first possibility and by dashed lines for the second. Within the three body model, the angular distribution spectra are calculated for different ℓ^2 configurations of the two emitted protons. The corresponding spectra (bottom part of Figure 5) show a double-hump structure, with one broad peak centered around 50° and a smaller one at about 145° . When the p^2 contribution becomes negligible, the second hump does not survive. Considering that the experimental distribution shows a double-hump structure, the results can be compared with the model predictions by looking at the ratio between the first and the second hump. From an interpolation of the theoretical ratios, we obtain an experimental p^2 contribution of $30^{+33}_{-21}\%$.

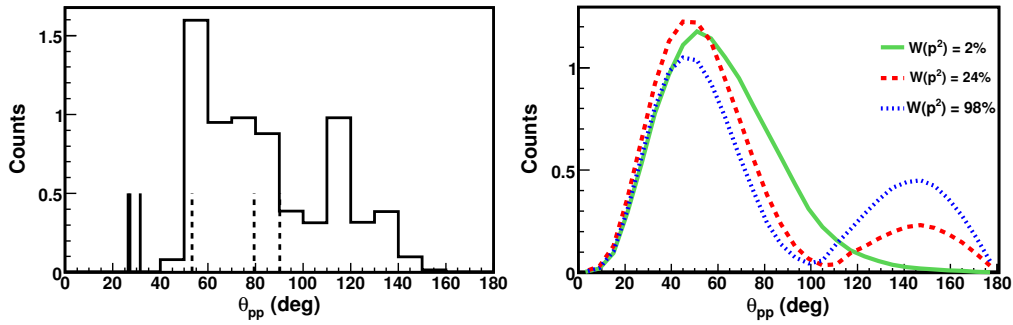


FIGURE 5. Top: Experimental angles between the two protons in the three dimensional space. Each event is convoluted with a Gaussian representing the angular resolution. Middle: Experimental angular distribution between the two protons. Seven events are represented in the histogram. The dashed and full lines represent two possible angles for three not fully reconstructed events. Bottom: The three lines are the theoretical predictions of the three-body model, each line corresponding to different weights of the p^2 configuration. These model distributions are folded with a Gaussian function representing the detector angular resolution.

CONCLUSION

In summary, we observed directly for the first time the two protons emitted in the decay of ^{54}Zn with a TPC. Energy and angular distributions could be obtained and allowed a first rough comparison with theoretical models giving information about nuclear structure. However, to establish a detailed picture of the decay process, higher statistics of implantation-decay events are needed, which can be obtained in a future experiment. In parallel, improvements of theoretical model predictions are essential to elucidate the decay mechanism which governs two-proton radioactivity.

REFERENCES

1. V. I. Goldansky, Nucl. Phys. **19**, 482 (1960).
2. J. Giovinazzo *et al.*, Phys. Rev. Lett. **89**, 102501 (2002).
3. M. Pfützner *et al.*, Eur. Phys. J. **A14**, 279 (2002).
4. B. Blank *et al.*, Phys. Rev. Lett. **94**, 232501 (2005).
5. C. Dossat *et al.*, Phys. Rev. C **72**, 054315 (2005).
6. B. Blank and M. Płoszajczak, Rev. Prog. Phys. **71**, 046301 (2008).
7. B. A. Brown and F. C. Barker, Phys. Rev. C **67**, 041304 (2003).
8. J. Rotureau, J. Okolowicz, and M. Płoszajczak, Nucl. Phys. **A767**, 13 (2006).
9. L.V. Grigorenko, R.C. Johnson, I.G. Mukha, I.J. Thompson, M.V. Zhukov, Phys. Rev. C **64**, 054002 (2001).
10. L.V. Grigorenko and M.V. Zhukov, Phys. Rev. C **68**, 054005 (2003).
11. J. Giovinazzo *et al.*, Phys. Rev. Lett. **99**, 102501 (2007).
12. K. Miernik *et al.*, Phys. Rev. Lett. **99**, 192501 (2007).
13. K. Miernik, Eur. Phys. J. **A42**, 431 (2009).
14. C. Dossat *et al.*, Nucl. Phys. A **792**, 18 (2007).
15. B. Blank *et al.*, Nucl. Instrum. Meth. **A613**, 65 (2010).
16. J. F. Ziegler, Nucl. Instrum. Meth. **B268**, 1818 (2010).

Spectroscopy of proton rich nuclei with the OTPC chamber

M. Pomorski^{*}, M. Pfützner^{*}, W. Dominik^{*}, R. Grzywacz^{†,**}, T. Baumann[‡], J.S. Berryman[‡], C.R. Bingham[†], H. Czyrkowski^{*}, M. Ćwiok^{*}, I.G. Darby[†], R. Dąbrowski^{*}, T. Ginter[‡], L. Grigorenko[§], Z. Janas^{*}, J. Johnson^{**}, G. Kamiński^{¶,§}, M. Karny^{*}, A. Korgul^{*}, W. Kuśmierz^{*}, A. Kuźniak^{†,*}, N. Larson^{‡,||}, S.N. Liddick^{‡,||}, M. Madurga[†], C. Mazzocchi^{*}, S. Mianowski^{*}, K. Miernik^{**,*}, D. Miller[†], S. Paulauskas[†], J. Pereira[‡], M. Rajabali[†], K.P. Rykaczewski^{**}, A. Stolz[‡] and S. Suchyta^{‡,||}

^{*}*Faculty of Physics, University of Warsaw, 00-681 Warsaw, Poland*

[†]*Department of Physics and Astronomy, University of Tennessee, Knoxville, TN 37996, USA*

^{**}*Physics Division, Oak Ridge National Laboratory, Oak Ridge, TN 37831, USA*

[‡]*National Superconducting Cyclotron Laboratory, Michigan State University, East Lansing, MI 48824, USA*

[§]*Joint Institute for Nuclear Research, 141980 Dubna, Moscow Region, Russia*

[¶]*Institute of Nuclear Physics PAN, 31-342 Kraków, Poland*

^{||}*Department of Chemistry, Michigan State University, East Lansing, MI 48824, USA*

Abstract. Decay studies of very neutron-deficient nuclei ^{43}Cr and ^{48}Ni with the application of a time projection chamber with optical readout are presented.

Keywords: gaseous detectors, β p decay, 2p emission

PACS: 23.50.+z, 23.90.+w, 27.40.+z, 29.40.Cs, 29.40.Gx

INTRODUCTION

In the region of mid-mass nuclei near the proton drip line we are able to witness interesting decays such as β -delayed multi proton emission or 2p emission from the ground state. To study these exotic decay modes a dedicated tool was constructed at the University of Warsaw - Optical Time Projection Chamber (OTPC) [1]. This device allows to register individual protons emitted in a decay and to reconstruct their tracks in 3D. This device already allowed the first study of angular distribution of protons emitted in the 2p decay of ^{45}Fe [2].

In this paper we will present results obtained with this detector on decay of ^{43}Cr as well as new results on the 2p decay of ^{48}Ni .

EXPERIMENTAL TECHNIQUE

The studies were conducted at National Superconducting Cyclotron Laboratory at Michigan State University, East Lansing, USA. The ^{43}Cr ions were registered as a byproduct of experiment dedicated to ^{45}Fe , performed in 2007, where they were col-

lected to monitor the performance of OTPC detector between rare events of ^{45}Fe . In this experiment we used fragmentation reaction of 161 AMeV beam of ^{58}Ni on a 800 mg/cm^2 natural nickel target. The fragments were separated using A1900 separator and identified in-flight using time-of-flight (TOF) and energy loss(ΔE) information for each ion.

Data on ^{48}Ni were collected in 2011 at the same laboratory. The conditions were almost identical with the primary beam energy of 160 AMeV and a natural nickel target of 580 mg/cm^2 thickness. In this experiment we used a rotating target assembly which was prepared in cooperation with University of Tennessee, Knoxville, and Oak Ridge National Laboratory.

The details of the OTPC detector were given in Ref. [1]. The changes made in the detector for 2011 experiment are described in Ref. [3]. In short OTPC is a gaseous detector with optical readout. The ions are implanted in the detector, where after short time the decay takes place. Primary ionisation electrons are travelling in electric field with a known velocity towards amplification stages. After the amplification, the signal is converted to visible light and registered with a CCD camera and a photomultiplier tube (PMT) read out by a fast oscilloscope. The CCD image provides information on event's 2D projection, while PMT records light intensity as a function of time, giving information on 3rd dimension as well as timing information of events registered.

CASE OF ^{43}Cr

The ^{43}Cr was studied at GANIL in several experiments, the results of which are presented in Ref. [4]. The half-life for ^{43}Cr was found to be $T_{1/2} = 21.1(4)\text{ms}$, and based on registered proton energies 10 transitions were identified. One of those transitions was suspected to come from $\beta 2p$ decay.

During 2007 experiment we collected in total 40000 events identified as ^{43}Cr . Due to different acquisition modes used (see Ref. [5]) only 30000 events were used to determine relative branching ratios. Among these we found 11502 βp events, 1010 $\beta 2p$ events and 12 events that pictured β -delayed emission of three protons. The $\beta 3p$ decay channel in ^{43}Cr was observed for the first time, and only one other nucleus is known to decay in such a way - ^{45}Fe studied in the same experiment [2]. Figure 1 shows one of the registered $\beta 3p$ events. Using above numbers we have determined relative branching ratios to be 91.8(3)%, 8.1(3)%, and 0.096(30)% for the β -delayed one-, two-, and three-proton emission, respectively. The half-life of ^{43}Cr was determined to be $T_{1/2} = 20.6(9)\text{ ms}$.

To determine the absolute branching ratio, one requires probability of β -decay without emission of any protons. This was found by using maximum likelihood method, as described in Ref. [5]. The resulting probability of β -decay without emission of protons was determined to be $b_0 = 0.12 \pm 0.04$. With this number the absolute branching ratios were calculated to be 81(4)%, 7.1(3)%, and 0.08(3)% for β -delayed one-, two-, and three-proton emission, respectively.

We note that probability of β decay of ^{43}Cr without emission of any protons is surprisingly high, as the transmission to ^{43}V ground state is first forbidden unique [6] and the proton separation energy is estimated to be only 280 keV [7].

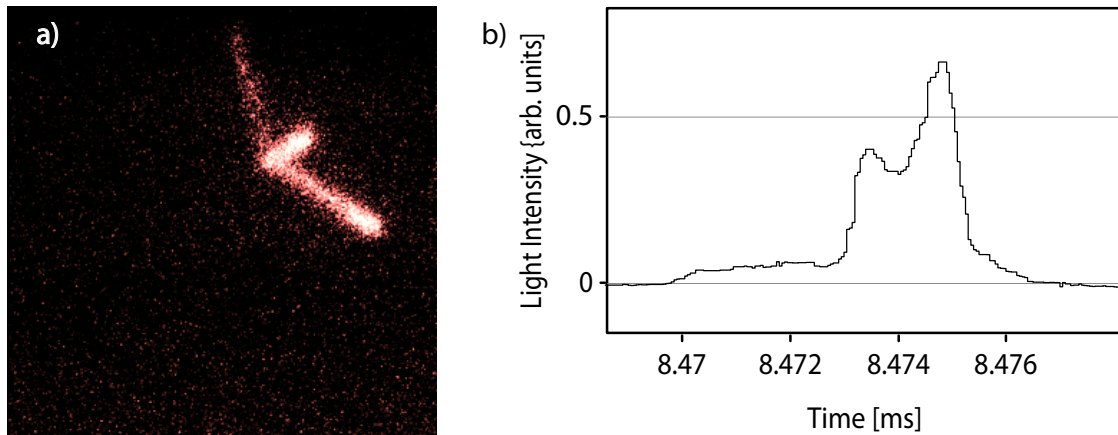


FIGURE 1. Example of a $3\beta p$ decay of ^{43}Cr . a) A CCD image showing tracks of 3 protons (ion's track is not visible). b) Signal from the PMT, where also 3 components are visible.

CASE OF ^{48}Ni

In the latest experiment with use of the OTPC, we were studying extremely neutron deficient ^{48}Ni , the nucleus with the third component of isospin $T_z = -4$. This nucleus was predicted to be a possible 2p precursor by a number of theoretical works [8, 9, 10, 11] and was first observed in GANIL by Blank et al. [12]. In later experiment Dossat et al. [13] were able to implement four ^{48}Ni ions in a Si detector and to record the emitted protons energy. Energy of one of the registered events was 1.35 MeV, which is consistent with predictions for 2p decay of ^{48}Ni [8, 9, 10, 11]. The half-life was determined to be $T_{1/2} = 2.1_{-0.7}^{+2.1}$ ms.

In our experiment, during 156 hours, we identified 10 events of ^{48}Ni . Only 6 of these could be further analysed, with 4 of them picturing 2p decays and remaining 2 β -delayed emission of proton. An example of a 2p event (followed by emission of a β -delayed proton from its daughter) is presented in Fig. 2.

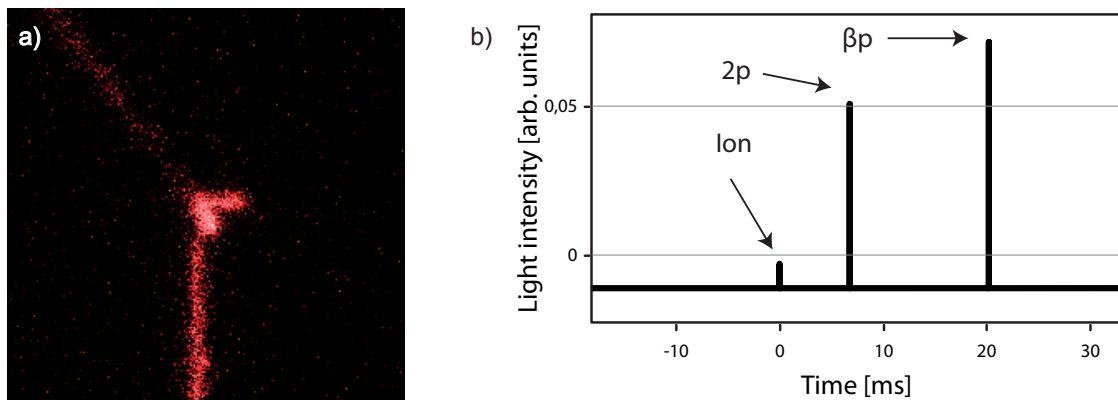


FIGURE 2. An example event of 2p decay of ^{48}Ni . a) CCD image showing a track of implantation of heavy ion (coming from the bottom), 2 short tracks of protons emitted in 2p decay, and a long track of a β -delayed proton from the daughter. b) Signal from the PMT presenting the timing sequence of events.

Using signals from the PMT and the CCD we have estimated the total energy of protons in four 2p events utilizing simplified 3D reconstruction procedure. Taking the tracks lengths and the SRIM code [14], we calculated energies of particles. The resulting decay energies are 1.35(12)MeV, 1.34(16)MeV, 1.27(10)MeV and 1.21(13)MeV. The average of these is 1.28(6)MeV which is in reasonable agreement with theoretical predictions [8, 9, 10, 11] and the value reported by Dossat et al. [13].

Based on the event counts, branching ratios are $P_{2p} = 0.7(2)$ and $P_{\beta p} = 0.3(2)$ for 2p emission and βp emission, respectively. Using the maximum likelihood method the half-life of ^{48}Ni is found to be $T_{1/2} = 2.1_{-0.6}^{+1.4}$ ms. The partial half-lives are $T_{1/2}^{2p} = 3.0_{-1.2}^{+2.2}$ ms and $T_{1/2}^{\beta} = 7.0_{-5.1}^{+6.6}$ ms for 2p and β decays, respectively. While the half-life is in excellent agreement with previous findings of Ref. [13], branching ratios and the partial half-lives differ significantly.

In the setting on ^{48}Ni also events of ^{46}Fe and ^{44}Cr were being recorded. The decay analysis of these nuclei will be soon carried out and published in a separate paper.

ACKNOWLEDGMENTS

This work was supported by the U.S. National Science Foundation under grant number PHY-06-06007, and the U.S. Department of Energy under contracts DE-FG02-96ER40983, DEFC03-03NA00143 and DOE-AC05-00OR22725, by the ORNL LDRD Wigner Fellowship WG11-035 (KM) and by the National Nuclear Security Administration under the Stewardship Science Academic Alliances program through DOE Cooperative Agreement No. DE-FG52-08NA28552.

REFERENCES

1. K. Miernik et al., Nucl. Instr. and Methods A 581, 194–197 (2007).
2. K. Miernik et al., Eur. Phys. J. A 42, 431–439 (2009).
3. M. Pomorski et al., Phys. Rev. C 83, 061303(R)-1–4 (2011).
4. C. Dossat et al., Nucl. Phys. A 792, 18–86 (2007).
5. M. Pomorski et al., Phys. Rev. C 83, 041306-1–5 (2011).
6. E.K. Warburton and D.E. Alburger, Phys. Rev. C 38, 2822–2837 (1988).
7. G. Audi et al., Nucl. Phys. A 729, 3–128 (2003).
8. B. A. Brown, Phys. Rev. C 43, R1513–R1517 (1991).
9. B. J. Cole, Phys. Rev. C 54, 1240–1248 (1996).
10. W. E. Ormand, Phys. Rev. C 55, 2407–2417 (1997).
11. W. Nazarewicz et al., Phys. Rev. C 53, 740–751 (1996).
12. B. Blank et al., Phys. Rev. Lett. 84, 1116–1119 (2000).
13. C. Dossat et al., Phys. Rev. C 72, 054315-1–5 (2005).
14. J.F. Ziegler, The Stopping and Range of Ions in Matter(SRIM), <http://www.srim.org>.

Lifetime Measurements of Tagged Exotic- and Unbound Nuclear States.

D.M. Cullen^a

^aSchuster Laboratory, School of Physics and Astronomy, The University of Manchester, Manchester, M13 9PL, UK

Abstract. A new Differential Plunger device for measuring pico-second lifetimes of Unbound Nuclear States (DPUNS) is being built at The University of Manchester. DPUNS has been designed to work with alpha-, beta- and isomer-tagging methods using the existing JUROGAM II – RITU - GREAT infrastructure at the University of Jyvaskyla, Finland. The importance of proton emission from nuclei is that it provides valuable nuclear-structure information as direct input to nuclear models beyond the drip line. New experimental data beyond the drip line can provide new extensions to these models especially with the possible coupling of weakly bound and unbound states to the continuum. The results of the first experiments to measure lifetimes of unbound nuclear states with this method was discussed along with possible future experiments which can be addressed with DPUNS using proton-, isomer- and alpha-tagging.

Keywords: Lifetime measurements, effective charges, Recoil-isomer tagging, Proton-decay tagging, Differential plunger.

PACS: 21.10.Tg, 23.20.Lv, 27.60.+j.

MOTIVATION

In recent years, the universal shell-model parameters are starting to be recognized as a more local concept for near-stable nuclei. As the nucleon drip lines are approached, the mean field is expected to be modified by various effects. In neutron-rich nuclei, the mean field was recently demonstrated to be dependent on the occupation of particular orbits due to Tensor components of the effective interactions [1]. At the other extreme, near the proton-drip line where separation energies are small, coupling to the continuum is expected to modify the energies of the states. Furthermore, as pointed out by Bohr and Mottelson, nuclear polarization charges depend on the coupling of the particle motion to the iso-scalar and iso-vector modes of the giant quadrupole resonances [2]. In this model, the iso-vector part is proportional to the deviation of the nuclear isospin from its mean value of $(N-Z)/A$. A study of this effect has been made by measuring lifetimes for a series of neutron-rich B isotopes [3]. This study in comparison with various shell model interactions revealed evidence for reduced neutron polarization charges as the deviation of the nuclear isospin from its mean value of $(N-Z)/A$ increased towards the neutron drip line. The focus of the present work is the corresponding study to measure the lifetimes of nuclear states at and beyond the proton drip line to gain information on the possible modification of the effective charges by the coupling to the continuum [4].

A study of the lifetimes of excited nuclear states beyond the proton drip line requires highly-selective techniques to be employed. These unbound nuclear states are produced with cross-sections of order $0.1 - 40 \mu\text{b}$ out of a total fusion cross section of order $\sim 1 \text{ mb}$. As an example, the ability to select such weakly produced nuclear states has relied on several tagging techniques such as Recoil-Decay (RD) and Isomer-Decay (ID) Tagging using the Recoil-Ion Transport Unit (RITU) at the University of Jyväskylä [5,6]. More recently, these selection techniques have been complemented by the addition of the Köln differential plunger to extract the lifetimes of weakly populated states above isomers [7] and proton-unbound states [8]. Figure 1 shows the schematic setup for extracting lifetimes of unbound nuclear states at the University of Jyväskylä.

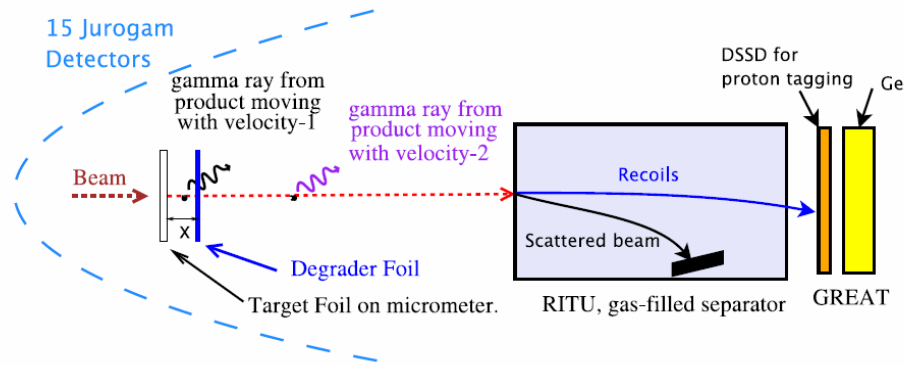


FIGURE 1. Schematic experimental setup used to extract lifetimes of unbound nuclear states at the University of Jyväskylä. Recoils are identified by their proton decay at the focal plane of RITU and are re-associated with the earlier prompt radiation at the target using the trigger-less Total Data Readout (TDR). The Köln plunger is placed around the target and lifetimes are deduced from consideration of the number of counts in the fully-shifted and degraded-components of a particular gamma-ray transition as a function of distance, x between the target and degrader foil.

These experiments typically require about 14 days of beam time to gain sufficient statistical accuracy in the final lifetime values. Figure 2 shows the lifetime measurements on the unbound nuclear states in the $T_Z=5$ nucleus ^{144}Ho using the Köln plunger with isomer-tagging methods [7].

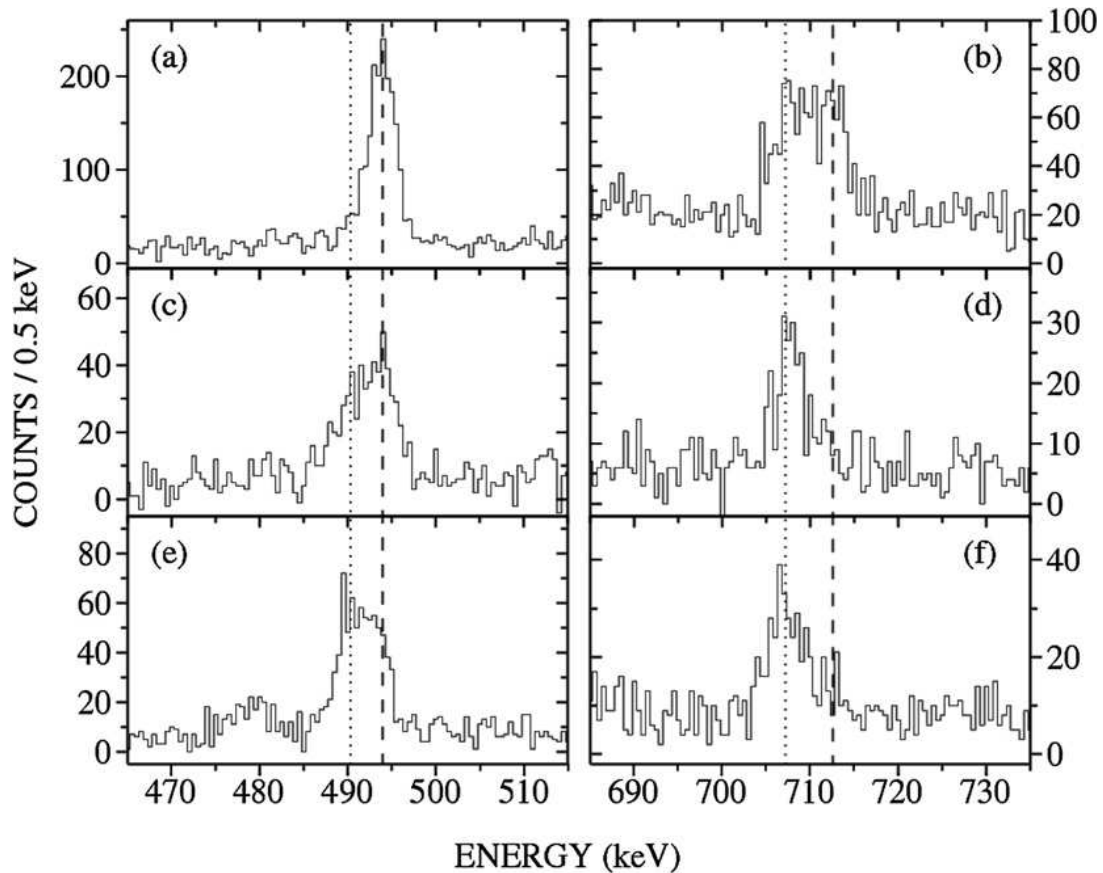


FIGURE 2. γ -ray spectra from the isomer-tagged differential plunger experiment on unbound states in ^{144}Ho [7]. The figure shows the splitting of the 502-keV transition (left) and the 724-keV transition (right) into their fully-shifted and degraded components in the Jurogam detectors at 134° . The spectra were recorded at target-to-degrader distances of $8.5(2) \mu\text{m}$ [Panels (a) and (b)], $42.3(2) \mu\text{m}$ [Panels (c) and (d)], and $68.7(6) \mu\text{m}$ [Panels (e) and (f)]. No Doppler correction has been applied to the spectra. The dotted and dashed lines show the approximate position of the fully-shifted and degraded components of the peaks, respectively.

The contribution by M.G. Procter at these proceedings showed the state-of-the-art results of what can be currently be achieved using the Köln plunger with proton tagging in ^{109}I at the University of Jyväskylä [8]. This experiment represents the current limit ($\sim 40 \mu\text{b}$) for extracting lifetimes beyond the proton drip line with 14 days of beam time. In order to progress further, a new differential plunger design has almost been completed at the University of Manchester. The contribution by M.J. Taylor at these proceedings discusses the design and status of construction of the new Differential-Plunger for Unbound Nuclear States (DPUNS). This device will allow nuclei with smaller cross-sections ($\sim 4 \mu\text{b}$) to be studied as it has been designed specifically to work within the 1mb He gas of the RITU gas-filled separator. Beam time has already been approved for the first commissioning experiments with DPUNS which are expected to take place in early 2012 at the University of Jyväskylä.

ACKNOWLEDGMENTS

DPUNS is based on the Köln differential plunger with several modifications. The work of A. Smith (design), V. Twist (manufacture) and M. Taylor (construction and assembly) at the University of Manchester are gratefully acknowledged. Some of the components have been constructed at the workshops of the Universities of Liverpool and Jyväskylä. This work has been supported by the EU 6th Framework Programme, "Integrating Infrastructure Initiative Transnational Access," Contract 506065 (EURONS), and by the Academy of Finland under the Finnish Centre of Excellence Programme 2006-2011 (Nuclear and Accelerator Based Physics Programme at JYFL). The authors acknowledge the support of the EPSRC/IN2P3 LOANPOOL and GAMMAPOOL for the loan of the JUROGAM detectors. DPUNS and D.M.C. are supported by STFC under the grant number ST/G008787.

REFERENCES

1. T. Otsuka et al., *Phys. Rev. Lett.* 104, 012501 (2010); G. Colo et al., *Phys. Letts. B*, 646 (2007) 227; T. Otsuka et al., *Phys. Rev. Lett.* 97, 162501 (2006).
2. A. Bohr and B.R. Mottelson, *Nuclear Structure* (Benjamin Reading, MA 1969), Vol. 1;
3. H. Ogawa, *Phys. Rev. C* **67**, 064308 (2003).
4. I. Hamamoto and B.R. Mottelson, *C.R. Physique* 4 (2003) 433.
5. M. Petri *et al.* *Phys. Rev. C* **76** 054301 (2007).
6. D.M. Cullen *et al.*, *Phys. Rev. C* **58**, 847 (1998).
7. P.J. R. Mason *et al.*, *Phys. Lett. B* 683, 17 (2010).
8. M.G. Procter *et al.* Submitted to *Phys. Lett. B* (June 2011).

Lifetime measurement in the proton-unbound nucleus ^{109}I .

M.G. Procter^{*}, D.M. Cullen^{*,†}, P. Ruotsalainen[†], C. Scholey[†], L. Angus^{**},
T. Bäck[‡], B. Cederwall[‡], A. Dewald[§], C. Fransen[§], T. Grahn^{¶,†},
P.T. Greenlees[†], M. Hackstein[§], U. Jakobsson[†], P. M. Jones[†], R. Julin[†],
S. Juutinen[†], S. Ketelhut[†], M. Leino[†], N.M. Lumley^{*}, P.J. R. Mason^{*},
P. Nieminen[†], M. Nyman^{†,||}, J. Pakarinen[¶], T. Pissulla[§], P. Peura[†],
P. Rahkila[†], J. Revill[¶], S. V. Rigby[¶], W. Rother[§], M. Sandzelius[†], J. Sarén[†],
J. Sorri[†], M.J. Taylor^{*}, J. Uusitalo[†], P. Wady^{**}, C. Qi[‡] and F.R. Xu^{††}

^{*}*Schuster Laboratory, University of Manchester, Manchester M13 9PL, UK*

[†]*Department of Physics, University of Jyväskylä, FIN-40014 Jyväskylä, Finland*

^{**}*University of The West of Scotland, High Street, Paisley PA1 2BE, UK*

[‡]*Department of Physics, Royal Institute of Technology, SE-10691 Stockholm, Sweden*

[§]*Institut für Kernphysik, Universität zu Köln, D-50937, Köln, Germany*

[¶]*Oliver Lodge Laboratory, University of Liverpool, Liverpool L69 7ZE, UK*

^{||}*Department of Physics, University of Helsinki, FIN-00014 Helsinki, Finland*

^{††}*Department of Technical Physics, Peking University, Beijing 100871, China*

Abstract. The Recoil-Distance Doppler-shift method has been combined with Recoil-Decay Tagging for the first time to measure a lifetime in the proton-unbound nucleus ^{109}I . The lifetime value was determined using the Differential Decay-Curve method in singles mode. The result has been compared to theoretical shell-model calculations in order to better understand the nature of unbound valence nucleons at the proton drip line.

Keywords: RDDS, Lifetimes, DDCM, proton-unbound

PACS: 21.20.Tg, 23.20.Lv, 27.60.+j.

INTRODUCTION

The lifetimes of states in exotic nuclei, specifically those residing along the proton drip line, are neither well established nor understood. This results from the subtle interplay between *microscopic* single-particle and *macroscopic* collective effects, which are difficult to model at such extremes of existence. Knowledge of the effects of axially asymmetric shapes on the proton tunnelling rates of these nuclei is required in order to be able to assign specific single-particle configurations to the decaying states [1–5]. In this work, a lifetime measurement has been made for the first excited $11/2^+$ state in the proton-unbound nucleus ^{109}I using the Recoil-Distance Doppler-shift (RDDS) technique in conjunction with Recoil-Decay Tagging (RDT), for the first time.

EXPERIMENT

Excited states were populated in ^{109}I via the $^{58}\text{Ni}(^{54}\text{Fe},\text{p}2\text{n})^{109}\text{I}$ reaction. The K130 cyclotron at the Accelerator Laboratory of the University of Jyväskylä was used to accelerate an $^{54}\text{Fe}^{11+}$ beam at an energy of 206 MeV onto a 1 mg/cm^2 ^{58}Ni foil located at the centre of the PRE-JUROGAM II spectrometer [6]. The beam current averaged 2.5 pA over an approximate running time of 245 h. Prompt transitions were observed in Ring 2 of the PRE-JUROGAM II array, comprising 10 single-crystal Ge detectors, at a backward angle of 134° to the beam line. The photopeak efficiency of Ring 2 was $\sim 1.5\%$ at 1332 keV. The fusion-evaporation products passed through a 1 mg/cm^2 Mg degrader foil, housed within the Köln plunger device [7]. The degrader foil was used to reduce the full velocity of recoiling reaction products from $v/c = 0.036(3)$ to $0.027(4)$. The reaction products were separated from beam-like nuclei by the gas-filled recoil separator, RITU [8, 9] and transported to the GREAT focal-plane spectrometer [10], where they implanted into the Double-sided Silicon Strip Detectors (DSSD) [11]. Subsequent proton decays were detected and correlated with ^{109}I recoils using a pixel-by-pixel search routine within the sort-code. A search time of $300\ \mu\text{s}$ between recoil implantation and proton emission allowed delayed proton decays associated with ^{109}I to be correlated with prompt γ decays at the target position. Figure 1 shows both the recoil and recoil-proton tagged spectra for a target-to-degrader distance of $73(1)\ \mu\text{m}$ as well as the DSSD proton-decay spectrum for ^{109}I . All events were time stamped by a 100 Mhz clock through the

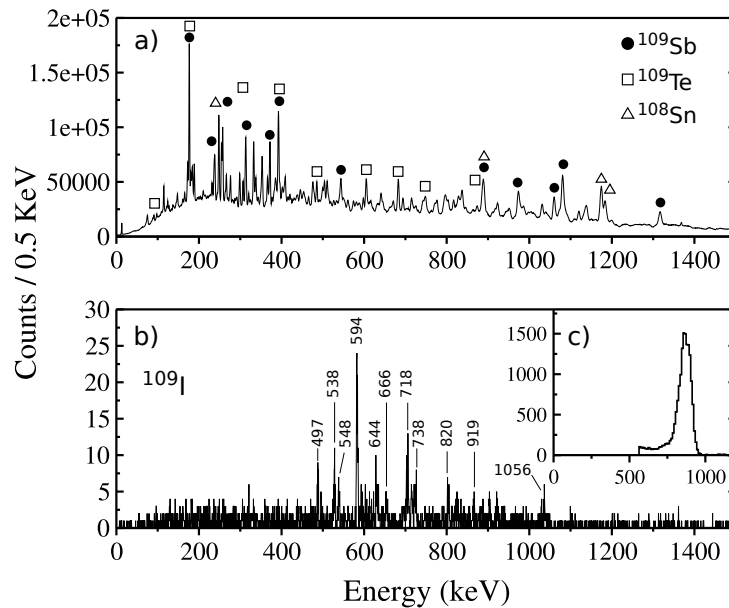


FIGURE 1. (a) Recoil-gated prompt γ -ray transitions in Ring 2 of the PRE-JUROGAM II spectrometer at a target-to-degrader distance of $73(1)\ \mu\text{m}$. Transitions associated with the nuclei ^{109}Sb , ^{109}Te and ^{108}Sn , produced with the highest cross sections, are highlighted. (b) Prompt γ -ray spectrum gated by the energy window from 600 to 920 keV and the region of time from 0 to $300\ \mu\text{s}$. (c) DSSD spectrum of proton decays associated with ^{109}I gated on a time region between 0 and $300\ \mu\text{s}$.

triggerless Total Data Readout (TDR) acquisition system [12] and collected to disk. On- and off-line sorting was carried out using the GRAIN software package [13].

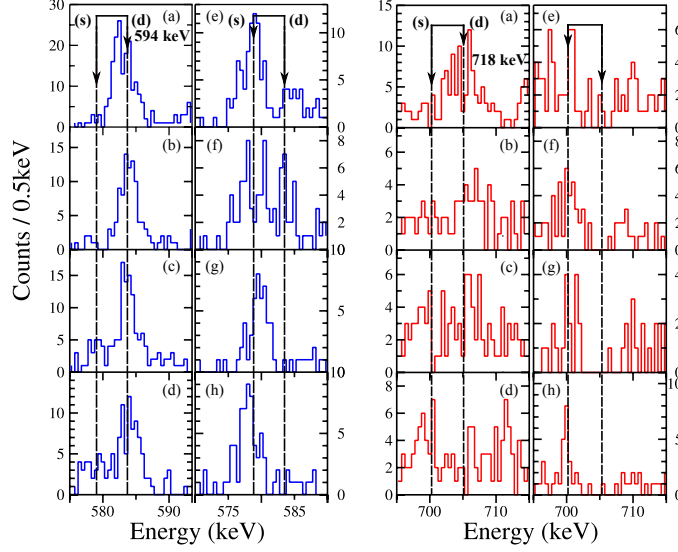


FIGURE 2. (Color online) Recoil-proton-tagged prompt spectra of the $(11/2^+) \rightarrow (7/2^+)$ and $(15/2^+) \rightarrow (11/2^+)$ transitions in ^{109}I . Each panel corresponds to a specific target-to-degrader distance: (a) 9.0(1)-; (b) 73(1)-; (c) 101(3)-; (d) 215(5)-; (e) 415(5)-; (f) 500(4)-; 801(6)- and (g) 1995(25) μm . The fully Doppler-shifted and degraded peaks for both the 594- and 718-keV transitions have been highlighted. No Doppler correction has been applied to the spectra.

Lifetime data were collected using the Recoil-Distance Doppler-Shift (RDDS) technique. Fully Doppler-shifted and degraded photo-peaks were tracked through eight target-to-degrader distances of 9.0(1), 73(1), 101(3), 215(5), 415(5), 500(4), 801(6) and 1995(25) μm . The lifetime data were analyzed using the Differential Decay Curve Method (DDCM) [14, 15]. In the DDCM, lifetime values are determined for each target-to-degrader distance by a χ^2 minimization fit to the normalized fully-shifted components of each transition. The final lifetime value is determined from a weighted average of lifetime values that lie within the so-called ‘region of sensitivity’. This region covers the particular range within which the final lifetime can be determined with a relatively small error. It is also important to note that within this technique it is only the relative target-to-degrader distances which are required and not the absolute distances.

RESULTS AND DISCUSSION

Figure 2 shows spectra obtained for each of the eight distances for both the 594- and 718-keV transitions. The positions of the fully Doppler-shifted and degraded peaks have been highlighted. In order to determine a value for the lifetime of the $(11/2^+)$ state, it was necessary to include in the DDCM analysis the measured intensities of the fully Doppler shifted and degraded components of the two other feeding transitions; 548- and 1056-keV γ rays. Assuming that the time behavior of the observed feeding transitions were similar to that of the $(11/2^+)$ state allowed a lifetime of ~ 15 ps to be measured. Figure 3 shows the fitting procedure used to determine the lifetime of the $(11/2^+)$ state. The near unity value of the summed intensities of the feeding transitions showed that

any contributions from unobserved side feeding would be very small and consequently effects from such feeding was not incorporated into the analysis.

The experimentally derived value of $\beta_2 = 0.11(1)$ is in agreement with that predicted by Möller *et al.* [16], however comparisons with shell-model calculations reveal an overestimation of the reduced transition probability [17]. This theoretical overestimation is not observed in comparisons with the experimental data for the lower-mass $N = 56$ isotone ^{108}Te [18]. The reason behind the differences observed in ^{109}I is thought to arise from the inability of shell-model calculations to correctly account for the properties of unbound nuclear states. The core-polarization effects from unbound nucleons is not well known, and an *ad hoc* modification of the effective charges is not sufficient to be able to resolve this discrepancy, especially when so far from stability. The full details of the theoretical calculations and comparisons with the data is given in Ref. [17].

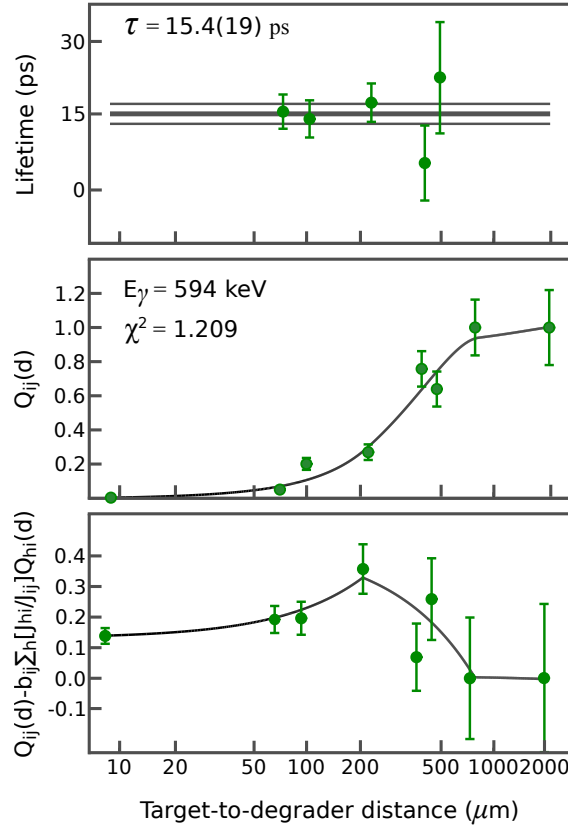


FIGURE 3. (Color online) Lifetime analysis using the DDCM for the $(11/2^+) \rightarrow (7/2^+)$ transition in the ground-state band of ^{109}I . The middle panel shows the Intensity of the Doppler-shifted component of the 594-keV transition feeding the ground state. The values were taken from data collected in Ring 2 of the PRE-JUROGAM II array. The data points have been fitted piecewise with a number of second-order polynomials. The bottom panel displays the difference in intensities of the degraded components of the 594-keV γ ray and the combined 1056-, 718- and 548-keV γ rays that feed the $(11/2^+)$ state. These points have been simultaneously fitted with the derivative of the fitting function in the middle panel multiplied by the value of the lifetime $\tau_i(d)$. A χ^2 minimisation of the fit yields the values of the lifetime, displayed in the top panel, for each target-to-degrader distance.

ACKNOWLEDGMENTS

This work has been supported by the EU 6th Framework Programme, “Integrating Infrastructure Initiative Transnational Access,” Contract 506065 (EURONS), and by the Academy of Finland under the Finnish Centre of Excellence Programme 2006-2011 (Nuclear and Accelerator Based Physics Programme at JYFL). The authors acknowledge the support of the GAMMAPOOL for the loan of the JUROGAM detectors. MGP/DMC/MJT acknowledge support by the STFC. PTG acknowledges the support of the Academy of Finland through Contract No. 119290. TB/BC/RL/CQ acknowledge the support of the Swedish Research Council under Grant Nos. 623-2009-7340, 621-2010-3694 and 2010-4723, and The Nordic Infrastructure support under NordForsk (Project No. 070315).

REFERENCES

1. S. Åberg, P. B. Semmes, and W. Nazarewicz, *Phys. Rev. C* **56**, 1762–1773 (1997).
2. E. Medeiros, M. Rodrigues, S. Duarte, and O. Tavares, *The European Physical Journal A - Hadrons and Nuclei* **34**, 417–427 (2007).
3. L. S. Ferreira, and E. Maglione, *Nuclear Physics A* **752**, 223 – 226 (2005), proceedings of the 22nd International Nuclear Physics Conference (Part 2).
4. E. Maglione, L. S. Ferreira, and R. J. Liotta, *Phys. Rev. C* **59**, R589–R592 (1999).
5. E. Maglione, L. S. Ferreira, and R. J. Liotta, *Phys. Rev. Lett.* **81**, 538–541 (1998).
6. P. T. Greenlees, N. Amzal, J. E. Bastin, E. Bouchez, P. A. Butler, A. Chatillon, O. Dorvaux, S. Eeckhaudt, K. Eskola, B. Gall, J. Gerl, T. Grahn, A. Görgen, N. J. Hammond, K. Hauschild, R.-D. Herzberg, F.-P. H. berger, R. D. Humphreys, A. Hürstel, D. G. Jenkins, G. D. Jones, P. Jones, R. Julin, S. Juutinen, H. Kankaanpää, A. Keenan, H. Kettunen, F. Khalfallah, W. Korten, P. Kuusiniemi, Y. L. Coz, M. Leino, A.-P. Leppänen, M. Muikku, P. Nieminen, J. Pakarinen, P. Rahkila, P. Reiter, M. Rousseau, C. Scholey, C. Theisen, J. Uusitalo, J. Wilson, and H.-J. Wollersheim, *AIP Conference Proceedings* **764**, 237–242 (2005), URL <http://link.aip.org/link/?APC/764/237/1>.
7. L. Cleemann, J. Eberth, W. Neumann, N. Wiehl, and V. Zobel, *Nuclear Instruments and Methods* **156**, 477 – 482 (1978), ISSN 0029-554X, URL <http://www.sciencedirect.com/science/article/B73DN-471XJ0B-1YX/2/d0f6566401c643e115d9de8ac130cc9c>.
8. M. Leino, J. ÄdystÄü, T. Enqvist, P. Heikkinen, A. Jokinen, M. Nurmia, A. Ostrowski, W. H. Trzaska, J. Uusitalo, K. Eskola, P. Armbruster, and V. Ninov, *Nuclear Instruments and Methods in Physics Research Section B: Beam Interactions with Materials and Atoms* **99**, 653 – 656 (1995), ISSN 0168-583X, URL <http://www.sciencedirect.com/science/article/B6TJN-43JWW5R-67/2/47f1773b6eb6b4121236943396feef57>.
9. M. Leino, *Nuclear Instruments and Methods in Physics Research Section B: Beam Interactions with Materials and Atoms* **126**, 320 – 328 (1997), ISSN 0168-583X, URL <http://www.sciencedirect.com/science/article/B6TJN-3V15680-2D/2/c964bf63386872dd1a25ae512cb28ddc>.
10. R. D. Page, A. N. Andreyev, D. E. Appelbe, P. A. Butler, S. J. Freeman, P. T. Greenlees, R. D. Herzberg, D. G. Jenkins, G. D. Jones, P. Jones, D. T. Joss, R. Julin, H. Kettunen, M. Leino, P. Rahkila, P. H. Regan, J. Simpson, J. Uusitalo, S. M. Vincent, and R. Wadsworth, *Nuclear Instruments and Methods in Physics Research Section B: Beam Interactions with Materials and Atoms* **204**, 634 – 637 (2003), ISSN 0168-583X, URL <http://www.sciencedirect.com/science/article/B6TJN-47MHV52-B/2/5407c5ba07f5804725a2636a7bc02384>.
11. P. T. Greenlees, N. Amzal, J. E. Bastin, E. Bouchez, P. A. Butler, A. Chatillon, O. Dorvaux, S. Eeckhaudt, K. Eskola, B. Gall, J. Gerl, T. Grahn, A. Görgen, N. J. Hammond, K. Hauschild, R. D. Herzberger, F. P. Hessberger, R. D. Humphreys, A. Hürstel, D. G. Jenkins, G. D. Jones, P. Jones, R. Julin, S. Juutinen, H. Kankaanpää, A. Keenan, H. Kettunen, F. Khalfallah, T. L. Khoo, W. Korten, P. Kuusiniemi, Y. L. Coz, M. Leino, A. P. Leppänen, M. Muikku, P. Nieminen, J. Pakarinen, P. Rahk-

- ila, P. Reiter, M. Rousseau, C. Scholey, C. Theisen, J. Uusitalo, J. Wilson, and H. J. Wollersheim, *European Physical Journal A* **25**, 599–604 (2005), URL <http://www.springerlink.com/content/k32r5g8462323708/>.
12. I. Lazarus, E. Appelbe, P. Butler, P. Coleman-Smith, J. Cresswell, S. Freeman, R. Herzberg, I. Hibbert, D. Joss, S. Letts, R. Page, V. Pucknell, P. Regan, J. Sampson, J. Simpson, J. Thornhill, and R. Wadsworth, *Nuclear Science, IEEE Transactions on* **48**, 567–569 (2001), ISSN 0018-9499.
 13. P. Rahkila, *Nuclear Instruments and Methods in Physics Research Section A: Accelerators, Spectrometers, Detectors and Associated Equipment* **595**, 637 – 642 (2008), ISSN 0168-9002, URL <http://www.sciencedirect.com/science/article/B6TJM-4T84JX6-3/2/1cda064f7c44c3eb26086fa5b03490f7>.
 14. A. Dewald, S. Harissopulos, and P. von Brentano, *Z. Phys. A* **334**, 163–175 (1989), ISSN 0930-1151, URL <http://www.springerlink.com/content/g240486w70504872/>.
 15. G. Böhm, A. Dewald, P. Petkov, and P. von Brentano, *Nuclear Instruments and Methods* **329**, 248 – 261 (1993), ISSN 0168-9002, URL <http://www.sciencedirect.com/science/article/B6TJM-4731HF1-20/2/45af3f8a1a118400b33182d569d20fcb>.
 16. P. Möller, R. Bengtsson, B. Carlsson, P. Olivius, T. Ichikawa, H. Sagawa, and A. Iwamoto, *Atomic Data and Nuclear Data Tables* **94**, 758 – 780 (2008), ISSN 0092-640X, URL <http://www.sciencedirect.com/science/article/pii/S0092640X08000399>.
 17. M. G Procter *et. al.*, *to be published* (2011).
 18. T. Bäck *et. al.*, *to be published* (2011).

Phoswich scintillator for proton and gamma radiation of high energy

O. Tengblad^{*}, T. Nilsson[†], MJG. Borge^{*}, J.A. Briz^{*}, M. Carmona-Gallardo^{*}, C. Cruz^{*}, V. Gugliemina^{*}, E. Nácher^{*}, A. Perea^{*}, J. Sanchez del Rio^{*}, M. Turrion Nieves^{*}, H. T. Johansson[†], J. Bergström[†], E. Blomberg[†], A. Bülling[†], E. Gallneby[†], J. Hagdahl[†], L. Jansson[†], K. Jareteg[†], R. Masgren[†], M. Nordström[†], G. Risting[†], S. Shojae[†] and H. Wittler[†]

^{*}*Instituto de Estructura de la Materia, CSIC, E-28006 Madrid, Spain*

[†]*Department of fundamental Physics, Chalmers Univ. of Technology, S-41296 Göteborg*

Abstract. We present here a Phoswich scintillator design to achieve both high resolution gamma ray detection, and good efficiency for high energy protons. There are recent developments of new high resolution scintillator materials. Especially the LaBr₃(Ce) and LaCl₃(Ce) crystals have very good energy resolution in the order of 3% for 662 keV gamma radiation. In addition, these materials exhibit a very good light output (63 and 32 photons/keV respectively).

A demonstrator detector in the form of an Al cylinder of 24 mm diameter and a total length of 80 mm with 2 mm wall thickness, containing a LaBr₃(Ce) crystal of 20 mm diameter and 30 mm length directly coupled to a LaCl₃(Ce) crystal of 50 mm length, and closed with a glass window of 5 mm, was delivered by Saint Gobain. To the glass window a Hamamatsu R5380 Photomultiplier tube (PMT) was coupled using silicon optical grease.

Keywords: scintillator material, phoswich, LaBr, LaCl, gamma detection

PACS: 20, 29.30, 29.40.Mc, 29.40.V

INTRODUCTION

The project R³B (Reactions with Relativistic Radioactive Beams) of FAIR (Facility for Antiproton and Ion Research) has as objective to study reactions with highly unstable exotic nuclei at high momentum transfer. Surrounding the target position a high efficiency gamma and proton spectrometer will be placed. This spectrometer should be able to measure the total energy of the cascade, the multiplicity and the individual energies of each gamma or proton with great efficiency and high resolution.

Here we are discussing a novel solution using scintillators of a new generation and detectors formed by two layers of crystals with a single readout, so called Phoswich.

Scintillators in phoswich formation

A phoswich (phosphor sandwich) detector consists of two or more layers of different scintillating materials. Here a phoswich combining two scintillators, LaBr₃(Ce) and LaCl₃(Ce) have been fabricated and tested. These relatively new materials are consid-

ered to be among the best inorganic scintillators available. $\text{LaBr}_3(\text{Ce})$ exhibits a bit better characteristics than $\text{LaCl}_3(\text{Ce})$, i.e. shorter decay time, higher stopping power, and higher energy resolution.

The signal from the phoswich detector will consist of a superposition of two pulses, originating in light emitted from the two crystals. A photon emitted from the $\text{LaBr}_3(\text{Ce})$ does not correspond to the same amount of deposited energy as a photon emitted by the $\text{LaCl}_3(\text{Ce})$. To determine the energy absorbed in each crystal, the information in the combined pulse has to be separated into its components. The factors of proportionality between the deposited energy in each scintillator have to be determined through a calibration process. Figure 1 illustrates how the expected superposed pulse along with its components may look like.

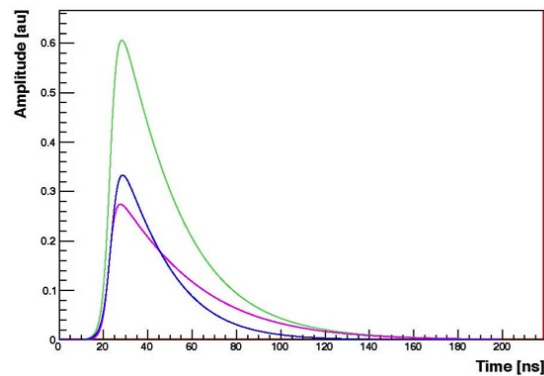


FIGURE 1. Example of a superimposed pulse (green, largest amplitude) and its two components: $\text{LaBr}_3(\text{Ce})$ (blue, second largest amplitude) and $\text{LaCl}_3(\text{Ce})$ (magenta). Note the different decay times of the two scintillator components.

The combination of scintillators used in a phoswich detector must be chosen carefully so that the scintillator attached to the PMT is transparent to the light emitted by the other crystal. Further, the pulse shapes of the light emitted from the different crystals must differ, e.g. by having different decay times. In our case the Brilliance350 [1] is transparent to the light emitted by the Brilliance380 [2], further, the decay time of the emission signals are slightly different, 28 and 16 ns respectively [3], which makes it possible to separate the output signal from each detector.

EXPERIMENTAL TEST OF PHOSWICH

Laboratory results using standard gamma sources

The phoswich prototype was tested in the laboratory using standard low-energy gamma sources (^{137}Cs , ^{60}Co and ^{22}Na). The following results were obtained with the phoswich detector mentioned above coupled to an 8 stage PMT-base. The aim was to distinguish the energy deposited in each of the two crystals, $\text{LaBr}_3(\text{Ce})$ and the $\text{LaCl}_3(\text{Ce})$.

For this test a standard slow coincidence set-up was used where the last dynode signal of the PMT was fed to a Timing Filter Amplifier (TFA) and from there to two separate Constant Fraction Discriminators (CFD) each with a different constant fraction delay.

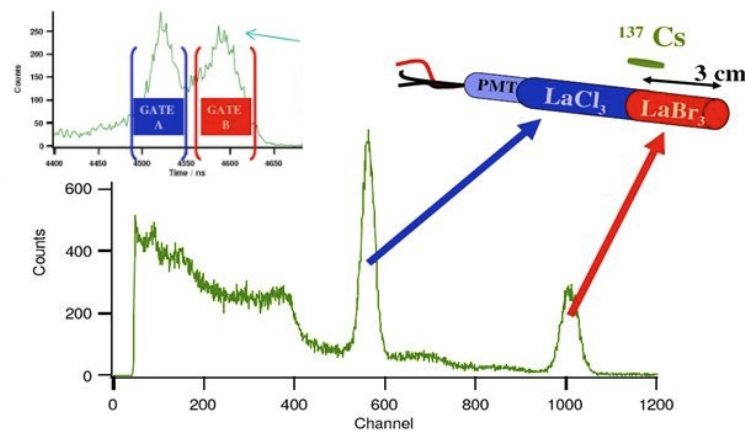


FIGURE 2. The resulting non-gated energy spectrum obtained when placing a ^{137}Cs source so that it irradiates the two crystal materials simultaneously. Due to the almost a factor of two difference in light yield, the 662 KeV gamma line show up twice at ch 1.000 due to the absorption in $\text{LaBr}_3(\text{Ce})$ and at 590 for the absorption in $\text{LaCl}_3(\text{Ce})$. The upper left inset shows the time spectrum obtained when passing the TFA signal via two separate CFD channels having different CFD-delays in order to optimize for the decay time of each scintillator.

The CFD signals were further coupled as START respectively STOP onto a Time to Amplitude Converter (TAC) and finally to a Multi Channel Analyzer (MCA) in order to optimize the CF delay for each module. Once optimized the CF-delay a threshold could be set on the TAC module and the output signal used as coincidence GATE onto the MCA when fed with the energy signal on the input. This energy signal was obtained from the anode pulse of the PMT that was sent via a preamplifier and a Spectroscopy Amplifier to the MCA.

It was shown possible to separate the two spectra of the two crystals in the phoswich detector, the one from the $\text{LaBr}_3(\text{Ce})$ crystal from the one from $\text{LaCl}_3(\text{Ce})$. Figure 2 shows the non-gated energy and time spectra obtained for a ^{137}Cs source in the position indicated in the figure. Depending on which gate (A or B) is being used the spectrum originating from the $\text{LaBr}_3(\text{Ce})$ and $\text{LaCl}_3(\text{Ce})$ respectively could be selected (not shown separately in the figure). The $\text{LaCl}_3(\text{Ce})$ has about half the light-yield compared to the $\text{LaBr}_3(\text{Ce})$ and thus the photo peak in the spectrum is situated at about half in channel number in comparison to the one of the $\text{LaBr}_3(\text{Ce})$ scintillator.

Response to high energy protons at TSL Uppsala

Experimental data for protons impinging on the phoswich detector were recorded in March 2009 at the The Svedberg Laboratory (TSL), Uppsala. A low intensity proton beam at 180 MeV provided by the Gustaf Werner Cyclotron [4] passed in air through an annular degrader of 25 mm Al in order to simultaneously obtain protons of 150

MeV (degraded) and 180 MeV (via hole) energy respectively. The detector prototype was positioned behind a Double Sided Si Strip Detector, providing position data of the incoming proton beam.

A flash ADC [5] was used to digitize the entire pulse using a 1 ns resolution for off-line analysis. The energy spectra and the resolution obtained for the high energy protons are shown in figure 3. Using the sampled signal a resolution (FWHM) of about 1 % was obtained. The standard electronic chain with PA and Shaper gave slightly better resolution but showing more pile-up events that were avoided by the sampling electronics.

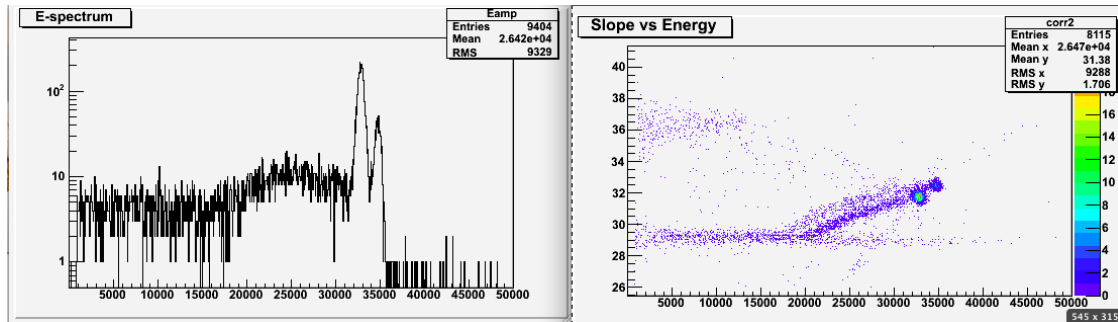


FIGURE 3. Energy spectrum for high energy protons of 150 and 180 MeV impinging on the phoswich. To the left it is shown the energy spectrum (*intensity vs adc channel*), and to the right it is shown the *pulse height vs total pulse*. The two strongly enhanced intensities are obtained when the protons are fully stopped in the detector. The 180 MeV protons leave less energy in the 1:st crystal and thus leaves the horizontal line (LaBr response) and goes onto the diagonal (LaCl response) earlier than in the case of the 150 MeV protons. All events outside the two main intensities are due to protons escaping the detector before depositing all energy.

ACKNOWLEDGMENTS

This work was partly financed by the Spanish Ministry of Science and Innovations under project FPA2009-07387, and partly by the Swedish Research Council. T.N. acknowledges support from the Royal Swedish Academy of Sciences via the Knut and Alice Wallenberg Foundation.

REFERENCES

1. BriLanCe 350 data sheet, Tech. rep., Saint-Gobain Ceramics & Plastics, Inc. (2004).
2. BriLanCe 380 data sheet, Tech. rep., Saint-Gobain Ceramics & Plastics, Inc. (2004).
3. O. Guillot-Noel, *Journal of Luminescence* **85**, 21 (1991).
4. The svedberg laboratory, Tech. rep. (2011), URL <http://www.tsl.uu.se/>.
5. E. Delagnes, and D. Breton, Documentation of the MATAQC32 board Rev. 1.8, Tech. rep., Dourdan, France (2006), URL <http://www.m2j-electronique.com/acquisition-boards/acquisition-boards.php>.

Digital signal processing for radioactive decay studies

D. Miller^{*}, D. Ackermann[†], R. Grzywacz^{*,**}, S. Heinz[†], F.P. Heßberger[†],
S. Hofmann[†], M. Madurga^{*}, K. Miernik^{**}, S.V. Paulauskas^{*},
K. Rykaczewski^{**} and H. Tan[‡]

^{}Department of Physics and Astronomy, University of Tennessee, Knoxville, TN 37996, United States*

[†]GSI Helmholtzzentrum für Schwerionenforschung, D-64220, Darmstadt, Germany

*^{**}Physics Division, Oak Ridge National Laboratory, Oak Ridge, TN 37831, United States*

[‡]XIA LLC, Hayward, CA 94544, United States

Abstract. The use of digital acquisition system has been instrumental in the investigation of proton and alpha emitting nuclei. Recent developments extend the sensitivity and breadth of the application. The digital signal processing capabilities, used predominately by UT/ORNL for decay studies, include digitizers with decreased dead time, increased sampling rates, and new innovative firmware. Digital techniques and these improvements are furthermore applicable to a range of detector systems. Improvements in experimental sensitivity for alpha and beta-delayed neutron emitters measurements as well as the next generation of superheavy experiments are discussed.

Keywords: Digital signal processing, data acquisition, superheavy elements, beta-delayed neutron emission

PACS: 29.85.Ca, 29.85.Fj, 29.30.-h

INTRODUCTION

Digital signal processing in nuclear structure experiments brings a host of benefits which improve the sensitivity of current experimental methods. Digital acquisition systems also are compact and versatile. For a number of different detector arrangements, digital electronics allow the correlation of events on arbitrary time scales with each electronics channel processed independently with the possibility of recording the shapes of the raw signals (“traces”) induced in the detector for further offline analysis.

Digital electronics have been instrumental in recent discoveries at the Holifield Radioactive Ion Beam Facility (HRIBF) [1, 2] enabling a host of experiments, many of which would not have been possible with traditional analog electronics [3, 4, 5, 6, 7, 8, 9]. The acquisition system has combined digitizers in the product line of XIA LLC with the traditional analysis framework in place at HRIBF. New Pixie-16 Revision D modules [10] now instrument several experimental setups. The versatility of the electronics allows the adaptation to research using a variety of detector systems. Recent developments focused on temporal correlations for superheavy element identification and beta-delayed neutron emission are discussed here.

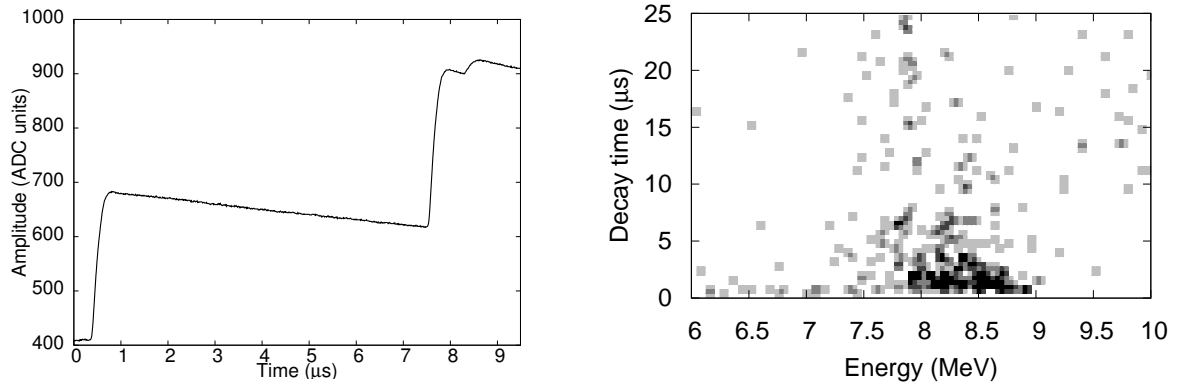


FIGURE 1. (Left) A trace captured in the “alpha catcher” mode where a pile-up is detected in the implantation detector and recorded. This event corresponds to two successive 7 MeV alpha decays followed by a low energy (~ 500 keV) scattered projectile-like implant during the beam-on period. (Right) Energy and time since the last correlated event for decays happening during the beam-off period in the silicon strip detector. Several weak alpha decays are visible with halfives on the order of several microseconds.

SUPERHEAVY ELEMENT SEARCH

A digital acquisition system consisting of five Pixie-16 module instrumented the detectors at the SHIP [11, 12] end-station in a recent experiment at GSI. Traditional analog electronics ran in parallel to the digital system. Correlations between the systems are possible using a combination of internal Pixie timestamp with either a standard time reference (“wall” clock) or an analog trigger counter included in the digital readout.

The primary goal of the experiment was to identify fusion residues following the reaction $^{248}\text{Cm} + ^{54}\text{Cr} \rightarrow ^{302}\text{120}^* \rightarrow ^{298,299}\text{120} + (4,3)n$. The expected halfives are on the order of $10 \mu\text{s}$ which lies on the limit of the capabilities of traditional analog electronics. If element 120 has a substantially shorter halfife, digital acquisition of the induced signal becomes imperative. Previous experiments have exhibited a sensitivity to decay halfives as small as 620 ns in a silicon strip detector using digital electronics [5]. The present experiment can easily identify decays which happen as soon as 300 ns following implantation, and the techniques are theoretically extensible down to ~ 100 ns. For time correlations smaller than $10 \mu\text{s}$, sufficient sensitivity requires analyses of recorded traces. To avoid the burden of high data rates associated with trace capture, the system used an innovative firmware which only captured traces when a second on-board trigger signal was detected in a short time window after an initial event (e.g. Figure 1).

This window corresponds to the time required for the energy filter to reach its peak amplitude for sampling. An energy filter with a long integration time was used to minimize noise and record all signals where the decay happened within $9 \mu\text{s}$ of the corresponding fusion residue implantation. A FIFO buffer for storing the relevant event data decreases the dead time of the acquisition sytem to virtually zero, which has been separately demonstrated up to count rates of 250 kHz per module recording $1 \mu\text{s}$ traces (~ 72 MB/s) where it becomes limited by the PCI bus readout.

The system considers all auxiliary information to categorize each event in a flexible developed software. This information includes: discriminated signal from a foil in front

of the implantation setup, digitized time-to-amplitude converter signals which measure the time of flight between 3 upstream foils as well as relative to the implantation signal, a silicon veto detector downstream of the implantation detector, as well as an upstream box of silicon detectors for decays that escape the implantation detector. After a cleanly-identified implant, correlated decays occur in the same strip with their characteristic decay energy and time as illustrated in Figure 1.

BETA-DELAYED NEUTRON EMISSION

Digital electronics also will implement the Versatile Array of Neutron Detectors at Low Energy (VANDLE) [13]: an array of plastic scintillator bars which will determine the neutron energy in the 100 keV to 10 MeV range using the time-of-flight method. These electronics are critical here to obtain a low energy threshold, but in order to obtain adequate energy resolution, the timing of the neutron interaction must be determined with a resolution finer than the sampling frequency of the Pixie-16 digitizers [14, 15].

Several considerations are important to obtain a sub-sample timing resolution for fast detectors (decay time ~ 2.1 ns). Here, it is vitally important to recognize that the front-end of the Pixie-16 modules includes an active Sallen-Key filter which cuts off sharply at the Nyquist frequency. The apparent digitized signal from a fast plastic scintillator only contains the remaining low-frequency components of the waveform. To accurately characterize the digitizer response, we first analyzed a varying amplitude signal with frequency characteristics similar to the BC-408 plastic scintillator. A functional form,

$$f(t) = \alpha e^{-\frac{t-t_0}{\lambda}} \left(1 - e^{-\frac{(t-t_0)^2}{\sigma}}\right), \quad (1)$$

characterized the response of the digitizer well, where the amplitude α and time t_0 are determined by minimizing the χ^2 on an event-by-event basis with fixed parameters λ and σ . The fluctuations in the time difference between the first signal and a delayed second signal from the same pulser determined the timing resolution for a given voltage as shown in Figure 2. We then performed a similar characterization for the plastic scintillator utilized in the VANDLE detectors. The results for a proof-of-principle experiment with the resulting resolution for beta-delayed neutrons are discussed elsewhere [14].

CONCLUSION

Digital acquisition systems can be applied with a high throughput to a wide variety of detectors with the same kind of module. Their use enables correlations to the shortest time scales, which may play a key importance for the newest superheavy element discovery. At the shortest time scales, detailed pulse-shape analysis can be employed for sub-sample time resolution for neutron time-of-flight measurements and is extensible for fast gamma-ray timing with BaF₂ detectors. Digital systems have been essential to the investigation of proton-emitting systems and will continue to be vital in discoveries on the forefront of nuclear structure research.

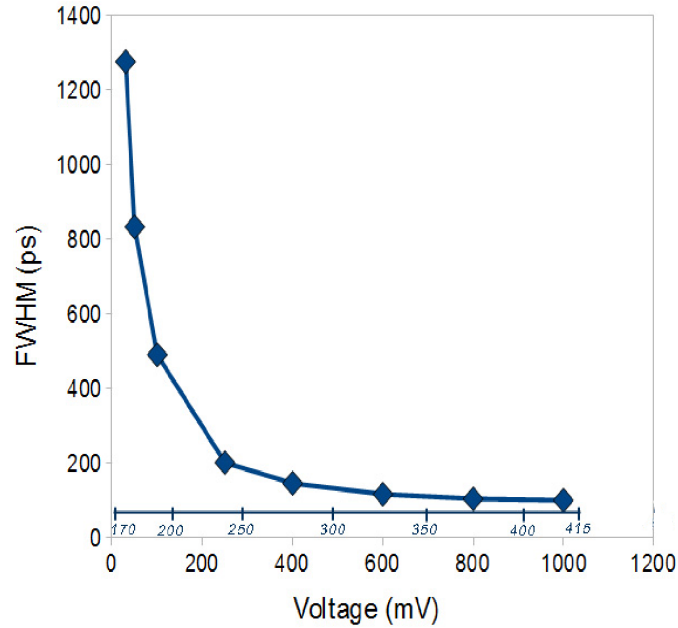


FIGURE 2. Time resolution obtained for pulser signals of different amplitudes from a Tektronix Arbitrary Function Generator. The inset scale shows the equivalent energy in keV deposited in the plastic scintillator by a proton for a signal of a given amplitude.

ACKNOWLEDGMENTS

This work is supported by the U.S. Department of Energy (DOE) under Grant No. DE-FG02-96ER40983 and in part by the National Nuclear Security Administration under the Stewardship Science Academic Alliances program through the DOE cooperative agreement DE-FG52-08NA28552.

REFERENCES

1. R. Grzywacz, *Nucl. Instrum. Methods B* **204**, 649 – 659 (2003).
2. R. Grzywacz, et al., *Nucl. Instrum. Methods B* **261**, 1103–1106 (2007).
3. W. Królas, et al., *Phys. Rev. C* **65**, 031303(R) (2002).
4. M. Karny, et al., *Phys. Rev. Lett.* **90**, 012502 (2003).
5. S. Liddick, et al., *Phys. Rev. Lett.* **97**, 082501 (2006).
6. C. Mazzocchi, et al., *Phys. Rev. Lett.* **98**, 212501 (2007).
7. M. Karny, et al., *Phys. Lett. B* **664**, 52 – 56 (2008).
8. J. Winger, et al., *Phys. Rev. Lett.* **102**, 142502 (2009).
9. I. G. Darby, et al., *Phys. Rev. Lett.* **105**, 162502 (2010).
10. DGF Pixie-16 – 100 MHz multichannel digital gamma finder in PXI format (2010), URL http://www.xia.com/DGF_Pixie-16.html, online, accessed 14 July 2011.
11. G. Münzenberg, et al., *Nucl. Instrum. Methods B* **26**, 294 – 300 (1987).
12. S. Hofmann, *Nucl. Instrum. Methods B* **126**, 310 – 315 (1997).
13. C. Matei, et al., *AIP Conf. Proc.* **1099**, 790–793 (2009).
14. M. Madurga, et al., *AIP Conf. Proc.* **1336**, 586–589 (2011).
15. S. Paulauskas, et al., Sub-nanosecond timing using 100 MHz digitizers (2011), in preparation.

A new differential plunger to measure lifetimes of unbound states in tagged exotic nuclei

M. J. Taylor^{*}, D. M. Cullen^{*}, A. J. Smith^{*}, V. Twist^{*}, P. M. Jones[†], P. Nieminen[†], T. Grahn[†], P. A. Butler^{**} and M. Scheck^{**}

^{*}*School of Physics & Astronomy, University of Manchester, Manchester M13 9PL, UK*

[†]*Department of Physics, University of Jyväskylä, FIN-40014 Jyväskylä, Finland*

^{**}*Department of Physics, University of Liverpool, Liverpool L69 7ZE, UK*

Abstract. A new differential plunger is being designed and built at the University of Manchester to measure lifetimes of unbound states in exotic nuclei approaching the proton drip-line. The device is designed to work in both vacuum and gas environments and will primarily be used in conjunction with the gas filled separator RITU at the University of Jyväskylä, Finland. This will enable the accurate measurement of excited state lifetimes identified via isomer and charged-particle tagging. The plunger will be used to address many key facets of nuclear structure physics with particular emphasis on the effect of deformation on proton emission rates.

Keywords: differential plunger, lifetimes, deformation, emission rates

PACS: PACS

INTRODUCTION

Proton emission rates are highly sensitive to nuclear deformation but in all known cases the deformation has never been experimentally determined. Currently, proton emission calculations rely on theoretically determined deformations [1] therefore the experimental determination of deformation parameters is crucial to our complete understanding of proton emission. A new differential plunger (DPUNS) is being developed to measure the lifetimes of unbound states in proton-dripline nuclei. With the aid of state-of-the-art theoretical models [2–7], accurate state lifetime measurements above proton emitting states can be used to determine the effects of deformation on the proton emission rate.

The Köln plunger device [8] has been used at the accelerator laboratory of the University of Jyväskylä (JYFL) to measure the lifetimes of γ -ray transitions in nuclei with great success. The design of the Köln plunger along with the installed components, however, has limited its use to nuclei with production cross-sections above $\sim 50 \mu\text{b}$. The Köln device is therefore proving inadequate for studying exotic nuclei approaching the proton dripline with sub-microbarn production cross-sections. The new differential plunger device has been designed to overcome the technical limitations of the Köln plunger for use at JYFL with the gas-filled separator RITU. The overall design of DPUNS, figure 1, is based on the successful Köln plunger [8] but with some technical improvements.

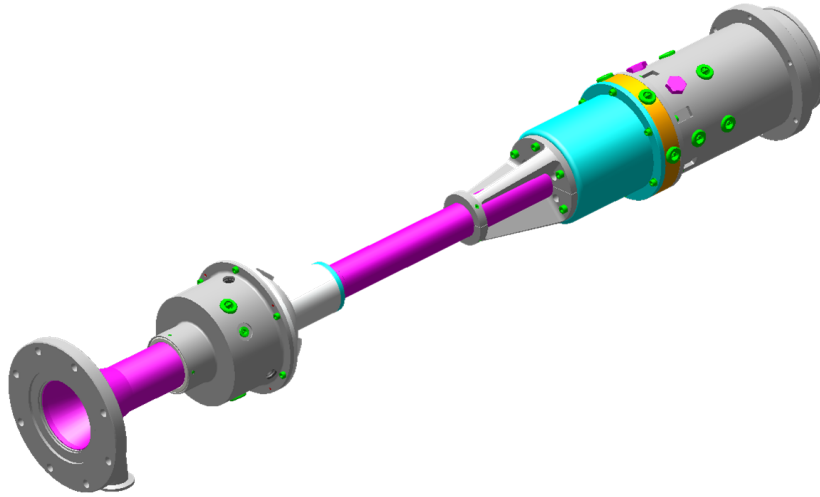


FIGURE 1. Schematic representation of the new DPUNS device for which the overall design is based on the Köln plunger device [8].

TECHNICAL DETAILS

Currently the Köln plunger has to be isolated from RITU with carbon foils due its 1 kV motors which were intended for use solely in a vacuum environment. The isolating carbon foils increases the γ -ray background arising from scattered recoils as well as reducing the transmission efficiency of RITU due to straggling. DPUNS incorporates a low voltage (45 V) stepping motor along with a low voltage (150 V) piezo actuator (see figure 2) which are manufactured by Physik Instrumente (PI) GmbH [9]. These low-voltage motors allow DPUNS to be used in the helium gas environment of RITU thus alleviating the need for carbon isolating foils. DPUNS also incorporates an improved inner plunger design and it is envisaged that a new in-situ optical telescope will be installed to improve the accuracy with which the target and degrader foils are aligned. It is estimated that all of these improvements will increase the overall efficiency of DPUNS over the Köln plunger. The measurement efficiency will be augmented further through improvements to the ancillary apparatus. For example, a thinner than usual ($< 300 \mu\text{m}$) double-sided silicon strip detector (DSSD) will be utilised for proton-tagging experiments to reduce the background from β and escaping α particles. The use of digital electronics will significantly increase (up to $\sim 60 \text{ kHz}$) the maximum counting rate of the JUROGAM-II detectors allowing larger beam currents to be used. This will be an invaluable improvement for studies where the proton decay half lives are on the order of a ms or less as this will result in a much improved tagging efficiency compared to what is achievable with conventional analogue electronics (maximum 10 kHz counting rate). Also one side of the DSSD will use digital electronics so that proton decays can be discriminated from recoil implantations via pulse shape analysis. All of the detailed improvements coupled with the high efficiency of RITU will enable the measurement of the lifetimes of unbound states in exotic nuclei produced with sub-microbarn cross-sections.



FIGURE 2. The new low-voltage stepper motor and piezo actuator, along with supports, being used in the DPUNS device.

EXPERIMENTAL PROGRAMME

The first DPUNS (commissioning) experiment will investigate the low-energy structure of ^{98}Ru via the measurement of excited state lifetimes. The basic low-energy structure of the Ru isotopes and in particular ^{98}Ru is still not fully understood. Figure 3a shows the low-energy level scheme for ^{98}Ru which at first glance resembles a structure that one may observe for a harmonic vibrator. The transition widths in figure 3a represent the reduced quadrupole transition probabilities which disagree with that expected for a harmonic vibrator. Indeed, lifetime [10], excitation energy [10], transition probability [11] and g -factor measurements [12] have all raised conflicting ideas as to the true nature of the low-lying excitations. In particular, anomalous $B(E2:4_1^+ \rightarrow 2_1^+) / B(E2:2_1^+ \rightarrow 0_1^+) < 1$ and $B(E2:6_1^+ \rightarrow 4_1^+) / B(E2:2_1^+ \rightarrow 0_1^+) < 1$ ratios [13] have been observed in contradiction to the predictions of collective models. Although the $B(E2:4_1^+ \rightarrow 2_1^+) / B(E2:2_1^+ \rightarrow 0_1^+) < 1$ anomaly has been addressed to some extent by Williams et al. [14], large uncertainties (the currently adopted 4_1^+ state lifetime has a 20% uncertainty) inhibit clarification of the type and degree of collectivity in ^{98}Ru . A choice of reactions are available to populate the excited states of interest, all with large ^{98}Ru production cross-sections. The reaction kinematics will yield a large energy separation between the shifted and degraded components for decays recorded by the JUROGAM-II detectors at angles of 157° (ring 1) and 133° (ring 2) (see Ref [15] for more details on the Differential Decay Curve Method (DDCM) for lifetime determination). This large separation along with the large cross-section will enable the performance of DPUNS to be easily evaluated.

The second experiment will measure, for the first time, the lifetimes of the proton-unbound states in ^{151}Lu [16] (see figure 3b). There is a long standing issue as to whether the proton emission in ^{151}Lu arises from a spherical [17] or deformed [18] nuclear system. The measurement of the proton-unbound excited state lifetimes in ^{151}Lu will therefore aid in the resolution of this debate. These measurements will also allow an investigation into the possible role of coupling to the continuum for these unbound states. The work of Liu et al., [16] showed evidence for proton emission from an unplaced isomeric state with a half life of $16(1) \mu\text{s}$ which will also be investigated. Excited states in ^{151}Lu will be populated in the reaction $^{96}\text{Ru}(^{58}\text{Ni}, p2n)^{151}\text{Lu}$ with an estimated cross-

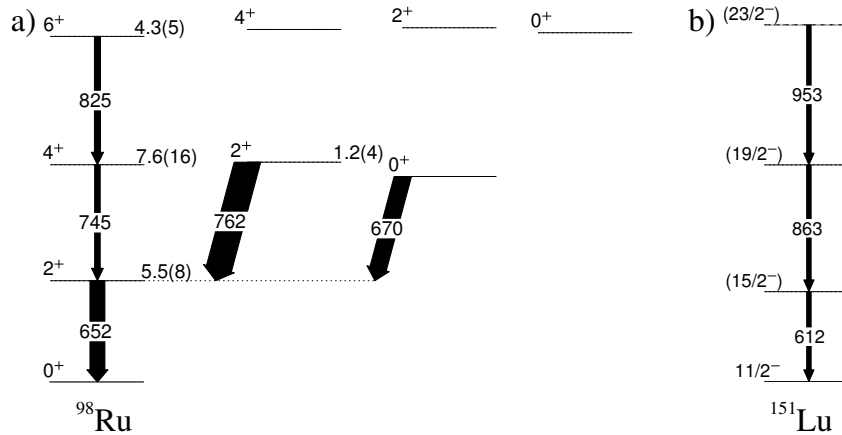


FIGURE 3. a) The low-energy structure of ^{98}Ru from [10] with transition widths representing the reduced transition probabilities. b) Tentative level scheme for ^{151}Lu deduced from [16] highlighting the excited states to be measured by DPUNS.

section of $\sim 70\mu\text{b}$. This experiment will therefore test DPUNS in a low cross-section, proton-tagging environment for which the device is primarily designed.

ACKNOWLEDGMENTS

DPUNS is based on the Köln differential plunger with several modifications therefore the authors wish to thank the Köln staff and students for their help and expertise in developing the new device. Some of the components have been constructed at the workshops of the Universities of Liverpool and Jyväskylä. This work is funded by the STFC under a standard grant D.M. Cullen EP/E02551X/1.

REFERENCES

1. P. Möller et al., Phys. Rev. Lett. 97, 162502 (2006)
2. P. Arumugam, L. S. Ferreira, E. Maglione, Phys. Rev. C 78, 041305(R) (2008)
3. E. Maglione, L. S. Ferreira, R. J. Liotta, Phys. Rev. Lett. 81, 538 (1998)
4. E. Maglione, L. S. Ferreira, R. J. Liotta, Phys. Rev. C 59, 589(R) (1999)
5. L. S. Ferreira, E. Maglione, Phys. Rev. Lett. 86, 1721 (2001)
6. L. S. Ferreira and E. Maglione, Nucl. Phys. A 752, 223 (2005)
7. D. S. Delion, R. J. Liotta and R. Wyss, Physics Reports 424, 113 (2006)
8. L. Cleemann, J. Eberth, W. Neumann, N. Wiehl and V. Zobel, Nucl. Instr. & Meth. 156, 477 (1978)
9. Physik Instrumente (PI) GmbH & Co., <http://www.pi.ws>
10. B. Singh and Z. Hu, Nucl. Data Sheets 98, 335 (2003)
11. S. Landsberger et al., Phys. Rev. C 21, 588 (1980)
12. M. J. Taylor et al., Phys. Rev. C 83, 044315 (2011)
13. R. B. Cakirli et al., Phys. Rev. C 70, 047302 (2004)
14. E. Williams et al., Phys. Rev. C 74, 024302 (2006)
15. A. Dewald, S. Harissopulos and P. von Brentano, Z. Phys. A 334, 163 (1989)
16. Z. Liu, Proceedings of PROCON Conference, A.I.P. 961, 34 (2007)
17. C. Bingham et al. Phys. Rev. C 59, R2984 (1999)
18. L. S. Ferreira and E. Maglione, Phys. Rev. C 61, 021304(R) (2000)

Momentum correlations in the two-proton decay of light nuclei

R.J. Charity

Department of Chemistry, Washington University, St. Louis, Missouri 63130, USA.

Abstract. Momentum correlations in two-proton and other multi-body decays of light proton-rich nuclei are discussed. The variety of such decays are illustrated by a number of examples. The measured correlations for the ground state of ${}^6\text{Be}$ are found to be consistent with the cluster-model calculations of Grigorenko *et al.* The ground state of ${}^8\text{C}$ decays by two sequential steps of 3-body (two-proton) decay passing through the ${}^6\text{Be}_{g.s.}$ intermediate state. The isobaric analog of ${}^8\text{C}$ in ${}^8\text{B}$ undergoes two-proton decay to the isobaric analog state in ${}^6\text{Li}$. To the extent that isospin is conserved, this is a Goldansky-type decay, i.e. the isospin-allowed immediate state in ${}^7\text{Be}$ is energetically forbidden. An excited state in ${}^{10}\text{C}$ is found to have a $\sim 50\%$ four-body-decay branch where the protons have a strong diproton character.

Keywords: two-proton decay, three-body decay, sequential decay

PACS: 21.10.-k, 25.70.Ef, 25.60.-t, 27.20.+n

INTRODUCTION

Two-proton and related multi-body decays of ground and excited states are found in amazing variety in light proton-rich nuclei. None of these decays are strictly of the Goldansky type [1], where a single proton decay is energetically forbidden. However, some approach this in a variety of ways. Also compared to the heavier Goldansky cases like ${}^{45}\text{Fe}$ and ${}^{54}\text{Zn}$ which have lifetimes in the ms time scale, the light nuclei are very short lived ($\sim 10^{-20}$ s) and decay in the target.

EXAMPLES

In this work a number of cases of two-proton decay are presented from experiments using the HiRA array developed jointly by Indiana University, Washington University, Michigan State University, and Western Michigan University.

${}^6\text{Be}$

The ground state of ${}^6\text{Be}$ is the most studied light two-proton decay nucleus. Previous studies by Geesaman *et al.* [2] and Bochkarev *et al.* [3] of the momentum correlations of the decay products ($2p+\alpha$) have demonstrated that it cannot be understood as a sequential two-proton decay through the ${}^5\text{Li}_{g.s.}$ intermediate state. Barker also showed its decay width of $\Gamma=92$ keV was larger than estimates of sequential decay based on the

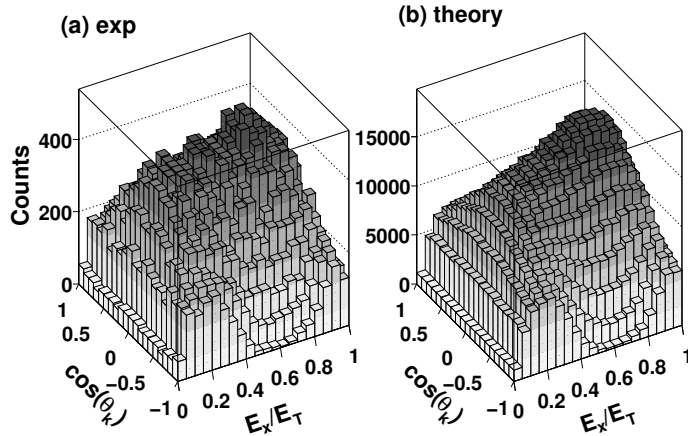


FIGURE 1. Comparison between (a) experimental momentum correlations measured for the ${}^6\text{Be}$ ground state and (b) the predictions of the quantum-mechanical cluster model. For the latter, the effect of the detector acceptance and resolution has been incorporated.

R -matrix formalism [4, 5]. In fact, ${}^6\text{Be}_{g.s.}$ is almost a Goldansky-type nucleus as only the low-energy tail of the ${}^5\text{Li}_{g.s.}$ intermediate state is energetically accessible.

We have studied the momentum correlations in the decay of ${}^6\text{Be}$ in two separate experiments. Once by using the α decay of an inelastically-excited ${}^{10}\text{C}$ beam at Texas A&M University [6] and more recently via neutron knockout from a ${}^7\text{Be}$ beam at the NSCL at Michigan State University. The correlations obtained in both experiments are consistent, but the number of ${}^6\text{Be}$ events detected in the latter experiment was significantly larger.

The correlations can be uniquely defined as a two-dimensional distribution (ignoring spin information) which can be represented in either the Jacobi T or Y system [6]. In the T system, we have used the variables, E_x/E_T , the fraction of the total decay kinetic energy in the p - p relative motion and θ_k , the angle between the p - p relative momentum vector and the core (α particle) momentum.

The experimental correlations from the latter experiment are displayed in Fig. 1 and compared to predictions from the three-body quantum-mechanical cluster model [6]. The reproduction of the experimental data is very good. We note the full two-dimensional parameter space of the correlations is essentially occupied. However there are regions of suppression associated with Coulomb interactions which are expected in a three-body decay, i.e., for $E_x/E_T \sim 0.62$, $\cos(\theta_k) \sim \pm 1$, where one of the protons has almost the same velocity vector as the α particle and $E_x/E_T \sim 0$ where the two protons have almost the same velocity vector.

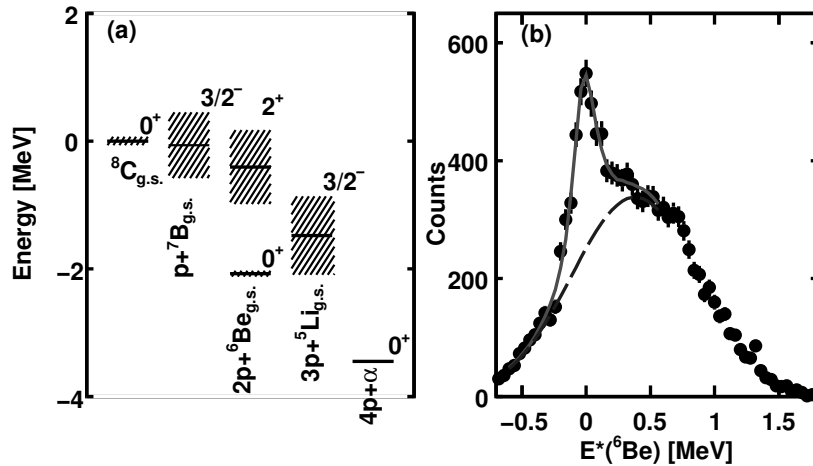


FIGURE 2. (a) Level scheme showing the potential intermediate states in the decay of the ground state of ${}^8\text{C}$. (b) Excitation energy spectrum of potential ${}^6\text{Be}$ fragments determined from each possible $2p+\alpha$ subevents in each detected ${}^8\text{C}_{g.s.}$ event. The solid curve shows a fit to this data assuming a ${}^6\text{Be}$ ground-state peak plus background (dashed curve).

${}^8\text{C}$

The ground state of ${}^8\text{C}$ is known to be unstable for decay into four protons and an α particle. We created ${}^8\text{C}_{g.s.}$ nuclei following the neutron knockout of a ${}^9\text{C}$ beam at Michigan State University and detected the five decay products for the first time.

It is interesting to establish whether this state decays via a series of two or more sequential steps or via a direct 5-body decay. A level scheme showing the possible intermediate states is shown in Fig. 2(a). Of the possible intermediate states only the ground state of ${}^6\text{Be}$ is narrow (long-lived) and allows for a meaningful description of a sequential decay scenario. To determine if a ${}^6\text{Be}$ fragment is produced in the decay, we have tried to find the products of ${}^6\text{Be}$ decay. For each detected $4p+\alpha$ event, it is possible to construct six possible $2p+\alpha$ subevents one of which maybe the product of this ${}^6\text{Be}$ decay. For each of these, a ${}^6\text{Be}$ excitation energy is determined. The spectrum of these excitation energies for all six subevents is displayed in Fig. 2(b). It shows a peak at zero energy associated with the correctly identified ${}^6\text{Be}$ subevents and an approximately Gaussian-shaped background associated with the incorrectly identified ${}^6\text{Be}$ subevents. The solid curve shows a fit to the spectra, with the dashed curve indicating the fitted background under the peak. The peak shape was taken from experimental ${}^6\text{Be}$ events created following neutron knockout of the ${}^7\text{Be}$ beam where the effects of the detector resolution is expected to be identical.

From this fit, we determined that 1.01 ± 0.05 ${}^6\text{Be}_{g.s.}$ fragments are created in each ${}^8\text{C}_{g.s.}$ decay, essentially all ${}^8\text{C}_{g.s.}$ decays produce one ${}^6\text{Be}$ fragment. Only a few percent of 5-body decay is possible within the error bars. The two-proton decay of ${}^8\text{C}$ to ${}^6\text{Be}$ is similar to the two-proton decay of ${}^6\text{Be}_{g.s.}$. The possible intermediate state ${}^7\text{B}_{g.s.}$ is very wide and only the low-energy tail is energetically accessible. An R -matrix calculation of

sequential decay gives a decay width of 12 keV, significantly smaller than our measured value of 130 ± 50 keV. Therefore this decay should also be considered a prompt 3-body decay like ${}^6\text{Be}_{g.s.}$ decay. Thus ${}^8\text{C}_{g.s.}$ decays by two sequential steps of prompt two-proton decay. For the first step of ${}^8\text{C}_{g.s.}$ decay (${}^8\text{C}_{g.s.} \rightarrow 2p + {}^6\text{Be}_{g.s.}$), it was found that the correlations are enhanced in the diproton region (low E_x/E_T values) compared to the second step (${}^6\text{Be}_{g.s.} \rightarrow 2p + \alpha$).

${}^8\text{B}$ Isobaric Analog State

In the same experiment that the ${}^8\text{C}_{g.s.}$ was detected, we also detected $2p + {}^6\text{Li}$ events associated with ${}^8\text{B}$ excited states. These were created following proton knockout from the ${}^9\text{C}$ projectile. The excitation-energy spectrum obtained from these events shows a narrow peak ($\Gamma < 75$ keV) at 7.05 MeV. The excitation energy was calculated assuming that the ${}^6\text{Li}$ fragment was created in its ground state. However, there is one excited state of ${}^6\text{Li}$, the 3.652 MeV isobaric analog state (IAS), which decays essentially 100% by γ -ray emission. All other ${}^6\text{Li}$ excited states particle decay. If the ${}^6\text{Li}$ fragment was formed in this state, then the peak would actually correspond to an excitation energy of 10.61 MeV.

There is no known narrow ${}^8\text{B}$ state at 7.05 MeV and no consistent candidates in the mirror nucleus where more levels are known. However, a 10.619 ± 0.009 MeV state is known in ${}^8\text{B}$ with a width consistent with our experimental value. This is the most likely candidate for the peak and it will be confirmed in future when we expect to detect the 3.652 MeV γ -ray from the decay of the ${}^6\text{Li}$ isobaric analog state.

The 10.61-MeV state is the isobaric analog of the ${}^8\text{C}$ ground state and it two-proton decays to the isobaric analog of ${}^6\text{Be}_{g.s.}$ and thus we are seeing the analog to the two-proton decay of ${}^8\text{C}_{g.s.}$. The level scheme of ${}^8\text{B}$ and its possible proton decay products is shown in Fig. 3 for isospin allowed decays. To the extent that isospin is conserved in the decay, then ${}^8\text{B}_{IAS}$ has a Goldansky-type two proton decay, i.e., the isospin allowed levels in the intermediate state ${}^7\text{Be}$ are energetically inaccessible. As isospin is generally conserved with high precision for these light nuclei, one might expect the two-proton decay to be dominated by the prompt emission of a $T=1$ proton pair. Future experiments will measure the correlations in the two-proton decay. The 10.61-MeV state was also found to have a small isospin-violating decay branch ($\sim 2\%$) to the $2p + d + \alpha$ channel.

9.69 MeV ${}^{10}\text{C}$ State

${}^{10}\text{C}$ nuclei were produced following neutron pickup from the ${}^9\text{C}$ beam. Apart from the first excited state, all excited states with $E^* < 15$ MeV must decay to the $2p + 2\alpha$ channel in some manner [7]. We have previously reported on ${}^{10}\text{C}$ excited states which two-proton decay to the ${}^8\text{Be}$ ground state [7]. In the experiment with the ${}^9\text{C}$ beam, a state at 9.69 MeV with $\Gamma = 490$ keV was strongly populated. This state decays 17% of the time by proton emission to the unstable 2.345-MeV level in ${}^9\text{B}$, 35% of the time by α emission to ${}^6\text{Be}_{g.s.}$, and 48% by a four-body process. For the four-body-decay branch,

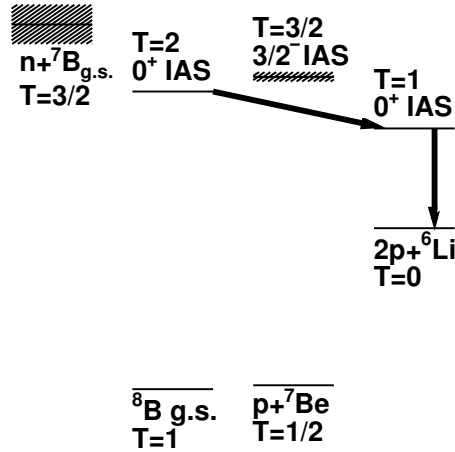


FIGURE 3. Level diagram for the decay of the isobaric analog state in ${}^8\text{B}$ showing the isospin-allowed decay mode.

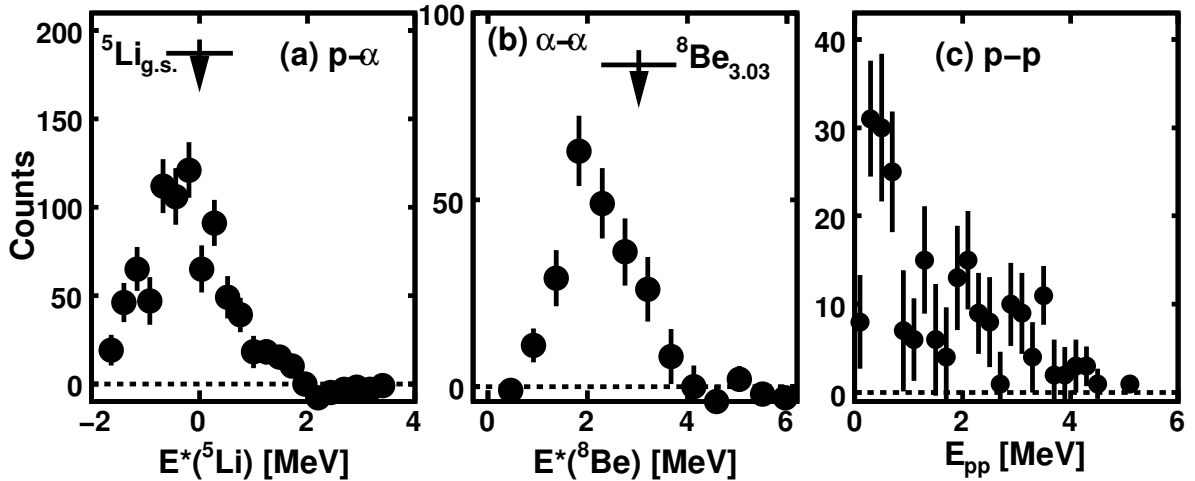


FIGURE 4. Correlations associated with the four-body decay of the 9.69-MeV state in ${}^{10}\text{C}$. (a) The ${}^5\text{Li}$ excitation-energy spectrum from all p - α pairs, (b) the ${}^8\text{Be}$ excitation-energy spectrum from the α - α pair, the (c) the p - p relative-energy distribution.

we have examined the correlations between the fragments by looking at the relative energies between all pairs of particles. These are displayed in Fig. 4.

There are four p - α pairs in each event and the ${}^5\text{Li}$ excitation-energy spectrum from these pairs is shown in Fig. 4(a). This distribution has a peak which overlaps with the location of the ${}^5\text{Li}$ ground state. It is surprising there is no tail in this distribution to higher energies. A ${}^5\text{Li}+{}^5\text{Li}$ decay would be expected to give rise to a tail when correlating a proton from one ${}^5\text{Li}$ decay with an α from the other. However, in this case all four possible p - α pairs are consistent with the ${}^5\text{Li}$ resonance. This can be understood as the p - p relative-energy is enhanced at small relative energies, the diproton region. In

addition the ${}^8\text{Be}$ excitation energy spectrum for the α - α pairs overlaps strongly with the wide first-excited state of ${}^8\text{Be}$ [Fig. 4(b)]. Possible we are seeing a decay where the α - α pairs are in a ${}^8\text{Be}$ resonance, all p - α pairs are simultaneously in ${}^5\text{Li}$ resonances and the two protons are strongly correlated. Alternatively some of the possible peaks in the excitation-energy spectra may not be resonances, but associated with energy conservation. In any case, the correlations in Fig. 4 cannot be explained by a sequential decay scenario.

SUMMARY

The data presented shows the variety of two-proton decays in light-proton rich nuclei. These include some exotic decays such as ${}^8\text{C}_{g.s.}$ which decays by two sequential steps of two-proton decay. Its analog in ${}^8\text{B}$, which two-proton decays to the isobaric analog state in ${}^6\text{Li}$ and the 9.69-MeV state in ${}^{10}\text{C}$ which undergoes a four-body decay where the two protons have a strong diproton character. Other examples of decays similar to these undoubtedly exist in other light nuclei and thus future studies in this region of the table of isotopes may prove fruitful.

ACKNOWLEDGMENTS

The data in this work is from a HiRA experiment at Michigan State University performed with J.M. Elson, J. Manfredi, R. Shane, L.G. Sobotka, B.A. Brown, Z. Chajecki, D. Coupland, H. Iwasaki, M. Kilburn, Jenny Lee, W.G. Lynch, A. Sanetullaev, M.B. Tsang, J. Winkelbauer, M. Youngs, S.T. Marley, D.V. Shetty, A.H. Wuosmaa, T.K. Gosh, and M.E. Howard.

REFERENCES

1. V. I. Goldansky, *Nuclear Physics* **19**, 482 (1960).
2. D. F. Geesaman, et al., *Phys. Rev. C* **15**, 1835 (1977).
3. O. V. Bochkarev, et al., *Nucl. Phys.* **A505**, 215 (1989).
4. F. C. Barker, *Phys. Rev. C* **66**, 047603 (2002).
5. F. C. Barker, *Phys. Rev. C* **67**, 049902(E) (2003).
6. L. V. Grigorenko, et al., *Phys. Rev. C* **80**, 034602 (2009).
7. R. J. Charity, et al., *Phys. Rev. C* **80**, 024306 (2009).

High Precision Atomic Mass Measurements: Tests of CVC and IMME

Tommi Eronen and the JYFLTRAP collaboration

Department of Physics, University of Jyväskylä, FI-40014 University of Jyväskylä, Finland

Abstract. Atomic mass is one of the key ingredients in testing the Conserved Vector Current (CVC) hypothesis and Isobaric Mass Multiplet Equation (IMME). With JYFLTRAP Penning trap installation at the University of Jyväskylä, Finland, several atomic masses related to these studies have been measured. The performed atomic mass measurements for CVC tests cover almost all the nuclei that are relevant for these studies. To test IMME, masses in two isobaric mass chains ($A=23$ and $A=32$) have been determined.

Keywords: Penning trap, Q-value, IMME, superallowed beta decay

PACS: 21.10.Dr 23.40.Bw

INTRODUCTION

The studies related to CVC and IMME benefit more from atomic mass difference measurements than absolute mass measurements. By knowing atomic mass differences one can calculate decay energies and reaction Q values. If both decay parent and daughter are easily available, a mass difference measurement with a Penning trap system can easily produce an order-of-a-magnitude better precision due to cancellation of systematic uncertainties since the two ions are relatively close in mass (see for instance [1, 2] and references therein).

According to CVC hypothesis, the ft values of the superallowed $0^+ \rightarrow 0^+$ β decays between isospin $T = 1$ analog states should be constant irrespective of the transition. Such transitions either having parent state $T_z = -1$ or $T_z = 0$ range from ^{10}C up to ^{74}Rb and beyond though cases heavier than ^{74}Rb are not yet so thoroughly studied [2].

The decay energy, commonly denoted as Q_{EC} value, is needed for f determination. Thus far Q_{EC} values of 14 different superallowed β emitters with JYFLTRAP have been measured with comparable or much better accuracy than the previously adopted values. These measurements include both $T_z = -1$ and $T_z = 0$ emitters ranging from ^{10}C to ^{62}Ga .

To test validity of IMME of $A = 23$ quartet and $A = 32$ quintet, atomic masses of ^{23}Al [3] and ^{31}S [4] have been determined.

EXPERIMENT

For these studies the short-living ions were produced using IGISOL method [5]. Here an ion guide optimized for light-ion induced fusion reactions was used which is optimal for producing ions via (p, xn) , $(^3\text{He}, xn)$ or similar reaction channels [6].

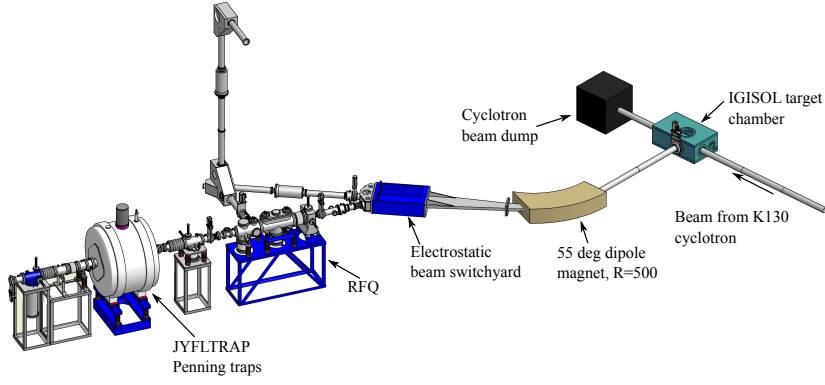


FIGURE 1. The IGISOL and JYFLTRAP installations. The primary beam from JYFL K130 cyclotron is incident from left. The ions of interest are created in nuclear reactions inside the target chamber. The ions are extracted out (perpendicular to the cyclotron beamline) and mass separated with a dipole magnet. After the magnet the ions are deflected inside the electrostatic switchyard 30 degrees towards the JYFLTRAP setup.

The reaction products are stopped in helium gas, extracted out from the gas volume in flowing gas with guiding electric fields and finally accelerated to $30q$ keV [7]. The ion beam is mass separated with a dipole magnet having mass resolving power $M/\Delta M$ of about 500. After 30 degree electrostatic deflection system located at the focal plane of the magnet, only ions with a chosen mass number are left in the beam.

The mass-number selected beam is injected into a radio-frequency quadrupole cooler and buncher [8] in where energy spread and emittance is considerably reduced. Additionally, ions are collected into a potential well. Upon lowering the exitside potential the accumulated ions are released as a short, about $10 \mu\text{s}$ wide bunch which is transferred to the JYFLTRAP Penning trap setup for actual mass measurements. A layout of the whole setup is shown in Fig. 1.

The JYFLTRAP Penning trap setup consists of two geometrically identical Penning traps located symmetrically about the magnet center 20 cm apart. The first trap in line is used for isobaric purification with mass resolving power $M/\Delta M$ of about 10^5 [9, 10]. The other trap is used for high precision mass measurements with time-of-flight ion-cyclotron resonance (TOF-ICR) technique [11, 12]. Once the cyclotron frequency ν_c of the ion is determined, the mass is obtained using equation $\nu_c = \frac{1}{2\pi} \frac{q}{m} B$, where q and m are charge and mass of the ion and B the magnetic field. Using cyclotron frequency ratio of the parent and daughter ions the Q_{EC} value of the ions becomes

$$Q_{\text{EC}} = M_m - M_d = \left(\frac{\nu_d}{\nu_m} - 1 \right) (M_d - m_e) - \Delta B_{m,d}, \quad (1)$$

where M_m and M_d are the masses of the parent and daughter atoms, respectively; ν_d/ν_m is their cyclotron frequency ratio with singly-charged ions, m_e is the electron mass; and $\Delta B_{m,d}$ arises from the electron binding-energy differences between the parent and daughter atoms. Since the term $(\frac{\nu_d}{\nu_m} - 1) < 10^{-3}$, the precision of the daughter atomic mass has very little contribution to the obtained Q_{EC} value. Additionally, since both

are mass doublets having the same mass-over-charge ratio, mass-dependent systematic errors cancel out. Overall, a Q_{EC} value precision $\Delta Q/M$ of about 2×10^{-9} has been reached [1, 13].

Q_{EC} VALUES OF SUPERALLOWED β EMITTERS

Superaligned beta decays occur between nuclear 0^+ isobaric analog states. These are pure Fermi decays, rendering the decay matrix element to be very simple. According to the conserved vector current (CVC) hypothesis, the decay ft values should be the same for any superallowed decay and is given by

$$ft = \frac{K}{G_V^2 |M_F|^2} = \text{const}, \quad (2)$$

where K is constant, G_V the vector coupling constant for semileptonic weak interactions and M_F the Fermi matrix element ($M_F = \sqrt{2}$ for $T = 1$ decays). The ft values, however, need to be corrected with small terms to compensate for instance isospin mixing [14, 15] in order to get corrected values denoted $\mathcal{F}t$. The mass measurements contribute to f determination which requires the decay energy Q_{EC} . Actually $f \propto Q_{EC}^5$ and thus very precise Q_{EC} determination is required.

The corrected ft value, denoted $\mathcal{F}t$ is given as

$$\mathcal{F}t = ft(1 + \delta_R)(1 - \delta_C) = \frac{K}{2G_V^2(1 + \Delta_R^V)} = \text{const}, \quad (3)$$

where δ_C is the isospin-symmetry-breaking correction, δ_R the transition-dependent radiative correction and Δ_R^V the transition-independent radiative correction.

The most recent survey [2] lists the relevant experimental data and theoretical corrections. Currently there are 13 superallowed transitions that significantly contribute to the world average $\mathcal{F}t$ value. Other cases are usually limited by the poor knowledge of the branching ratio or in some cases also by the half-life.

JYFLTRAP is ideally suited for Q_{EC} value measurements because both the decay parent and daughter nuclei—whether being radioactive or not—are simultaneously available in the ion beam produced by the IGISOL method.

By June 2011, the Q_{EC} values of ^{10}C , $^{26}\text{Al}^m$, ^{26}Si , ^{30}S , ^{34}Cl , ^{34}Ar , $^{38}\text{K}^m$, ^{38}Ca , ^{42}Sc , ^{42}Ti , ^{46}V , ^{50}Mn , ^{54}Co and ^{62}Ga have been determined at JYFLTRAP (see also Fig. 2). Thus far only Q_{EC} value of ^{14}O remains to be measured with a Penning trap of the 13 cases that are precise enough to contribute to the current world average value.

Most of the cases had their Q_{EC} values already precisely determined (see compilation by Hardy and Towner [2]) prior to Penning trap measurements. The measurements at JYFLTRAP have not merely improved the Q_{EC} value precision but have also found significant deviations to old data in the cases of ^{46}V , ^{50}Mn and ^{54}Co [16, 17].

In the most recent work [1], a small difference to Q_{EC} value of ^{10}C was found which had a consequence of shifting its $\mathcal{F}t$ value to be off slightly more than 1σ from the world average $\mathcal{F}t$ value.

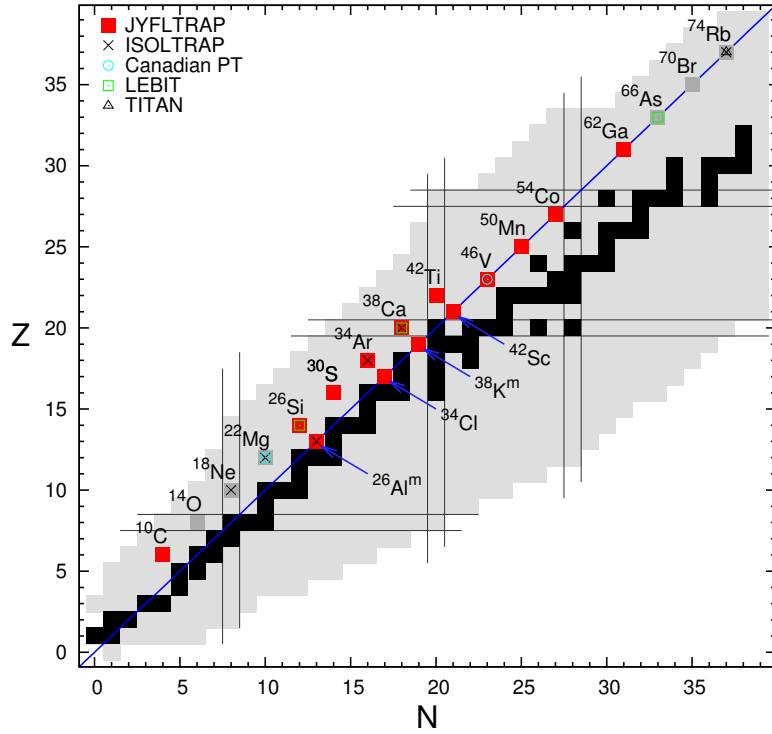


FIGURE 2. (Color online) Chart of the superallowed β emitters. Nuclei whose mass or Q_{EC} values have been measured with Penning traps have been indicated. JYFLTRAP measurements are indicated with solid red squares.

MASSES FOR TESTING IMME

It is shown with the isobaric mass multiplet equation (IMME) that the masses of the isospin $2T + 1$ nuclear states belonging to a given isospin multiplet are related as

$$M(A, T, T_z) = a(A, T) + b(A, T) \times T_z + c(A, T) \times T_z^2, \quad (4)$$

when charge-dependent effects and Coulomb force between the nucleons are treated by first-order perturbation theory. T_z is the z projection of the isospin T [18]. Higher order terms may arise for instance from isospin mixing between the isobaric analog and neighbouring states. The most significant deviations from Eq. (4) have been found in the $A = 8, T = 2$ quintet and the $A = 9, T = 3/2$ quartet [19]. Since the compilation in Ref. [19] the sd -shell nuclei in particular have been studied further to obtain more accurate data.

To obtain masses of the isobaric analog states, not only the ground state masses are needed but also energies of the excited states. JYFLTRAP has contributed to these studies by measuring the ground state mass of ^{23}Al , which is the $T_z = -3/2$ nucleus of the $(A, T) = (23, 3/2)$ quintet. The new measurement provides about two orders of magnitude improvement over the existing mass value [3]. Fit of the coefficients given in Eq. 4 to experimental is gives excellent agreement between the equation and experimental values.

The other case in which JYFLTRAP has contributed is the $(A, T) = (32, 2)$ quintet. Here, a new mass value for ^{31}S was obtained which improved the ground state mass of the $T_z = -1$ nucleus ^{32}Cl using proton separation energy from Ref. [20] to link the ^{31}S and ^{32}Cl masses. A slight deviation of about 1.4σ to the previously adopted value was found. Even with this significant offset the quadratic IMME form still remains broken [4].

SUMMARY AND OUTLOOK

JYFLTRAP has been extensively used to measure Q_{EC} values of superallowed β emitters and also in some extent masses of nuclei relevant to test the IMME. Measured as A/q doublets the systematic uncertainties could be greatly reduced.

In summer 2010 both IGISOL and JYFLTRAP installation were shutdown for relocation. The upgraded IGISOL facility will be served by two cyclotrons: the new K-30 and also by the existing K-130 cyclotron. The new facility is expected to be running in early 2012.

ACKNOWLEDGMENTS

This work has been supported by the EU 6th Framework programme “Integrating Infrastructure Initiative - Transnational Access”, Contract Number: 506065 (EURONS) and by the Academy of Finland under the Finnish Centre of Excellence Programme 2006-2011 (Nuclear and Accelerator Based Physics Programme at JYFL).

REFERENCES

1. T. Eronen, D. Gorelov, J. Hakala, J. C. Hardy, A. Jokinen, A. Kankainen, V. S. Kolhinen, I. D. Moore, H. Penttilä, M. Reponen, J. Rissanen, A. Saastamoinen, and J. Äystö, *Phys. Rev. C* **83**, 055501– (2011), URL <http://link.aps.org/doi/10.1103/PhysRevC.83.055501>.
2. J. C. Hardy, and I. S. Towner, *Phys. Rev. C* **79**, 055502 (2009), URL <http://link.aps.org/abstract/PRC/v79/e055502>.
3. A. Saastamoinen, T. Eronen, A. Jokinen, V. V. Elomaa, J. Hakala, A. Kankainen, I. D. Moore, S. Rahaman, J. Rissanen, C. Weber, J. Aysto, and L. Trache, *Phys. Rev. C* **80**, 044330–5 (2009), URL <http://link.aps.org/abstract/PRC/v80/e044330>.
4. A. Kankainen, T. Eronen, D. Gorelov, J. Hakala, A. Jokinen, V. S. Kolhinen, M. Reponen, J. Rissanen, A. Saastamoinen, V. Sonnenschein, and J. Äystö, *Phys. Rev. C* **82**, 052501– (2010), URL <http://link.aps.org/doi/10.1103/PhysRevC.82.052501>.
5. J. Äystö, *Nucl. Phys. A* **693**, 477–494 (2001), URL <http://www.sciencedirect.com/science/article/B6TVB-43W5CYS-11/1/290d952179e1ba0fbdc179ecbf4e3cd>.
6. J. Huikari, P. Dendooven, A. Jokinen, A. Nieminen, H. Penttilä, K. Peräjärvi, A. Popov, S. Rinta-Antila, and J. Äystö, *Nucl. Instrum. Methods Phys. Res., Sect. B* **222**, 632–652 (2004), ISSN 0168-583X, URL <http://www.sciencedirect.com/science/article/B6TJN-4CG2CG5-2/2/dfd21dc4051d81a20c68be45a2ef55be>.
7. P. Karvonen, I. Moore, T. Sonoda, T. Kessler, H. Penttilä, K. Peräjärvi, P. Ronkanen, and J. Äystö, *Nucl. Instrum. Methods Phys. Res., Sect. B* **266**, 4794–4807 (2008), ISSN 0168-583X, URL <http://www.sciencedirect.com/science/article/B6TJN-4T2S8KR-1/2/1d7624cd369335096dcb1fd81a410fea>.

8. A. Nieminen, J. Huikari, A. Jokinen, J. Äystö, P. Campbell, and E. C. A. Cochrane, *Nucl. Instrum. Methods Phys. Res., Sect. A* **469**, 244–253 (2001), URL <http://www.sciencedirect.com/science/article/B6TJM-43PGJKX-C/1/93d5587efba5cfe8571b63228952dab8>.
9. G. Savard, S. Becker, G. Bollen, H. J. Kluge, R. B. Moore, T. Otto, L. Schweikhard, H. Stolzenberg, and U. Wiess, *Phys. Lett. A* **158**, 247–252 (1991), ISSN 0375-9601, URL <http://www.sciencedirect.com/science/article/B6TVM-46T4MHS-17Y/2/cda0251d2c9698b6b249f2cd4b4ff7eb>.
10. V. S. Kolhinen, S. Kopecky, T. Eronen, U. Hager, J. Hakala, J. Huikari, A. Jokinen, A. Nieminen, S. Rinta-Antila, J. Szerypo, and J. Äystö, *Nucl. Instrum. Methods Phys. Res., Sect. A* **528**, 776–787 (2004), URL <http://www.sciencedirect.com/science/article/B6TJM-4CHG99P-9/1/255b97da47f4d0e492d99d4d9ebc4f09>.
11. G. Gräff, H. Kalinowsky, and J. Traut, *Z. Phys. A* **297**, 35 (1980).
12. M. König, G. Bollen, H. J. Kluge, T. Otto, and J. Szerypo, *Int. J. Mass Spectrom.* **142**, 95–116 (1995), ISSN 0168-1176, URL <http://www.sciencedirect.com/science/article/B6TG6-405JY09-8/2/4fc84d7352db90c3329ca812cf47e325>.
13. T. Eronen, V.-V. Elomaa, J. Hakala, J. C. Hardy, A. Jokinen, I. D. Moore, M. Reponen, J. Rissanen, A. Saastamoinen, C. Weber, and J. Aysto, *Phys. Rev. Lett.* **103**, 252501–4 (2009), URL <http://link.aps.org/abstract/PRL/v103/e252501>.
14. I. S. Towner, and J. C. Hardy, *Phys. Rev. C* **77**, 025501–15 (2008), URL <http://link.aps.org/abstract/PRC/v77/e025501>.
15. W. Satuła, J. Dobaczewski, W. Nazarewicz, and M. Rafalski, *Phys. Rev. Lett.* **106**, 132502– (2011), URL <http://link.aps.org/doi/10.1103/PhysRevLett.106.132502>.
16. T. Eronen, V. Elomaa, U. Hager, J. Hakala, A. Jokinen, A. Kankainen, I. Moore, H. Penttilä, S. Rahaman, J. Rissanen, A. Saastamoinen, T. Sonoda, J. Äystö, J. C. Hardy, and V. S. Kolhinen, *Phys. Rev. Lett.* **97**, 232501–4 (2006), URL <http://link.aps.org/abstract/PRL/v97/e232501>.
17. T. Eronen, V.-V. Elomaa, U. Hager, J. Hakala, J. C. Hardy, A. Jokinen, A. Kankainen, I. D. Moore, H. Penttilä, S. Rahaman, S. Rinta-Antila, J. Rissanen, A. Saastamoinen, T. Sonoda, C. Weber, and J. Äystö, *Phys. Rev. Lett.* **100**, 132502–4 (2008), URL <http://link.aps.org/abstract/PRL/v100/e132502>.
18. E. P. Wigner, Robert A. Welch Foundation, Houston, Texas, 1958, vol. 1 of *Proceedings of the Robert A. Welch Conferences on Chemical Research*, p. 67.
19. J. Britz, A. Pape, and M. S. Antony, *At. Data Nucl. Data Tables* **69**, 125–159 (1998), ISSN 0092-640X, URL <http://www.sciencedirect.com/science/article/B6WBB-45KKT5W-Y/2/2cd436aa3bbf94ee8fe79ac18c0b891e>.
20. M. Bhattacharya, D. Melconian, A. Komives, S. Triambak, A. Garcia, E. G. Adelberger, B. A. Brown, M. W. Cooper, T. Glasmacher, V. Guimaraes, P. F. Mantica, A. M. Oros-Peusquens, J. I. Prisciandaro, M. Steiner, H. E. Swanson, S. L. Tabor, and M. Wiedeking, *Phys. Rev. C* **77**, 065503 (2008), URL <http://link.aps.org/abstract/PRC/v77/e065503>.

Decay Spectroscopy for Nuclear Astrophysics: β -delayed Proton Decay

L. Trache^a, E. Simmons^a, A. Spiridon^a, M. McCleskey^a, B.T. Roeder^a,
R.E. Tribble^a, A. Saastamoinen^b, A. Jokinen^b, J. Aysto^b, T. Davinson^c,
P.J. Woods^c, E. Pollacco^d, M. Kebbiri^d and G. Pascovici^e

^aTexas A&M University, College Station, TX 77845, USA

^bUniversity of Jyväskylä, Jyväskylä, Finland, ^cUniversity of Edinburgh, Edinburgh, UK,

^dCEA/IRFU Saclay, France, ^eIKP, Universitaet zu Koeln, Germany

Abstract. Decay spectroscopy is one of the oldest indirect methods in nuclear astrophysics. We have developed at TAMU techniques to measure beta- and beta-delayed proton decay of sd-shell, proton-rich nuclei. The short-lived radioactive species are produced in-flight, separated, then slowed down (from about 40 MeV/u) and implanted in the middle of very thin Si detectors. These allowed us to measure protons with energies as low as 200 keV from nuclei with lifetimes of 100 ms or less. At the same time we measure gamma-rays up to 8 MeV with high resolution HPGe detectors. We have studied the decay of ²³Al, ²⁷P, ³¹Cl, all important for understanding explosive H-burning in novae. The technique has shown a remarkable selectivity to beta-delayed charged-particle emission and works even at radioactive beam rates of a few pps. The states populated are resonances for the radiative proton capture reactions ²²Na(p, γ)²³Mg (crucial for the depletion of ²²Na in novae), ^{26m}Al(p, γ)²⁷Si and ³⁰P(p, γ)³¹S (bottleneck in novae and XRB burning), respectively. More recently we have radically improved the technique using a gas based detector we call AstroBox.

Keywords: nuclear astrophysics, b-delayed proton decay, H-burning, resonant proton capture.

PACS: 26.50.+x, 23.40.-s, 23.50.+z, 27.30.+t

INTRODUCTION

While the study of nuclear structure and of the emission mechanism(s) in proton decay are the main motivations for most of the other presentations at this conference, our motivation is nuclear astrophysics. The connection is simple: many (p, γ) reactions on the proton-rich side of the nuclide chart, important in H-burning processes in stars, are dominated by resonant proton capture. To determine the corresponding reaction rates what is needed is to determine the properties of the relevant resonances: position (energy), spin and parity and the resonance strengths. These could be determined by direct measurements in some cases, but in many others, involving radioactive targets, they can only be extracted from the population and study of the metastable states that produce these resonances. In our case we use β -delayed proton-decay spectroscopy (βp): in the same compound nucleus the states are populated by β -decay, and then they decay emitting a proton. Provided the selection rules for (p, γ) and βp allow for the population of the same states, of course. One can determine that way the energy of the

resonance, restrict the spins and parity and determine the branching ratios. This simple connection is schematically presented in figure 1. One important point here is that, on the nuclear scale, the stars are cold! Even for explosive burning processes, like novae and X-ray bursts (XRB) that are our particular focus here, at temperatures $T=0.1-0.3$ GK, the energies in the Gamow peak are of the order of a few hundred keV, therefore we need to measure proton energies $E_p \sim 100-400$ keV. This is the challenge we are addressing in this work. I will concentrate on the methodical aspects of the work, not on the astrophysical results.

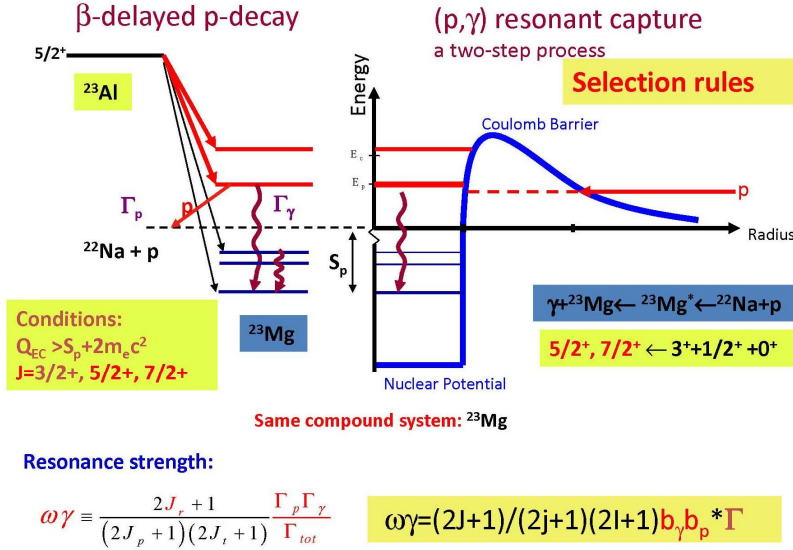


FIGURE 1. (Color online) Schematic presentation of the use of β -delayed proton decay to study H-burning in nuclear astrophysics.

EXPERIMENTAL METHODS

The focus of our interest is on H-burning reactions involving proton-rich nuclei in the *sd*-shell region, reactions important in classical novae, or in XRB. In particular we were looking at 3 cases: $^{22}\text{Na}(p,\gamma)^{23}\text{Mg}$ (crucial for the depletion of ^{22}Na in novae), $^{26}\text{mAl}(p,\gamma)^{27}\text{Si}$ and $^{30}\text{P}(p,\gamma)^{31}\text{S}$ (bottleneck in novae and XRB H-burning), respectively [1]. The resonances dominating these reaction rates at astrophysical energies can be populated in the β -decay of ^{23}Al , ^{27}P and ^{31}Cl , respectively. We have studied them using methods developed specifically to detect very low energy protons. The radioactive species were produced and separated with beams from the superconducting K500 cyclotron and the MARS spectrometer at Texas A&M University. For the first time, relatively intense (2-4000 pps) and pure secondary beams (>85%) were obtained in all 3 cases. The measurements for ^{27}P are very recent and the data are still being analyzed; those for ^{31}Cl will be discussed in more detail in the next presentation. I will concentrate here on the case of ^{23}Al , which is the one studied most exhaustively, so far. Parts of the data were published recently [2].

We realized that in order to detect protons with energies ~ 200 keV we want to implant the source nuclei in the detectors, rather than stopping them in a material

outside the detector. The first method was to implant them in very thin Si detectors; the second was to construct a special gas detector.

Implantation in very thin Si detectors

The short-lived radioactive species are produced in-flight with (p,2n) reactions in inverse kinematics on a cryogenic H₂ gas target, separated in MARS, then slowed down (from about 40 MeV/u) and implanted in the middle of a very thin Si detector. Then the beam is stopped and the decay is measured. The primary beams used were ²⁴Mg at 48 MeV/u, ²⁸Si and ³²S @ 40 MeV/u, respectively. Two different double sided strip Si detectors (DSSSD), 65 or 45 μm thick (W1-65 and BB2-45 [3], respectively), were used as proton detectors. A 1 mm thick Si detector was placed behind the proton detector to measure betas in coincidence. One or two HpGe detectors were put outside the implantation chamber, as close as possible to the implantation site, to measure gamma-rays. Protons and gamma-rays in coincidence with the beta-detector were measured simultaneously. An important and delicate part of the experiments was to precisely implant the source nuclei in the middle of the very thin detectors; we obtained depths distributions of 17-20 μm. While implanting the β-decaying nuclei in the proton detector has the advantage that it avoids losses in the implantation material and in any dead layers a detector

may have, there is an important limitation due to the fact that the detectors may also be sensitive to the positrons emitted in the obligatory first step of the βp-decay process: the signal collected is a sum of the proton energy and of the energy loss of the β. Moreover, the spectrum of the latter is inherently continuous: these lead to proton peaks that are shifted and have a tail on the high energy side and to a large continuous background at low energies from the β events not followed by proton emission. To reduce this background and the tail it is necessary to minimize the β energy loss. With these thin detectors we have background free

proton spectra at energies $E_p > 400$ keV or so, but the background becomes considerable at lower energies. We could, however, determine reliable proton spectra down to about 200 keV by subtracting a purely β background measured from an emitter that does not emit protons. For the ²³Al case we have used a background from ²²Mg. The process is shown in Figure 2. Locations of low-energy resonances were determined, as well as branchings by comparing with our earlier βγ-decay studies [4].

²³Al βp measured with Si det

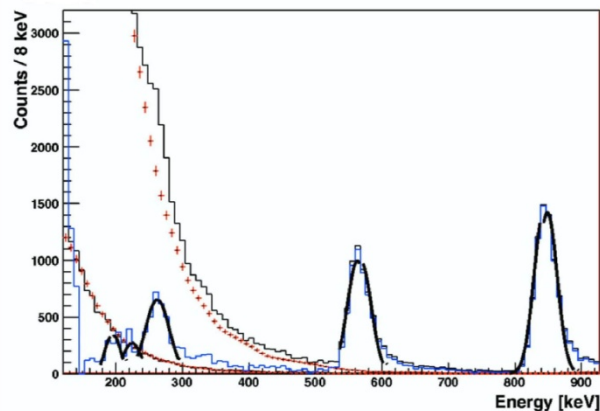


Figure 2. Detail of the low energy part of a proton spectrum measured with DSSSD W1-65. The useful proton spectrum at 200-400 keV is obtained after subtracting a large continuum background (dotted line) due to positrons only.

AstroBox

In a very recent development, this spring, we have replaced the Si detector with a gas based detector, part of a small project that we call AstroBox. It was developed with people from CEA-Saclay and IKP Koln. Using a P5 gas we could reduce drastically the beta background that has hindered the measurement of low energy proton branches while improving the resolution. The charge produced by protons in gas is further amplified by micromegas detectors. The beta background was pushed down to energies lower than about 80 keV (figure 3, right), opening an important window for further studies.

ACKNOWLEDGMENTS

More people were involved in this cycle of measurements at Texas A&M University. Their contributions are shown in the published material cited here. This work has been supported in part by the US DOE under Grant DE-FG02-93ER40773 and by the Academy of Finland under the Finnish Centre of Excellence Programme 2006-2011. PJW and TD would like to acknowledge support from the STFC.

Run0311B: ^{23}Al β p-decay with ASTROBOX

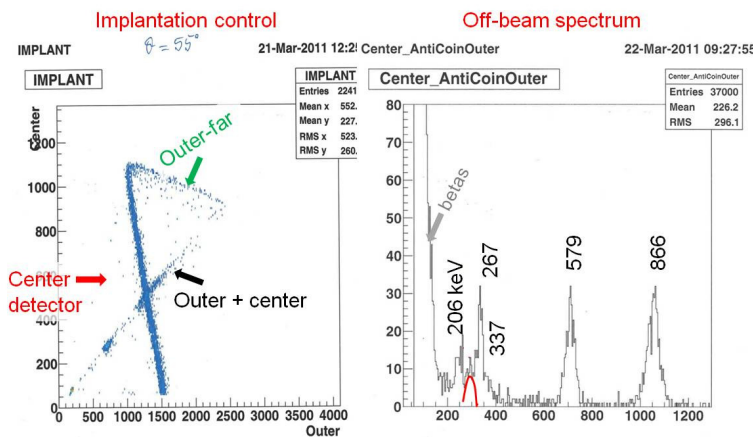


Figure 3. Spectra from the ^{23}Al β p-decay study taken using the AstroBox. The left hand side shows how the implantation in the middle of the gas detector was controlled. The right part shows a proton spectrum. The beta background is pushed down below ~ 80 keV.

REFERENCES

1. see, e.g. J. Jose, M. Hernanz and C. Illiadis, Nucl. Phys. A 777, 550 (2006).
2. A. Saastamoinen, L. Trache et al., Phys. Rev. C 83, 045808 (2011).
3. Micron Semiconductor Ltd. Catalogue 2010. <http://www.micronsemiconductor.co.uk>.
4. VE Iacob et al., Phys. Rev. C 74, 045810 (2006).

Study of excited states of ^{31}S through beta-decay of ^{31}Cl for nucleosynthesis in ONe novae

A. Saastamoinen^{*}, L. Trache[†], A. Banu^{†,**}, M. A. Bentley[‡], T. Davinson[§],
J. C. Hardy[†], V. E. Iacob[†], A. Jokinen^{*}, M. McCleskey[†], B. Roeder[†],
E. Simmons[†], G. Tabacaru[†], R. E. Tribble[†], P. J. Woods[§] and J. Äystö^{*}

^{*}*Department of Physics, University of Jyväskylä, P.O.Box 35 (YFL), FI-40014, Finland*

[†]*Cyclotron Institute, Texas A&M University, College Station, TX 77843, USA*

^{**}*Present address: James Madison University, Harrisonburg, VA 22807, USA*

[‡]*Department of Physics, University of York, Heslington, York, YO10 5DD, UK*

[§]*School of Physics and Astronomy, University of Edinburgh, Edinburgh, EH9 3JZ, UK*

Abstract. We have produced an intense and pure beam of ^{31}Cl with the MARS Separator at the Texas A&M University and studied β -decay of ^{31}Cl by implanting the beam into a novel detector setup, capable of measuring β -delayed protons and γ -rays simultaneously. From our data, we have established decay scheme of ^{31}Cl , found resonance energies with 1 keV precision, have measured its half-life with under 1% accuracy, found its Isobar Analog State decay and by using the IMME obtained an improved mass excess for its ground state. In this contribution, a description of the used method along with selected preliminary experimental results are given and their relevance for novae nucleosynthesis discussed.

Keywords: βp , $\beta\gamma$, classical novae

PACS: 26.50.+x, 23.40.-s, 27.30.+

INTRODUCTION

Classical novae are relatively common events in our galaxy with a rate of a few per year detected. Present understanding is that novae occur in interacting binary systems where hydrogen-rich material accretes on a white dwarf from its low-mass main-sequence companion. At some point in the accretion the hydrogen-rich matter compresses leading to a thermonuclear runaway [1]. An understanding of the dynamics of nova outbursts and of the nucleosynthesis fueling them is crucial in testing our understanding of the dynamics of stellar phenomena in general. Novae are relatively frequent phenomenon and they are observed throughout the whole electromagnetic spectrum and therefore the models can be compared more easily with the observations. Many H-burning reactions important here are dominated by resonant capture. The key parameters in understanding the astrophysical reaction rates are the energies and decay widths of the associated nuclear states near the particle separation threshold of the compound nucleus formed in the capture reaction. Reaction rate sensitivity studies [2, 3] have identified key reactions with large uncertainties and large variations in the end products of the nova outbursts. One such reaction is $^{30}\text{P}(p, \gamma)^{31}\text{S}$ that is a mandatory passing point to elements beyond sulfur [4]. The relevant states in ^{31}S can be studied via β -decay of ^{31}Cl , populating the excited states of ^{31}S that are decaying by both proton and γ -emission.

EXPERIMENTAL TECHNIQUE

The β -decay of ^{31}Cl was studied at Cyclotron Institute of the Texas A&M University. In this experiment the ^{31}Cl beam was produced in inverse-kinematics reaction $^1\text{H}(^{32}\text{S}, ^{31}\text{Cl})2n$ by bombarding a hydrogen gas target with ^{32}S beam at 40 MeV/u. The recoil products were separated and with the Momentum Achromat Recoil Separator (MARS) [5], resulting a beam of ^{31}Cl with typical intensity of 2-3000 pps and purity better than 85%.

Ions of interest were implanted into a detector setup consisting of a $69\mu\text{m}$ Double-Sided Silicon Strip Detector (DSSSD), a 1 mm thick Si-pad detector and a 70% high-purity germanium detector (HPGe). The beam implantation depth was controlled by using a rotatable $300\mu\text{m}$ Al degrader, allowing us to tune the beam into the middle of the DSSSD. The beam was pulsed with implantation period of 300 ms and decay period of 300 ms and the data was collected only during the decay part. A more detailed description of the experimental technique is given in Ref. [6].

The particle detectors were calibrated online with ^{29}S beam and the HPGe detector with ^{32}Cl and standard offline sources. Both, the DSSSD and the HPGe were required to be in coincidence with the Si-pad detector and gated with the β -spectrum acquired by the Si-pad.

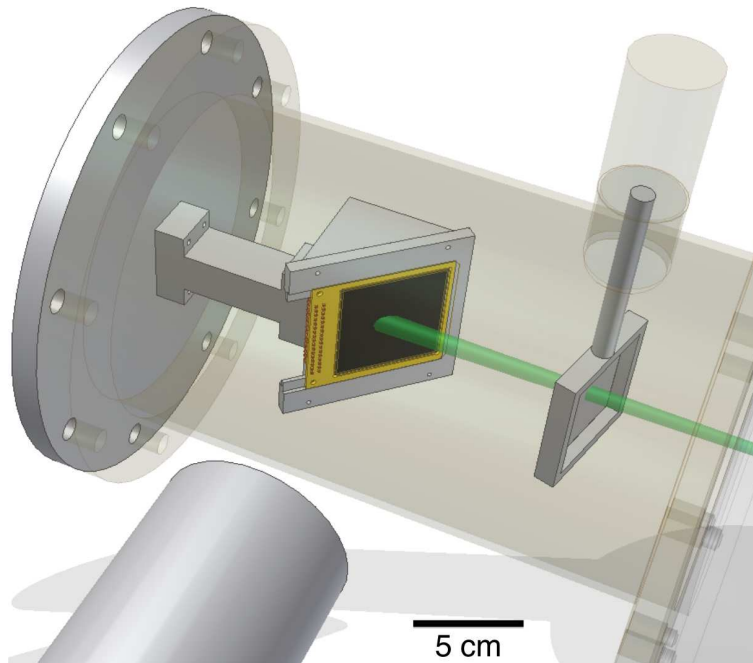


FIGURE 1. Illustration of the experimental setup at the focal plane of MARS. Beam enters the chamber from right, through the tunable aluminum degrader and finally into the detector setup consisting of a DSSSD backed with a thick Si-pad detector. The HPGe detector was installed outside the measurement chamber.

RESULTS

In the proton spectrum, the measured energy is sum of the energies of the emitted proton, the recoil and average energy deposited by the preceding β -particle:

$$E_{\text{obs.}} = \left(1 + k \cdot \frac{M_{\text{p}}}{M_{\text{rec.}}}\right) \cdot E_{\text{p}} + E_{\langle\beta\rangle}, \quad (1)$$

where k denotes the fraction of the recoil energy that is actually deposited to the detector due to ionization. The total β -gated proton spectrum is illustrated in Fig. 2. Our spectrum agrees with the evaluation [7] as well as the latest β -decay study [8], confirming the proton group at 894 keV discovered in the latter. Our spectrum has some ^{29}S contamination and somewhat high β -background covering the very low end of the spectrum.

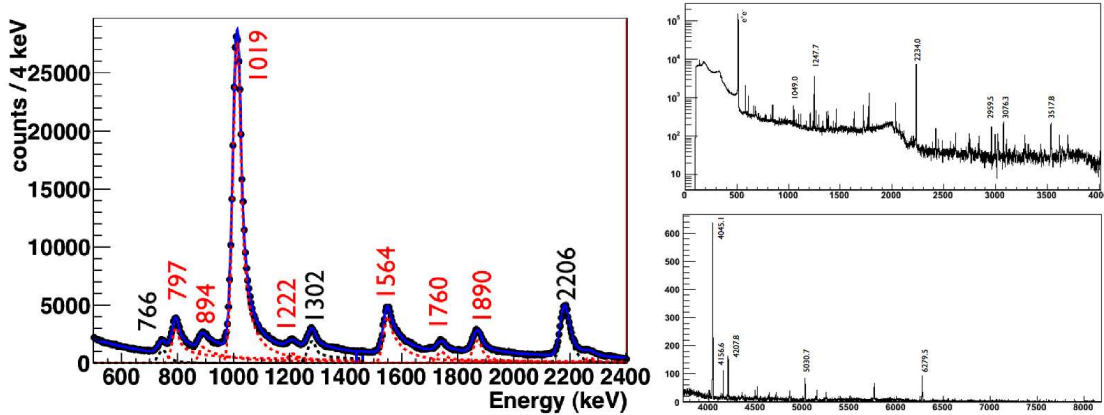


FIGURE 2. The β -delayed proton spectrum collected in this work is shown in left. The major proton groups from both ^{31}Cl (red, dashed) and ^{29}S (black, dashed) β -decay are identified. The solid blue line indicates the sum fit of all peaks as well as an exponential background. All the energies are given in c.m.s. The γ -ray spectrum collected with same conditions is given on right with the major lines from ^{31}Cl given.

The γ -ray spectrum, gated by same β -spectrum as the proton spectrum, is shown also in Fig. 2. We verify the observations by Kankainen et al. [8], but extend the γ -data significantly. Most notably, we do observe for the first time the γ -decay from the $T = 3/2$ isobaric analogue state (IAS) of ^{31}Cl ground state in ^{31}S with $E_{\gamma} = 6279.7 \pm 0.3(\text{stat}) \pm 1.5(\text{syst})$ keV. We do observe it decaying also through other transitions, e.g. to the first and second excited states. We observe also several other transitions from the excited states of ^{31}S , extending the decay scheme of ^{31}Cl significantly. We measured also the half-life of ^{31}Cl by using a 4π proportional gas counter coupled to a tape transport system. The half-life was improved to 190(1) ms, compared to the old value of 150(25) ms [9].

DISCUSSION

In conclusion, we have produced a very clean and intense beam of ^{31}Cl . Excited states of ^{31}S have been studied through β -decay of ^{31}Cl . By using the isobaric multiplet mass equation (IMME) with our excitation energy for the IAS of ^{31}Cl in ^{31}S and the latest mass values for the other members of this $T = 3/2$ multiplet [10, 11], we obtain an improved value for the mass excess of ^{31}Cl ground state to be $-7058.9(32)$ keV. This value agrees with the previous value of $-7070(50)$ keV [12] and improves also the $Q_{EC}(^{31}\text{Cl})$ and $S_p(^{31}\text{Cl})$, the latter being important for $^{30}\text{S}(p,\gamma)^{31}\text{Cl}$ in novae. Our decay data about the states above the $S_p(^{31}\text{S})$ can be used to improve the knowledge on the resonances of $^{30}\text{P}(p,\gamma)^{31}\text{S}$ in novae. The detailed analysis is in progress and all results presented here should be treated as preliminary. We have also performed another experiment of the β -decay of ^{31}Cl with an improved setup, consisting a thinner DSSSD and two HPGe detectors for improved detection efficiency and the setup has been used to study e.g. β -decays of ^{23}Al and ^{27}P . New detection techniques, discussed in more detail in Ref. [6], may yield information on the possible proton decays from the lowest $T = 3/2$ state in ^{31}S .

REFERENCES

1. J. Jose, M. Hernanz, and C. Iliadis, *Nucl. Phys. A* **777**, 550 – 578 (2006).
2. C. Iliadis, A. Champagne, J. Jose, S. Starrfield, and P. Tupper, *The Astrophys. J. Supp. Series* **142**, 105 (2002).
3. A. Parikh, J. Jose, F. Moreno, and C. Iliadis, *New Astronomy Reviews* **52**, 409 – 411 (2008), astronomy with Radioactivities. VI - Proceedings of International Workshop Held at Ringberg Castle of Max Planck Gesellschaft in Kreuth, Germany, 7-10 January 2008.
4. J. Jose, A. Coc, and M. Hernanz, *Astrophys. J* **560**, 897–906 (2001).
5. R. Tribble, A. Azhari, C. Gagliardi, J. Hardy, A. Mukhamedzhanov, X. Tang, L. Trache, and S. Yen-nello, *Nucl. Phys. A* **701**, 278 – 281 (2002).
6. L. Trache et al., in these proceedings (2011).
7. P. Endt, *Nucl. Phys. A* **633**, 1 (1998).
8. A. Kankainen, T. Eronen, S. Fox, H. Fynbo, U. Hager, J. Hakala, J. Huikari, D. Jenkins, A. Jokinen, S. Kopecky, I. Moore, A. Nieminen, H. Penttila, S. Rinta-Antila, O. Tengblad, Y. Wang, and J. Aysto, *Eur. Phys. J. A* **27**, 67–75 (2006).
9. J. Aysto, J. Honkanen, K. Vierinen, A. Hautojarvi, K. Eskola, and S. Messelt, *Phys. Lett. B* **110**, 437–440 (1982).
10. G. Audi, A. Wapstra, and C. Thibault, *Nucl. Phys. A* **729**, 337–676 (2003).
11. A. Kankainen, T. Eronen, D. Gorelov, J. Hakala, A. Jokinen, V. S. Kolhinen, M. Reponen, J. Rissanen, A. Saastamoinen, V. Sonnenschein, and J. Aysto, *Phys. Rev. C* **82**, 052501(R) (2010).
12. W. Benenson, D. Mueller, E. Kashy, H. Nann, and L. Robinson, *Phys. Rev. C* **15**, 1187–1190 (1977).

Exotic modes of excitation in proton rich nuclei

N. Paar

Physics Department, Faculty of Science, University of Zagreb, Croatia

Abstract. The framework of relativistic energy density functional has been applied in description of excitation phenomena in nuclei close to the proton drip line. In particular, low-lying dipole excitations have been studied using relativistic quasiparticle random phase approximation, based on effective Lagrangians with density dependent meson nucleon couplings. In the isovector dipole channel, the occurrence of pronounced low-lying dipole peaks is predicted, corresponding to the proton pygmy dipole resonance. Since this exotic mode still awaits its experimental confirmation, systematic calculations have been conducted within a pool of neutron deficient nuclei, in order to identify the best possible candidates for measurements.

Keywords: soft modes, giant resonances, exotic nuclei, proton drip-line

PACS: 21.10.Gv, 21.30.Fe, 21.60.Jz, 24.30.Cz

INTRODUCTION

Nuclei away from the valley of stability exhibit unique structure phenomena in multipole response. In neutron-rich nuclei the low-energy dipole excitations indicate possible occurrence of the pygmy dipole resonance (PDR), i.e. the resonant oscillation of the weakly-bound neutron skin against the isospin saturated proton-neutron core (for more details see Ref. [1] and references therein). The onset of low-lying E1 strength has been experimentally observed not only in exotic nuclei [2], but also in stable nuclei with neutron excess, like $^{44,48}\text{Ca}$ and ^{208}Pb [3, 4]. Exotic modes of excitation in proton-rich nuclei still remain mainly unexplored and represent an open problem for future studies [5]. Because the proton drip-line is much closer to the line of β -stability than the neutron drip-line, bound nuclei with an excess of protons over neutrons can be only found in the region of light $Z \leq 20$ and medium mass $20 < Z \leq 50$ elements. For $Z > 50$, nuclei in the region of the proton drip-line are neutron-deficient rather than proton-rich. In addition, in contrast to the evolution of the neutron skin in neutron-rich systems, because of the presence of the Coulomb barrier nuclei close to the proton drip-line generally do not exhibit a pronounced proton skin, except for very light elements. Since in light nuclei the multipole response is generally less collective, all these effects seem to preclude the formation of the pygmy dipole states in nuclei close to the proton drip-line. However, model calculations based on relativistic nuclear energy density functional [6] and nonrelativistic framework with Skyrme functional [7] indicate that proton pygmy dipole states can develop in light and medium mass proton-rich nuclei. The analyses of the transition matrix elements and transition densities show that these low-energy states correspond to an exotic mode of excitation, proton pygmy dipole resonance (PPDR), i.e., excitation of protons from weakly bound orbitals, including those which are bound only due to the presence of Coulomb barrier. Since the nature of these states still has not been experimentally confirmed, more systematic model analysis has been conducted in order

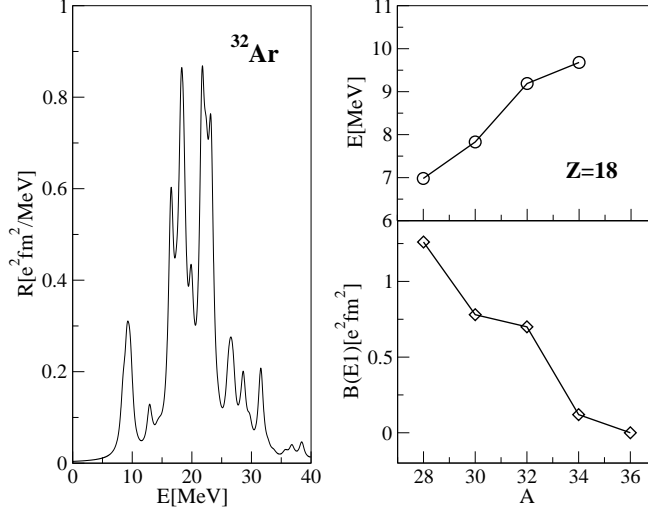


FIGURE 1. The E1 transition strength distribution in ^{32}Ar (left panel). Centroid energies and integrated B(E1) strength below 10 MeV excitation energy for Ar isotopes (right panel).

to identify nuclei with reasonable proton excess and half-lives where the PPDR is the best pronounced.

PROTON PYGMY DIPOLE RESONANCE

The relativistic nuclear energy density functional (RNEDF) represents feasible theory framework of choice for the studies of exotic modes of excitation in nuclei. By employing the RNEDF, the self-consistent relativistic QRPA has been formulated in the canonical single-nucleon basis of the relativistic Hartree-Bogoliubov (RHB) model [1]. For the interaction in the particle-hole channel effective Lagrangians with density-dependent meson-nucleon couplings are used (DD-ME2 [9]), and pairing correlations are described by the pairing part of the finite-range Gogny interaction (D1S [10]). Both in the particle-hole and pairing channels, the same interactions are used in the RHB equations that determine the canonical quasiparticle basis, and in the matrix equations of the RQRPA. This feature is essential for the decoupling of the zero-energy mode which corresponds to the spurious center-of-mass motion. Figure 1 shows the RHB+RQRPA electric dipole strength distribution in ^{32}Ar . One can observe that in addition to the rather fragmented GDR structure at ≈ 20 MeV, several prominent E1 peaks are obtained just below 10 MeV. Detailed analysis of the transition densities and transition amplitudes showed that the low-energy states constitute the structure characteristic for the PPDR [6]. The RQRPA amplitudes of the low-lying states present superpositions of many proton $2qp$ configurations, with negligible neutron contributions. The dominant configurations correspond to transitions from the proton states $1d_{3/2}$ at -2.09 MeV and $2s_{1/2}$ at -4.07 MeV. The right panel of Fig. 1 shows the mass dependence of the centroid energy of the pygmy

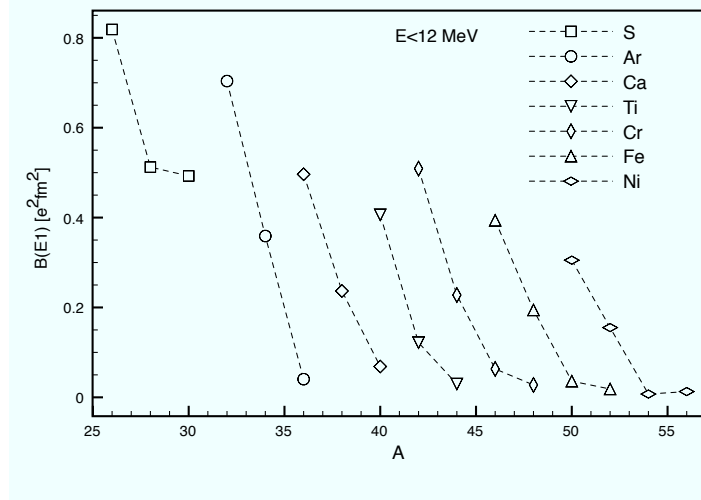


FIGURE 2. The RQRPA low-lying E1 transition strength integrated up to 12 MeV for a set of isotopes from S toward Ni.

peaks and the corresponding values of the integrated $B(E1)$ strength below 10 MeV excitation energy. It is interesting to note that in contrast to the case of medium-heavy and heavy neutron-rich isotopes, in which both the PDR and GDR are lowered in energy with the increase of the neutron number [1], in proton-rich isotopes the mass dependence of the PDR excitation energy and $B(E1)$ strength is opposite to that of the GDR. This mass dependence is intuitively expected since, the PPDR is dominated by transitions from the weakly-bound proton orbitals. As the proton drip-line is approached, either by increasing the number of protons or by decreasing the number of neutrons, due to the weaker binding of higher proton orbitals one expects more inert oscillations, i.e. lower excitation energies. The number of $2qp$ configurations which include weakly-bound proton orbitals increases towards the drip-line, resulting in an enhancement of the low-lying $B(E1)$ strength.

The occurrence of low-energy E1 transition strength has been explored in more details for a pool of nuclei from S toward Ni, from the valley of stability toward the proton-drip line. The calculated $B(E1)$ values for the whole pool involving only nuclei with reasonable decay half-lives that could be experimentally observed, are shown in Fig. 2. Similar as in the case of Ar isotopes, other neighboring nuclei also develop low-energy E1 strength with increasing proton number. Fig. 3 shows the same transition strength but displayed as function of the proton excess, $Z - N$. Obviously the low-energy E1 transition strength systematically increases with the proton excess, in accordance with the detailed structure analysis conducted in the case for Ar isotopes. The PPDR represents unique exotic mode of excitation that appears in nuclei toward the proton drip-line and its strength becomes more pronounced in lighter systems in the pool under consideration, i.e. the strongest PPDR states have been obtained for the proton-rich nuclei ^{26}S and ^{32}Ar .

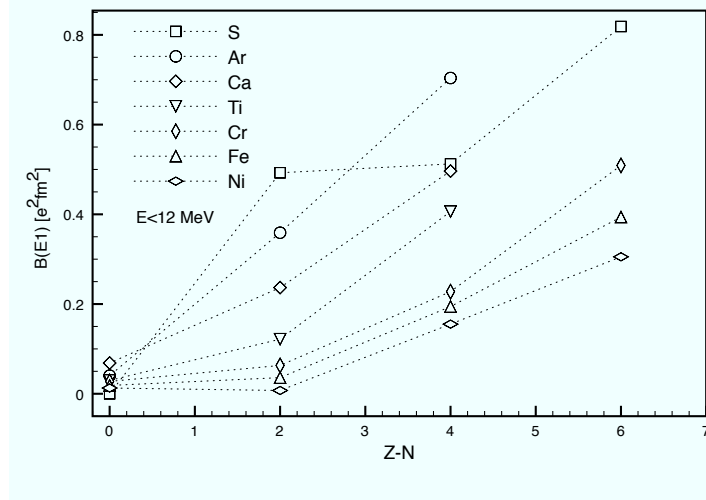


FIGURE 3. The same as in Fig. 2, but displayed as function of the proton excess $Z-N$.

CONCLUSION

The analysis of low-energy E1 strength in proton rich nuclei based on the RNEDF framework predicts the occurrence of low-energy exotic mode, the PPDR corresponding to the oscillation of the proton excess against an approximately isospin-saturated core. The PPDR states are represented by a superposition of many proton $2qp$ configurations, whereas the contribution of neutron excitations is negligible. With the decrease of the number of neutrons, for the chains of proton-rich S toward Ni isotopes, the proton PDR is lowered in energy, and the integrated $B(E1)$ strength in the low-energy region increases accordingly. It is shown that the best realistic candidates for experimental verification of the PPDR mode with the most pronounced $B(E1)$ strength are ^{26}S and ^{32}Ar .

ACKNOWLEDGMENTS

This work was supported by MZOS - project 1191005-1010 and Croatian foundation for science (HRZZ).

REFERENCES

1. N. Paar, D. Vretenar, E. Khan, and G. Colo, Rep. Prog. Phys. 70, 691 (2007).
2. P. Adrich, A. Klimkiewicz, M. Fallot, et al., Phys. Rev. Lett. 95, 132501 (2005).
3. T. Hartmann et al., Phys. Rev. Lett. 93, 192501 (2004).
4. N. Ryezayeva et al., Phys. Rev. Lett. 89, 272502 (2002).
5. N. Paar, J. Phys. G: Nucl. Part. Phys. 37, 064014 (2010).
6. N. Paar, D. Vretenar, and P. Ring, Phys. Rev. Lett. 94, 182501 (2005).
7. N. Paar, P. Papakonstantinou, V. Yu. Ponomarev, and J. Wambach, Phys. Lett. B 624, 195 (2005).
8. N. Paar, P. Ring, T. Nikšić, and D. Vretenar, Phys. Rev. C 67, 034312 (2003).
9. G. A. Lalazissis, T. Nikšić, D. Vretenar, and P. Ring, Phys. Rev. C 71, 024312 (2005).
10. J. F. Berger, M. Girod, and D. Gogny, Comp. Phys. Comm. 63, 365 (1991).

Beta delayed alpha emission from the neutron deficient rare earth isotopes ^{152}Tm and ^{150}Ho

E. Nácher^{*,†}, J.L. Taín^{*}, B. Rubio^{*}, A. Algora^{*}, L. Batist^{**}, J.A. Briz[†], D. Cano-Ott[‡], J. Döring[§], M. E. Estévez Aguado^{*}, A. Gadea^{*}, M. Gierlik[¶], Z. Janas[¶], I. Mukha[§], C. Plettner[§] and E. Roeckl[§]

^{*}*Instituto de Física Corpuscular, CSIC - Univ. de Valencia, Spain*

[†]*Instituto de Estructura de la Materia, CSIC, Madrid, Spain*

^{**}*PNPI, Gatchina, Russia*

[‡]*CIEMAT, Madrid, Spain*

[§]*GSI, Darmstadt, Germany*

[¶]*University of Warsaw, Poland*

Abstract. The study of beta-delayed proton emission is a well known method to aid the determination of the beta strength distribution in nuclei far from the stability line. At the neutron deficient side of the nuclear chart the process of proton or alpha emission from excited states is energetically allowed when one goes far enough from stability. However, beta-delayed alphas have seldom been measured for nuclei heavier than $A=20$. Here we present a study of the beta-delayed alpha-particle emission from ^{152}Tm and ^{150}Ho and their importance in the full B(GT) distribution.

Keywords: Beta decay, beta-delayed particles, beta-delayed alphas, Gamow-Teller resonance, Total Absorption Spectroscopy

PACS: 23.35.+g; 23.40.-s; 23.60.+e; 27.70.+q; 29.30.Ep

THE PHYSICS CASE

Beta delayed alpha particle emission is a rare process not frequently found along the nuclear chart. For nuclei heavier than $A \approx 20$ the coulomb barrier is high enough to suppress the emission of α particles from excited states in favor of the emission of γ -rays or even protons. However, for nuclei that are α emitters in their ground state, one might expect to observe the emission of α particles from excited states populated in the β^+ -decay of the parent. This process will, in general, compete with the prompt gamma de-excitation of the populated state, but if the β intensity distribution ($I_\beta(E)$) is such that high lying levels are strongly populated in the β^+ -decay, then the β delayed α branching ratio ($\text{BR}(\beta\alpha)$) will not be negligible and one should be able to measure such a rare process. Summarizing, in order to observe β delayed α emission two conditions must be fulfilled:

1. very low alpha separation energy (S_α) in the daughter nucleus
2. enough β population to high energy levels in the daughter nucleus

There are not many cases among the known medium mass and heavy nuclei in which these two conditions are fulfilled. The $N=83$ rare earths above ^{146}Gd are good candidates as they decay through the fast Gamow-Teller transition $h_{11/2} \rightarrow h_{9/2}$ populating a

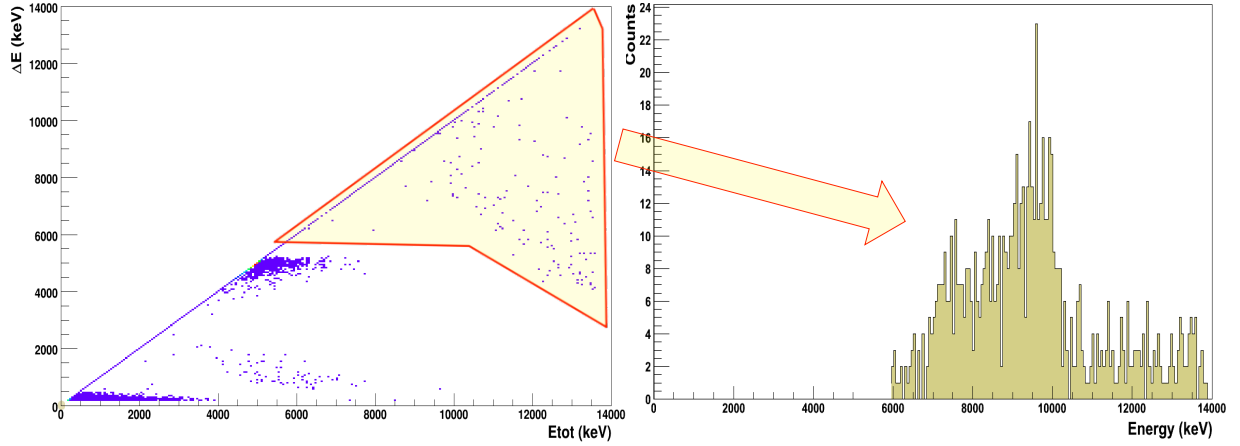


FIGURE 1. Left: ΔE -E plot obtained with the Si telescope in the decay of ^{152}Tm . Right: Total energy in the Si telescope for the β delayed α events inside the condition window shown in the left panel.

narrow resonance at ≈ 4.5 MeV in the daughter $N=84$ nuclei [1]. These latter isotopes have negative S_α and therefore one would expect to observe β delayed α 's. In what follows we report on our measurement of β delayed α emission from the low spin isomer (2^-) of ^{152}Tm and ^{150}Ho .

EXPERIMENT AND RESULTS

Beta decay of $^{152}\text{Tm}(2^-)$

The main goal of our experiment was to measure the Gamow-Teller strength distribution (B(GT)) in the β^+ -decay of the odd- $N=83$ rare earths above ^{146}Gd . The production and separation of the isotopes of interest was carried out at the GSI on-line mass separator [2]. The separated beam (in vacuum) was implanted on a tape and moved to the measuring station (in air). As most of the β^+ -decay populates levels that de-excite through the emission of prompt gamma cascades, the Total Absorption gamma Spectroscopy (TAS) technique was used to measure the β feeding properly [3]. This technique was combined with charged particle spectroscopy to estimate the amount of B(GT) missing from the former TAS measurement as a small fraction of the β^+ -decay might proceed through β delayed α emission. With this aim in mind we placed a Silicon telescope at a distance of 2.6 mm to the radioactive source inside the TAS detector. It was made of a thin ΔE detector (35 μm thick) and a thicker E detector (550 μm thick). The left panel of Fig. 1 shows a ΔE vs total E plot in which one can identify the charged particles emitted in the decay. The upper right section of this plot corresponds to the β delayed α particles emitted in the decay of ^{152}Tm . In the right panel of the same figure one can see the total energy deposited by these β delayed α particles. We clearly observe a distribution peaked at ≈ 9.5 MeV, in agreement with expectations: that the states underneath the Gamow-Teller resonance at ≈ 4.5 MeV in the daughter nucleus

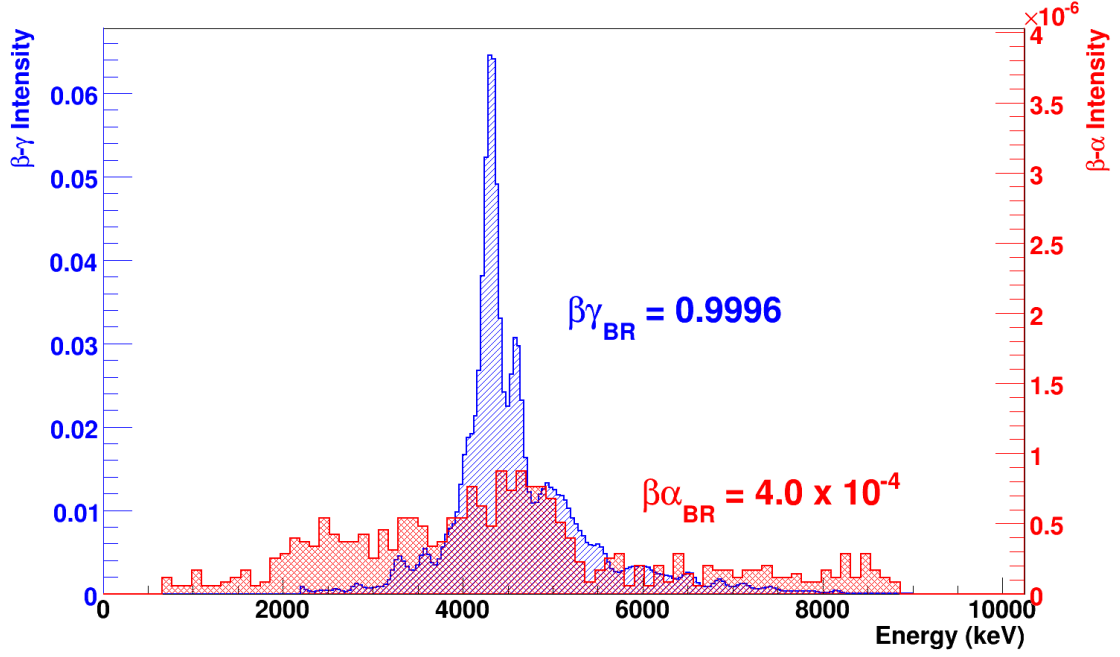


FIGURE 2. Beta intensity distributions. Blue, left axis: obtained with the TAS measuring β delayed γ -rays. Red, right axis: obtained with the Si telescope measuring β delayed α particles.

^{152}Er might decay by α emission to the ground state of ^{148}Dy ($S_{\alpha}(^{152}\text{Er}) = -4.93$ MeV).

From the time distribution of the α particles in the condition window shown in Fig. 1 we calculate a half-life of 8.7(8) s for $^{152}\text{Tm}(2^-)$, in good agreement with that of Ref. [4]. Comparing now these results for the α 's with the results from the TAS measurement one can calculate the $\text{BR}(\beta\alpha)$ as defined below:

$$\text{BR}(\beta\alpha) = \frac{I_{\beta\alpha}}{I_{\beta\alpha} + I_{\beta\gamma}} = 4.0(2) \times 10^{-4} \quad (1)$$

This small branching ratio in comparison with the $\text{BR}(\beta\gamma) = 0.9996(2)$ indicates that the B(GT) missing in the TAS measurement due to the α emission is negligible. There is an indication of β delayed protons in the left panel of Fig. 1 as well. Unfortunately, the statistics is not enough to reach any strong conclusion on these delayed protons apart from estimating an upper limit for the branching ratio: $\text{BR}(\beta p) < 3.0 \times 10^{-5}$.

At this stage one can compare the β intensity distribution proceeding through delayed γ -rays ($I_{\beta\gamma}$) or α particles ($I_{\beta\alpha}$) as shown in Fig. 2. The left vertical axis affects the $I_{\beta\gamma}$ distribution obtained with the TAS (in blue), whereas the right vertical axis applies only to the $I_{\beta\alpha}$ distribution obtained with the Silicon telescope. We see a similar structure except for the fact that there is a second bump at the left side of the main peak in the $I_{\beta\alpha}$ distribution. This, we think, might be due to the fact that sometimes the α -decay of ^{152}Er populates the first excited state in ^{148}Dy and not the ground state. Consequently,

the energy of the alpha particles is sifted by almost 2 MeV downwards in energy, which means that in reality, strictly speaking, all the counts in this bump should be placed in the main peak in the $I_{\beta\alpha}$ distribution.

Beta decay of $^{150}\text{Ho}(2^-)$

The beta decay of ^{150}Ho is very similar to that of ^{152}Tm as it is due to the same Gamow-teller transition but with lower proton occupation of the $h_{11/2}$ orbital in the initial state. Being the S_{α} negative and the I_{β} peaked at ≈ 4.5 MeV as in the previous case, one would expect very similar results as in the decay of ^{152}Tm . The measurement of the β^+ -decay of ^{150}Ho was very similar to the one described above except for the fact that in this occasion the charged particles were measured with a similar Si telescope but placed in a different beam line than the one for the TAS detector. In this way the charged particle spectroscopy could be done in vacuum and therefore in more favorable conditions.

The branching ratios for β delayed α particles and γ -rays were different in this case: $\text{BR}(\beta\alpha) = 9.2(2) \times 10^{-5}$ and $\text{BR}(\beta\gamma) = 0.999908(2)$. This might be related to the higher alpha separation energy of the daughter in this case ($S_{\alpha}(^{150}\text{Dy}) = -4.35$ MeV). These results, as well as the comparison of the beta intensity distributions of the two measurements were already presented in a report [5].

SUMMARY AND CONCLUSIONS

We have reported on two new β delayed α precursors: ^{152}Tm and ^{150}Ho , amongst the heaviest β delayed α emitters ever measured. The $\text{BR}(\beta\alpha)$ amounts to 4.0×10^{-4} in the case of ^{152}Tm and 9.2×10^{-5} in the case of ^{150}Ho , both negligible for B(GT) determination as compared to the $\text{BR}(\beta\gamma)$. There is a strong indication of β delayed protons from ^{152}Tm with $\text{BR}(\beta p) < 3 \times 10^{-5}$ still to be confirmed.

REFERENCES

1. A. Algora *et al.*, *Phys. Rev. C* **68**, 034301 (2003).
2. C. Bruske *et al.*, *Nucl. Instrum. Methods* **186**, 61 (1981).
3. M. Karny *et al.*, *Nucl. Instrum. Methods B* **126**, 411 (1997).
4. E. Nolte *et al.*, *Z. Phys. A* **309**, 33–40 (1982).
5. A. Algora *et al.*, *GSI Scientific Report* **99-1**, 23 (1999).

Nuclear structure studies along the proton dripline at ATLAS

D. Seweryniak^a, G. Lotay^b, P.J. Woods^b, M.P. Carpenter^b, C.J. Chiara^c,
H.M. David^a, T. Davinson^b, C. Hoffman^a, T.L. Khoo^a, T. Lauritsen^a, C.J.
Lister^a, Z. Liu^b, E.A. McCutchan^a, R.V.F. Janssens^a, A.M. Rogers^a,
W.B. Walters^c, S. Zhu^a

^a*Physics Division, Argonne National Laboratory, Argonne, IL 60565, USA*

^b*University of Edinburgh, Edinburgh, UK*

^c*University of Maryland, Maryland, USA*

Abstract. Nuclei far from the line of stability is one of the focal points of contemporary nuclear physics. Nuclear structure studies along the proton dripline remain an important component of the scientific program at the ATLAS facility. The GAMMASPHERE gamma-ray array and the Fragment Mass Analyzer offer unprecedented sensitivity and selectivity required to study nuclei at and beyond the proton dripline. Recent results in proton decay studies, in-beam γ -ray spectroscopy around ^{100}Sn and studies of proton resonances in light rp-process nuclei are presented. Future prospects in the context of planned and undergoing upgrades of ATLAS and experimental apparatus are also discussed.

Keywords: rp-process, proton decay, doubly magic nucleus, shell model

PACS: 21.60.Cs, 23.20.Lv, 23.20.Eu, 23.50.+z, 26.30.Ca, 27.30.+t, 27.60.+j

INTRODUCTION

Properties of nuclei far from the line of stability provide a stringent test for nuclear models and constitute critical input for understanding the nucleosynthesis. Fusion-evaporation reactions are the preferred reaction mechanism for populating proton-rich exotic nuclei. Recent improvements in experimental techniques resulted in significant progress on the proton rich side of the line of stability. In this paper, some of the experiments performed at the ATLAS facility at the Argonne National Laboratory using the Gammasphere array Ge detectors and the Fragment Mass Analyzer will be presented. Recent examples of spectroscopy of proton emitters, in-beam spectroscopy near the doubly magic ^{100}Sn nucleus, and γ -decay spectroscopy of proton resonances in light nuclei located along the path of the astrophysical rp-process will be discussed.

EXPERIMENTAL SETUP

The combination of the Gammasphere array of ~ 100 HPGe detectors in BGO Compton shields and the Argonne Fragment Mass Analyzer (FMA) offers an unprecedented gamma-ray detection efficiency and high reaction channel selectivity.

This setup has been successfully used to study many exotic nuclei. The most sensitive studies were performed using the Recoil-Decay Tagging (RDT) method. In this technique, recoiling reaction products were implanted in a double-sided Si strip detector (DSSD) placed at the FMA focal plane and correlated with their characteristic decays. In studies of light nuclei the FMA is complemented with an ionization chamber which facilitates atomic number assignment.

PROTON EMITTERS

The phenomenon of spontaneous proton emission is characteristic of nuclei with positive proton separation energy. The proton decay width is determined by the transmission through the centrifugal and the Coulomb barrier and depends on the energy and the orbital angular momentum of emitted protons. Consequently, the proton decay is a sensitive probe of wave functions of proton emitting states and provide information on nuclear masses far from the line of stability.

At least one proton emitting isotope was observed for all odd-Z elements from iodine through bismuth except promethium. The known proton emitters exhibit a variety of shapes from spherical, through transitional to highly prolate deformed. The WKB approximation can be used to calculate proton-decay widths in spherical proton emitters. In this case, orbital angular momentum, l_p , is a good quantum number. In contrast, single-proton wave functions in deformed nuclei have different l_p components and protons tunnel through a 3-dimensional barrier, which requires more sophisticated models. One of the outstanding theoretical issues is the role played by the Coriolis interaction in proton emitters. In the most recent model, the description of the Coriolis interaction was improved by considering quasi-particles rather than particles, which automatically takes into account Coriolis attenuation due to pairing [1].

In-beam spectroscopy of proton emitters provide complementary information on their structure. Recently, results from a Gammasphere experiment on excited states in the proton emitter ^{117}La were published [2]. The quasi-particle model [1] predicts that the ^{117}La proton width is consistent with the emission from a $7/2^-$ partially aligned member of the $h_{11/2}$ band. However, γ -ray transitions correlated with the ^{117}La proton decay are indicative of the $K^\pi=3/2^+$ band. This discrepancy reflects uncertainties in the choice of parameters such as the Coriolis attenuation or the pairing strength. More detailed studies of known deformed proton emitters and search for new cases would help to constrain these parameters.

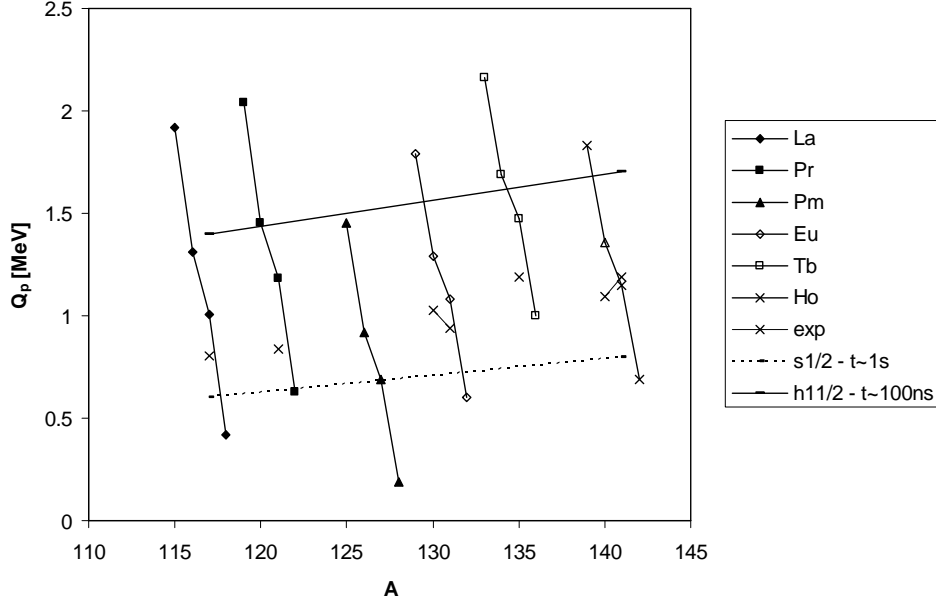


FIGURE 1. Proton decay Q-values for highly deformed proton emitters as a function of the mass number. The measured values represented by crosses are compared with the calculations of Liran and Zeldes [2]. The solid and the dashed line represent Q-values for which the $h_{11/2}$ state would have lifetime of about 100 ns and the $s_{1/2}$ states would have the lifetime of about 1 s, respectively.

Observation of other even more exotic highly deformed proton emitters is hampered by small crosssections and lifetimes which are shorter than a time of flight through a recoil mass separator. Figure 1 shows proton Q-values of known highly-deformed proton emitters as a function of the mass number. For comparison, proton Q-values calculated using the Liran-Zeldes model [3] are included. The area between the line corresponding to the $s_{1/2}$ emission with a lifetime of about 1s and the line corresponding to the $h_{11/2}$ emission with a lifetime of about 100 ns represents Q-values which are experimentally accessible. Close examination of Fig. 2 indicates that the ^{125}Pm , ^{139}Eu , ^{139}Ho odd-Z, odd-Z even-N and ^{116}La , ^{120}Pr , ^{134}Pr odd-Z, odd-N fast deformed proton emitters could still be within experimental reach.

SINGLE-NEUTRON STATES IN ^{101}Sn

The doubly magic ^{100}Sn nucleus determines the structure of proton rich mid mass nuclei. It is located at the point where the $N=Z$ line crosses the proton drip line. The rp-process was proposed to terminate with α decays of light Te isotopes. The states in nuclei containing one or two nucleons outside of the ^{100}Sn core provide information on single-particle energies and nucleon-nucleon interactions which are essential ingredients in shell model calculations used to assign multi-particle configurations in nuclei around ^{100}Sn .

The ^{100}Sn region has been studied in the past using variety of probes and experimental methods. The β decay of ^{100}Sn was recently characterized at GSI after fragmentation. Until recently, nothing was known about excited states in nuclei with

one valence particle or hole in the ^{100}Sn core or in ^{100}Sn itself. A single 172-keV γ -ray transition was assigned to ^{101}Sn for the first time using Gammasphere and the FMA [4]. In this experiment, prompt γ -ray transitions in ^{101}Sn were tagged by β -delayed protons using the RDT method. The 172-keV transition was proposed to connect the $g_{7/2}$ and $d_{5/2}$ single-neutron states. Recently, observation of the ^{109}Xe - ^{105}Te - ^{101}Sn α -decay chain was reported [5]. Two α lines were assigned to the ^{105}Te ground state decay. Surprisingly, the strong 90% branch, which was associated in the past with the ground state to ground state decay, was found to feed the excited state at 172 keV. In contrast, the corresponding branch in ^{107}Te is only 0.5%. This observation led authors to the conclusion that the order of the two lowest states in ^{101}Sn is inverted implying that the $g_{7/2}$ single-neutron orbital is located below the $d_{5/2}$ orbital in ^{101}Sn .

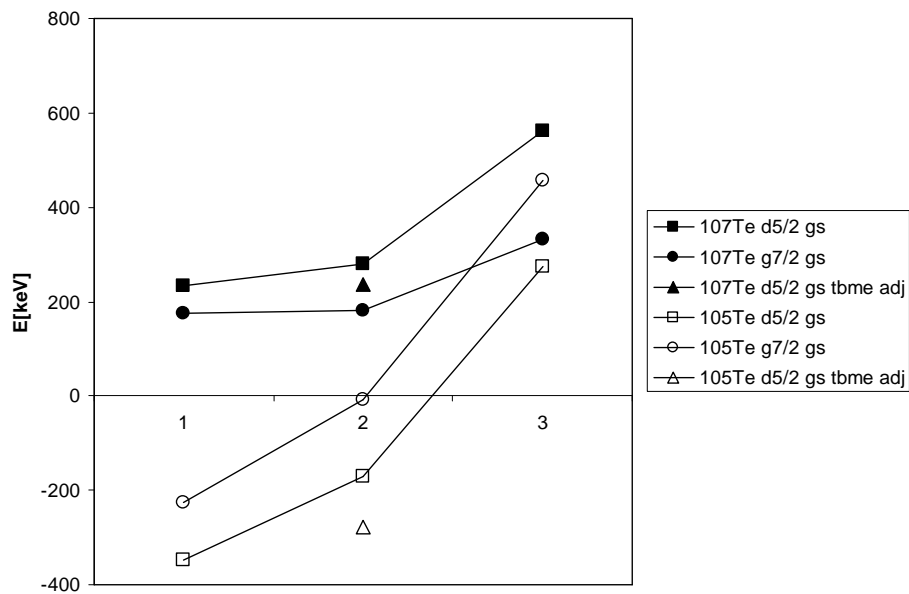


FIGURE 2. Calculated energy of the $7/2^+$ state relative to the $5/2^+$ state in ^{105}Te and ^{107}Te as a function of the $s_{1/2}$ and $d_{3/2}$ single-neutron energies (1-2.5 MeV, 2-3.5 MeV, 3-infinite) relative to $d_{5/2}$ and $g_{7/2}$.

Both papers concluded that their assignments are in agreement with shell model calculations for the light Sn isotopes. Given the inherent uncertainties of the shell model calculations this argument has to be considered as inconclusive. Also, the observed α decay pattern in ^{105}Te can be explained by assuming the $7/2^+$ ground state in ^{105}Te instead of $5/2^+$ and leaving the order in ^{101}Sn unchanged. This hypothesis was tested by calculating the lowest excited states in ^{105}Te . Similarly to the light odd Sn isotopes, a doublet with spins $5/2^+$ and $7/2^+$ was predicted at low energies. In Fig. 2 the calculated separation between the two states in ^{105}Te and ^{107}Te is shown as a function of the energy of the $s_{1/2}$ and $d_{3/2}$ orbitals assuming different order of the $d_{5/2}$ and $g_{7/2}$ orbitals in ^{101}Sn . It is clear from Fig. 2 that in ^{107}Te the $5/2^+$ state is the ground state. In ^{105}Te the $5/2^+$ ground state is predicted only when the $d_{3/2}$ and $s_{1/2}$ states were not included in the calculations. Already at the $s_{1/2}$, $d_{3/2}$ energy of 3.5 MeV the lowest calculated state in ^{105}Te has spin $7/2^+$. The $s_{1/2}$, $d_{3/2}$ energies in the 2-3 MeV range are

consistent with data on odd Sb isotopes. This indicates that the inversion of the $5/2^+$ and $7/2^+$ states in ^{107}Te is plausible and could be responsible for the observed ^{105}Te α -decay pattern. However, in view of the uncertain $s_{1/2}$ and $d_{3/2}$ energies, unambiguous assignment will require more experimental evidence.

LIGHT NUCLEI ALONG THE RP-PROCESS PATH

The astrophysical rapid proton capture process was proposed to be one of the processes which are responsible for the synthesis of nuclei heavier than Oxygen in exploding stars such as novae, X-ray bursters and super novae. The rp-process is a sequence of (p,γ) reactions competing at high temperatures during the explosion with β decays in these hydrogen rich environments. Proton capture cross sections are essential for calculating the rp-process path. Only a few of these reactions were studied directly in recent years using radioactive beams. In the majority of cases the cross sections must be calculated. These calculations require knowing properties of a handful of states located above the proton threshold. The cross sections depend sensitively on the energies, spins and parities of these resonant states.

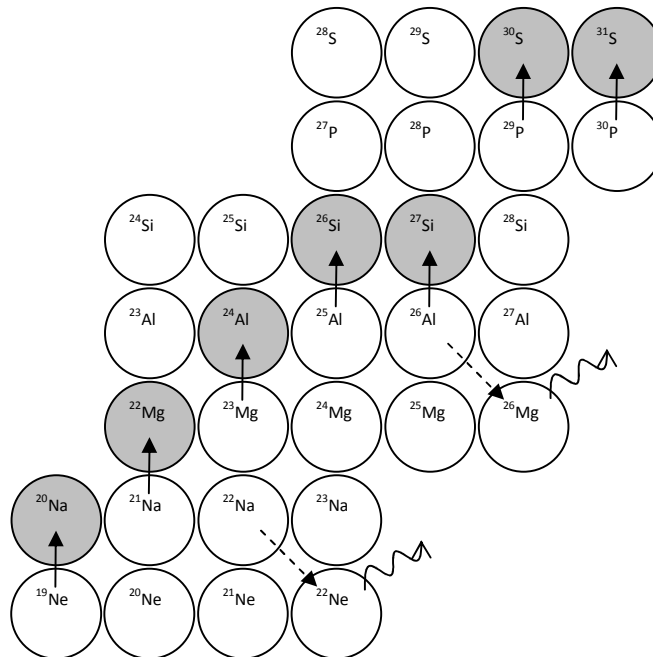


FIGURE 3. Light nuclei along the path of the rp-process. Shaded circles mark nuclei which have been studied with Gammasphere and the FMA. Solid and dashed arrows represent (p,γ) reactions and β decays, respectively. The ^{22}Na and ^{26}Al β decays are followed by emission of γ rays.

Several light proton-rich nuclei were populated in heavy-ion fusion evaporation reactions at ATLAS. Gamma-ray emission from levels above the proton threshold was characterized in nuclei shown in Fig. 3. These nuclei are important for production of ^{22}Na and ^{26}Al , which are candidates for cosmogenic γ -ray emitters. Their abundances can be measured using satellite borne γ -ray detector arrays and compared with rp-process network calculations.

The proton capture on the 5^+ ground state and the 0^+ isomer in ^{26}Al destroy ^{26}Al thus having direct impact on the ^{26}Al abundance. The states above the proton threshold in ^{27}Si were studied using the $^{12}\text{C}(^{16}\text{O}, p)^{27}\text{Si}$ reaction. Gamma rays deexciting the states populated in ^{27}Si were detected using Gammasphere. Since the one-proton evaporation was one of the strongest reaction channels the FMA was not used in this case. In particular, γ -ray transitions from the 68 keV and 126 keV resonances were observed leading to the $5/2^+$ and $9/2^+$ spin assignments, respectively, and implying the $l=2$ and $l=0$ proton capture on the 5^+ ground state [6]. As a result, the uncertainty of the proton capture to these two states, which dominate the total cross section at temperatures around $T\sim 0.5$ GK, was reduced by two orders of magnitude. Such low temperatures are characteristic of Wolf-Rayet stars believed to be significant sources of ^{26}Al in the Galaxy. In addition, a $1/2^+$ resonance at 146 keV ($l=0$) and a $3/2^-$ resonance at 378 keV ($l=1$), which dominate the proton capture on the 0^+ , were found [7]. It is noteworthy that a counterpart was found in the mirror ^{27}Al nucleus for all observed states in ^{27}Si validating mirror symmetry as a tool for spin and parity assignment in light nuclei [8].

OUTLOOK

The ATLAS facility is undergoing efficiency and intensity upgrade. At the same time Gammasphere and the Fragment Mass Analyzer are being prepared to run with higher beam intensities. A digital data acquisition system will be used for Gammasphere. This will limit pileup in the Ge detectors. Waveforms from the DSSD will be also digitized so signals in rapid succession corresponding to fast activities can be disentangled. The system will be operated in the triggerless mode which will significantly reduce the dead time. It is expected that a gain of about 10 in sensitivity can be achieved after the upgrades are completed. These improvements will benefit in-beam studies of one- and two-quasi particle neighbors of and ^{100}Sn itself. They will facilitate searches for more deformed proton emitters discussed above. They will also help to extend in-beam studies of proton resonances to heavier rp-process nuclei.

ACKNOWLEDGMENTS

This work was supported by the U. S. Department of Energy, Office of Nuclear Physics, under contract No. DE-AC02-06CH11357.

REFERENCES

1. G. Fiorin et al., *Phys. Rev. C* **99**, 054302 (2007).
2. S. Liran and N. Zeldes, *At. Data and Nucl. Data Tables* **17**, 431 (1976).
3. Z. Liu et al., *Phys. Lett.*, accepted.
4. D. Seweryniak et al., *Phys. Rev. Lett.* **99**, 022504 (2007).
5. I.G. Darby et al., *Phys. Rev. Lett.* **105**, 162502 (2010).
6. G. Lotay et al., *Phys. Rev. Lett.* **102**, 162502 (2009).
7. G. Lotay et al., *Phys. Rev. C* **102**, 055802 (2009).
8. G. Lotay et al., *Phys. Rev. C*, accepted.

Nonadiabatic effects in odd-odd deformed proton emitters

M. Patial*, P. Arumugam*,[†], A.K. Jain*, E. Maglione** and L.S. Ferreira[†]

**Department of Physics, Indian Institute of Technology Roorkee, Uttarakhand 247 667, India*
[†]*Centro de Física das Interações Fundamentais, and Departamento de Física, Instituto Superior Técnico, Avenida Rovisco Pais, P1049-001 Lisbon, Portugal*

***Dipartimento di Fisica “G. Galilei”, Via Marzolo 8, I-35131 Padova, Italy and Istituto Nazionale di Fisica Nucleare, Padova, Italy*

Abstract. We present for the first time, the nonadiabatic quasiparticle approach to study proton emission from odd-odd deformed nuclei. Coriolis effects are incorporated in both the parent and daughter wavefunctions and hence our formalism allows us to study their complete role on the decay widths. First results obtained for the nucleus ^{112}Cs suggest a weak dependence on Coriolis effect. However, we are able to reproduce the experimental half-lives without assuming the exact Nilsson orbital from which the decay proceeds.

Keywords: Proton emission, Dripline nuclei, odd-odd deformed nuclei

PACS: 23.50.+z, 21.10.Tg, 27.60.+j

INTRODUCTION

It is well established [1, 2, 3, 4] that decay from deformed nuclei proceeds from a single-particle Nilsson resonance of the unbound proton with respect to the core, generated by the Coulomb and centrifugal barriers. However it is important to consider the non-adiabatic effects, which take care of the rotational excitations of the daughter nucleus, through the Coriolis interaction in a particle-plus-rotor model approach. A proper treatment of the pairing residual interaction [2] provides a more complete and consistent description of proton emission in agreement with the experimental data.

Recently with this description it was possible to obtain [5], for the first time, a clear evidence for partial rotation alignment in a proton emitting nucleus and the angular momentum $J^\pi = 7/2^-$ was assigned for the decaying state in ^{121}Pr . Our approach has been extended successfully to explain proton emission from triaxial nuclei as well. In the case of ^{161}Re [6] inclusion of triaxial deformation could explain experimental data, with angular momentum $1/2^+$ for the proton emitting state. For the nucleus ^{145}Tm [7] the analysis of the energy spectra of parent and daughter nuclei, half-life and fine structure confirmed a large triaxiality with a high degree of confidence. All experimental data corresponding to the unique case of ^{141}Ho namely, the rotational spectra of parent and daughter nuclei, decay widths and branching ratios for ground and isomeric states, have been well explained with a strong triaxial deformation $\gamma \sim 20^\circ$ [8]. These studies reveal that proton emission measurements can be a precise tool to probe triaxial deformations and other structural properties of exotic nuclei beyond proton drip-line.

The nonadiabatic effects which play crucial role in our calculations, are considered so far in the case of odd-even nuclei only and the odd-odd nuclei were studied [4] within

the strong coupling limit. Odd-odd nuclei are more interesting due to the complexities involved in the coupling of proton as well as neutron with the core [9, 10, 11]. However, this area is least explored [10] and hence the theoretical study of structure of these nuclei has not been carried out extensively despite rich experimental data being available. In the present work we undertake the important task of formulating a proper theoretical framework comprising the Coriolis interaction, to study proton emission from odd-odd deformed nuclei. We also discuss our preliminary results in the case of ^{112}Cs .

THEORETICAL FRAMEWORK

We consider the parent nucleus as a deformed core plus proton plus neutron system and the daughter nucleus as a deformed core plus neutron system. The decay width is obtained by calculating microscopically the overlap of the initial state wave-function of the odd-odd nucleus (two quasiparticles plus rotor model) with the final state wave-function which is for the proton coupled with daughter nucleus (quasiparticle plus rotor model).

The total Hamiltonian in case of two quasiparticle plus rotor model (TQPRM) [9] can be written as $H = H_{int} + H_{rot}$ where

$$H_{rot} = \frac{\hbar^2}{2\mathfrak{S}} [(I^2 - I_z^2) - (I^+ j^- + I^- j^+) + j_p^+ j_n^- + j_p^- j_n^+ + (j_p^2 - j_{p_z}^2) + (j_n^2 - j_{n_z}^2)]. \quad (1)$$

Here I is the total angular momentum of the nucleus, given by $I = R + j$ with R and j ($= j_n + j_p$) as angular momentum of core and particles respectively, and all other symbols used have their usual meanings. The variable moment of inertia (VMI) is defined as $\mathfrak{S}(I) = \mathfrak{S}_0 \sqrt{1 + b I(I+1)}$, where b is the VMI parameter and the constant \mathfrak{S}_0 is evaluated by fitting the energy of the first excited 2^+ state of the core. The single-particle wavefunctions are generated with the deformed Wood-Saxon potential using parameters from Ref. [12]. Pairing interactions are considered within constant gap BCS approach, where the pairing gap is chosen as $12/\sqrt{A}$ MeV. The wavefunction of the daughter nucleus is calculated using the quasiparticle plus rotor model which is presented in Ref. [2].

The components of the eigenvectors from Coriolis coupled calculations for both parent ($a_{K_T, K_n, K_p}^{I, M}$) and daughter nuclei ($a_{K_n}^{I_d, M_d}$), are used to calculate the partial decay width given by

$$\Gamma_{l_p j_p}^{I, I_d}(r) = \frac{\hbar^2 k}{\mu} \left| \sum_{K_n, K_p (K_T = K_n \pm K_p)} a_{K_T, K_n, K_p}^{I, M} a_{K_n}^{I_d, M_d} \times \sqrt{\frac{(2I_d + 1)}{(2I + 1)}} \langle I_d, K_n, j_p, K_p | I, K_T \rangle u_{K_p} \frac{\phi_{j_p, K_p}^p(r)}{G_{l_p} + iF_{l_p}} \right|^2, \quad (2)$$

where $\phi_{j_p, K_p}^p(r)$ are the radial components of the eigenfunctions of the Nilsson Hamiltonian. The quantity $|u_{K_p}|^2$ gives the probability that the proton single-particle level in

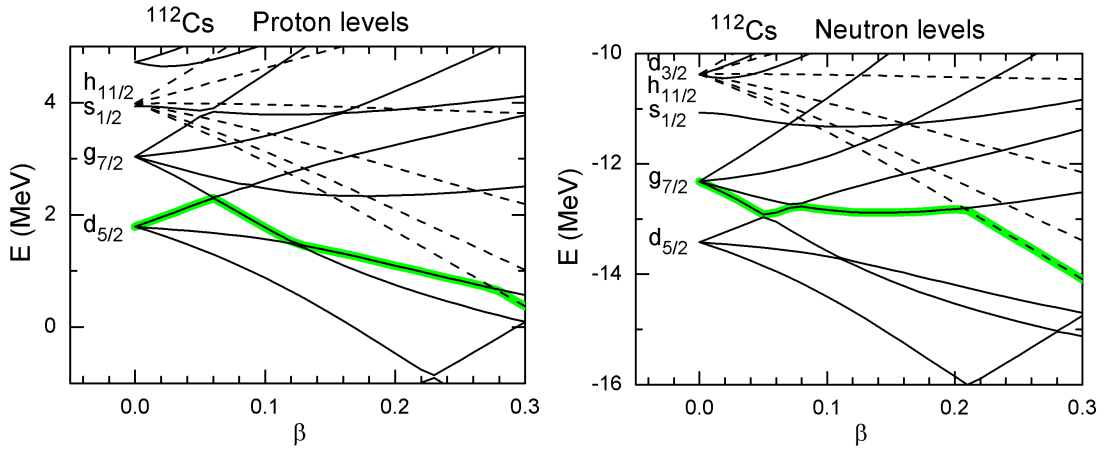


FIGURE 1. Single-particle levels of interest for ^{112}Cs as a function of axial quadrupole deformation with $\beta_4 = 0$. The solid and dashed lines stand for positive and negative parity levels respectively. The Fermi level is shaded.

TABLE 1. The half-life of ^{112}Cs in milliseconds.

Theory ($\beta = 0.22, I_d^\pi = 3/2^+$)	$I^\pi = 0^+$	$I^\pi = 3^+$
Adiabatic	0.579	0.460
Nonadiabatic		
$\rho = 0.5$	0.632	0.515
$\rho = 1.0$	0.742	0.648
Experiment [13]	0.5 ± 0.1	

the daughter nucleus is empty and is obtained from the BCS calculation. F and G are regular and irregular Coulomb functions, respectively. The decay width is calculated at an asymptotic distance, as a sum of all the partial decay widths over allowed j_p values.

RESULTS AND DISCUSSION

As a first case we studied the nucleus ^{112}Cs for which adiabatic calculations are already presented in Ref. [4]. The first step is to look at the Nilsson levels (Fig. 1) to choose the important states around the Fermi level, to be included in the Coriolis mixing. At the deformation 0.22 (suggested by Moller, Nix and Swiatecki [14]), interestingly, for both protons and neutrons it is the same set of levels which are important. In both the cases the positive parity states are more probable except at higher deformations. If we choose to use four levels each for proton and neutron, then the states getting priority will be the Nilsson levels denoted by the asymptotic quantum numbers $3/2[422]$, $1/2[420]$, $3/2[411]$ and $1/2[431]$.

Our next step is to fix the angular momentum of the daughter nucleus ^{111}Xe which can be done by looking at the minimum in energy, for various combinations of spin and parity (I_d^π), calculated in the nonadiabatic quasiparticle approach. In the nonadiabatic

calculation with quasiparticles, the ground state for a given spin and parity should come out automatically as the least energy state [2]. For these calculations we need the moment of inertia (\mathcal{I}_0) of the core and the VMI parameter (b). \mathcal{I}_0 is obtained from the energy of 2^+ state in ^{110}Xe (469.7 keV [15]). The parameter b is obtained by fitting the rotational spectrum of ^{110}Xe . At the deformations near 0.2 the least energy state comes out to be that of $3/2^+$ in ^{111}Xe .

We have calculated the half-life of ^{112}Cs for two probable angular momenta, namely 0^+ and 3^+ . The results are presented in Table 1 along with the experimental value. The nonadiabatic calculations are carried out with (50%, $\rho = 0.5$) and without (0%, $\rho = 1.0$) attenuation of the Coriolis interaction. The results of nonadiabatic calculations are very similar to the adiabatic calculations. Considering the uncertainty in the experimental half-life and in the Q -value for proton emission (which result in uncertainty in our calculations), the role of nonadiabatic effects are weak to ascertain them. Nevertheless, the nonadiabatic calculations give a good fit for systematically calculated daughter nucleus angular momentum along with the probable angular momenta for the parent nucleus, without the assumption of the decaying state.

In summary, we have extended our nonadiabatic approach for calculating proton emission half-lives, to odd-odd deformed nuclei. The Coriolis effects seem to be weak in the case of ^{112}Cs . Without assuming the decaying state, we could reproduce the half-life of ^{112}Cs .

ACKNOWLEDGMENTS

This work was supported by the Fundação para a Ciência e a Tecnologia (Portugal), Projects: PTDC/FIS/68340/2006, SFRH/BPD/26642/2006 and CERN/FP/116385/2010. Financial support from C.S.I.R. (MP) and D.S.T. (AKJ), Govt. of India is acknowledged.

REFERENCES

1. E. Maglione, L. S. Ferreira, and R. J. Liotta, *Phys. Rev. Lett.* **81**, 538 (1998).
2. G. Fiorin, E. Maglione, and L. S. Ferreira, *Phys. Rev. C* **67**, 054302 (2003).
3. E. Maglione, L. S. Ferreira, and R. J. Liotta, *Phys. Rev. C* **59**, R589 (1999).
4. L. S. Ferreira, and E. Maglione, *Phys. Rev. Lett.* **86**, 1721 (2001).
5. M. C. Lopes, E. Maglione, and L. S. Ferreira, *Phys. Lett. B* **673**, 15 (2009).
6. P. Arumugam, E. Maglione, and L. S. Ferreira, *Phys. Rev. C* **76**, 044311 (2007).
7. P. Arumugam, L. S. Ferreira, and E. Maglione, *Phys. Rev. C* **78**, 041305 (2008).
8. P. Arumugam, L. S. Ferreira, and E. Maglione, *Phys. Lett. B* **680**, 443 (2009).
9. A. K. Jain, J. Kvasil, R. K. Sheline, and R. W. Hoff, *Phys. Rev. C* **40**, 432 (1989).
10. A. K. Jain, R. K. Sheline, D. M. Headly, P. C. Sood, D. G. Burke, I. Hrivnácová, J. Kvasil, D. Nosek, and R. W. Hoff, *Rev. Mod. Phys.* **70**, 843 (1998).
11. D. M. Headly, R. K. Sheline, P. C. Sood, R. W. Hoff, I. Hrivnácová, J. Kvasil, D. Nosek, A. K. Jain, and D. G. Burke, *At. Data Nucl. Data Tables* **69**, 239 (1998).
12. H. Esbensen, and C. N. Davids, *Phys. Rev. C* **63**, 014315 (2000).
13. R. D. Page, P. J. Woods, R. A. Cunningham, T. Davinson, N. J. Davis, A. N. James, K. Livingston, P. J. Sellin, and A. C. Shotton, *Phys. Rev. Lett.* **72**, 1798 (1994).
14. P. Moller, J. Nix, W. Myers, and W. Swiatecki, *At. Data Nucl. Data Tables* **59**, 185 (1995).
15. M. Sandzelius, et al., *Phys. Rev. Lett.* **99**, 022501 (2007).

Microscopic calculations of Q_p -values in well-deformed odd- Z proton emitters

L. Bonneau, J. Le Bloas and P. Quentin

*Université Bordeaux I, CNRS/IN2P3, Centre d'Etudes Nucléaires de Bordeaux-Gradignan,
Gradignan F-33175, France*

Abstract. Within the Hartree–Fock–BCS and Highly Truncated Diagonalization microscopic approaches we have calculated the ground-state binding energies of axially-deformed odd- Z , even- N nuclei in the $A \sim 130$ region and of the even-even daughter nuclei resulting from one-proton emission. The deduced Q_p values are in fair agreement with available experimental data.

Keywords: Binding energy, beyond Hartree–Fock approach, pairing correlations, odd-mass nuclei

PACS: 21.10.Dr, 21.60.Jz, 23.50.+z

INTRODUCTION

The calculation of one-proton emission Q -values represents a challenge for nuclear-structure models since their ingredients are not fitted on experimental data in the proton-emitting nuclei. This is particularly true for the microscopic approaches—such as the mean-field-plus-correlations approaches—involving an effective nucleon-nucleon interaction usually fitted in the valley of stability. The goal of the present work is to assess the reliability of the Hartree–Fock–BCS approach and the Highly Truncated Approach (HTDA) which both use the Skyrme force and include the effects of core polarization in odd-mass nuclei and pairing correlations—especially their quenching in odd-mass nuclei.

THEORETICAL FRAMEWORK

To describe the ground state of well-deformed odd-mass nuclei we start from the mean-field solution obtained within the HFBCS approximation in which all nucleons participate in the creation of the mean field in which they move. This self-consistent problem is solved iteratively by blocking the extra nucleon—with respect to the underlying even-even core which corresponds here to the daughter nucleus—in a chosen single-particle state (see, e.g., Ref. [1]). The ground-state solution is then obtained by retaining the lowest-energy solution among those corresponding to all possible blocked states. In practice, the relevant blocked states lie near the Fermi level of the even-even core. As discussed in, e.g., Ref. [1], the neutron and proton single-particle spectra do not exhibit the Kramers degeneracy owing to the time-reversal symmetry breaking by the HF approximation and the resulting core polarization allows to quantitatively account for the empirically observed quenching of the spin gyromagnetic ratio [6].

In order for the above iterative scheme to converge, one often needs to incorporate the one-body effect of pairing correlations in the form of non-integer occupation numbers

for all the single-particle states except the blocked state which is fully occupied and does not participate in the pairing correlations. After this HFBCS calculation, one extracts the Slater determinant $|\Phi_{K\pi}\rangle$ filled with the lowest-energy single-particle states including the blocked state with quantum numbers K (projection of angular momentum on the symmetry axis) and π (intrinsic parity).

Two remarks are in order in the context of Q_p calculations. On the one hand, the notion of pair of single-particle states has to be properly defined in odd-mass nuclei. To do so we calculate the overlap of a given state $|i\rangle$, whose quantum numbers are K and π , with the time-reversed conjugate $|\bar{j}\rangle$ of each state $|j\rangle$ having quantum numbers $-K$ and π . The pair partner $|\bar{i}\rangle$ of the state $|i\rangle$ is the one whose absolute value of the overlap is maximum (close to 1 in practice) [3]. On the other hand, the question of the treatment of the exchange Coulomb terms in the mean-field potential and the binding energy arises. For computation time reasons we have used the Slater approximation. However, according to Ref. [4], this is expected to be appropriate in open-shell nuclei such as those considered in this work.

For the above mean-field solution to be relevant, it is necessary to restrict oneself to nuclei exhibiting a well-pronounced deformation, to avoid strong degeneracy and particle-vibration coupling in spherical nuclei and shape-mixing in soft nuclei. Therefore the HFBCS approach is suited to mid-shell nuclei, as in the rare-earth region ($A \sim 130$ for the considered proton-emitting nuclei). For simplicity we restrict ourselves to axially-deformed nuclei assuming, in addition, left-right reflection symmetry. However the BCS treatment of pairing correlations in these open-shell nuclei yields ground-state solutions which are superpositions of many-body states corresponding to different nuclei. To solve this problem, we have chosen to use the HTDA framework, which can be interpreted as a shell-model type of approach based on a mean-field solution. It has been recently applied in various contexts such as isospin mixing in $N = Z$ even-even nuclei with pairing correlations [2], magnetic moments of odd-mass nuclei [3], and the giant quadrupole resonance in ^{40}Ca [5].

In HTDA calculations, the hamiltonian $\hat{H} = \hat{K} + \hat{V}$, where \hat{K} denotes the kinetic energy and \hat{V} the effective nucleon-nucleon interaction (here the Skyrme force in its SIII parametrization [7]), is split into the expectation value of \hat{H} in the Slater determinant $|\Phi_{K\pi}\rangle$, the independent quasi-particle hamiltonian \hat{H}_{IQP} , and the residual interaction \hat{V}_{res}

$$\hat{H} = \langle \Phi_{K\pi} | H | \Phi_{K\pi} \rangle + \underbrace{\hat{K} + \hat{V}_{\text{HF}} - \langle \Phi_{K\pi} | \hat{H}_{\text{HF}} | \Phi_{K\pi} \rangle}_{\hat{H}_{\text{IQP}}} + \underbrace{\hat{V} - \hat{V}_{\text{HF}} + \langle \Phi_{K\pi} | \hat{V} | \Phi_{K\pi} \rangle}_{\hat{V}_{\text{res}}}, \quad (1)$$

where \hat{V}_{HF} denotes the HF potential and $\hat{H}_{\text{HF}} = \hat{K} + \hat{V}_{\text{HF}}$ is the HF hamiltonian. Since the SIII pairing matrix elements do not have satisfactory properties, they are replaced by those of a delta interaction [8], with a strength $V_0^{(T=1)}$ in the $T = 1$ channel and a strength $V_0^{(T=0)}$ in the $T = 0$ channel as in Ref. [10]. The many-body basis in which the HTDA hamiltonian is diagonalized is made of single-pair excitations created on the quasi-vacuum $|\Phi_{K\pi}\rangle$, truncated using a cut-off on their unperturbed excitation energy chosen as $3\hbar\omega(A)$ with $\hbar\omega(A) = 41A^{-\frac{1}{3}}$ MeV.

The binding energy $E(N, Z)$ of the HTDA ground-state solution $|\Psi_{K\pi}\rangle$ can thus be written as $E(N, Z) = E_{\text{MF}}(N, Z) + E_{\text{corr}}(N, Z)$, where the mean-field contribution

$E_{\text{MF}}(N, Z)$ and the correlation energy $E_{\text{corr}}(N, Z)$ are given by

$$E_{\text{MF}}(N, Z) = \langle \Phi_{K\pi} | \hat{H} | \Phi_{K\pi} \rangle, \quad E_{\text{corr}}(N, Z) = \langle \Psi_{K\pi} | \hat{H}_{\text{IQP}} | \Psi_{K\pi} \rangle + \langle \Psi_{K\pi} | \hat{V}_{\text{res}} | \Psi_{K\pi} \rangle. \quad (2)$$

The proton-decay Q -value can therefore be decomposed as the sum of the mean-field contribution $Q_p^{(\text{MF})}$ and the contribution $Q_p^{(\text{corr})}$ brought by correlations

$$Q_p(N, Z) = \underbrace{E_{\text{MF}}(N, Z) - E_{\text{MF}}(N, Z-1)}_{Q_p^{(\text{HF})}} + \underbrace{E_{\text{corr}}(N, Z) - E_{\text{corr}}(N, Z-1)}_{Q_p^{(\text{corr})}}. \quad (3)$$

RESULTS AND DISCUSSION

The HFBCS calculations have been performed using the seniority force with the strengths (in MeV) $g_n = -17.7/(11 + N)$ for neutrons and $g_p = -17.7/(11 + Z)$ for protons, and a single-particle valence space made of all states up to 6 MeV above the chemical potential. The one-body states are expanded in the cylindrical harmonic-oscillator basis with $N_0 = 12$ and optimized parameters b and q in the notation of Ref. [11]. In the HTDA framework, the results are obtained with the strength $V_0^{(T=1)} = -300 \text{ MeV} \cdot \text{fm}^3$ of the delta residual interaction (see Ref. [12]). As it turns out, the Q_p -value has been found to be insensitive to the $T = 0$ channel, although the neutron-proton pairing is active in both channels. Therefore we present and discuss the results obtained without $T = 0$ pairing correlations.

In table 1 the Q_p -values calculated in the HFBCS and HTDA models are compared with the measured values taken from Ref. [9] when available. Overall the order of magnitude of HFBCS and HTDA results is consistent with the experimental data. More precisely, the root-mean-square (rms) deviations amount to 282 keV and 467 keV, respectively. In fact, if one discards the case of ^{131}Eu in the HTDA calculations, the rms error reduces to about 300 keV, comparable to the HFBCS one. It is interesting to

TABLE 1. Comparison of Q_p -values (in MeV) calculated in the HFBCS and HTDA models with the experimental data taken from Ref. [9] when available. Following the K^π values is given the dominant spherical configuration resulting from the HFBCS calculations.

Proton emitter	Experiment		K^π	Theory	
	$J^\pi(\text{g.s.})$	$Q_{p,\text{nucl.}}$		$Q_p^{(\text{HFBCS})}$	$Q_p^{(\text{HTDA})}$
^{127}Pm			$\frac{5}{2}^-(h11/2)$	0.556	0.078
			$\frac{5}{2}^+(g7/2)$	0.923	0.442
			$\frac{3}{2}^+(d5/2)$	1.307	0.873
^{131}Eu	$\frac{3}{2}^+$	0.959	$\frac{3}{2}^+(d5/2)$	1.168	0.198
^{135}Tb	$(\frac{7}{2}^-)$	1.200	$\frac{7}{2}^-(h11/2)$	1.696	1.109
^{141}Ho	$\frac{7}{2}^-$	1.190	$\frac{7}{2}^-(h11/2)$	1.106	1.224
^{141m}Ho	$\frac{1}{2}^+$	1.255	$\frac{1}{2}^+(d3/2, d5/2)$	1.109	0.723

note that, where the HFBCS approximation leads to the poorer agreement, namely in ^{135}Tb , the HTDA calculation provides a good agreement. The overall larger scattering of HTDA results as compared to the HFBCS results could be due to the mean-field contribution $Q_p^{(\text{MF})}$. Indeed this term is calculated using an underlying Slater determinant $|\Phi_{K\pi}\rangle$ which is not, strictly speaking, a variational solution, contrary to the BCS wave function.

An important observation about the HTDA Q_p -values is that they generally underestimate the experimental values. Apart from the above consideration about the mean-field contribution, the inclusion of missing correlations could improve the HTDA results. In particular the pairing correlations should provide a larger contribution to $Q_p^{(\text{corr})}$ if we include double-pair excitations in addition to single pairs. Indeed it has been shown that their role is to enhance the weight of single-pair excitations in the correlated wave function while their weight remains small (see, e.g., ref. [10]). Because of the quenching of pairing in odd-mass nuclei, the effect of double pairs is expected to be stronger in the daughter nucleus and thus to increase Q_p .

Finally, in the case of ^{127}Pm , both models predict the ground-state spin and parity to be $5/2^-$ but the HTDA values of Q_p are much smaller than in the HFBCS calculations, as in the other studied nuclei.

CONCLUSION

This first investigation of proton-decay Q -values within the HTDA framework has yielded very encouraging results even if the HFBCS values of Q_p prove to be overall in better agreement with experimental data. Moreover this HTDA study has shown that the neutron-proton pairing correlations in the $T = 0$ channel can be neglected in the considered decaying nuclei ($Z \sim 60$, $A \sim 130$). To improve these results it seems important to include double-pair excitations in the HTDA calculations and to improve the nonvariational underlying Slater determinant by performing self-consistent HTDA calculations (see Ref. [8]).

REFERENCES

1. P. Quentin, L. Bonneau, N. Minkov, and D. Samsøen, *Int. J. Mod. Phys. E* **19**, 252–258 (2010).
2. J. Le Bloas, L. Bonneau, P. Quentin, J. Bartel, and D. Strottman, *Int. J. Mod. Phys. E* **19**, 568–574 (2010).
3. L. Bonneau, J. Le Bloas, P. Quentin, and N. Minkov, *Int. J. Mod. Phys. E* **20**, 252–258 (2011).
4. J. Le Bloas, Meng Hock Koh, P. Quentin, L. Bonneau and J. I. A. Ithnin, *Phys. Rev. C* **84**, 014302 (2011).
5. H. Naïdja, P. Quentin, T. L. Ha, and D. Samsøen, *Phys. Rev. C* **81**, 044320 (2010).
6. Å. Bohr and B. Mottelson, *Nuclear Structure* (Vol. 1), Benjamin, New York, 1975, pp. 336–340.
7. M. Beiner, H. Flocard, Nguyen Van Giai, and P. Quentin, *Nucl. Phys. A* **238**, 29–69 (1975).
8. N. Pillet, P. Quentin, and J. Libert, *Nucl. Phys. A* **697**, 141–163 (2002).
9. B. Blank and M.J.G. Borge, *Prog. Part. Nucl. Phys.* **60**, 403–483 (2008).
10. K. Sieja, T. L. Ha, P. Quentin, and A. Baran, *Int. J. Mod. Phys. E* **16**, 289–297 (2007).
11. H. Flocard, P. Quentin, A. K. Kerman, and D. Vautherin, *Nucl. Phys. A* **203**, 433–472 (1973).
12. L. Bonneau, P. Quentin, and K. Sieja, *Phys. Rev. C* **76**, 014304 (2007).

Theoretical studies of proton emission from drip-line nuclei.

L.S. Ferreira*, E. Maglione[†] and P. Ring**

**Centro de Física das Interações Fundamentais, and Departamento de Física, Instituto Superior Técnico, Avenida Rovisco Pais, P1049-001 Lisbon, Portugal*

[†]*Dipartimento di Fisica “G. Galilei”, Via Marzolo 8, I-35131 Padova, Italy
and Istituto Nazionale di Fisica Nucleare, Padova, Italy*

***Physik-Department der Technischen Universität München, D-85748 Garching, Germany*

Abstract. In this work, we discuss proton radioactivity from spherical nuclei in a modern perspective, based on a fully self-consistent relativistic density functional calculation with fundamental interactions.

Keywords: Proton decay, relativistic density functionals

PACS: 23.50.+z, 27.60.+j

INTRODUCTION

Since the first measurements on proton radioactive nuclei [1], it was recognized they were a unique probe of nuclear structure at the extremes of stability. Through the theoretical interpretation of the decay observables to ground and excited states, one could establish the shape of the emitter, and assign the quantum numbers of the decaying state, as well as specific features of its spectra.

Proton emitters range from spherical or quasi spherical nuclei, up to nuclei with large deformations. Deformed proton emitters were quite successfully described within the nonadiabatic quasiparticle approach [2] developed initially to account for odd-even nuclei with axial symmetry, generalized afterwards to account for triaxial degrees of freedom [3], and lately [4] for odd-odd emitters. In the model, the nucleus has a finite moment of inertia, and the rotational spectrum of the daughter is taken into account, as well as the pairing residual interaction between the valence nucleons. The proton state was treated exactly [5] as a single proton resonance in the nuclear mean-field, justified by the fact that the observed proton emitters are very close to the drip-line, where the density of states in the continuum is quite low allowing for a single particle resonance, with practically no mixing with the other states.

Concerning spherical emitters, the first systematic study of half-lives and spectroscopic properties was performed by Åberg and collaborators [6]. A standard WKB calculation of the transmission through the Coulomb and centrifugal barriers of a proton in a defined spherical state, can suggest the order of magnitude of the decay rate, and the angular momentum of the decaying state. Perturbative approaches, like the distorted wave Born Approximation (DWBA) and the two potential model were used, and compared with the semi-classical WKB tunneling probability, leading to very similar results, and essentially showing a strong dependence on the orbital angular momentum of the

single particle orbital, and on the mixing due to the residual interaction or deformation.

In fact, the existence of deformed emitters was clearly established in Ref. [6] from a comparison between experimental and theoretical spectroscopic factors for odd Z and even or odd N emitters. Experimental spectroscopic factors were defined as the ratio between the calculated half-lives, with a simple or an improved version of WKB approach, and the measured ones. The theoretical factors were evaluated within the BCS approach, representing the probability that the spherical orbital in the daughter nucleus is empty. The comparison between them, has shown a strong correlation except for few cases where the experimental value is below or sometimes above the theoretical prediction, indicating a different tunneling probability or fragmentation of the single particle strength, which was attributed to deformation.

Other authors have extended and refined the methods of Ref. [6], using different models to describe the nuclear part of the potential entering the WKB calculation. Various parameterizations of the nuclear mean field available in the literature from the fit to single particle properties of stable nuclei or by semiclassical considerations based on the liquid drop model and the proximity force, were used. The potential was also determined by folding an effective two-body force with the nuclear density $\rho(r)$ of the daughter nucleus, as described in Ref. [7], and references therein. These densities, can be purely phenomenological or calculated in a self-consistent way in the framework of relativistic mean field theory (RMF) and superfluidity is taken into account in the BCS framework [8]. Often, the proton in the odd parent nucleus cannot be described by a pure single particle wave function, and the spectroscopic factor reduces the transition probability. The BCS-model provides a simple way to calculate these factors in open shell nuclei in the framework of RMF theory [9, 10, 11].

A draw back of these approaches, is their strong dependence on a large number of phenomenological parameters to describe the nucleus. It is well known, for example, how the shape and radius of the tunneling interaction directly control the magnitude of the decay times, since a potential with a small radius will lead to a large half-life and vice-versa.

Covariant density functional theory (CDFT), can provide a frame to overcome these uncertainties. As a relativistic quantum field approach, first introduced by Walecka [12], it has a density dependence to allow for a quantitative description of nuclear surface properties, and is able to interpret a large variety of nuclear structure phenomena of β stable and exotic nuclei at the extremes of stability. In the CDFT theory, the treatment of the spin-orbit interaction arises in a natural way, without any additional adjustable parameters. The empirical pseudospin symmetry is also explained, and the model is also consistent with the non linear realization of chiral symmetry. Therefore, the model needs only a relatively small number of parameters determined by a global fit to ground state properties of spherical nuclei and to nuclear matter properties. The functionals can be considered universal since they are valid all over the periodic table, where mean field theory is applicable. The density dependence is introduced either by using non-linear coupling terms or by considering coupling constants dependent on the density of the exchanged mesons. Two examples of these interactions are the non-linear meson exchange model NL3 [13] and the density dependent point coupling model DD-PC1 [14].

They have been successfully applied to describe ground state properties in finite spherical and deformed nuclei over the entire nuclear chart [15] from light nuclei

to super-heavy elements and from the neutron drip line, where halo phenomena are observed, to the proton drip line. Time-dependent versions of this theory have been successfully used for the description of excited states such as rotational bands or giant resonances. There are also investigations in the framework of spherical and deformed relativistic Hartree-Bogoliubov (RHB) theory for spherical and deformed nuclei at the proton dripline [16, 17]. In these calculations the proton dripline is mapped with high precision [18, 19, 20], and the single particle configurations and spectroscopic factors are been derived very successfully.

In this work, we present a fully self-consistent relativistic description of proton emission from spherical nuclei, based on relativistic density functionals derived from meson exchange and point coupling models.

COVARIANT DENSITY FUNCTIONAL THEORY FOR PROTON EMITTING NUCLEI

The nucleons are described by the Dirac spinors ψ , interacting in an effective Lagrangian through the exchange of the isoscalar scalar σ , isoscalar vector ω , and isovector vector ρ mesons, and the electromagnetic field. This simple model, with interaction terms linear in the meson fields, does, however, not provide a quantitative description of the nuclear surface properties. An effective density dependence was introduced [21] by replacing the quadratic σ -potential with a quartic potential that includes non-linear σ self-interactions depending on two parameters. This model has been widely used [22, 15] with the parameter set NL3 [13].

From the Lagrangian density the classical variation principle leads to the equations of motion, which are the Dirac equation for the nucleons, equivalent to the Kohn-Sham equations in non-relativistic density functional theory, and the Klein-Gordon equations for the meson fields. Pairing correlations are taken into account in the constant gap approximation. This set of equations is non-linear and is solved by iteration starting with an initial guess for the potentials, until self-consistency is achieved, and the final mean field interaction obtained, from which the proton resonances and their decay probabilities can be determined. For details, see Ref. [7]

The mesonic degrees of freedom in the non-linear meson models are only introduced to provide an effective interaction between the Dirac particles which obeys Lorentz invariance and causality. Relativistic mean field models can be also formulated replacing finite range meson-exchange interactions in the Lagrangian, by local four-point interactions between the nucleons [23], and including the density dependence in the coupling constants [14]. Following this approach, a very successful parameter set DD-PC1 [14] has been derived from a high precision fit to nuclear matter data and to the binding energies of 64 deformed nuclei in the rare earth and actinide regions.

The non-linear meson exchange model NL3 and the density dependent point coupling model DD-PC1 were applied to the calculation of decay by proton emission from spherical nuclei. The half-lives are given by [24],

$$T_{1/2} = \ln 2 \frac{m}{S \hbar k \alpha^2} \quad (1)$$

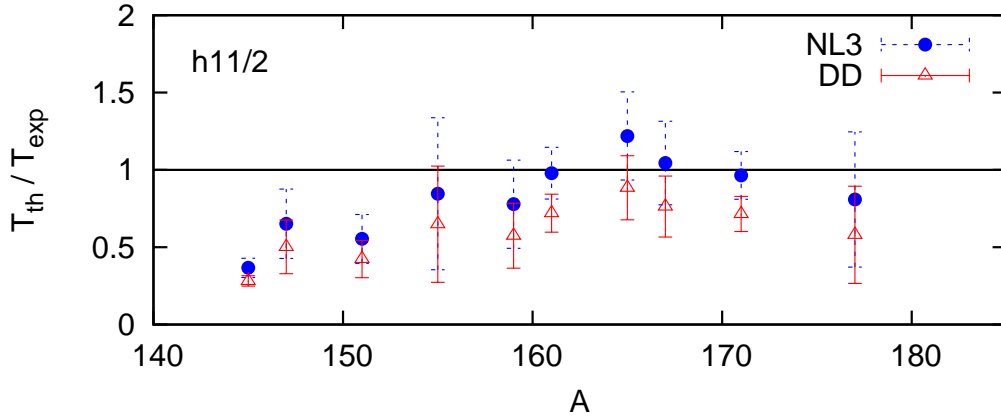


FIGURE 1. Ratio between the theoretical and experimental half-lives as a function of the atomic number for decay from the $h_{11/2}$ single particle level, using the NL3 (dot) and DD-PC1 fields (triangles). The error bars take into account the experimental error on the half-life, and the theoretical error induced by the experimental error on the energy.

with m and k standing for the mass and wave number of the proton. S is a spectroscopic factor, and the quantity α the asymptotic normalization of the proton wave function. The latter is a solution at the experimental energy, of the Dirac equation with outgoing wave boundary conditions in the spherical NL3 and DD-PC1 fields. The spectroscopic factor in the case of nuclei where the residual interaction is mainly due to pairing, is simply the probability u_k^2 that the single particle level k is empty in the daughter nucleus.

The results for proton emission from the $h_{11/2}$ state shown in Fig. 1, prove that for nuclei approaching a magic number, that is, the number of protons or neutrons is ≈ 82 , the description is very good for both models. Far from this N or Z value, the ratio is much smaller than one, pointing to the existence of correlations in the nuclear medium away from a closed shell. Strong mixing of wave functions and coupling to phonon states is possible. In fact, spherical nuclei have the possibility of collective excitations and display a vibrational spectrum with some anharmonicity. It is reasonable to expect a correlation between the outgoing proton and the lowest 2^+ excited state of the daughter nucleus, and great sensitivity of the spectroscopic factor to this coupling. In addition, for open proton and neutron shells, deformations will set in. The spectroscopic factor will become smaller than the one derived from the BCS model, since pairing is not the only dominating effective interaction in this case. It is clearly seen in Fig. 1 that, as expected, the discrepancy between theory and experiment increases as one is moving away from magic numbers.

In fact, there is now strong evidence that ^{145}Tm [3, 25] is triaxial deformed. Similar calculations were performed [7] for decay from other spherical orbitals, leading to equivalent conclusions. A strong mixing between states in decay from positive parity levels, should be responsible for lowering the spectroscopic factor and making the experimental half-life longer than the one obtained in the calculation.

CONCLUSIONS

In conclusion, we have presented the first fully self-consistent model without free parameters, that accounts for the experimental data of proton radioactivity from spherical nuclei, providing clear evidence for a mixing of configurations. It is very desirable to have a unique parameterization for the Lagrangian of relativistic mean field models, which is able to describe properties of nuclei from light to very heavy, and from the proton drip-line to the neutron one. In the present study, we have shown how the non-linear meson exchange NL3 [13] and density dependent point coupling DD-PC1 [14] models, derived from relativistic density functional theory, are also able to describe proton radioactive nuclei, and predict their properties. The present studies provide new theoretical tools to access nuclear structure properties far from the stability domain.

ACKNOWLEDGMENTS

This work was supported by the Fundação para a Ciência e a Tecnologia (Portugal), Project: CERN/FP/116385/2010.

REFERENCES

1. A. A. Sonzogni, Nuclear Data Sheets **95**, 1 (2002).
2. G. Fiorin, E. Maglione and L. S. Ferreira, Phys. Rev. **C 67**, 054302 (2003).
3. P. Arumugam, E. Maglione and L. S. Ferreira, Phys. Rev. **C 78**, 041305 (2008).
4. M. Patial, P. Arumugam, A.K. Jain, E. Maglione and L.S. Ferreira, in these proceedings.
5. L. S. Ferreira, E. Maglione and R. J. Liotta, Phys. Rev. Lett. **78**, 1640 (1997).
6. S. Åberg, P. B. Semmes and W. Nazarewicz, Phys. Rev. **C 56**, 1762 (1997).
7. L. S. Ferreira, E. Maglione and P. Ring, Phys. Lett. **B 701**, 508 (2011).
8. M. Bhattacharya and G. Gangopadhyay, Phys. Lett. **B 651**, 263 (2007).
9. J. M. Dong, H. F. Zhang and G. Royer, Phys. Rev. **C 79**, 054330 (2009).
10. H. F. Zhang, Y. J. Wang, J. M. Dong, J. Q. Li, and W. Scheid, J. Phys. **G 37**, 085107 (2010).
11. Y.-B. Qian, Z.-Z. Ren, D.-D. Ni, and Z.-Q. Sheng, Chin. Phys. Lett. **27**, 072301 (2010).
12. B. D. Serot and J. D. Walecka, Adv. Nucl. Phys. **16**, 1 (1986).
13. G. A. Lalazissis, J. König, and P. Ring, Phys. Rev. **C 55**, 540 (1997).
14. T. Nikšić, D. Vretenar, and P. Ring, Phys. Rev. **C 78**, 034318 (2008).
15. Y. K. Gambhir, P. Ring, and A. Thimet, Ann. Phys. (N.Y.) **198**, 132 (1990).
16. D. Vretenar, G. A. Lalazissis, P. Ring, Phys. Rev. Lett. **82** (1999) 4595.
17. G. A. Lalazissis, D. Vretenar, and P. Ring, Phys. Rev. **C60**, 051302(R) (1999).
18. G. A. Lalazissis, D. Vretenar, and P. Ring, Nucl. Phys. **A650**, 133 (1999).
19. G. A. Lalazissis, D. Vretenar, and P. Ring, Nucl. Phys. **A679**, 481 (2001).
20. G. A. Lalazissis, D. Vretenar, and P. Ring, Phys. Rev. **C69**, 017301 (2004).
21. J. Boguta, A. R. Bodmer, Nucl. Phys. **A 292**, 413 (1977).
22. P.-G. Reinhard, Rep. Prog. Phys. **52**, 439 (1989).
23. P. Manakos, T. Mannel, Z. Phys. **A 334**, 481 (1989).
24. E. Maglione, L. S. Ferreira and R. J. Liotta, Phys. Rev. Lett. **81**, 538 (1998).
25. D. Seweryniak *et al.*, Phys. Rev. Lett. **99**, 082502 (2007).

Spectroscopy of the unbound nucleus ^{18}Na in link with ^{19}Mg two-proton radioactivity

M. Assié^{*}, F. de Oliveira[†] and e521as collaboration

^{*}*Institut de Physique Nucléaire, Université Paris-Sud-11-CNRS/IN2P3,91406 Orsay,France*

[†]*GANIL, BP 55027,14076 Caen Cedex 5, France*

Abstract. The unbound nucleus ^{18}Na , the intermediate nucleus in the two-proton radioactivity of ^{19}Mg , is studied through the resonant elastic scattering $^{17}\text{Ne}(p,^{17}\text{Ne})p$. The spectroscopic information obtained in this experiment is discussed and put in perspective with previous measurements and the structure of the mirror nucleus ^{18}N .

Keywords: two-proton radioactivity, resonant elastic scattering, ^{19}Mg , ^{18}Na

PACS: <23.50.+z, 24.30.-v, 25.60.Bx, 21.10.Tg>

INTRODUCTION

Near the proton drip-line, where nuclear binding energies are almost zero, the pairing force could play a more important role than in stable nuclei. Sometimes it leads to a situation where a drip-line nucleus is bound with respect to single-proton decay but unbound to two-proton radioactivity [1]. Then, this phenomenon can proceed: (i) either through simultaneous emission (^2He emission) where the two protons form a quasiparticle due to pairing force that facilitates the penetration of the Coulomb barrier; (ii) or by sequential emission through an intermediate state (or eventually the tail of a resonant state) that can be described by genuine three-particle decay. Direct two-proton radioactivity as defined by Goldansky [2] requires not only that the $2p$ emitter level lies lower in energy than the $1p$ daughter level but also that those states are narrow enough so that they would not overlap. Therefore, the structure of the intermediate nucleus plays an important role.

Among the two-proton emitters observed experimentally, the case of ^{19}Mg is still not very clear : its measured life-time is 4.0 (15) ps and the measured angular correlation between the two-emitted proton does not show strong di-proton correlation [3]. Its intermediate nucleus ^{18}Na is one of the rare $^A_{Z-1}\text{X}$ nucleus to be accessible experimentally. However it is almost not known. The only set of data available comes from stripping reactions [4]. Two peaks were observed, one with a proton separation energy of 0.41(16) MeV ($\Gamma=0.34(9)\text{MeV}$) and the other with $S_p=1.26(17)$ MeV ($\Gamma=0.54(13)\text{MeV}$). If the first peak corresponds to the ground state, then its position is in strong disagreement with the models predictions. Moreover, in this case, the ^{19}Mg lifetime could not be understood since this nucleus would decay with an extremely fast ($\tau_{1/2} \leq 10^{-18}$ s) sequential emission of two protons through the intermediate ^{18}Na ground state resonance. Even though the second peak seems more probable for the g.s., in order to identify its g.s. more experimental spectroscopic information is needed. In this letter, results concern-

ing ^{18}Na obtained from a recent experiment measuring the resonant elastic scattering reaction $^{17}\text{Ne}(p, ^{17}\text{Ne})p$ are presented.

EXPERIMENTAL SET-UP

The elastic scattering reaction $^{17}\text{Ne}(p, ^{17}\text{Ne})p$ was measured in inverse kinematics with a ^{17}Ne beam at 4 A.MeV and an intensity of 10^4 pps produced by the Spiral facility at GANIL. It was impinging on a $150\mu\text{m}$ thick polypropylen (CH_2) target where the beam was stopped. With this method, the full excitation function up to 4 MeV in the center-of-mass was obtained all at once (for details on the method see [5]). The out-

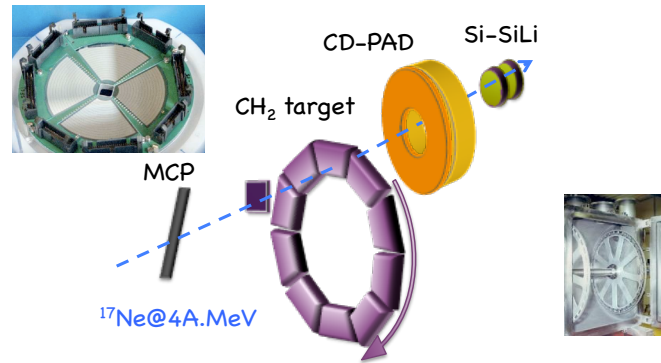


FIGURE 1. Experimental set-up for the study of $^{17}\text{Ne}(p, ^{17}\text{Ne})p$ resonant elastic scattering (see text for description).

coming protons were detected with two ΔE -E telescopes (see Fig. 1) : (i) the first one located at zero degree is composed of a $150\mu\text{m}$ thick Silicon detector and a 6 mm Silicon-Lithium detector which was cooled down to -20°C . It was covering from -2 to 2 degrees with a total resolution of 35 keV for the telescope (ii) the second one, called CD-PAD detector [6], is composed of a thin ($\sim 40\mu\text{m}$) double-sided stripped Silicon detector and a 1.5 mm thick Silicon detector covering from 5 to 25 degrees in the laboratory frame with an energy resolution of 50 keV. Rough calibration of Silicon telescopes was performed with 3α source. Then, more accurate calibration was obtained from ^{17}O runs and comparison with a previous measurement in direct kinematics of the $^{17}\text{O}(p,p)^{17}\text{O}$ reaction [7]. Moreover, the contamination from ^{17}Ne decay by βp (90%) was strongly reduced by the use of a target rotating at 1000 rpm. It was supplemented by a MultiChannel Plate (MCP) detector for time of flight (TOF) measurement with an efficiency close to 100%. 98% of the contamination was removed with this set-up.

ANALYSIS AND RESULTS

The selection of the kinematic line from TOF measurement and of protons from ΔE -E identification matrix makes it possible to reconstruct the excitation function in the laboratory frame. In order to infer this latter in the center-of-mass system, an algorithm based

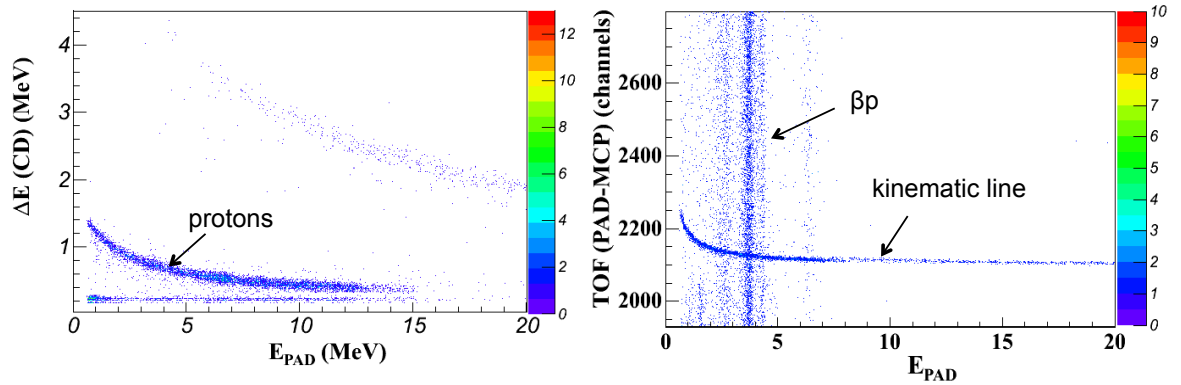


FIGURE 2. Left : ΔE -E matrix for identification of protons. Right : Time of flight versus energy loss in the PAD detector; the kinematic line of the protons coming out of the reaction is well separated from the βp background.

on Monte-Carlo simulation and on simulation of the experimental set-up was used. Starting from a flat distribution in the center-of-mass, the energy in the laboratory is deduced from kinematics calculations coupled to simulation of energy loss and straggling in the target and taking into account the energy resolution of each detector. These steps are iterated while χ^2 between experimental excitation function in laboratory frame and the simulated one is small. The center-of-mass excitation function obtained after this algorithm is shown on Fig. 3 where all rings' contributions in the CDPAD detector have been summed.

The excitation function shows two contributions: the Rutherford scattering (mainly at low energy) and some interfering resonances reflecting the compound nucleus ^{18}Na structure. Indeed, the position of these resonances is linked with the excited states of the compound nucleus whereas their widths give access to spectroscopic factors.

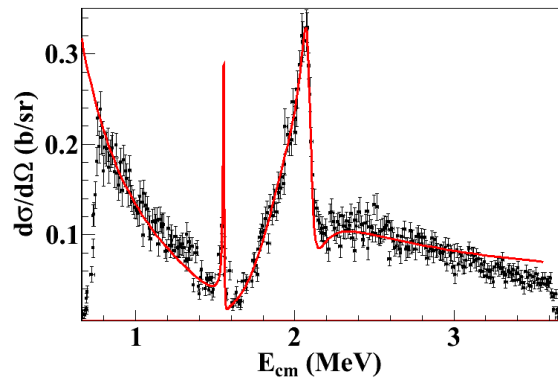


FIGURE 3. Excitation function in the center -of-mass framework corrected from ^{12}C background and residual βp background from ^{17}Ne decay. The red line represents the R-matrix fit of the data, taking as a starting point the shell model calculations

A R-matrix fit of the excitation function was performed using the code Anar χ [8]. As

TABLE 1. Dimensionless reduced width for ^{18}Na obtained from shell model calculations.

^{18}Na state	^{17}Ne core	protons	
		s1/2	d5/2
1_1^-	$3/2^-$	0.183	0.921
2_1^-	$1/2^-$	-	0.644
0_1^-	$1/2^-$	0.759	-
2_2^-	$3/2^-$	0.028	0.507
1_2^-	$1/2^-$	0.654	-
3_1^-	$1/2^-$	-	0.621

a starting point we have inferred the position of the state in ^{18}Na from the states known in its mirror nucleus ^{18}N , by adjusting a Saxon-Woods potential to reproduce the binding of the states in ^{18}N and taking into account the Coulomb shift in ^{18}Na . In the case of 0_1^- and 1_2^- states which are unknown in ^{18}N [9], we have assumed their position from the $1/2^+$ state in ^{19}O following ref.[10]. Our calculation shows a strong lowering of these states due to Coulomb shift. The energy of the states are in good agreement with the d-wave calculations of ref.[11] except for the 0_1^- and 1_2^- which are found much higher in energy in [11]. The widths of the states are deduced from the Wigner widths combined with the dimensionless reduced width obtained from shell model calculations performed with the Oxbash code and the ZBM interaction [12]. The first six states of ^{18}Na can be described as single particle states (see Tab.1) with a core of ^{17}Ne in the ground state or the first excited state. The agreement is quite good.

Level scheme of ^{18}Na

The first resonance in our excitation energy spectrum (see Fig. 3) is found at $S_p=1.54$ MeV corresponding to $\Delta M=25.30(2)$ MeV. This value is compatible with predictions based on mass measurement [13, 14, 15] but above the second peak value from ref [4]. From its mirror nucleus ^{18}N spectroscopic information [9] (see Fig. 4), the ground state (g.s.) spin should be 1^- . However the shape of a 1^- spin resonance obtained with the R-matrix theory code Anar χ [8] is not compatible with our peak. Thus there are two possibilities : (i) either there is a spin inversion between ^{18}Na and its mirror nucleus; (ii) or the first resonance is not the ground state and there is a narrow resonance ($\Gamma < 5$ keV) at lower energy that was not seen in this experiment. The first scenario is difficult to understand as the Coulomb shift tends to lower the 1^- state. As for the second hypothesis, the position of the g. s. of ^{18}Na inferred from the 1^- g. s. of ^{18}N should lie at an energy higher than 1.1 MeV with a width lower than 3 keV. This state can not be seen in our experiment even with our 13 keV resolution. Maybe there is a small enhancement of the cross-section around 1.3 MeV but this is also the position of the βp contamination.

The first resonance is compatible with a 2- state and then the second large peak

represents the contribution of three states : the 0_1^- , 1_2^- , 3_1^- . This confirms the strong lowering of the 0_1^- , 1_2^- states due to the Coulomb shift, predicted theoretically.

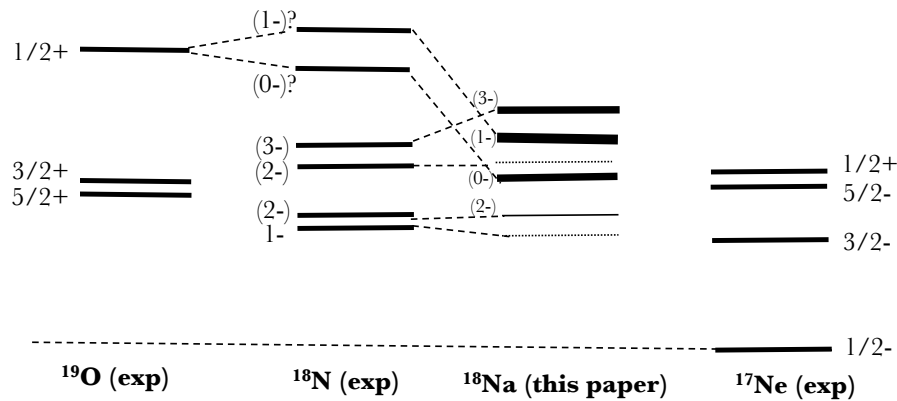


FIGURE 4. Experimental level scheme for ^{19}O , ^{18}N , ^{17}Ne and ^{18}Na as measured in this paper. The thickness of the line gives the width of the state (see text for more detailed information).

The obtained level scheme for ^{18}Na is shown on Fig. 4. The thickness of the lines represent the width of the states and the dotted lines represent the states which are too narrow ($\Gamma < 2$ keV) to be observed experimentally but which are predicted theoretically.

From these results the lifetime of ^{19}Mg as regards to sequential two-proton decay can be estimated. Taking into account spectroscopic factors for ^{19}Mg from shell model calculations and using the approximate formula from ref.[16], the calculated lifetime of ^{19}Mg is of the order of 1 ps. This is in good agreement with the measurement from ref.[3].

REFERENCES

1. B. Blank and M. Płoszajczak, *Rep. Prog. Phys.*, **71** (2008) 046301 and ref. therein.
2. V.I. Goldansky, *Nucl. Phys.*, **19** (1960) 482.
3. I.G. Mukha *et al*, *Phys. Rev. Lett.*, **99** (2007) 182501; *Phys. Rev. C*, **77** (2008) 061303(R).
4. T. Zerguerras *et al*, *Eur. Phys. J. A*, **20** (2004) 389.
5. V.Z. Goldberg *et al*, *Phys. At. Nucl.* **60** (1997) 1186.
6. A.N. Ostrowski *et al*, *Nucl. Instr. and Meth. A*, **480** (2002) 448.
7. J.C. Sens, S. M. Rafeai, A. Ben Mohamed and A. Pape, *Phys. Rev. C* **16** (1977) 2129.
8. E. Berthoumieux, B. Berthier, C. Moreau, J.P. Gallien and A.C. Raoux, *Nucl. Instr. and Meth. B*, **136-138** (1998) 55.
9. D. R. Tilley, H. R. Weller, C. M. Cheves, and R. M. Chasteler, *Nucl. Phys. A* **595** (1995) 1.
10. H.T. Fortune and R. Sherr, *Phys. Rev. C*, **76** (2007) 014313.
11. L. Grigorenko, I.G. Mukha and M.V. Zhikov, *Nucl. Phys. A*, **713** (2003) 372.
12. N. Smirnova, private communication.
13. G. Audi, A.H. Wapstra, *Nucl. Phys. A* **595** 1995 409.
14. J. Jänecke, P. Masson, *At. Data Nucl. Data Tables* **39** (1988) 265.
15. A. Pape M. Antony, *At. Data. Nucl. Data Tables* **39** (1988) 201.
16. R.A. Kyger *et al*, *Phys. Rev. Lett.*, **74** (1995) 860.

A reef in the sea of instability: Observation of a narrow state in ^{15}F

F. de Oliveira Santos and the E521S collaboration

GANIL, CEA/DSM-CNRS/IN2P3, Caen France.

Abstract. The properties of the low lying states of ^{15}F were studied by measuring the resonant elastic scattering of an ^{14}O radioactive beam on protons. This experiment was performed at GANIL with a post-accelerated beam produced by the SPIRAL1 facility. We confirm the existence of a second excited state in ^{15}F with a narrow width, which may seem particularly surprising for a state located above the Coulomb barrier.

Keywords: Nuclear Structure, Resonant Elastic Scattering, Unbound Nuclei, ^{15}F

PACS: 27.20.+n, 25.40.Cm, 25.60.Bx, 21.10.Dr, 21.10.Tg

INTRODUCTION

The unbound nucleus ^{15}F is located two steps beyond the proton drip-line. Its mirror nucleus ^{15}C is a well-known neutron halo nucleus. The ground and first excited states of ^{15}F were measured in several experiments [1, 2]. The second excited state was observed in three recent experiments [3, 4, 5], but with contradictory results.

The ground state of ^{15}F is located 1480 keV above the proton emission threshold. Its lifetime is extremely short since it is observed as a broad resonance with a width of about 800 keV. The spin was measured with the resonant elastic scattering technique, it is $J^\pi = \frac{1}{2}^+$, meaning that this unbound state emits a proton with an angular momentum $\ell = 0$. Such a large value of the width means that the corresponding spectroscopic factor is high, in fact it is very close to unity. So, this state is well described by a pure single particle configuration with an $^{14}\text{O}_{gs}$ core plus one proton in the $2s_{1/2}$ shell. Shell model calculations are in agreement with these results [1].

The first excited state of ^{15}F is located ~ 1.2 MeV above the ground state. Despite the fact it is less bound than the ground state, this state has a longer lifetime with a width of about 300 keV. The spin of the state is $J^\pi = \frac{5}{2}^+$, meaning that the proton is emitted with an angular momentum $\ell = 2$. The longer lifetime of the state is due to the centrifugal barrier which retains the proton inside the nucleus. The spectroscopic factor is close to unity, so this state is well described as $^{14}\text{O}_{gs} \otimes p(1d_{5/2})$, again in agreement with shell model calculations [1].

The second excited state of ^{15}F was not observed nor studied theoretically until recently. In the mirror nucleus, the second excited state has a spin $J^\pi = \frac{1}{2}^-$ and an excitation energy $E_x = 3.1$ MeV. Therefore, in ^{15}F this state should be unbound by about 4.6 MeV and should emit a proton with an angular momentum $\ell = 1$. With such an excitation energy, the state is located well above the Coulomb barrier, and the proton should leave the nucleus in an extremely short time. A simple estimate gives

a value of $\Gamma \sim 10$ MeV. Recently, Canton *et al* [6], using a multi-channel algebraic scattering theory with coupling to Pauli-hindered states, predicted a very narrow width of $\Gamma = 2$ keV. The narrow width is confirmed by shell model calculations [7]. This is very surprising for a state which is expected to be embedded in the continuum. Three experiments reported the observation of this state, but the results are in contradiction. In one case, a resonance was observed at the excitation energy $E_x = 3.23(21)$ MeV with a width of $\Gamma = 1.25(34)$ MeV [3], in an other experiment it is observed at $E_x = 3.92$ MeV with $\Gamma = 150$ keV [4], and in the last case it is observed at $E_x = 3.34(20)$ MeV with $\Gamma = 200(200)$ keV [5].

In order to investigate this intriguing state, we measured the properties of the ^{15}F low lying states using the intense ^{14}O radioactive beam available at SPIRAL1-GANIL and a high resolution resonant elastic scattering technique.

MEASUREMENT

Figure 1 shows the excitation function of the elastic scattering reaction $^{14}\text{N}(p,p)^{14}\text{N}$ measured recently at GANIL [8]. It was measured with a beam of ^{14}N , so in inverse kinematics, and with a thick target of plastic. The Rutherford formula for the elastic scattering describes very well the overall shape as it is shown with the continuous line up to 1 MeV, but a resonance is observed at an energy close to 1.06 MeV. Obviously, this resonance is not explained by a simple Coulomb scattering, while yet the incident energy is well below the Coulomb barrier energy (about 2 MeV). This resonance is the manifestation of another contribution, it is the fusion of the two incident nuclei forming the compound nucleus ^{15}O . This fusion reaction occurs for two reasons, firstly the penetration of the Coulomb barrier is possible through the quantum tunnel effect, and secondly the existence of a discrete state in the compound nucleus induced a resonant increase in the penetration probability, so-called resonant tunnel effect. Thus in general, this kind of measurement can be used to determine the properties of the compound nucleus. Excitation energies can be determined from the position of the peaks, the total and partial widths of the states can be extracted from the width and height of the peaks, and the spin and parity of the states from the shape of the resonances and the angular distributions of the scattered particles. The interest of using such kind of measurement to study the spectroscopy of unbound states is manifest: this measurement is simple, it gives pertinent properties of the states, and the cross sections are often high, these are essential conditions when dealing with RIB [9]. This technique is called Resonant Elastic Scattering (RES).

In order to confirm the existence of the second excited state in ^{15}F , we measured the RES reaction $^1\text{H}(^{14}\text{O},p)^{14}\text{O}$ optimizing the experimental conditions to obtain the best energy resolution. The experiment was performed at GANIL using the intense and high quality radioactive ^{14}O beam produced by the SPIRAL facility and post accelerated to 6 MeV/u with the CIME cyclotron. After using a stripper foil, the beam purity was close to 100 % (no contamination observed) and the mean intensity was 2×10^5 pps. The beam impinged on a $150\mu\text{m}$ thick rotating polypropylene target (the same system as in the ^{18}Na experiment presented in this conference by M. Assié). Scattered protons were detected with a $\Delta E(500\mu\text{m})$ -E(6mm SiLi) telescope of silicon detectors located

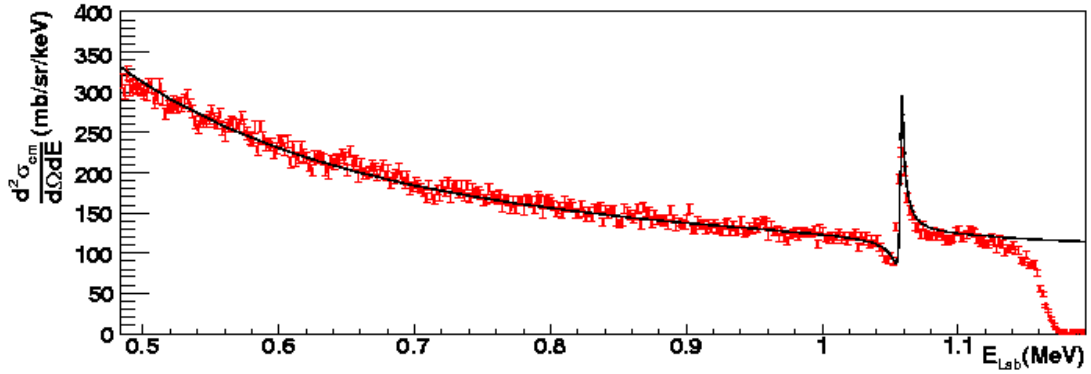


FIGURE 1. Measured excitation function of the elastic scattering reaction $^{14}\text{N}(p, p)^{14}\text{N}$ [8]. While the shape of the curve is very well reproduced by the Rutherford formula (continuous line on the left side up to about 1 MeV), a peak located at the energy of 1.06 MeV is clearly visible. This peak is due to the existence of a single state in the compound nucleus ^{15}O .

36.6 cm downstream the target. It resulted that the angular acceptance was limited to ± 2.16 degrees in laboratory. In this kind of experiment, it is well known that the angular acceptance has a strong impact on the final energy resolution. Our limited angular acceptance resulted in a total energy resolution of 50 keV in lab corresponding to 12 keV in center of mass. Such a good energy resolution provides good experimental conditions to observe a narrow resonance.

ANALYSIS AND DISCUSSION

The measured excitation function of the reaction $^1\text{H}(^{14}\text{O}, p)^{14}\text{O}$ is shown in Fig. 2. The first large dip observed at the energy close to 1 MeV corresponds to the ground state of ^{15}F . The peak observed at the energy close to 2.8 MeV corresponds to the known $5/2+$ first excited state. The analysis of the low energy part of the excitation function using the R-Matrix formalism (the code Anarki [10]) gives results that are in good agreement with the known properties of these states (energy, width, spin and parity) [11].

A dip can be observed in the excitation function at a resonance energy close to 4.8 MeV ($E_x \sim 3.3$ MeV). The shape of the cross section is in good agreement with the presence of a $1/2-$ resonance. The best fit (see continuous line in Fig. 2) is obtained with a width of about 50 keV. This observation definitively confirms the existence of a narrow $1/2-$ state in ^{15}F . The very small measured value of the width means that the spectroscopic factor for the emission of one proton is very small. A value of $\theta^2 = 3.3 \times 10^{-3}$ was extracted, which is in agreement with shell model calculations (made with the bwt interaction in the spsdpf space) where a value of $\theta^2 = 3 \times 10^{-3}$ is obtained. The same calculations show that this state is mainly described as a configuration: $^{13}\text{N} \otimes ^2\text{He}$, that is a $^2\text{He}(0+)$ cluster configuration in ^{15}F with a predicted spectroscopic factor close to 1. Whereas this state is located above the one proton emission Coulomb barrier, it is well below the two-proton emission Coulomb barrier. The emission of two proton is strongly reduced because the decay energy is small, less than 200 keV [11]. This is

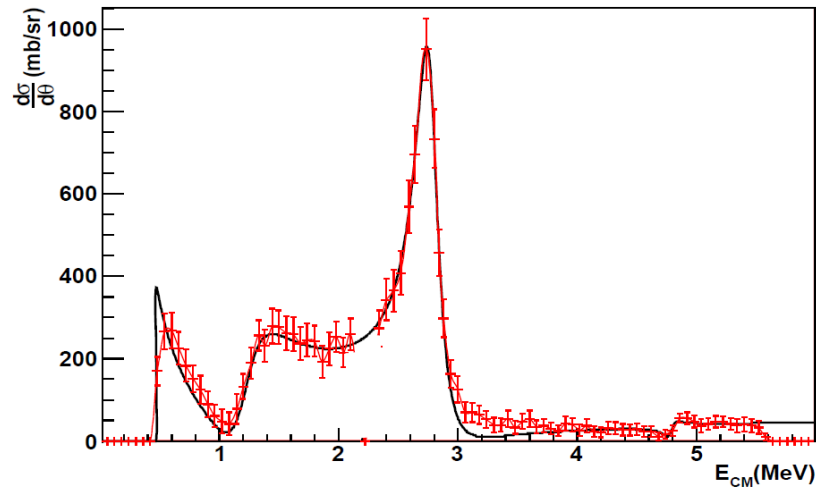


FIGURE 2. Measured excitation function of the reaction ${}^1\text{H}({}^{14}\text{O},\text{p}){}^{14}\text{O}$. At an energy close to 4.8 MeV a dip can be observed, corresponding to the presence of a narrow excited state in ${}^{15}\text{F}$ with a spin $1/2^-$. The continuous line is the best fit obtained using the R-Matrix formalism.

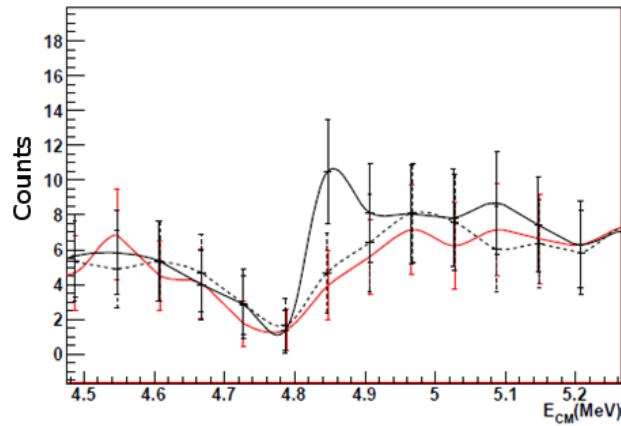


FIGURE 3. Zoom in the region of the excitation function where the second excited state is observed. The red line corresponds to the data, the continuous black line corresponds to a Monte Carlo simulation where only the elastic scattering channel is taken into account, the dashed line corresponds to a simulation where two channels are taken into account (elastic + inelastic, see text for details).

the explanation of the existence of this relatively long lived excited state.

The following discussion is more speculative. A thorough analysis of the shape of the $1/2^-$ resonance allowed us to determine that it is better fitted with two contributions, one for the elastic scattering channel with a partial width of 40 keV and another unknown channel with a partial width of 40 keV, see Fig. 3. The two-proton decay can not be the second channel since the maximum expected width (Wigner limit) is about 1 eV. Moreover, the experimental setup was also composed of a large acceptance DSSSD, and

no event of two-proton emission was observed. The introduction of a closed channel in the R-matrix calculations, the inelastic scattering reaction $H(^{14}\text{O}, p')^{14}\text{O}^*$ (first excited state at $E_x=5.17$ MeV), gives a good fit of the data. One possible interpretation of this result could be that the $1/2^-$ state in ^{15}F decays by one proton emission to the tail of the first excited state in ^{14}O , and is followed by one γ -ray emission. This $(p\gamma)$ decay can be calculated by simple models, and we obtained a partial width of 20 keV [11], a value not far from the measured one. Moreover, the protons emitted in this channel are also detected by our detector, and it could explain the additional counts that are observed at energies around 3.2 MeV in the excitation function (see Fig 2) and not well fitted. The exact shape of this additional contribution depends on the angular distribution of the protons, that is not known.

For the future, we would like to confirm this exotic decay channel with a dedicated experiment. For this purpose, a very intense beam of ^{14}O is under development at SPIRAL2 [12]. This beam could be produced by the reaction $^{12}\text{C}(^3\text{He}, n)^{14}\text{O}$ using the very intense beam of ^3He accelerated by the LINAC accelerator.

REFERENCES

1. V. Z. Goldberg *et al*, *Phys. Rev. C* **69**, 031302 (2004).
2. W. Benenson *et al*, *Phys. Rev. C* **17**, 1939 (1978).
3. T. Zerguerras *et al*, *Eur. Phys. J. A* **20**, 389 (2004).
4. A. Lépine-Szilý *et al*, *Nucl. Phys. A* **734**, 331–336 (2004).
5. I. Mukha *et al*, *Phys. Rev. C* **77**, 061303(R) (2008).
6. L. Canton *et al*, *Phys. Rev. Lett.* **96**, 72502 (2006).
7. H. T. Fortune and R. Sherr, *Phys. Rev. C* **99** 89201 (2007).
8. I. Stefan, *Thesis* (Université de Caen – France) (2007).
9. F. de Oliveira Santos *et al.*, *Eur. Phys. J. A* **24**, 237 (2005).
10. E. Berthoumieux, B. Berthier, C. Moreau, J.P. Gallien and A.C. Raoux, *Nucl. Instr. and Meth. B* **55** 136–138 (1998).
11. F. de Grancey *et al*, to be submitted and *Thesis* Université de Caen France, (2007).
12. A. Pichard *et al*, *Eur. Phys. J. A* **47**, 72 (2011).

Mass Evaluation for Proton Rich Nuclides

M. Wang^{a,b}, G. Audi^b, X. Xu^{a,b,c}, B. Pfeiffer^d and F. G. Kondev^e

^a *Institute of Modern Physics, Chinese Academy of Sciences, 730000 Lanzhou, China*

^b *CSNSM-IN2P3, Batiment 104,108, 91405 Orsay Campus, France*

^c *Graduate University of Chinese Academy of Sciences, Beijing, 100049, People's Republic of China*

^d *GSI Helmholtzzentrum für Schwerionenforschung, Planckstr. 1, D-64291 Darmstadt, Germany*

^e *Argonne National Laboratory, 9700 S. Cass Avenue, Argonne, Illinois 60439, USA*

Abstract. The Atomic mass evaluation (AME) provides the reliable resource for the values related to atomic masses. Since the publication of the latest version of AME in 2003, many developments for atomic mass determination have been done and important results changed significantly our knowledge. A preliminary version of AME was released in April 2011, and an official version is foreseen to be published in early 2013. The general status of AME is presented and some specific features of AME for proton-rich nuclides are discussed.

Keywords: Atomic mass evaluation (AME), Proton-rich nuclides, IMME.

PACS: 21.10.Dr

INTRODUCTION OF AME

Atomic masses are widely used in basic nuclear physics and astrophysics research, as well as in some other practical applications such as nuclear energy. The atomic mass tables, the main products of the Atomic mass evaluation (AME) [1], provide the reliable resource for the values related to atomic masses.

The AME was created by Aaldert H. Wapstra in the 1950's and following this concept, a series of Mass Tables has been produced over the years. The latest version of AME was published in 2003. Since then, a large amount of data emerged from the mass measurements by Penning traps and storage rings, as well as the nuclear decay and reaction energy measurements. A new project called "AME-future" is now running aiming at new tables to be published in early 2013: AME2013. Intensive work is continuing for this project under the collaboration with G. Audi as the coordinator, and contributors from IMP-Lanzhou, GSI-Darmstadt, ANL-Argonne and MPI-Heidelberg.

Meanwhile, many demands have been expressed by our colleagues for some updated tables. To answer these demands, a bulletin was edited in April 2011 from the atomic mass data center (AMDC) to introduce the present status and distribute the AME2011-preview, a preliminary version of AME2013 [2]. Many changes and improvements are included in the AME2011-preview. Up to now, 2376 masses of the ground-state nuclides have been obtained from around 9800 experimental data, compared to 2228 masses from around 7000 experimental data in AME2003, the latest published version.

THE POLICY FOR DATA TREATMENT

In general, there are two kinds of methods for atomic mass measurements: the so-called “direct method” where the inertial masses are determined with mass spectrometry, and the “indirect method” where the reaction energy, i.e. the difference of a few masses, is determined in a nuclear reaction or decay. In the AME, all the available experimental data related to atomic masses (energy data or mass-spectrometric data) are collected and carefully examined. With the least-squares method, the best values for atomic masses are recommended.

In AME data treatment, we try our best to use the primary experimental information. In this way, the masses can be recalibrated automatically for any changes, and the original correlation information can be preserved properly. As an example, we consider the recent publication of Wrede et al. [3], where a series of masses were determined from ($^3\text{He},t$) reactions. In Fig.1 of this reference, each peak in the spectra corresponds to an excited or ground state of various nuclides. From these complex correlations the masses of the nuclides were extracted. Rather than using the mass values in Table 4 of this paper, after communication with the authors and with their help, we built the input equations for AME as:

$$^{20}\text{Ne}(3\text{He},t)^{20}\text{Na} - ^{36}\text{Ar}(^{36}\text{K}) = -1078.06 (1.06) \text{ keV};$$

$$^{24}\text{Mg}(3\text{He},t)^{24}\text{Al} - ^{36}\text{Ar}(^{36}\text{K}) = -1071.48 (1.05) \text{ keV};$$

$$^{28}\text{Si}(3\text{He},t)^{28}\text{P} - ^{36}\text{Ar}(^{36}\text{K}) = -1530.58 (1.10) \text{ keV};$$

$$^{32}\text{S}(3\text{He},t)^{32}\text{Cl} - ^{36}\text{Ar}(^{36}\text{K}) = 133.01 (1.10) \text{ keV}.$$

Strictly speaking, these equations are not exact. Because of the mass differences between the measured nuclides and the reference, there should be a fractional coefficient for the reaction with the measured nuclides, depending on the angle where the spectra are obtained. While the coefficients are quite close to unity and the exact equations are quite complex, we believe this treatment is the best one to represent these data and most of the primary information is thus preserved.

AME FOR PROTON RICH NUCLIDES

The proton drip-line is much closer to the β stability valley than the neutron drip-line, due to the Coulomb effects between the protons. It is relatively easy to access the very proton-rich nuclides via the projectile fragmentation, fusion-evaporation reactions and proton induced spallation reactions. The limits of nuclear binding for proton-rich nuclides have been reached up to heavy elements in experiments. For them many researches using mass-spectrometry and decay spectroscopy studies have been performed, contributing importantly to the atomic mass determination.

In recent years, tremendous developments have been done in the field of direct mass measurements for radioactive nuclides. The landscape of nuclides with known masses has been extended importantly on the nuclear chart, and can be extended even further when combining with the decay spectroscopy data. For example, the long α decay chain $^{171}\text{Au}-^{167}\text{Ir}-^{163}\text{Re}-^{159}\text{Ta}-^{155}\text{Lu}$ is connected with another α decay chain $^{170}\text{Pt}-^{166}\text{Os}-^{162}\text{W}-^{158}\text{Hf}-^{154}\text{Yb}-^{150}\text{Er}$ by $^{171}\text{Au}(p)^{170}\text{Pt}$ and $^{167}\text{Ir}(p)^{166}\text{Os}$, where all of the decay energies are known from the spectroscopic studies. Since the mass of ^{150}Er is measured directly with ESR at GSI [4], all of the masses of the nuclides along these

two decay chains are now determined experimentally. So the surface of measured mass is extended significantly. There are similar decay chains like in parallel ^{170}Au - ^{166}Ir - ^{162}Re - ^{158}Ta - ^{154}Lu , connected to ^{169}Pt - ^{165}Os - ^{161}W - ^{157}Hf - ^{153}Yb - ^{149}Er with $^{170}\text{Au}(p)$ ^{169}Pt and $^{166}\text{Ir}(p)$ ^{165}Os . Unfortunately, none of the nuclides has known mass. If any masses of these nuclides can be measured, all of the masses along the decay chains will be determined.

Because of the Coulomb barrier, even nuclides beyond the proton drip-line can exist long enough for direct mass measurements. Some of them have been measured directly [5]. In this way, the location of the proton drip-line can be determined unambiguously.

Many proton-rich nuclides are studied with β decay spectroscopy and the decay energy can be obtained with the end point energy method. For nuclides far away from the stability valley, the decay energies become larger and larger, and many states can be accessed in the decay daughter nuclide, rendering the combination of the individual continuous spectrum quite complex. Using the end point energy method is also not quite reliable, since the level corresponding to the end point is not clear. This situation is well demonstrated in the case of ^{80}Y . The Q_{EC} were measured in two different groups as 6952(152) keV [6] and 6934(242) keV [7] respectively. While in a later study [8], with β - γ coincidence, only a lower limit of 8923(23) keV could be obtained because of the possibly missed levels. Recently the mass of ^{80}Y was measured directly with Penning Traps [9]. The Q_{EC} for ^{80}Y is determined eventually as 9163 keV, agree well with the result of [8]. Similarly, the Q_{EC} of ^{84}Nb is measured as 7200(300) keV [6], while systematical trends suggest ^{84}Nb 3200 keV less bound. We tentatively use the systematic value in AME and call for more experimental studies.

In a β^+ transition, the ratio of positron emission and electron capture in the transition to the same final level depends on Q_{EC} in a known way. Thus, the decay energy can be derived from a measurement of the relative positron feeding of the level, which is often easier than a measurement of the positron spectrum end-point. With the total-absorption spectrometer, decay energies can be determined with the end-point energy and EC/β^+ as well [10]. We believe the TAS could provide more reliable decay values.

Rather than the β^+ decay, a lot of the radioactive proton-rich nuclides decay by charged particles, which are much easier to be detected. Even with very few events, the decay energies can be determined precisely. But in some of the nuclei, more than one isomeric state could exist. The studies of the odd-odd nuclides are usually difficult as the coupling of the valence neutron and valence proton can result in complicated isomeric states. Here is one example. Two different alpha decay lines of ^{182}Tl were observed as 6406(10) keV [11] and 6050(20) keV [12]. The first one was adopted at AME2003 for it was published in a regular refereed journal. But recently we questioned the particle identification in this work, where $\sim 100\%$ α branching ratio was assumed, which contradicts the later works where the α decay was not observed in coincidence with α decay of ^{186}Bi [13]. Then we use at present the lower value [12], for there the dominant β decay mode of ^{182}Tl is consistent with other works. Since this value doesn't fit quite well the systematic trends, we suppose it decays to some excited levels rather than the ground state of ^{178}Au . So the masses of ^{182}Tl , as well as

^{186}Bi ground-states are experimentally unknown in the present AME. More experimental efforts are called to clarify this case.

For nuclides with masses not determined experimentally, extrapolation is used to assign the values, assuming the mass surface is smooth. Some local extrapolations are done for specific aims by some authors, like to set the limits of observable proton-emitting nuclei between the $N = 82$ and $Z = 82$ shell closures [14]. For some proton-rich nuclides, β delayed protons are observed. Then the mass of the isobaric analogue state can be determined from the proton energies and the mass of the more exotic nuclide of this isobaric chain can be derived from the isobaric multiplet mass equation (IMME), which is quite reliable and precise in most cases.

The IMME was used up to the AME1983 for deriving mass values for nuclides for which little information was available. This policy was questioned with respect to the correctness in stating a quantity that was derived by combination with a calculation as “experimental”. Since AME1993, it was decided not to present any IMME-derived mass values in the evaluation, but rather use the IMME as a guideline when estimating masses of unknown nuclides. We continue this policy at present, and do not replace experimental values by an estimated one from IMME, even if orders of magnitude more precise.

The mass of ^{41}Ti was determined with IMME [15]. And it was directly measured with the ESR ring at GSI [16]. We adopted the experimental value for ^{41}Ti , although with bigger error bar of 360 keV. This value is 600 keV less bound compared to IMME and we call for more experimental work to clarify this situation.

PERSPECTIVE

A large landscape with known masses has been discovered at the proton-rich side of the nuclear chart with experimental efforts. The direct mass measurements and decay spectroscopy studies benefit with each other. More experimental results are desirable to clarify some cases.

The new version of AME is planned to be published by the end of 2012 or early 2013. Half a year before the publication, a bulletin will be sent around from AMDC to call for available experimental results related to atomic masses that are not yet published but ready to be included in the AME.

ACKNOWLEDGMENTS

The founder of the Ame, Prof. Aaldert H. Wapstra passed away at the end of 2006. He made essential contributions to Ame2013 during the two years following the publication Ame2003. And more than those two years, this work is filled with his spirit.

M.W. acknowledges support from the International Agency for Atomic Energy, IAEA-Vienna. The work at ANL was supported by the U.S. Department of Energy, Office of Nuclear Physics, under Contract No. DE-AC02-06CH11357.

REFERENCES

1. G. Audi, A.H. Wapstra, and C. Thibault *Nucl. Phys. A* **729**, 337 (2003) and reference therein.
2. Bulletins of the Amdc: <http://amdc.in2p3.fr/bulletins/file.html>.
3. C. Wrede et al., *Phys. Rev. C* **81**, 055503 (2010) and private communication.
4. Yu. A. Litvinov et al., 2005 *Nucl. Phys. A* **756**, 3 (2005).
5. X.L. Tu et al., *Phys. Rev. Lett.* **106**, 112501 (2011); C. Rauth et al., *Phys. Rev. Lett.* **100**, 012501 (2008);
6. C. J. Lister et al., *Phys. Rev. C* **24**, 260 (1981).
7. S. Della Negra et al., *Z. Phys. A* **307**, 305-321 (1981).
8. C. J. Barton et al., *Phys. Rev. C* **67**, 034310 (2003).
9. E. Haettner et al., *Phys. Rev. Lett.* **106**, 122501 (2011); A. Kankainen et al., *Eur. Phys. J. A* **29**, 271 (2006); G. Sikler et al., *Nucl. Phys. A* **763**, 45 (2005).
10. M. Kavatsyuk et al., *Inter. J. Mass Spec.* **251**, 138-145 (2006).
11. J. G. Keller et al., *Nucl. Phys. A* 452, 173 (1986).
12. V. A. Bolshakov et al., *Inst. Phys. Conf. Ser. No 132 : Section 5*, 1992, pp. 743-745.
13. A. N. Andreyev et al., *Eur. Phys. J. A* 18, 55 (2003) ; J. C. Batchelder et al., *Z. Phys. A* 357, 121 (1997).
14. R. D. Page, *Phys. Rev. C* **83**, 014305 (2011)
15. C. Dossat et al., *Nucl. Phys. A* **792**, 18-86 (2007).
16. J. Stadlmann et al., *Phys. Lett. B* **586**, 27-33 (2004).

Beta-delayed Proton-emission: Peering into Nuclear Structure

M.J.G. Borge

Instituto de Estructura de la Materia, CSIC, Serrano 113bis, E-28006 Madrid, Spain

Abstract. The β decay data of $^{32,33}\text{Ar}$, recently revisited at the low energy line of SPIRAL at GANIL, is used to illustrate the structure information we can get from βp precursors when a highly performing setup is used.

Keywords: β -decay, delayed particle emission, GT strength distribution, quenching factor.

PACS: 23.40.-s, 23.40.Hc, 21.10.Dr, 21.10.Tg.

INTRODUCTION

The beta decay process dominates the way a nucleus changes into another one. The determination of the beta decay half-life of a nucleus and the comparison with the theoretical predictions give us the first glance into the global behavior of such a nuclear system. In the last half a century a great number of nuclear systems have been studied by the beta decay process and the interpretation of the results has allowed to advance greatly in the understanding of the organization and behavior of the nucleons inside the nuclei.

When moving away from the valley of stability, the isobaric mass differences grow roughly quadratically with isospin while the binding energy of the last nucleon decreases significantly so that it becomes feasible for particle-unbound states to be populated in the β decay process. The decay path hence opens up to many different processes: $\beta\gamma$, βp , βn , $\beta 2p$, $\beta 2n$...

The high efficiency for the charged particle detection makes the study of the beta delayed charged particle emission a unique tool to understand the nuclear structure of rare species. Beta-delayed α emission dates back to the early days of nuclear physics, but β -delayed proton emission and proton radioactivity were still not discovered in the late 1950's. The β -delayed proton emission was first identified in ^{25}Si in 1963 thanks to the use, for first time, of Si surface barrier detectors. Today close to 200 β -delayed proton emitters have been identified [1].

The delayed particle energy spectrum is determined by two factors: the intensity of the β transition from the precursor (parent) to the unbound state in the daughter, often called emitter, and the branching ratio for subsequent particle emission from the intermediate state to states in the so called particle-daughter. The process is well understood and the interpretation of the data yields a wide variety of spectroscopic information: level energies, spins, parities, widths and level densities.

The βp process is open for most elements for the isotopes close to the proton drip line. The lightest is ^9C with $\beta p = 62\%$ [2] and the heaviest is ^{183}Hg with $\beta p = 3.10^{-4}\%$ [3]. Heavier precursors might exist such as $^{200,202}\text{At}$ with βp at the level of 10^{-6} , but they have not been search for in their β decay study [4].

The Q-values are high in the neutron deficient side for light nuclei revealing the nuclear structure of the daughter in a large energy range. The effect is even higher in

the sd-shell ($Z \geq 8$) where there are many βp precursors. For nuclei with $Z > N$, the IAS falls into the Q_β -window. The IAS decays by isospin-forbidden transitions to the ground and excited states of the proton daughter. Coulomb force and the charge dependence of the nuclear forces tend to mix the states. The comparison of the IAS feeding to the $B(F)$ value can be used to investigate the *isospin mixing* of the states in the emitter. In this way a large isospin mixing up to 2 % was determined in ^{32}Ar [5].

We will summarize recent results from the light Ar isotopes which decays have been recently revisited in the low energy line of SPIRAL.

THE CASE OF THE LIGHT ARGON ISOTOPES

Often in nuclei of the sd-shell the IAS is in the middle of the Q_β -window. This is the case, for instance, for the β -decay of the ^{33}Ar ($Q_{\text{EC}} = 11.6193(6)$ MeV; $E^*(\text{IAS}) = 5.544(1)$ MeV) and ^{32}Ar ($Q_{\text{EC}} = 11.1344(19)$ MeV; $E^*(\text{IAS}) = 5.0463(4)$ MeV) nuclei. The decay of the IAS dominates the βp spectrum see Fig. 1. The Q_{EC} is large and a large part of the Gamow Teller (GT) strength, including the GT Giant Resonance becomes accessible. Furthermore the shell model predictions in the sd-shell give, in general, a good description of the excited states. So the analysis of the decay allows for the determination of the excitation energies of a large number of excited states in the daughter nucleus, and, in some cases, the spin and parities of the excited states. Thus the comparison of the deduced excited states with theory becomes a highly stringent test for these predictions.

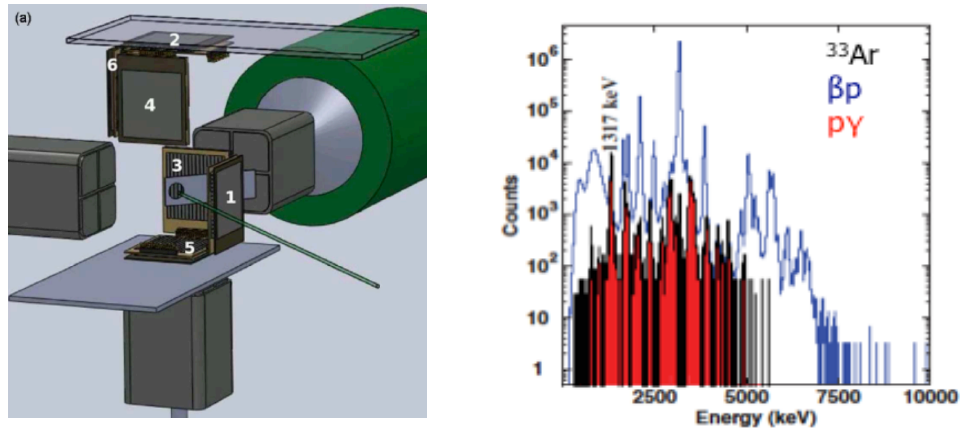


FIGURE 1. a) Set up used in the study of $^{33,32}\text{Ar}$ decay. b) The β -gated proton spectrum and γ -gated proton spectrum from the ^{33}Ar decay taken from [8]

Further the measured GT strength distribution can be compared with the sum rule. Comparison of the observed GT strength distribution with the theoretical prediction allows the *extraction of the* quenching of the axial-vector coupling constant. Effective values of the coupling constant, $q=(g'_A/g_A)$, have been deduced empirically from experiments, as the origin of this quenching is not well understood. Recently, the $^{90}\text{Zr}(p,n)$ and (n,p) reaction data up to 70 MeV were used to study the contribution of the continuum beyond the GTGR to the GT strength [6]. It was concluded that second-

order configuration mixing was the main mechanism responsible for the quenching of the Gamow-Teller strength.

The $^{32,33}\text{Ar}$ nuclei were produced at the low energy line of SPIRAL at GANIL. Beta-delayed proton and γ -ray emission from these decays were studied by means of the setup display in Fig. 1a). It consisted in a Silicon Cube detector array surrounded by three high-efficiency HPGe Clover telescopes, with efficiencies of 41(1) % of 4π for charged particles and 3.0(2) % for 1.25 MeV γ -ray. The added value of this experimental setup was the high py efficiency that allows to obtain a more realistic B(GT) strength distribution. Details about the complete analysis can be found in [7,8].

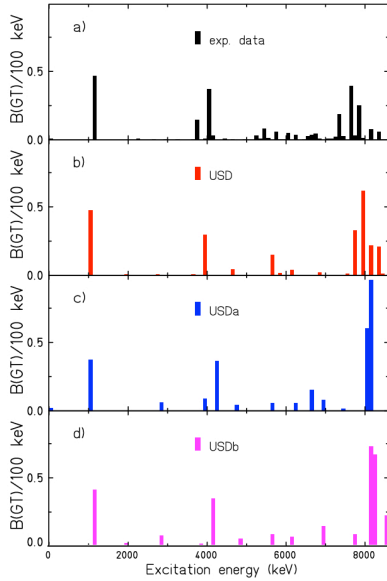


FIGURE 2. Experimental B(GT) strength for the ^{32}Ar decay is shown in a) for all levels. It is compared with shell model predictions using the interactions USD in b), USDa in c) and USDb in d) [11,12]. Notice that the experimental onset of GTGR is at lower energy than theoretically predicted.

The predicted excited states in ^{33}Cl are in good agreement with the experimentally found ones. The case is different for the excited states of ^{32}Cl as shown in Fig. 2.

With the new B(GT) distributions obtained from these data the problem of abnormal quenching factors obtained for these nuclei [9] have been addressed. It was found that the quenching factor, $q^2 = \Sigma\text{B(GT)}_{\text{exp}}/\Sigma\text{B(GT)}_{\text{th}}$ for the $^{32,33,34}\text{Ar}$ nuclei was close to unity and very far from the average of the sd-shell $q^2 = 0.58(5)$ [9]. Being the case of ^{33}Ar the more severe as the q^2 was equal to 1.19 when compared to the shell model calculations using the USD interaction [10]. Later on it was clear that this interaction worked very well for mid-shell nuclei, but it had problems for nuclei in the upper part of the sd-shell where the neutron deficient argon isotopes sit. New interactions, USDa and USDb, were developed [11]. The B(GT) strength for the ^{32}Ar case is displayed in Fig. 2a.

As the correspondence between experimental and predicted excited states in ^{32}Cl is not very good binning by 100 keV is done for the comparison of the experimental B(GT) strength with the shell model calculations using the different interactions, see Fig. 2b-d. It is clear that the calculations followed the main trend and reproduce the experimental characteristics mainly at low energy up to the IAS situated at 5046.3(4) keV. The shell model calculations fail to reproduce the excitation energy region between 6-7 MeV where many 1^+ states has been identified. Further the onset of the Gamow-Teller Giant Resonance is found experimentally at lower energy than theoretically predicted. Table 1 summarises the quenching factors deduced for $^{32,33}\text{Ar}$ decay studies using the half-lives and the $\Sigma\text{B(GT)}$ strength distribution. For the ^{33}Ar case a $q^2 = 0.58$ is obtained from the half-lives. This factor is not far from the one

obtained comparing individual allowed transitions ($\log(ft) \leq 6$) up to an energy of 9.2 MeV. The average q^2 value obtained from the half-lives for ^{32}Ar is 0.60. For the ^{32}Ar case, the USD interaction predicts different strength than the other two interactions from which an average quenching factor of 0.56 is found for the individual allowed transitions up to 7 MeV. When all transitions are taken into account a value of $q^2 = 0.45$ is obtained from both nuclei and all interactions.

TABLE 1 Quenching factor obtained from the $^{32,33}\text{Ar}$ decays by comparison of experimentally obtained and theoretically predicted half-lives and $\Sigma B(\text{GT})$ both for individual allowed transitions up to a certain energy and for the strength observed in the Q_{EC} window.

A_Z			Exp Value	USD	USDa	USDb	q^2 (USD)	q^2 (USDa)	q^2 (USDb)
^{33}Ar	$T_{1/2}(\text{ms})$		173.9(9)[8]	101.4	98.0	100.8	0.583	0.564	0.580
	$\Sigma B(\text{GT})$	7	0.5206	0.865	0.935	1.107	0.602	0.557	0.47
	Up to E^* (MeV)	9.2	1.814	2.434	3.55	3.198	0.745	0.511	0.567
		ALL	2.5674	5.613	5.703	5.403	0.457	0.450	0.475
^{32}Ar	$T_{1/2}(\text{ms})$		100.5(3)[7]	56.79	61.85	60.98	0.565	0.615	0.607
	$\Sigma B(\text{GT})$	4.5	1.039	1.664	1.883	1.862	0.624	0.552	0.558
	Up to E^* (MeV)	7	1.407	2.103	2.575	2.488	0.669	0.546	0.565
		ALL	2.303	5.109	5.728	5.47	0.451	0.402	0.421

SUMMARY

Rather complete studies of the $^{32,33}\text{Ar}$ decays were done recently [7,8] by the used of a high efficient setup that allowed for a meaningful proton and γ -ray coincident study. The information obtained on the excited excites of the daughters are a stringent test of the shell calculations and they have been compared with the three USD, USDa and USDb interactions [10,11]. The new USDa and USDb interactions reproduced better the behavior of the ^{32}Ar decay. From the comparison of the GT strength with the shell model calculations the quenching factor has been obtained. Quenching factors in the order of 0.55 are obtained when the $B(\text{GT})$ strength coming from individual allowed transition is compared with predictions for excitation energies below the onset of the Gamow-Teller Giant Resonance. This quenching factor diminishes to 0.45 when all transitions are taken into account. In short, we can conclude that the new data and new interactions indicate that the quenching factor deduced for these nuclei is the current one in the sd-shell, but the predictions still have problems in predicting the onset, the energy and width of the GT Giant Resonance. So care has to be taken when deducing the quenching factor from beta decay studies in the proximity of the GTGR.

REFERENCES

1. B. Blank and M. J. G. Borge, *Progress in Part. and Nuc. Phys.* **60**, 403-483 (2008)
2. www.tunl.duke.edu/nuclldata/General_Tables/9b.shtml
3. P. Hornshøj et al., *Phys. Lett.* **34B**, 591-593 (1971)
4. N. Bijmens et al., *Phys. Rev.* **C58**, 754-764 (1998)
5. M. Bhattacharya et al., *Phys. Rev.* **C77**, 065503-1-15 (2008)
6. M. Ichimura, H. Sakai and T. Wakasa, *Progress in Part. and Nuc. Phys.* **56**, 446- (2006)
7. N. Adimi et al., *Phys. Rev.* **C81**, 024311-1-14 (2010)
8. R. Dominguez-Reyes, et al., submitted to *J. Phys. G: Nucl. Phys.*
9. M. J. G. Borge et al., *Z. Phys.* **A332** 413-417 (1989)
10. B. A. Brown and B. H. Wildenthal, *At. Data Nucl. Data Tables* **34**, 347- (1985)
11. B. A. Brown and W.A. Richter, *Phys. Rev.* **C74** 034315- (2006)

β -delayed emission of protons at the proton drip-line: the cases of ^{43}Cr and ^{51}Ni

L. Audirac,^{a,b} N. Adimi,^a P. Ascher,^a B. Blank,^a C. Borcea,^d G. Cachel,^a C.E. Demonchy,^a I. Companis,^a F. Delalee,^a C.E. Demonchy,^a F. de Oliveira Santos,^c C. Dossat,^a J. Giovinazzo,^a S. Grévy,^a L. Hay,^a J. Huikari,^a T. Kurtukian-Nieto,^a S. Leblanc,^a I. Matea,^e J.-L. Pedroza,^a L. Perrot,^c J. Pibernat,^a L. Serani,^a C. Stodel,^c P. Strivatava,^c J.-C. Thomas^c

^a*CENBG, Chemin du Solarium, BP 120, F-33175 Gradignan Cedex, France*

^b*CEA Saclay, DSM/Irfu/SPhN, Orme des Merisiers, F-91191 Gif-sur-Yvette Cedex, France*

^c*GANIL, Bvd Henri Becquerel, BP 55027, F-14076 Caen Cedex 5, France*

^d*NIPNE, P.O. Box MG6, Bucharest-Magurele, Romagne*

^e*IPN, 15 rue Georges Clémenceau, F-91406 Orsay*

Abstract. Studies of β -delayed emission of protons for ^{43}Cr and ^{51}Ni were performed with a Time Projection Chamber. This detection setup allows to reconstruct in the three-dimensional space the tracks of the protons emitted. For the first time, β -delayed emission of two protons is directly observed for ^{43}Cr and ^{51}Ni . The question about correlations between protons can be accessed. Finally, we show that ^{43}Cr can emit up to three delayed protons.

Keywords: Exotic nuclei, β -delayed emission of protons, Time Projection Chamber.

PACS: 23.40.-s, 23.50.+z, 27.40.+z, 29.40.Cs, 29.40.Gx

INTRODUCTION

Proton-rich nuclei are firstly known to be unstable relative to β^+ disintegration. For nuclei very far from stability, β^+ emission can populate excited states in the daughter nucleus which are unstable relative to the emission of protons. This phenomenon is called β -delayed emission of protons. The most recent experimental results concerning the spectroscopy of ^{43}Cr and ^{51}Ni are presented in reference [1]. A detection setup consisting in silicon and germanium detectors allowed to identify β -delayed emission of one proton for both nuclei. Moreover, a possibly β -delayed emission of two protons could be attributed to ^{43}Cr without protons identified separately.

A NEW EXPERIMENTAL SETUP FOR THE STUDY OF β -DELAYED EMISSION OF PROTONS OF ^{43}Cr AND ^{51}Ni

A second opportunity to study ^{43}Cr and ^{51}Ni occurred during two experiments performed in 2006 and 2008 at the LISE3 separator of GANIL with a new detection setup consisting in a Time Projection Chamber (TPC). The TPC is a gaseous detector filled with P10 (a mixture of 90 % argon and 10 % methane) where the heavy ions are

implanted and the subsequent decays can occur. When a charged particle like heavy ions or protons loses energy in the gaseous medium, ionization electrons are created along the tracks of these particles. Electrons are then directed toward a detection plane thanks to an electric field. Before being detected, the number of electrons is amplified by a set of four GEMs (Gas Electron Multipliers). Electrons are finally detected on a two-dimensional matrix of two orthogonal sets of 768 strips with a pitch of 200 μm . Each strip gives information in energy and in time. The information in energy is directly proportional to the total energy deposited on the strip and the information in time is relative to the arrival time of the electronic signal on the strip. Energy signals allow to reconstruct the tracks projected on the detection plane and to access the total energy deposited by a particle. Then time spectra give the relative drift time of the particles, giving access to the third dimension.

β -DELAYED EMISSION OF PROTONS OF ^{43}Cr AND ^{51}Ni

The study of β -delayed emission of protons of ^{43}Cr [2] and ^{51}Ni [3] with the TPC was achieved during two different experiments initially dedicated to the study of two-proton radioactivity of ^{45}Fe and ^{54}Zn . It confirmed firstly β -delayed emission of one proton for both nuclei. Secondly, the observation of β -delayed emission of two protons was achieved for the first time with an individual detection of the two particles, both for ^{43}Cr and ^{51}Ni . Figure 1 shows an event of β -2p decay of ^{43}Cr .

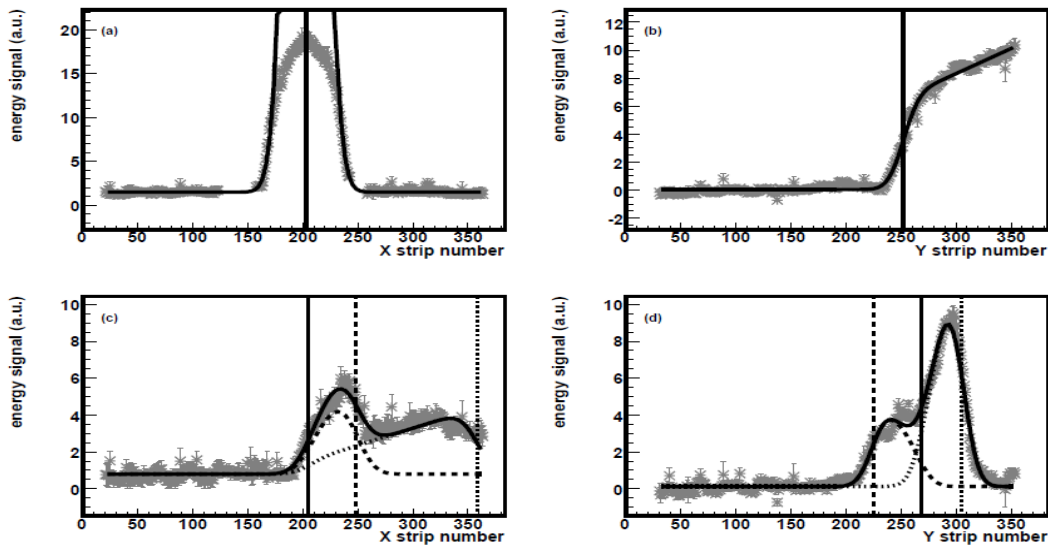


FIGURE 1. (a) Implantation signal of ^{43}Cr for the anodes (X strips). (b) Implantation signal for the cathodes (Y strips). Fitting the spectra gives the implantation positions (solid lines). (c) Correlated β -delayed emission of two protons for the anodes. The tracks of each proton (dashed and dotted curves) are obvious. The starting point of the decay (solid line) and the stopping points (dashed and dotted lines) are determined. (d) Same correlated decay event for the cathodes.

We first determine the implantation positions of the heavy ion by analyzing the implantation signals. As the beam enters the chamber parallel to the anodes, a Gaussian profile is used to adjust the data whereas a folding of a Gaussian and a straight line is a good approximation of the Bragg peak for the cathodes orthogonal to

the beam axis. For the correlated decay event, the sum of two foldings between a Gaussian and a straight line is used to determine the common starting point and the stopping points of the protons on the two dimensions which are fitted at the same time to constrain the energy deposited to be the same on both strip sets. Finally, drift time spectra of the protons (not shown on the figure) give the opportunity to obtain the proton tracks in the three-dimensional space.

The question of correlations between the protons could be studied in order to access the emission process. Analysis of the energy spectra allows to calculate the sharing between the two protons of the total energy deposited in the TPC. The left part of figure 2 shows the experimental data compared to a simulation taking into account the fact that the protons escape the active volume of the chamber. A non-equal sharing of the total decay energy is in good agreement with the data, showing a sequential emission of the protons via an intermediary state in ^{42}Ti . Moreover the relative angle between the protons is calculated. This needs the analysis of the drift time spectra. The right part of figure 2 shows the experimental data compared to a simulation of an isotropic emission of the protons. The lack of statistics limits the conclusions but the data do not contradict a sequential process for the angular correlations except the lack of events at around 90° .

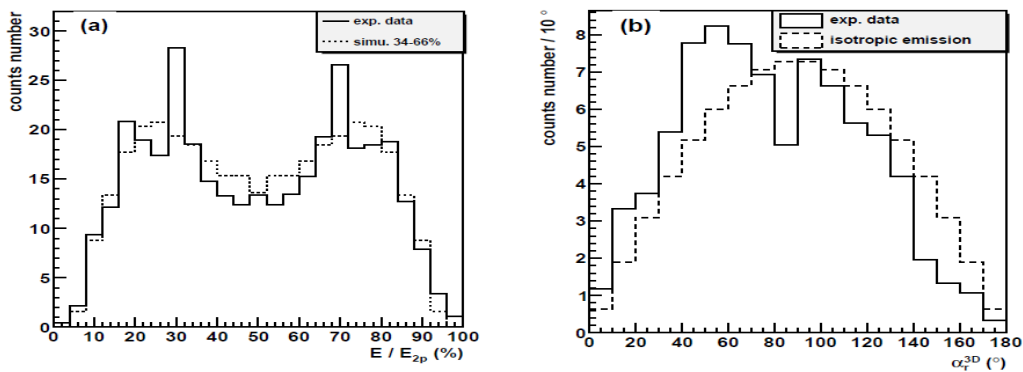


FIGURE 2. (a) Sharing of the total energy between the two delayed protons of ^{43}Cr . The solid histogram represents the data whereas dashed line is a simulation of a non-equal sharing (34-66 %) of the total energy deposited. Nice agreement is obtained. (b) Relative angle between the protons. Experimental data (solid curve) are compared to an isotropic emission (dashed curve). The two histograms do not contradict each other even though more statistics would be needed.

For the first time, β -delayed emission of two protons is identified for ^{51}Ni . Figure 3 shows an example of these decay events. Their analysis is going on.

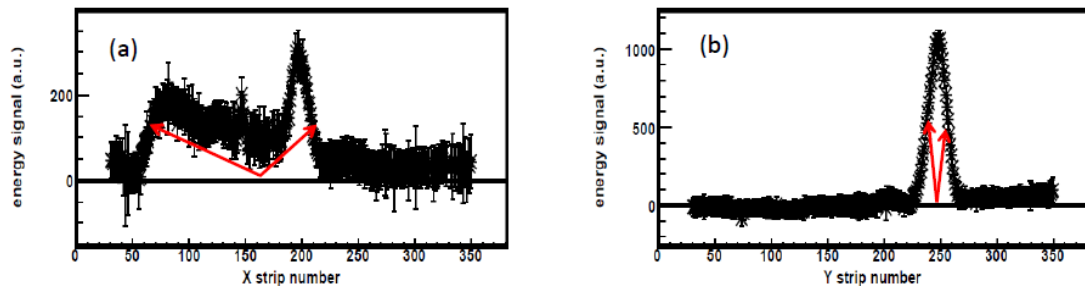


FIGURE 3. (a) β -delayed emission of two protons from ^{51}Ni for the anode strips. (b) Same decay event for the cathode strips. This is the first observation of such a decay mode for this nucleus.

Finally the β -delayed emission of three protons was observed for the first time for two decay events correlated to implantations of ^{43}Cr . Figure 4 presents one of these events. The decay energy spectra show obviously the tracks of three particles emitted. The data are fitted by the sum of three foldings of a Gaussian and a straight line which allows to determine the three proton tracks projected on the detection plane.

From all the analyzed decay events of ^{43}Cr , one can access the relative branching ratios for each type of β -delayed emission of protons. A branching ratio of (87.1 ± 2.5) % of the total emission of protons is found for β -p emission, (12.7 ± 1.0) % for β -2p emission and $0.14^{+0.19}_{-0.09}$ % for β -delayed emission of three protons. A nice agreement is observed with values obtained from another experiment [4].

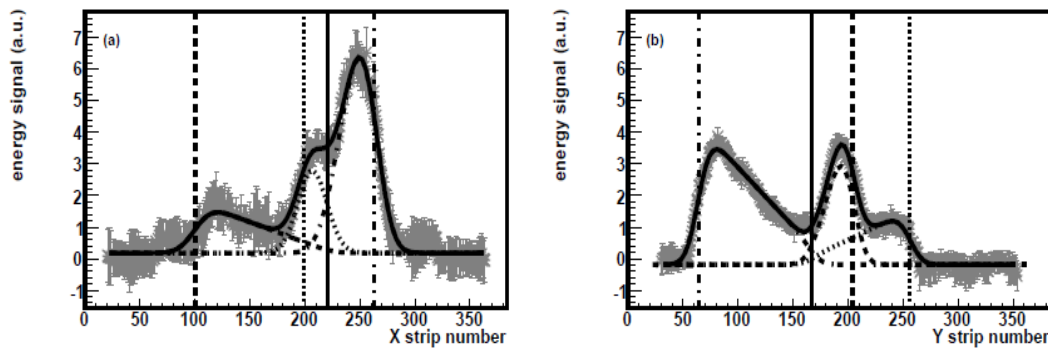


FIGURE 4. (a) β -delayed emission of three protons for the anode strips. The fit function allows to determine the tracks of the three protons (dashed, dotted and dashed-dotted curves) and their starting (solid line) and stopping positions (dashed, dotted and dashed-dotted lines). (b) Analysis of the same decay event for the cathode strips.

CONCLUSION

The study of β -delayed emission of protons of ^{43}Cr and ^{51}Ni was achieved with a TPC which allows to reconstruct in the three-dimension space the tracks of charged particles. For the first time, β -2p emission was observed with an individual detection of the two protons for ^{43}Cr and ^{51}Ni . Up to now, this decay mode was unknown for ^{51}Ni . The question about correlations between protons shows a sequential emission of the protons for ^{43}Cr . Moreover, the data showed that ^{43}Cr can emit up to three delayed protons. Analysis is going on for ^{51}Ni . These experiments show the capability of TPC to access the study of exotic decay modes by emission of protons for nuclei situated at the proton drip-line.

REFERENCES

1. C. Dossat et al., *Nucl. Phys. A* **792**, p. 18-86 (2007).
2. L. Audirac et al., *to be submitted*.
3. P. Ascher, Ph.D. Thesis, Université Bordeaux 1.
4. M. Pomorski et al., *Phys. Rev. C* **83**, 014306 (2011).

Recent experimental results of two-proton correlated emission from the excited states of $^{17,18}\text{Ne}$ and $^{28,29}\text{S}$

C. J. Lin^a, X. X. Xu^a, H. M. Jia^a, F. Yang^a, F. Jia^a, Z. D. Wu^a,
S. T. Zhang^a, Z. H. Liu^a, H. Q. Zhang^a, H.S. Xu^b, Z. Y. Sun^b,
J. S. Wang^b, Z. G. Hu^b, M. Wang^b, R. F. Chen^b, X. Y. Zhang^b,
C. Li^b, X. G. Lei^b, Z. G. Xu^b, and G. Q. Xiao^b

^aChina Institute of Atomic Energy, P. O. Box 275(10), Beijing 102413, China

^bInstitute of Modern Physics, The Chinese Academy of Science, Lanzhou 730000, China

Abstract. Two-proton emissions from the excited states of $^{17,18}\text{Ne}$ and $^{28,29}\text{S}$ were investigated by the radioactive beams bombarding on the ^{197}Au target via the Coulomb excitation. The complete-kinematics measurements were actualized by the stacks of silicon-strip detectors and CsI+PIN array detectors. The invariant mass of final systems as well as the relative momentum, opening angle, and relative energy of the two emitted protons were reconstructed under the framework of relativistic kinematics. The mechanisms of two-proton emission were analyzed in a simple schematic model. With the help of Monte-Carlo simulations, the two protons emitted from the 6.15 MeV excited state of ^{18}Ne and the excited states around 10 MeV of ^{29}S , respectively, exhibit prominent features of ^2He decay. While for the other states, no obvious diproton emissions were observed.

Keywords: Two-proton emission, complete-kinematics measurement, diproton decay, three-body phase-space decay, two-body sequential decay.

PACS: 23.50.+z, 25.60.-t, 25.70.De.

INTRODUCTION

Two-proton ($2p$) radioactivity was first proposed by Goldanskii [1] at the beginning of 1960s. More than forty years later, such an exotic decay mode was discovered in ^{45}Fe [2,3], ^{54}Zn [4], and most likely ^{48}Ni [5]. Nowadays, it becomes one of the most exciting topics in the field of radioactive-ion-beam physics [6]. Besides the ground state emitters mentioned above in the medium mass region, which have longer decay times due to the higher Coulomb barriers, a lot of lighter nuclei with very short decay times, such as ^6Be [7], ^{10}C [8,9], $^{12,14}\text{O}$ [10,11], $^{16,17,18}\text{Ne}$ [12-16], ^{19}Mg [17], ^{28}P [18], and ^{29}S [19] etc., have been extensively investigated to search for the correlated $2p$ emissions from the ground states and/or the excited states.

In the past years, we performed a series of experiments to study $2p$ emission from the proton-rich nuclei close to the drip line. In the $^{29}\text{S}+^{28}\text{Si}$ experiment, an abnormally large total reaction cross section has been detected [20], indicating the possibility of $2p$ halo/skin structure in ^{29}S . Moreover, signatures of $2p$ emission were observed in the $^{29}\text{S}+^{12}\text{C}$ reaction [21]. Later, we focus on $2p$ emission from the excited states of

$^{17,18}\text{Ne}$ and $^{28,29}\text{S}$ by means of the complete-kinematics measurements. Recent experimental results will be presented in this paper.

EXPERIMENTAL PROCEDURE

The experiments were done at the Institute of Modern Physics, Lanzhou, China. The secondary radioactive beams were produced by the primary beams of ^{20}Ne and ^{32}S , respectively, with typical current of 100 enA, bombarding on the $1589\ \mu\text{m}$ ^9Be target, transported and purified through the RIBLL facility [22] by means of the combined Bp- ΔE -Bp method, where ^{27}Al degraders with different thicknesses were chosen to get the suitable momentum dispersion. The excited states were populated by bombarding on a secondary ^{197}Au target via the Coulomb excitation. Typical secondary beam intensities were 200 and 800 pps for ^{17}Ne and ^{18}Ne with purities of 10% and 40%, respectively, 30 and 200 pps for ^{28}S and ^{29}S with purities of 1% and 3%, respectively.

A detector array consisting of two parallel plane avalanche counts, four large area silicon detectors, four single-sided silicon strip detectors, and a 6×6 array of CsI crystals coupled to PIN photodiodes (CsI+PIN) was employed to perform the complete-kinematics measurement. As an example, Figure 1 shows the schematic plot of the detector array used in the $^{28,29}\text{S}$ experiments. The secondary beams were identified by ΔE -ToF technique, as shown in Fig. 2 for the $^{28,29}\text{S}$ cases.

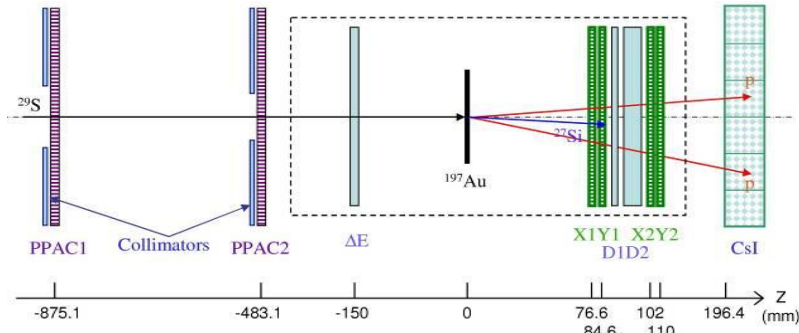


FIGURE 1. Schematic plot of detector array used in the $^{28,29}\text{S}$ experiments.

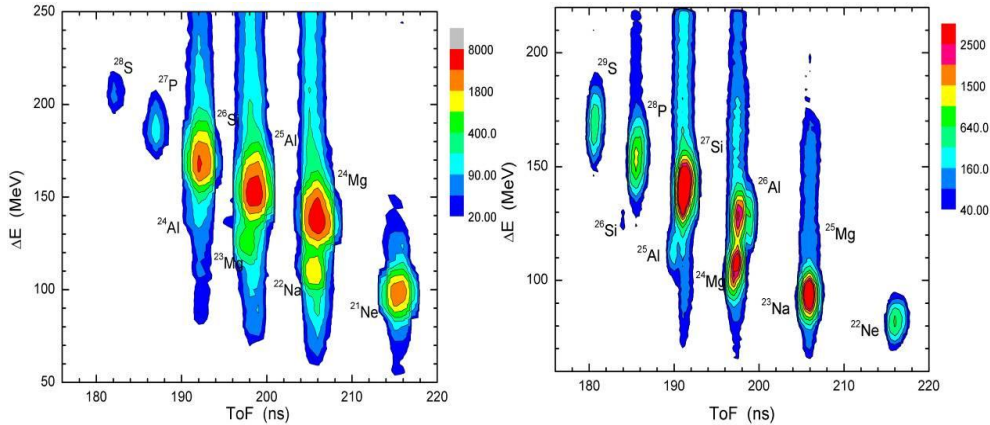


FIGURE 2. Contour plot of the particle identification for the ^{17}Ne secondary beam.

EXPERIMENTAL RESULTS

The effective $2p$ coincident events were selected under serial strict conditions. The invariant mass of final three-body system as well as the relative momentum ($q_{pp} = |\mathbf{p}_1 - \mathbf{p}_2|/2$), the opening angle ($\theta_{c.m.}^{pp}$), and the relative energy (E_{pp}) of two protons can be deduced, on event-by-event basis, by the relativistic-kinematics reconstruction under the constraints of energy and momentum conservation. Taking into account the energy and position resolutions of the detector array, the experimental excitation-energy resolution was estimated as 200–400 keV.

In order to investigate the mechanisms of $2p$ decay, MC simulations were carried out, in which all the possible decay channels should be included. For the sake of simplicity, three schematic decay modes were employed to describe $2p$ emission, i.e. ${}^2\text{He}$ decay, two-body sequential decay, and three-body phase-space simultaneous decay.

With the help of MC simulations, the mechanism of $2p$ decay can be understood by the relative momentum combined with opening angle of two protons. Figure 3 shows the experimental results for ~ 7.4 MeV and ~ 10.0 MeV excited states of ${}^{29}\text{S}$, respectively. An isotropic distribution in the opening angle and no peak at 20 MeV/c in the relative momentum can be seen for the 7.4 MeV states. But for the 10.0 MeV states, the opening angle shows a forward distribution with maximum around 35° and the relative momentum has an obvious peak at 20 MeV/c, indicating the features of ${}^2\text{He}$ decay. The MC results are also plotted in the figures for comparison. The dashed, dotted and dash-dotted curves are the results predicated by the ${}^2\text{He}$ decay, two-body sequential decay, and the three-body phase-space decay, respectively. Associated with the MC simulations, the branching ratio of ${}^2\text{He}$ decay was determined as $29^{+10}_{-11}\%$, where the errors were estimated by χ^2 analysis.

In the ${}^{17,18}\text{Ne}$ cases, visible p - p correlations were also observed. But no obvious diproton emission was found except the 6.15 MeV state in ${}^{18}\text{Ne}$ which is in good agreement with Raciti's results. Some preliminary results can be found in Ref. [23].

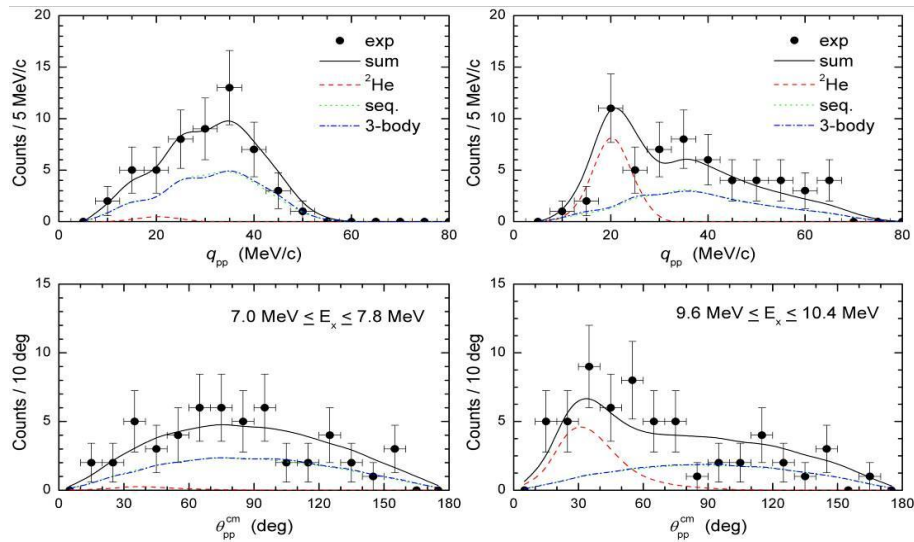


FIGURE 3. The relative momentum and opening angle for $2p$ emission from the excited states around 7.4 MeV (left) and 10.0 MeV (right) of ${}^{29}\text{S}$.

SUMMARY

In summary, a series of experiments have been performed to study $2p$ correlated emission from the excited states of $^{17,18}\text{Ne}$ and $^{28,29}\text{S}$. $2p$ emissions were induced by the Coulomb excitations via the radioactive secondary beams bombarding on the ^{197}Au targets. Complete-kinematics measurements were actualized by the stacks of silicon-strip detectors and CsI+PIN array detectors, allowing us to reconstruct invariant mass of final systems as well as the relative momentum, opening angle, and relative energy of emitted two protons under the framework of relativistic kinematics. The events of $2p$ coincident with heavy residua were picked out under strict conditions to unambiguously identify the rare events in the strong background. The mechanisms of $2p$ emission were analyzed in a simple schematic model. With helps of the MC simulations, the present results show that $2p$ emitted from the excited states around 10 MeV of ^{29}S exhibit the features of ^2He decay with a branching ratio of $29^{+10}_{-11}\%$. Visible p - p correlations were also observed in the cases of $^{17,18}\text{Ne}$. But no obvious diproton emission was found except the known 6.15 MeV state in ^{18}Ne , according to the MC simulations.

ACKNOWLEDGMENTS

This work was supported by the National Natural Science Foundation of China under Grants 10735100, 10727505, and 10975192, and by the Major State Basic Research Developing Program under Grant 2007CB815003.

REFERENCES

1. V. I. Goldanskii, *Nucl. Phys.* **19**, 482-495 (1960).
2. J. Giovinazzo, B. Blank, M. Chartier et al., *Phys. Rev. Lett.* **89**, 102501 (2002).
3. M. Pfutzner, E. Badura, C. Bingham et al., *Eur. Phys. J.* **A14**, 279-285 (2002).
4. B. Blank, A. Bey, G. Canchel et al., *Phys. Rev. Lett.* **94**, 232501 (2005).
5. C. Dossat, A. Bey, B. Blank et al., *Phys. Rev. C* **72**, 054315 (2005).
6. B. Blank, M. Ploszajczak, *Rep. Prog. Phys.* **71**, 046301 (2008).
7. O. V. Bochkarev, L. V. Chulkov, A. A. Korsheninnicov et al., *Nucl. Phys.* **A505**, 215-240 (1989).
8. R. J. Charity, K. Mercurio, L. G. Sobotka et al., *Phys. Rev. C* **75**, 051304R (2007).
9. K. Mercurio, R. J. Charity, R. Shane et al., *Phys. Rev. C* **78**, 031602R (2008).
10. R. A. Kryger, A. Azhari, M. Hellstrom et al., *Phys. Rev. Lett.* **74**, 860-863 (1995).
11. C. R. Bain, P. J. Woods, R. Coszach et al., *Phys. Lett.* **B373**, 35-39 (1996).
12. I. Mukha, L. Grigorenko, K. Summerer et al., *Phys. Rev. C* **77**, 061303R (2008).
13. M. J. Chromik, P. G. Thirolf, M. Thoennessen et al., *Phys. Rev. C* **66**, 024313 (2002).
14. T. Zerguerras, B. Blank, Y. Blumenfeld et al., *Eur. Phys. J.* **A20**, 389-396 (2004).
15. J. Gomez del Campo, A. Galindo-Uribarri, J. R. Beene et al., *Phys. Rev. Lett.* **86**, 43-46 (2001).
16. G. Raciti, G. Cardella, M. De Napoli et al., *Phys. Rev. Lett.* **100**, 192503 (2008).
17. I. Mukha, K. Summerer, L. Acosta et al., *Phys. Rev. Lett.* **99**, 182501 (2007).
18. X. X. Xu, C. J. Lin, H. M. Jia et al., *Phys. Rev. C* **81**, 054317 (2010).
19. C. J. Lin, X. X. Xu, H. M. Jia et al., *Phys. Rev. C* **80**, 014310 (2009).
20. Zu-Hua Liu, Ming Ruan, Yao-Lin Zhao et al., *Chin. Phys. Lett.* **21**, 1711-1713 (2004).
21. C. J. Lin, X. X. Xu, G. L. Zhang et al., *AIP Conf. Proc.* **961**, 117-119 (2007).
22. Z. Sun, W. L. Zhan, Z. Y. Guo, et al., *Nucl. Instr. Meth. Phys. Res.* **A503**, 496-503 (2003).
23. Fei Jia, Cheng-Jian Lin, Huan-Qiao Zhang et al., *Chin. Phys. Lett.* **26**, 032301 (2009).

The $T_z = -1 \rightarrow T_z = 0$ beta decays and comparison with Charge Exchange reactions

F.Molina¹, B.Rubio¹, Y.Fujita², W.Gelletly³ for the Valencia, Osaka, Surrey, GSI, Istanbul, Legnaro, Leuven, Lund, Madrid, New Delhi, Santiago Collaboration

¹*Instituto de Física Corpuscular, CSIC-Universidad de Valencia, E-46071 Valencia, Spain.*

²*Department of Physics, Osaka University, Toyonaka, Osaka 560-0043, Japan.*

³*Department of Physics, University of Surrey, Guildford GU7XH, Surrey, UK*

Abstract. Gamow-Teller (GT) transitions can be studied in both β decay and charge exchange (CE) reactions. If isospin is a good quantum number, then the $T_z = -1 \rightarrow 0$ and $T_z = +1 \rightarrow 0$ GT mirror transitions, are identical. Therefore, a comparison of the results from studies of β decay and CE should shed light on this assumption. Accordingly we have studied the β decay of the $T_z = -1$ fp-shell nuclei, ^{54}Ni , ^{50}Fe , ^{46}Cr , and ^{42}Ti , produced in fragmentation and we have compared our results with the spectra from (^3He , t) measurements on the mirror $T_z = +1$ target nuclei studied in high resolution at RCNP, Osaka. The β decay experiments were performed as part of the STOPPED beam RISING campaign at GSI.

Keywords: Beta decay, Charge Exchange reactions, B(GT), Isospin Symmetry

PACS: 21.10 Hw, 23.20 Lv, 23.40 -s, 25.40 Kv, 27.40+z

MOTIVATION

Gamow-Teller (GT) transitions can be studied in two very different ways, namely in beta decay, involving the Weak Interaction, and in Charge Exchange(CE), which involves the Strong interaction. Assuming the same GT response, one can combine them to produce a complete picture of the GT strength for a particular nucleus. The β decay has the advantage that it provides absolute B(GT) values but is limited by the energy window available. In contrast CE reactions provide only relative B(GT) values, but have no restrictions in energy. Ideally one would like to study both on the same nucleus (also the same final nucleus) and compare the results. This would provide a comparison of the two probes and determine whether they can be combined. However, this experiment, which would involve intense radioactive beams of exotic nuclei and a highly demanding experimental set up is not yet feasible although it is firmly on the agenda for several future facilities [1]. A possible alternative is to assume isospin symmetry and to compare β -decay and CE reactions in mirror nuclei. This is possible when a stable target is available for the appropriate CE study. From all possible mirror combinations the $T_z = \pm 1$ transitions into the final $T_z = 0$ nucleus is the simplest since we need only to assume isospin symmetry for the initial two nuclei.

With this idea in mind we have launched a series of experiments at Leuven, GSI and GANIL. Here we present part of the GSI experiments where we have studied the β decay of the $T_z = -1$, fp-shell nuclei, ^{54}Ni , ^{50}Fe , ^{46}Cr , and ^{42}Ti and compared the

results with the corresponding CE reactions studied at Osaka on the ^{54}Ni , ^{50}Cr , ^{46}Ti and ^{42}Ca stable targets [2-4].

In order to deduce the B(GT) values for each state fed in beta decay in the daughter nucleus one has to use the following expression

$$B(GT)^\beta = k \frac{I_\beta(E)}{f(Q_\beta - E, Z)T_{1/2}}$$

where $I_\beta(E)$ is the β feeding to a level at excitation energy E , $f(Q_\beta - E, Z)$ is the value of the Fermi function for $(Q_\beta - E)$ energy and a daughter nucleus of atomic number Z , $T_{1/2}$ is the parent beta half life and $k=3809.0$ (1.0) [5]. Thus we need the following observables, the β feeding, the $T_{1/2}$ and the Q_β value. In our experiments we have measured the first two quantities while the Q_β value (the factor which dominates the error in the B(GT)) is available in the literature [6, 7].

EXPERIMENTAL DETAILS

The β -decay experiments were performed as part of the STOPPED beam RISING campaign at GSI. The ^{54}Ni , ^{50}Fe , ^{46}Cr and ^{42}Ti nuclei were produced by the fragmentation of a ^{58}Ni beam (680 MeV/u) on a 400 mg/cm² Be target. The primary beam consisted of beam spills of 10 s on and 3 s off and an intensity of 2×10^9 particles per spill. The reaction fragments were separated in-flight in the FRS. The time-of-flight of the ions was measured using two plastic scintillators sci21 and sci41 (Fig 1), and their energy loss was measured with two MUSIC ionization chambers. Multiwire detectors were used for angular correction of the ion trajectory. The separated ions were implanted in one of six Double Sided Silicon Strip Detectors (DSSSD) forming an array (16 x and 16 y strips and 50 x 50 x 1 mm³ volume) [8] (Fig 1). The separator was operated in achromatic mode. Although the ions of interest dominated at the final focal plane, several other ion species survived the several filters and were implanted in the implantation detector. The aluminium energy degrader was adjusted so that most of the desired ions were implanted in the DSSSD M2. In the off-line analysis we have restricted ourselves to cases where the implantations occurred in this detector which resulted in very clean selection of the nucleus of interest. The β -decay signals were detected in the same DSSSD detectors. A logarithmic amplifier was used in order to amplify the energy signals produced by the β -particles (few hundreds of keV) and the energy signals produced by the implants (few tens of GeV). Two kinds of trigger were used in the present experiment: namely an implantation signal (sci41 and DSSSD) or a decay signal (only the DSSSD). This trigger separation allows a software correlation analysis between the implant and the decay demanding that the two signals occurred in the same pixel of the DSSSD. Surrounding the implantation setup was the RISING γ -ray array [9] consisting of 15 Euroball CLUSTER detectors (Fig.1). In the following we will present the results for the ^{46}Cr decay case as an example. In Fig. 2, lower panel, we show the corresponding gamma spectrum. All strong peaks could be identified as gamma lines originating from transitions in ^{46}V with the exception of the

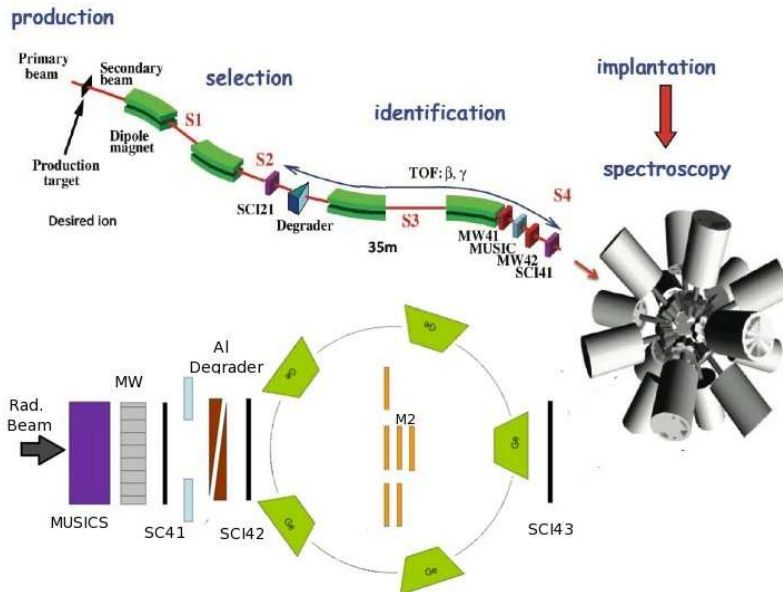


FIGURE 1. Upper part, experimental setup at the FRS at GSI. The RISING Ge-array surrounded the six DSSSD array. Lower part, top view of the implantation focal plane showing the arrangement of the array of six DSSSDs

well known gamma transition at 5522.6(4) in ^{44}Ti . In the upper panel of Fig. 2, we show the results from the (^3He , t) experiment at Osaka. A nice correspondence is observed between the triton and the gamma peaks. The decrease in intensity of the gamma peaks as a function of the energy is a consequence of the reduction imposed by the Fermi function in combination with the natural decrease in efficiency of the RISING array. The decay scheme for ^{46}Cr (Fig.3) was constructed based mainly on the association of gamma lines with the de-excitation of 1^+ states observed in the $^{46}\text{Ti}(^3\text{He},t)^{46}\text{V}$ spectrum and an exhaustive search for contaminant peaks. This decay scheme clearly improves our knowledge of this decay since only the first 1^+ state at 993 keV was previously observed [10]. The parent half-life is a very important quantity and, as mentioned before, essential to extract $B(\text{GT})$ values. In the present experiment we have used time correlations between the ^{46}Cr heavy ion implantation signal (defining $t=0$) and the decay signal happening in the same pixel of the M2 DSSSD detector. In our experiments how to treat random correlations was important and therefore we correlated each decay with all implants happening before and after it to make sure that the true correlation was included in the analysis. This method includes many random correlations which increase the background which has to be properly subtracted. The background was determined by constructing a “wrong” correlation spectrum by correlating decays in pixel ij with implants in pixel ji . The spectrum resulting from the subtraction is shown in Fig 4. It can be seen that the resulting background is flat and close to zero counts. The ^{46}Cr and the daughter activity contribute to the decay curve. The experimental points are fitted with the ^{46}Cr decay curve and the growth and decay curve for the ^{46}V superallowed β emitting

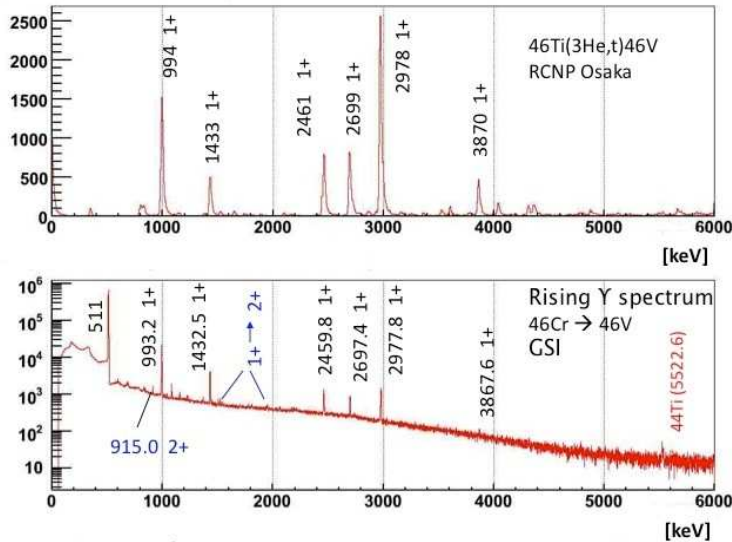


FIGURE 2. Lower panel: Rising add-back gamma spectrum obtained in the ^{46}Cr run, all the levels labeled with energies in keV correspond to gamma transitions in ^{46}V except for the peak at 5522.6 keV in ^{44}Ti (see text). Upper panel: triton spectrum for the $^{46}\text{Ti}(^3\text{He},t)^{46}\text{V}$ reaction obtained at RCNP [4].

activity. The daughter half-life is precisely known (422.50(1) ms [5]) and was a fixed parameter in the fit. The absolute intensity of the 993 keV gamma line, the only line which had enough intensity to allow implant-decay-gamma correlations, could be determined. Thus we have compared all implant-beta correlations with the implant-beta-gamma (993 keV) correlations. We have used this intensity to normalize all gamma intensities and extracted the feeding to the ground state by subtraction. Using these absolute intensities and the intensity balance method we have determined the absolute beta feeding to each individual state including the feeding to the ground state of ^{46}V . These values are also shown in Fig. 3. Using these experimental values and the Q_β from [6] we have deduced the $B(\text{GT})$ values for the transitions in ^{46}Cr . They are shown in Fig. 5 and compared with the results from the CE experiment. All the levels previously observed in the CE reaction experiment and inside our sensitivity limit have been observed in the decay experiment. The $B(\text{GT})$ value reported in [4] for the 2460 keV level contains the contributions from two levels which could be resolved in the decay experiment. Comparing the $B(\text{GT})$ values from the two experiments we see that they are similar but not identical. Several factors could contribute to these differences. A) The two initial ground states are not identical (isospin symmetry breaking). B) The reaction mechanism of the CE reaction is not simple enough, more specifically we know that the CE explores the “crust” of the nucleus while the beta decay can happen anywhere inside the nucleus. C) The “Pandemonium” effect [11] may result in missing strength in the beta decay experiment (although level density arguments suggest this is unlikely here), and D) Since the CE reactions are measured

“close” to zero degrees but not at zero degrees contributions other than $\sigma\tau$ may be present. It should be noted that the other three cases are very similar.

In summary we have presented the cleanest and simplest cases where CE and beta decay experiments have been studied and compared to date. This has been possible

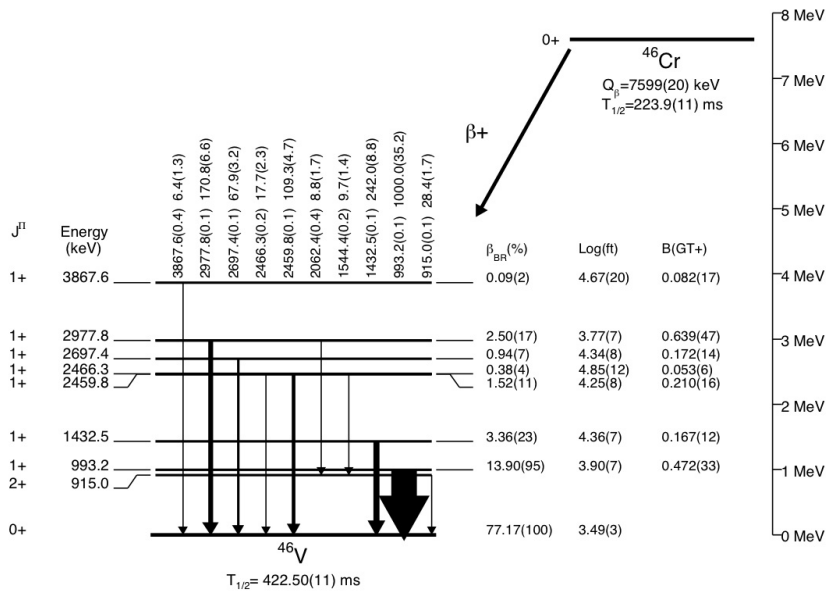


FIGURE 3. ^{46}Cr β -decay scheme. All the values given in this figure were determined in the present work except for the Q_β -value which is from [6] and the daughter half-life which is from [5].

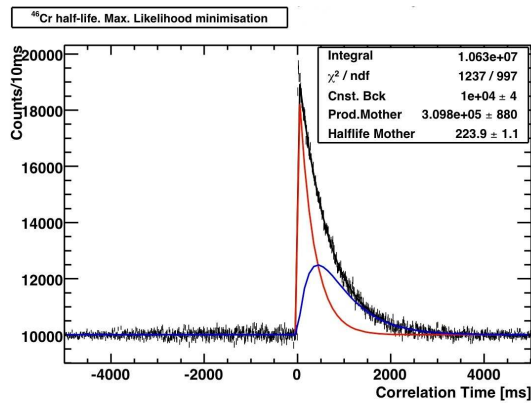


FIGURE 4. ^{46}Cr β -decay half-life determination from heavy-ion implant-beta decay correlations using least squares fit minimization (see text). $T_{1/2} (^{46}\text{Cr}) = 223.9(11)$.

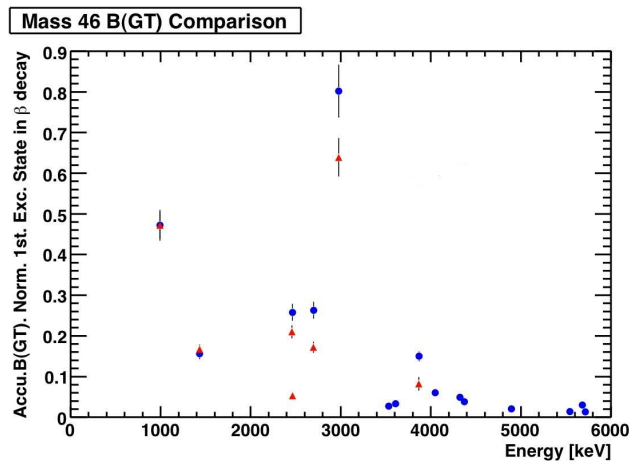


FIGURE 5. ^{46}Cr B(GT) values deduced from the present experiment (triangles) and comparison with the CE results. The reaction B(GT) values are normalised to the beta decay value for the 993 keV level.

thanks to the very good resolution achieved in the $(3\text{He}, t)$ reaction at RCNP in recent years and to the progress in terms of beta decay experiments at fragmentation facilities. In making this comparison we have observed some differences and we have given a number of reasons for their possible origin. In order to progress further in this direction and pin down the dominant contribution, we require some theoretical input or have to wait for the time when CE reactions can be done on the beta decaying nucleus using radioactive beams, although this still lies in the future.

ACKNOWLEDGMENTS

This work has been partially supported by MICINN-Spain, FPA200806419-C02-01), MEXT-Japan, 22540310, the Japan-Spain collaboration programme JSPS-CSIC, Brix(STFC)-UK ST/F012012/1 and EC EURONS No. 506065.

REFERENCES

1. http://www.gsi.de/forschung/fair_experiments/NUSTAR/Proposals.htm
2. T. Adachi et al, Nucl. Phys. **A 788**, 70c (2007)
3. Y. Fujita et al, Phys. Rev. Lett. **95**, 212501 (2005)
4. T. Adachi et al, Phys. Rev. **C 73**, 024311 (2006)
5. J. C. Hardy and I. S. Towner Phys. Rev. **C 70**, 055502 (2009)
6. J. Audi Nucl. Phys. **A 729**, 337 (2003)
7. T. Kurtukian et al. Phys. Rev. **C 80**, 035502 (2009)
8. R. Kumar et al Nucl. Instr. and Meth. **A 598**, 745 (2009)
9. H.J. Wollersheim et al, Nucl. Inst. and Meth **A 537** 637 (2005)
10. T.K. Onishi et al, Phys. Rev. **C 72** 024308 (2005)
11. B. Rubio et al., J. Phys. G, Nucl. Part. Phys. **31**, S1477 (2005)

Code de champ modifié

Mis en forme : Français (France)

Mis en forme : Français (France)

Shell Model Depiction of Isospin Mixing in sd Shell

Yi Hua Lam (蓝乙华)*, Nadya A. Smirnova* and Etienne Caurier†

*CENBG (CNRS/IN2P3 - Université Bordeaux 1) Chemin du Solarium, 33175 Gradignan, France

†IPHC, IN2P3-CNRS et Université Louis Pasteur, 67037 Strasbourg, France

Abstract. We constructed a new empirical isospin-symmetry breaking (ISB) Hamiltonian in the sd ($1s_{1/2}$, $0d_{5/2}$ and $0d_{3/2}$) shell-model space. In this contribution, we present its application to two important case studies: (i) β -delayed proton emission from ^{22}Al and (ii) isospin-mixing correction to superallowed $0^+ \rightarrow 0^+$ β -decay ft -values.

Keywords: Isospin-symmetry breaking, shell model, superallowed $0^+ \rightarrow 0^+$ Fermi beta decay, isospin-forbidden nucleon emission.

PACS: 21.10.Hw, 21.10.Jx, 21.60.Cs, 27.30.+t

INTRODUCTION

Accurate theoretical description of the isospin mixing in nuclear states plays the key role in tests of the fundamental symmetries underlying the Standard Model such as the conserved vector current (CVC) hypothesis and the unitarity of Cabibbo-Kobayashi-Maskawa (CKM) quark-mixing matrix. Any failure would signify the existence of new physics beyond standard concepts.

Besides, Coulomb and charge-dependent nuclear forces are very important for the structure of proton-rich nuclei. An ISB model is required to study isospin-forbidden decay modes, such as β -delayed proton emission, and thus it can help to fine tune the theoretical description. Precise prediction of spectroscopic factors for proton capture has important implications for nuclear reaction rates in an astrophysical context.

Hence, the construction of an ISB Hamiltonian has pivotal consequences for these two applications. Within the microscopic shell-model formalism, we have derived a set of ISB Hamiltonians of high precision to describe the isospin-mixing effects in the sd shell.

ISOSPIN SYMMETRY BREAKING HAMILTONIAN

We assumed that the two-nucleon interaction has both (1) charge-asymmetry $V_{pp} \neq V_{nn}$ and (2) charge-dependence $V_{pp} \neq V_{nn} \neq V_{np}^{T=1}$. To fix the parameters of the ISB shell-model Hamiltonian we used a perturbation theory. First, we obtained nuclear $|\psi^T\rangle$, via diagonalization of an isospin-invariant Hamiltonian, e.g., USD [1], USDA and USDB [2] in a full sd space. Then, the set of functions $|\psi^T\rangle$ was used to get an expectation value of the ISB interaction, $\langle \psi^T | v_{ISB} | \psi^T \rangle$, consisted of the Coulomb potential (v_{coul}), Yukawa π (or ρ) exchange potentials (v_π or v_ρ , respectively) to model

charge-dependent forces of nuclear origin, and isovector single particle energies, $\varepsilon_i^{(1)}$, i.e.

$$v_{ISB} = \sum_{q=1,2} \left(\lambda_{coul}^{(q)} v_{coul}^{(q)}(r) + \lambda_{\pi}^{(q)} v_{\pi}^{(q)}(r) + \lambda_{\rho}^{(q)} v_{\rho}^{(q)}(r) \right) + \sum_i \varepsilon_i^{(1)}. \quad (1)$$

Here q refers to the tensorial character of the operator in isospace and λ_v are the strength parameters. Instead of meson-exchange potentials, we have also used the $T = 1$ two-body matrix elements of the original isospin-conserving Hamiltonian to represent the charge-dependent nuclear forces.

The two-body matrix elements of v_{coul} and $v_{\pi,\rho}$ have been calculated using the harmonic-oscillator wave functions with experimentally determined $\hbar\omega$. The short range correlations (SRC) have been taken into account by four different techniques: (i) via Jastrow-type function with Miller-Spencer parametrization [3], Argonne V18 (AV18), and CD-Bonn [4]¹, or (ii) by a unitary correlation operator method (UCOM) [5].

To find the most optimal strength parameters (λ_v), we used the fact that masses of isobaric multiplets are well described by the second-order isobaric-multiplet mass equation (IMME) [9]

$$M(\alpha, T, T_z) = a(\alpha, T) + b(\alpha, T)T_z + c(\alpha, T)T_z^2 \quad (2)$$

where $\alpha = (A, J^\pi, N_{exc}, \dots)$ denotes all other quantum numbers, besides the isospin, necessary to label an isobaric multiplet of states, whereas a , b and c are coefficients. The strength parameters (λ_v) have been obtained from a least-squares fit of the energy splittings of the isobaric multiplets (due to v_{ISB}) to experimental b and c coefficients. An updated experimental IMME data base was used (to be published in a forthcoming paper [10]) where the latest compilation done by Britz *et al.* [8] was re-evaluated and extended, by taking into account recently (re-)measured mass excesses and updated level schemes.

Our method allowed us to obtain a set of globally fitted ISB Hamiltonians which can reproduce the experimental isobaric mass splittings with low discrepancies, i.e., ~ 34.5 keV for b coefficients, and ~ 8.5 keV for c coefficients. A detailed description of the formalism, SRCs effect and theoretical values for the IMME b and c coefficients can be found in Ref. [6]. A similar procedure was used in Ref. [7], however, based on older experimental data, relied on some truncations and different approaches to the SRC and harmonic oscillator parameter.

BETA-DELAYED PROTON EMISSION OF ²²Al

A β -delayed proton is emitted from the IAS populated in a β -decay of a parent nucleus (precursor). The process goes via isospin-symmetry breaking and thus, to describe the proton branching ratios, one needs to have an ISB Hamiltonian. As an example, we consider here ²²Al. A partial decay scheme is given in Fig. 1, while the calculated

¹ Proposed parameters for Jastrow-type function on the basis of coupled-cluster calculations with Argonne V18 or CD-Bonn nucleon-nucleon potential.

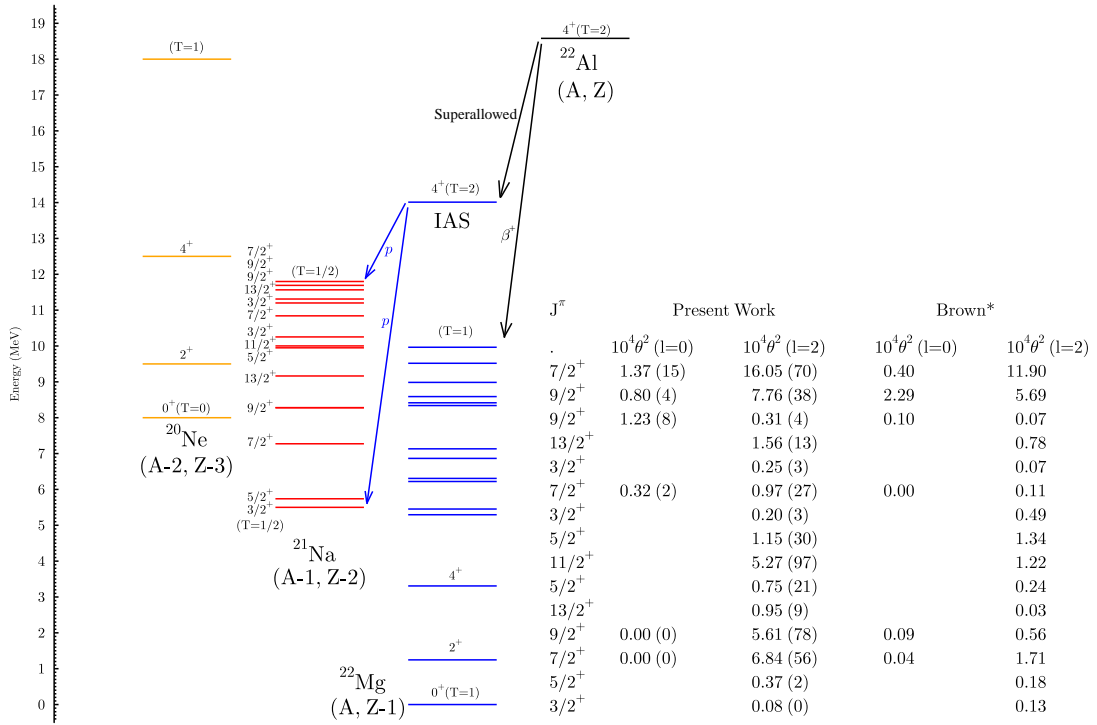


FIGURE 1. Partial decay scheme of ^{22}Al and calculated isospin-forbidden proton spectroscopic factors in comparison with Ref. [11]. Present θ^2 are averaged values calculated from each SRC, i.e., UCOM, CD-Bonn and AV18.

spectroscopic factors, θ^2 , are summarized in an inserted table. We can notice an overall enhancement of the θ^2 obtained in this work compared to the previous results [11], especially, for the transitions to the lowest $7/2^+$, $9/2^+$ and $11/2^+$ states. This is due to a slightly higher degree of impurity of the IAS predicted by the new Hamiltonian. The values of the spectroscopic factors come out to be very sensitive to subtle details of the ISB part of the Hamiltonian. More results will be published elsewhere [12].

SUPERALLOWED $0^+ \rightarrow 0^+$ BETA DECAY

The constancy of the absolute $\mathcal{F}t$ value of superallowed $0^+ \rightarrow 0^+$ β transitions would validate the CVC hypothesis and then would allow to test the unitarity of the CKM matrix. To get it from a given ft -value, a number of corrections should be applied (Ref. [13] and refs. therein). The nuclear structure correction (δ_C) due to the ISB in nuclear states is the one which provides the largest uncertainty to the unitarity test.

We have calculated the contribution to δ_C from configuration mixing of the shell-model basis states, referred as δ_{C1} in [13] or δ_{IM} in [14] see Table 1. Discrepancies between the present results and those from the previous works [14, 13] may be ascribed to different fitting strategies and updated values of experimental b and c coefficients. The difference between our method and that of Ref. [14] was already noted before. The authors of Ref. [13] adjusted strength parameters locally for each multiplet under

TABLE 1. δ_{IM} (in %) of superallowed $0^+ \rightarrow 0^+$ transition in sd shell

Parent Nucleus	Present Work		Previous Work	
	With SRC*	Without SRC	Ormand & Brown	Towner & Hardy [†]
²² Mg	0.0244 (11)	0.0236	0.017 [‡]	0.010 (10)
^{26m} Al	0.0148 (10)	0.0137	0.01**	0.025 (10)
²⁶ Si	0.0513 (4)	0.0511	0.028 [‡]	0.022 (10)
³⁰ S	0.0237 (18)	0.0221	0.056 [‡]	0.137 (20)
³⁴ Cl	0.0313 (3)	0.0316	0.06**	0.091 (10)
³⁴ Ar	0.0070 (4)	0.0065	0.008 [‡]	0.023 (10)

* Averaged δ_{IM} from different SRCs, and the standard deviation.

[†] δ_{IM} or unscaled δ_{C1} from Table III. of Ref. [13].

** δ_{IM} from [14].

[‡] δ_{IM} calculated in present work by using strength parameters from TABLE 2 Ref. [7] without truncation.

consideration (case by case). Calculated $\mathcal{F}t$ values of ²²Mg, ^{26m}Al, ³⁴Cl and ³⁴Ar will be shown in Ref. [6].

In this paper, we presented two important applications of the newly developed ISB shell-model Hamiltonian for the calculation of the branching ratios of the β -delayed proton emission from ²²Al and of the nuclear structure correction (a part due to configuration mixing) for superallowed β -decay. Further analysis and comparison between theoretical predictions and available experimental data is required to elucidate the impact of the new parametrization. All calculation were performed by using ANTOINE [15].

We thank B. Blank for fruitful discussions, S. Triambak and J. Giovinazzo for error estimations, and M. S. Antony for some newly adopted experimental b and c coefficients.

REFERENCES

1. B. A. Brown and B. H. Wildenthal, *Ann. Rev. Nucl. Part. Sci.* **38**, p. 29 (1988).
2. B. A. Brown and W. A. Richter, *Phys. Rev. C* **74**, 034315 (2006).
3. G. A. Miller and J. E. Spencer, *Ann. Phys. (N.Y.)*, **100**, p. 562 (1976).
4. F. Šimkovic, A. Faessler, H. Mütter, V. Rodin, and M. Stauf, *Phys. Rev. C* **79**, 055501 (2009).
5. R. Roth, T. Neff and H. Feldmeier, *Prog. Part. Nucl. Phys.* **65**, p. 50 (2010).
6. Y. H. Lam, N. A. Smirnova, E. Caurier (submitted).
7. W. E. Ormand and B. A. Brown, *Nucl. Phys. A* **491**, p. 1 (1989).
8. J. Britz, A. Pape and M. S. Antony, *At. Data Nucl. Data Tables* **69**, 125 (1998).
9. E. P. Wigner, *Proceedings of the Robert A. Welch Foundation Conference on Chemical Research*, edited by W. O. Milligan, 1958, Vol. 1, p. 67.
10. Y. H. Lam, B. Blank, M. S. Antony, N. A. Smirnova (in preparation).
11. B. A. Brown, *Phys. Rev. Lett.* **65**, p. 2753 (1990).
12. Y. H. Lam, N. A. Smirnova, B. Blank and E. Caurier (in preparation).
13. I. S. Towner and J. C. Hardy, *Phys. Rev. C* **77**, 025501 (2008).
14. W. E. Ormand and B. A. Brown, *Phys. Rev. Lett.* **62**, p. 866 (1989); *Phys. Rev. C* **52** p. 2455 (1995).
15. E. Caurier *et al.*, *Rev. Mod. Phys.* **77**, p. 427 (2005).

Production and Separation of T=1/2 Nuclides for $\beta - \nu$ angular correlation measurements

P. Delahaye^a, C. Couratin^{a,b}, E. Liénard^b, O. Bajeat^a, G. Ban^b, D. Durand^b, X. Flécharde^b, O. Naviliat-Cuncic^c, M. G. Saint Laurent^a, T. Stora^d, J. C. Thomas^a, E. Traykov^a, and the GANISOL group^a

^aGANIL, CEA/DSM-CNRS/IN2P3, Bd. Becquerel, BP 55027, 14076 CAEN Cedex 05, France.

^bLPC Caen, 6 bd Maréchal Juin, 14050 CAEN Cedex, France.

^cNSCL, Michigan State University, 1 Cyclotron, East Lansing, Michigan 48824-1321

^dISOLDE, CERN, 1211 Geneva 23, Switzerland.

Abstract. The SPIRAL facility at GANIL, which uses the so-called ISOL method to produce radioactive ion beams, is being upgraded to extend its production capabilities to the metallic beams of neutron deficient isotopes. We discuss here the potentialities offered by this upgrade for the measurement of the $\beta - \nu$ angular correlation in the $\beta - \nu$ decay of mirror nuclides.

Keywords: β - decay, $\beta - \nu$ angular correlation, radioactive beams.

PACS: 23.40.Bw, 27.30.+t, 29.25.Rm, 29.38.-c.

MIRROR NUCLIDES AND THE CVC HYPOTHESIS

According to the Conserved – Vector – Current (CVC) hypothesis, the corrected Ft-value of all super-allowed β decays is constant. This hypothesis is extensively used for the determination of V_{ud} [1], which is the dominant term appearing in the test of the unitarity of the first row of the CKM matrix. V_{ud} is presently most precisely determined from the Ft – value from 13 nuclear $0^+ \rightarrow 0^+$ decays. The Ft – value inferred from neutron and a set of mirror nuclides [2] arrives then second with an uncertainty 6 to 8 times larger, in front of pion decay. As for the neutron, the determination of V_{ud} from the decay of mirror transitions requires the experimental measurement of correlation parameters from which the Gamow – Teller to Fermi mixing ratio can be deduced.

Using the same conventions as in [3], the corrected Ft-value for the transition of mirror nuclides Ft^{Mirror} is related to the Ft-value for the super-allowed $0^+ \rightarrow 0^+$ transition $Ft^{0^+ \rightarrow 0^+}$ via the following equation:

$$Ft^{Mirror} \equiv ft(1 + \delta'_R)(1 + \delta_{NS}^V - \delta_C^V) = \frac{2Ft^{0^+ \rightarrow 0^+}}{(1 + f_A / f_V \cdot \rho^2)} \quad (1)$$

where δ'_R , δ_{NS}^V are respectively nucleus dependent and nuclear structure dependent radiative corrections, δ_C^V an isospin-symmetry breaking correction, f_A and f_V the

statistical rate functions for the Axial – Vector and Vector interactions respectively, and ρ the Gamow – Teller to Fermi mixing ratio:

$$\rho \approx \frac{C_A M_{GT}^0}{C_V M_F^0} \quad (2)$$

C_A, C_V, M_{GT}^0 and M_F^0 are the Gamow Teller and Fermi coupling constants and matrix elements in the isospin symmetry limit. Assuming CVC, V_{ud} can be deduced from $Ft^{0^+ \rightarrow 0^+}$ and Ft^{Mirror} average values:

$$V_{ud}^2 = \frac{K}{2Ft^{0^+ \rightarrow 0^+} G_F^2 (1 + \Delta_R^V)} = \frac{1}{(1 + f_A / f_V \cdot \rho^2)} \cdot \frac{K}{Ft^{Mirror} G_F^2 (1 + \Delta_R^V)} \quad (3)$$

where $K / (\hbar c)^6 = 2\pi^3 \hbar \ln 2 / (m_e c^2)^5 = 8120.2787(11) \times 10^{-10} \text{ GeV}^4$, $\Delta_R^V = 2.361(38)\%$ is a nucleus independent radiative correction [4], $G_F / (\hbar c)^3 = 1.16637(1) \times 10^{-5} \text{ GeV}^{-2}$ is the Fermi constant [5].

Recently, a number of mirror nuclides were proposed as candidates for the measurement of $\beta - \nu$ angular correlations at SPIRAL, GANIL, using an upgraded target – ion source setup [6]. The list of these nuclides is shown in Tab. 1.

TABLE 1. List of nuclides candidates for the measurement of $\beta - \nu$ angular correlation parameter of non – oriented nuclei. The two columns on the right are the standard deviation that could be obtained on ρ and V_{ud} assuming a measurement of the $\beta - \nu$ angular correlation parameter with an uncertainty as described in the text.

Isotope	ρ [3]	σ_ρ assuming	$\sigma_{V_{ud}}$ with/without uncertainty on Ft
		$\sigma_a = \text{Max}(0.005 \cdot a, 0.00167)$	([3])
¹⁹ Ne	1.5933(30)	0.0041	2.9E-3 / 2.8E-3
²¹ Na	-0.7034(32)	0.0028	2.4E-3 / 1.9E-3
²³ Mg	0.5426(44)	0.0034	2.5E-3 / 1.8E-3
²⁵ Al	-0.7973(27)	0.0025	2.3E-3 / 2.1E-3
²⁹ P	-0.5209(48)	0.0035	2.7E-3 / 1.9E-3
³¹ S	0.5167(84)	0.0035	3.8E-3 / 1.8E-3
³³ Cl	0.3076(42)	0.0054	1.9E-3 / 1.6E-3
³⁵ Ar	-0.2841(25)	0.0058	1.7E-3 / 1.6E-3
³⁷ K	0.5874(71)	0.0032	3.3E-3 / 1.5E-3
³⁹ Ca	-0.6504(41)	0.0029	2.3E-3 / 1.3E-3

Proposed $\beta - \nu$ angular correlation measurements

Operational since 2006, the LPCtrap setup has originally been developed in the low energy beam lines of SPIRAL by LPC Caen for the measurement of the $\beta - \nu$ angular correlation in the decay of ⁶He [7]. LPCtrap consists of a RFQ cooler buncher, a measurement trap and a detection setup. The RFQ cooler buncher optimizes the transfer of the radioactive ion into the measurement trap. This latter is a transparent Paul whose open structure permits the detection in coincidence of the electrons and recoiling ions. A $\Delta E - E$ (Si plus plastic) telescope for the electron and a micro-channel plates assembly for the recoiling ions allow one to measure for each detected decay the electron energy, the recoil ion time of flight and the angle between both particles. The $\beta - \nu$ angular correlation parameter is deduced from the recoil ion time-

of-flight spectrum, while the other observables are used for checking data consistency. During the two last experiments with ${}^6\text{He}$, up to $4 \cdot 10^6$ coincidences could be collected. Based on the data of the first experiment, and despite an experimental bias on the recoil ion detector, a complete analysis procedure could be developed and a precise knowledge of the setup and of its present limitations could be gained [8]. It is expected that in nominal conditions the eventual total uncertainty (statistical + systematic) on the $\beta - \nu$ angular correlation parameter (denoted a in the following) should reach the 0.5% level. This analysis is being applied to the data of the latest experiment with ${}^6\text{He}$ which additionally permitted the precise measurement of the charge state distribution of the recoil nucleus after decay [9].

In contrast with comparable setups using magnetic optical traps, LPCtrap can be used for measuring $\beta - \nu$ angular correlations for β - decaying ions of any chemical nature. A test was lately done with ${}^{35}\text{Ar}$ which is already produced by the SPIRAL facility. For all isotopes shown in Tab. 1 it was estimated that a production of 10^7 $1+$ ions to LPCtrap is required for obtaining comparable total uncertainty to the one obtained with ${}^6\text{He}$ in one week beam time [6].

Sensitivity of the Measurements to New Physics

In the limit of zero momentum transfer, the expression of a is quite simple:

$$a = (1 - \rho^2 / 3) / (1 + \rho^2) \quad (4)$$

the correct formula in first order in recoil being developed in [2]. The second column of Tab. 1 shows the error that could be obtained on ρ from the measurement of the angular correlation parameter a with an accuracy of 0.5% for all isotopes as assumed in [10], except for ${}^{19}\text{Ne}$ for which the expected amplitude of a is much smaller: $a_{SM} = 0.0435(10)$ as calculated in [3]. In this particular case, it was assumed as conservative estimate that the same absolute accuracy as in the case of ${}^6\text{He}$ could be achieved: $\sigma_a \approx 0.00167$.

As a result from Eq. 3, the last column of Tab. 1 shows the error that could be obtained on V_{ud} from each of these measurements with the present uncertainty on the Ft-values, and assuming a negligible contribution from the Ft - values in the error budget. As in [3], a conservative error was applied to the ratio f_A/f_V of 20% on the deviation from unity. Alone, this campaign of measurement would yield an error on the determination of V_{ud} in the order of $8.4 \cdot 10^{-4}$, or $5.9 \cdot 10^{-4}$ if it is accompanied by the re-measurements of the ft values to high accuracies, such as those achieved for the $0^+ \rightarrow 0^+$ decays ($\sigma_{ft}/ft \leq 5 \cdot 10^{-4}$, see [11]). Assuming that the ratio f_A/f_V can be determined to the percent level, this error drops to $4.6 \cdot 10^{-4}$, which is only about two times larger than the present precision on V_{ud} from the $0^+ \rightarrow 0^+$ transitions: $\sigma_{V_{ud}} = 0.0022$ [1]. In addition, this set of data would permit testing CVC by comparing the Ft-values of these mirror nuclides and eventually the two left members of Eq. 3 to a level of 10^{-3} . Finally, assuming CVC the coherence of the theoretical corrections for these mirror nuclides could be tested, although for these latter the

expected errors from experiment $\sigma_{\delta_C^V - \delta_{NS}^V} \approx 2\sigma_{V_{ud}}$ would be 3 to 10 times bigger than those quoted from calculations [3].

NEW BEAMS FROM THE SPIRAL UPGRADE

Since 2001, the SPIRAL facility has been delivering radioactive ion beams of gaseous elements of unique intensity and purity for physics experiments [12]. SPIRAL makes use of the so – called Isotope Separation On Line (ISOL) method: the intense heavy ion beams from the GANIL facility impinge on thick graphite targets where the fragmentation products are stopped. After diffusion in the target material and effusion in a cold transfer tube the radioactive atoms are ionized in an ECR ion source. The transfer tube permits to protect the ECR source from the demagnetization of the permanent magnets by heat and secondary neutron flux. A drawback of this ionization system is that only gaseous elements can be ionized, as all condensable elements stick onto the cold surfaces of the transfer tube and eventually ion source.

In order to extend the capabilities of SPIRAL to condensable elements, it is planned to couple the so-called VADIS [13] which is the latest FEBIAD source developed at ISOLDE, CERN, to the SPIRAL targets. Hot FEBIAD ion sources are usually capable to ionize any element to 1+ charge state with melting point below 2000°C, provided that the element of concern can effuse to the ion source volume. During two beam times, a prototype of SPIRAL target heated by an external oven coupled via a hot transfer tube to the VADIS was tested in the SIRa test bench. A complete description of the prototype of target - ion source system and its performances will be discussed in a forthcoming article [14]. The ionization efficiency of stable Ne injected as tracer in the target volume was monitored during the two tests. During the first beam time, a ^{58}Ni beam at 72 AMeV was impinging on the target with a maximum power of 45W. An efficiency up to 5% with stable Ne, close to the nominal efficiency of 6.7% as measured at ISOLDE, could be obtained after a couple of days of conditioning. During the second test, a ^{36}Ar beam with maximum power of 13W was used. Only 0.5% ionization efficiency could be obtained with Ne because of a lack of conditioning of the ion source and of misbehaving extraction optics. Tab. 2 shows the preliminary results for the two tests corresponding to 1+ intensities deduced from gamma lines measured at saturation on the SIRa tape station using a Ge detector. The last column of Tab. 2 shows extrapolated SPIRAL 1+ intensities, scaled to a nominal power of 1500W and normalized to an ionization efficiency of 5% for Ne. Comparing to Tab. 1, 5 over 10 isotopes candidates for the $\beta - \nu$ angular correlation measurements have been observed. Among them, ^{33}Cl , ^{37}K and ^{35}Ar exhibit extrapolated yields which are compatible for the measurements. Using ^{24}Mg as primary beam instead of ^{36}Ar , this should also be the case for ^{23}Mg , as an EPAX calculation shows that the in – target production yield would be then multiplied by more than one order of magnitude. In the case of ^{25}Al , a slow effusion of Al on the graphite and Tantalum surfaces is probably the cause of the low 1+ intensity. ^{29}P and ^{31}S were not observed during the last beam time. For these three isotopes one shall test in the future the use of the technique of molecular sideband (formation of molecules by the injection of a reactive gas into the target volume) for easing their effusion to the ion source in the form of

molecules such as AlF, HP or HS. ^{21}Na , ^{19}Ne (already available from the present SPIRAL) and ^{39}Ca are expected to be produced to the required yields using suitable primary beams.

TABLE 2. Results of the two test beam times for the new target – ion source prototype tested at SIRa. See text for explanations.

Isotope	Half life	Primary beam	Power (W)	Measured 1+ intensity	Extrapolated to 1500W and nominal ionization efficiency
23Mg	11.3s	36Ar	~13	1.73E+03	2.00E+06
25Al	7.18s	36Ar	~13	2.60E+02	3.00E+05
33Cl	2.5s	36Ar	~13	6.93E+03	8.00E+06
35Ar	1.775s	36Ar	~13	8.67E+03	1.00E+07
37K	1.226s	36Ar	~13	1.10E+04	1.27E+07
38K	6.3min	36Ar	~13	1.30E+04	1.50E+07
38K	6.3min	58Ni	4	3.80E+04	1.50E+07
38mK	923ms	36Ar	~13	1.30E+04	1.50E+07
38mK	923ms	58Ni	4	-	-
53Fe	8.51 min	58Ni	34	6.60E+04	2.90E+06
53mFe	2.526min	58Ni	34	1.40E+04	6.10E+05
58Cu	3.204s	58Ni	37	4.30E+03	1.80E+05
58Mn	3s	58Ni	37	5.70E+04	2.30E+06
59Cu	81.5s	58Ni	38	7.30E+04	2.90E+06

Beam separation

As the FEBIAD source is by principle a non - selective ion source, beam contamination issues can eventually hinder the precise measurement of the $\beta - \nu$ angular correlation parameters with the condensable isotopes as proposed in Tab. 1. For this reason, the use of a Time – Of – Flight Mass Spectrometer of a similar type as the one developed at RIKEN [15] is being investigated. This device would be placed in-between the RFQ cooler buncher and measurement trap. First simulations show that a resolving power of 10.000 could be obtained for time – of – flights within the 10 ms range, which is enough to efficiently suppress eventual isobar contamination for the mass range of Tab. 1. The timing properties of the extracted bunch being very similar to the injected one, the injection into the measurement trap should be as efficient as with the present setup.

REFERENCES

1. I. S. Towner and J. C. Hardy, Rep. Prog. Phys. 73 (2010) 046301 .
2. O. Naviliat-Cuncic and N. Severijns, Phys. Rev. Lett. 102 (2009) 142302.
3. N. Severijns, M. Tandecki, T. Phalet, and I. S. Towner, Phys. Rev. C **78** (2008) 055501.
4. Marciano W J and Sirlin APhys. Rev. Lett. 96 (2006) 032002.
5. C. Amsler et al. (Particle Data Group), Phys. Lett. B 667 (2008) 1.
6. E. Lienard et al., letter of intent to the GANIL PAC, March 2010, and letter of intent to the SPIRAL 2 SAC, SPIRAL 2 Week, Feb. 2010.
7. X. Flécharde et al., J. Phys.: Conf. Ser. 58 431
8. P. Velten, PhD thesis, 2011, Université de Caen, France.
9. X. Flécharde et al, in preparation.
10. O. Naviliat-Cuncic and N. Severijns, Eur. Phys. J. A 42 (2009) 327.
11. T. Kurtukian - Nieto et al., this volume.

12. A Navin, F. de Oliveira Santos, P Roussel-Chomaz and O Sorlin., *J. Phys. G: Nucl. Part. Phys.* **38** (2011) 024004.
13. L. Penescu, R. Catherall, J. Lettry, and T. Stora , *Rev. Sci. Instrum.* **81** (2010) 02A906
15. Y. Ishida, M. Wada, Y. Matsuo, I. Tanihata, A. Casares and H. Wollnik, *Nucl. Instrum. And Meth. B*, 219–220 (2004) 468

High-precision β decay half-life measurements of proton-rich nuclei for testing the CVC hypothesis

T. Kurtukian-Nieto by the NEX group of CENBG

*Centre d'Etudes Nucléaires de Bordeaux-Gradignan (CENBG), Université Bordeaux 1,
CNRS/IN2P3, Chemin du Solarium, BP 120, F-33175 Gradignan cedex, France*

Abstract. The experimental study of super-allowed nuclear β decays serves as a sensitive probe of the conservation of the weak vector current (CVC) and allows tight limits to be set on the presence of scalar or right-handed currents. Once CVC is verified, it is possible to determine the V_{ud} element of the CKM quark-mixing matrix. Similarly, the study of nuclear mirror β decays allows to arrive at the same final quantity V_{ud} . Whereas dedicated studies of $0^+ \rightarrow 0^+$ decays are performed for several decades now, the potential of mirror transitions was only rediscovered recently. Therefore, it can be expected that important progress is possible with high-precision studies of different mirror β decays. In the present piece of work the half-life measurements performed by the CENBG group of the proton-rich nuclei ^{42}Ti , $^{38-39}\text{Ca}$, $^{30-31}\text{S}$ and ^{29}P are summarised.

Keywords: Weak-interaction, lifetimes

PACS: 21.10.Tg, 23.40.-s, 23.40.Bw

INTRODUCTION

The nuclear β^+ decay is a purely weak process in which a proton (two up quarks and one down, uud) decays to become a neutron (one up quark and two down quarks, udd) plus a positron e^+ and an electron-type neutrino ν_e . According to the Standard Model (SM), an up quark disappears in this process and a down quark and a virtual W^+ boson is produced. The W^+ boson then decays to produce a e^+ and a ν_e . The β decay is inherently sensitive to the physics of the weak interaction and small deviations of experimental results from SM predictions translate directly into new physics beyond SM.

In particular, the study of the super allowed $0^+ \rightarrow 0^+$ β^+ decay between $T = 1$ analog states provides valuable information for testing SM since it depends uniquely on the vector part of the weak interaction and, according to the conserved vector current (CVC) hypothesis, its experimental ft value is related to the vector coupling constant g_V , a fundamental constant that is the same for all such transitions. A universal $\mathcal{F}t$ value, which depends only on the isospin of the decaying nucleus, can be determined after applying the theoretical corrections which are necessary due to isospin impurities of the nuclear states, nuclear structure differences impacting on radiative corrections as well as nucleus dependent and nucleus independent radiative corrections (see ref. [1] and references therein for a review). Once the CVC hypothesis is verified, these data, together with the muonic vector coupling constant, allow for the determination of the up-down quark element V_{ud} of the Cabibbo-Kobayashi-Maskawa quark-mixing matrix which, according to the SM, is unitary. Similarly, the study of nuclear mirror β^+ decays allows to arrive at the same final quantity V_{ud} (see ref. [2]). Consequently, the

experimental study of these transitions serves as a sensitive probe of the conservation of the weak vector current and allows tight limits to be set on the presence of scalar or right-handed currents.

Dedicated studies of super-allowed $0^+ \rightarrow 0^+$ Fermi transitions has been performed for several decades now, allowing to reach a precision close to or better than 10^{-3} for the experimental ingredients of ft , yielding a V_{ud} value of 0.97425(22) [1]. A value of 0.9719(17) for V_{ud} was recently determined [3] from a compilation of the relevant data from literature [2] with nuclear mirror β^+ decays. Nuclear mirror transitions provide an independent sensitive source for the determination of V_{ud} and significant progress can be achieved when better precision is reached in both the experimental inputs and the theoretical corrections.

In the present piece of work, the summary of a series of measurements performed both at the IGISOL facility at the Accelerator Laboratory of the University of Jyväskylä and at ISOLDE-CERN is given.

EXPERIMENTAL TECHNIQUE

Experiments performed at the ISOLDE/CERN facility

The isotopes are produced by spallation reactions induced by the CERN PS Booster proton beam. The ion source allows for the production of molecules, which are mass separated by the ISOLDE High-Resolution Separator (HRS) and accumulated in the REXTRAP Penning trap facility. After an accumulation time of one half-life, an ejection pulse empties the trap and send the sample to a tape station. This ejection allows a time-of-flight (TOF) selection of mass which is operated by means of a pulsed deflection plate. The TOF analysis eliminates any contamination and an ultra-pure sample is deposited on the tape. Details of the method are described in ref. [4].

The sample is then transported to the experimental set-up consisting of a 4π gas (CF₄) counter (with a tape passing between two subdivided halves) for β particles and two germanium detectors for γ detection. Figure 1 shows a schematic drawing of the experimental set-up. Its purpose is to detect the β particles from the decay of the mother and of the daughter isotopes. The decay time is measured with respect to the REXTRAP extraction pulse. The germanium detectors allow to verify the sample purity.

Experiments performed at the IGISOL facility

The Ion Guide Isotope Separator On-Line (IGISOL) facility is placed at the Accelerator Laboratory of the University of Jyväskylä. The isotopes are produced by means of fusion-evaporation reactions. The reaction products are thermalized in the helium gas of the IGISOL target chamber, extracted by means of a helium gas flow and a sextupole ion guide (SPIG), accelerated and A/q selected by the IGISOL magnet (see ref. [5] and reference therein). The JYFLTRAP facility-consisting of a radio frequency cooler-buncher (RFQ) and two Penning traps- is used to prepare pure samples of the isotope of interest to be sent to the experimental setup for half-life measurements.

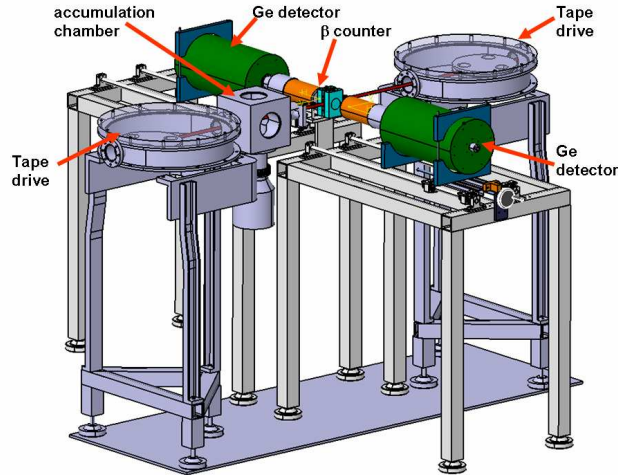


FIGURE 1. (Color online) Schematic drawing of the experimental set-up used in ISOLDE/CERN experiments. The activity accumulated in REXTRAP is transported and deposited on a tape in the cubic collection chamber. The tape is then moved into a 4π gas counter for β detection. Two germanium detectors, facing each side of the counter, detect γ -rays in coincidence with β -particles in the gas counter.

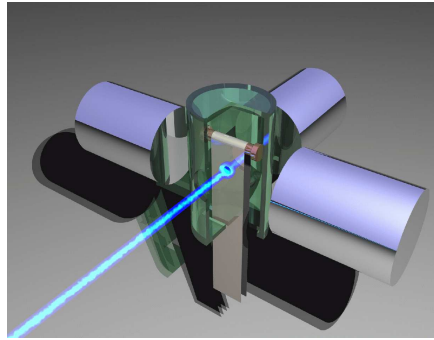


FIGURE 2. (Color online) Schematic drawing of the experimental setup used in the IGISOL-JYFL experiments showing the plastic scintillator to detect the β particles and the moving mylar tape as well as three germanium detectors for the γ rays.

The pure samples are implanted on a moving mylar tape, placed at the end of the JYFLTRAP extraction beam line (See Figure 2). The collection spot is located at the center of a 2 mm thick, 4π cylindrical plastic scintillator, which is used to detect the positrons emitted by the implanted nuclei. The plastic scintillator had an entrance hole of 12 mm in diameter and an entrance hole for the tape on the bottom of the cylinder, yielding a β -particle detection efficiency of 90%. The scintillation light is collected by two photomultiplier tubes, which view a special light guide connected to the scintillator. The two photomultipliers are run in coincidence to eliminate most of the noise of the individual tubes. To provide $\beta - \gamma$ coincidence data for measuring the superallowed branching ratio, and for a further control of the background, three coaxial germanium detectors are placed around the plastic scintillator detector at -90° , 0° , and $+90^\circ$, with respect to the extraction beam line.

DATA ANALYSIS

The first step in the analysis is the selection of valid cycles. The criteria for accepting a cycle are: (i) the number of counts in a cycle had to be larger than a user chosen limit, (ii) the fit of the experimental decay time spectrum converges, yielding a reduced χ^2 lower than a user chosen value. The accepted cycles, with identical experimental conditions, are then dead-time corrected and grouped in runs. The fit of these runs with the theoretical curve yield the final half-life of a run. The average of all runs yield the final result with its statistical uncertainty. The final step of the analysis is to search for bias on the result. The half-life is investigated as a function of both the experimental and the analysis parameters which are varied within reasonable limits to check their influence on the final result. From these considerations, the systematic uncertainties are deduced and added quadratically to the statistical uncertainty.

SUMMARY OF RESULTS AND CONCLUSIONS

In the present piece of work the half-life measurements of ^{42}Ti , $^{38-39}\text{Ca}$, $^{30-31}\text{S}$ and ^{29}P are summarised. ^{42}Ti decays by super-allowed β^+ emission to its isobaric analog state ($J^\pi = 0^+$, $T = 1$), the g.s. of ^{42}Sc . Our experimental result, $T_{1/2} = 208.14 \pm 0.45$ ms, is the most precise measurement for this nucleus. Compared with previous measurements (see ref. [6] and references therein), our result is 15 times more precise. ^{38}Ca is one of the $T_z = -1$, $0^+ \rightarrow 0^+$ β -emitting nuclides used to determine the vector coupling constant and the V_{ud} quark-mixing matrix element in ref. [1]. Our result, $T_{1/2} = 443.8(19)$ ms [7], is four times more precise than the average of previous measurements. For ^{30}S , another super-allowed β -emitter, the result of $T_{1/2} = 1175.9(17)$ ms obtained in this work [8] is in agreement with older half-life values from the literature and is a factor of 3 more precise than the previous experimental average. During the experiment of ^{30}S , the half-lives of the mirror β decays of ^{29}P and ^{31}S were also measured. Both data sets are presently under analysis. The expected precision for both isotopes is of the order 10^{-3} [9]. For ^{39}Ca , another $T = 1/2$ mirror nuclei, a half-life of $T_{1/2} = 860.7(10)$ ms is obtained [7], a result in agreement with the average value from the literature.

With the half-life measurements summarised here, all $T_z = -1$ nuclei up to ^{42}Ti are now known with good precision. Further experimental campaigns will mainly concentrate on mirror β decay, where significant progress can be achieved.

REFERENCES

1. J. C. Hardy, and I. S. Towner, *Physical Review C* **79**, 055502 (2009).
2. N. Severijns, M. Tandecki, T. Phalet, and I. Towner, *Phys. Rev. C* **78**, 055501 (2008).
3. O. Naviliat-Cuncic, and N. Severijns, *Phys. Rev. Lett.* **102**, 142302 (2009).
4. P. Delahaye, B. Blank, and S. Sturm, *Nucl. Instrum. Methods B* **266**, 4647 (2008).
5. P. Karvonen, et al., *Nucl. Instrum. Methods B* **266**, 4794 (2008).
6. T. Kurtukian-Nieto, et al., *Phys. Rev. C* **80**, 035502 (2009).
7. B. Blank, et al., *Eur. Phys. J. A* **44**, 363-372 (2010).
8. J. Souin, et al., *Eur. Phys. J. A* **47**, 40 (2011).
9. A. Bacquias, et al., *Eur. Phys. J. A* (2011).